Investigating the role of Nicotinamide phosphoribosyltransferase (NAMPT) in cartilage catabolism

Laura Evans BSc (Hons) MRes

Thesis presented for the degree of Philosophiae Doctor

September 2013

Acknowledgements

First and foremost, I would like to thank my supervisors Mari Nowell, Anwen Williams and Anthony Hayes for their continued guidance, support and above all, patience. They have taught me so much, and made my PhD experience truly invaluable and enjoyable.

I give thanks also to Bruce Caterson, Claire Hughes, and the staff and students within BIOSI who have assisted me with my *ex vivo* studies; including Amy Morgan, Shane Wainright, Ilyas Khan, and Emma Blain.

I would also like to thank Naz, Sara and Louise for their excellent work on NAMPT within the Nowell group: that has benefited my thesis enormously.

I am also indebted to the past and present staff in Central Biotechnology Services for providing training and essential facilities; including Jennifer Stott, Ayman Hawrani, and Claudia Consoli. I am also grateful to the staff within JBIOS for their support and guidance, including Deborah and Martin. I would also like to take this opportunity to thank all the company reps that have provided technical support over the years, including Tim Devlin and Ardy Arjomandi.

I would also like to thank all my colleagues, staff and students alike, who have offered me advice and practical assistance over the years, and for keeping me sane.

Last but not least, thank you to my friends and family for their continued love and support. This thesis is dedicated to them.

Summary

NAMPT (nicotinamide phosphoribosyltransferase) is a universally expressed protein elevated in the serum and synovial fluid of rheumatoid arthritis (RA) sufferers. NAMPT is a rate-limiting enzyme in the biosynthesis of (nicotinamide adenine dinucleotide) NAD^+, an essential cellular coenzyme, and has also been shown to exert cytokine-like activities as a mediator of innate immunity. However little is currently known of the role of NAMPT in cartilage metabolism. In this thesis, the role and regulation of NAMPT was studied in a variety of model systems. Addition of exogenous (e)NAMPT to fibroblasts *in vitro* increased MMP-3 release, an effect attenuated by APO866. *In vivo* studies in a murine arthritis model showed APO866 treatment reduced arthritis index, with a slight reduction in synovial hyperplasia, inflammatory infiltrate and cartilage degradation. *In vivo* imaging with MMP activatable fluorescent probes showed a reduction in MMP activity in APO866-treated animals compared with placebo. Analyses of archived tissue indicated that APO866 reduced MMP gene expression in affected limbs in a time and dose dependent manner. In a cartilage explant culture system, APO866 significantly attenuated cytokine-mediated proteoglycan (PG) depletion and MMP-2 and -9 release. This was associated with a dose-dependent loss of cell viability. These effects were reversed by co-incubation with NAD^+ metabolites NMN and NA, suggesting that cell survival was highly NAD^+-dependent, and that cytokine-induced MMP expression could be NAMPT independent. Finally, *in vitro* studies in RA synovial fibroblasts revealed that intracellular (i)NAMPT is upregulated by cytokine stimulation, with concurrent upregulation of MMPs -1 and -3. The data emphasise the pleiotropic function of NAMPT in health and disease, and suggest a role for extracellular (but not intracellular) NAMPT in cartilage catabolism. Finally, NAMPT inhibition is highlighted as a promising therapeutic strategy for RA.

Publications and Presentations

Publications

Jackman, S., Evans, L.A., Moideen, A., Blain, E., Nowell, M.A. (2012) Regulation of NamPRT following cyclic tensile mechanical loading of synovial fibroblasts. British Society for Matrix Biology- Autumn 2011. International Journal of Experimental Pathology **93**(4): A27-28.

Nowell, M.A., Evans, L.A., Williams, A.S. (2012). PBEF/NAMPT/visfatin: a promising target for treating rheumatoid arthritis? Future Medicinal Chemistry **4**(6): 751-769.

Moideen, A.N., Evans, L.A., Osgood, L., Williams, A.S., Jones, S.A., Nowell, M.A. (2012). Nicotinamide adenine dinucleotide (NAD^+) biosynthesis enzymes in rheumatoid arthritis. Rheumatology **51**(supp 3): 142-142.

Evans, L.A., Williams, A.S., Hayes, A.J., Nowell, M.A. (2011). Investigating the role of PBEF on cartilage integrity. British Society for Matrix Biology- Autumn 2010 Meeting Report. International Journal of Experimental Pathology **92**(3): A33-A34.

Evans, L.A., Williams, A.S., Hayes, A.J., Jones, S.A., Nowell, M.A. (2011). Suppression of leukocyte infiltration and cartilage degradation by selective inhibition of pre-B cell colony-enhancing factor/visfatin/nicotinamide phosphoribosyltransferase: Apo866-mediated therapy in human fibroblasts and murine collagen-induced arthritis. Arthritis and Rheumatism **63**(7): 1866-1877.

Presentations

Evans, L.A., Williams, A.S., Hayes, A.J., Nowell, M.A. (2011). Investigating the role of NAMPT in cartilage metabolism. (Poster) 26th Annual Postgraduate Research Day, Cardiff University, November 11th 2011.

Evans, L.A., Williams, A.S., Hayes, A.J., Nowell, M.A. (2011). Investigating the role of nicotinamide phosphoribosyl transferase (NAMPT) on cartilage metabolism. (Oral) I3-IRG Meeting 2011, Cardiff, September 29th 2011.

Evans, L.A., Williams, A.S., Hayes, A.J., Nowell, M.A. (2010). Investigating the effect of PBEF on cartilage integrity. (Oral) 25th Annual Postgraduate Research Day, Cardiff University, November 19th 2010.

Evans, L.A., Williams, A.S., Hayes, A.J., Nowell, M.A. (2010). Investigating the effect of PBEF on cartilage integrity. (Oral) 9th Annual Cardiff Institute of Tissue Engineering and Repair (CITER) group meeting, Eastwood Park, Gloucestershire, September 17th 2010.

Evans, L.A., Williams, A.S., Hayes, A.J., Nowell, M.A. (2010). Investigating the effect of PBEF on cartilage integrity. (Oral) British Society for Matrix Biology (BSMB) Meeting Autumn 2010, University of East Anglia, Norwich, September 7th 2010.

Evans, L.A., Williams, A.S., Hayes, A.J., Nowell, M.A. (2010). The effect of PBEF on cartilage integrity. (Poster) I3-IRG Meeting 2010, Atlantic college, Llantwit Major, July 8th and 9th 2010.

Evans, L.A., Williams, A.S., Hayes, A.J., Nowell, M.A. (2009). Investigating the effect of PBEF on cartilage integrity. (Poster) 24th Annual Postgraduate Research Day, Cardiff University, November 20th 2009.

Abbreviations

ACPA	Anti-citrullinated protein antibody
ADAM	A disintegrin and metalloproteinase
ADAMTS	A disintegrin and metalloproteinase with thrombospondin motifs
AI	Arthritis index
AIA	Antigen-induced arthritis
ATP	Adenosine Triphosphate
BSA	Bovine Serum Albumin
CCL	CC chemokine ligand
cDNA	Complementary deoxyribonucleic acid
CIA	Collagen-induced arthritis
CII	Collagen Type II
COX	Cyclooxygenase
CRP	C-reactive protein
CXCL	CXC chemokine ligand
DMARD	Disease-modifying anti-rheumatic drug
DMEM	Dulbecco's Modified Eagle's Medium
DMMB	Dimethylmethylene blue
DNase	deoxyribonuclease
dNTP	Deoxyribonucleotide triphosphate
ECM	Extracellular Matrix
EDTA	Ethylenediaminetetraacetic acid
EGF	Epidermal growth factor
ELISA	Enzyme-linked immunosorbent assay
EMMPRIN	Extracellular matrix metalloproteinase inducer
eNAMPT	Extracellular Nicotinamide phosphoribosyltransferase
ERK	Extracellular signal-regulated kinase
ESR	Erythrocyte sedimentation rate
FBS	Fetal bovine serum
GAG	Glycosaminoglycan
GM-CSF	Granulocyte macrophage-colony-stimulating factor
HDAC	Histone deacetylase
HRP	Horseradish peroxidase
HUVEC	Human umbilical vein endothelial cells
IDO	Indoleamine 2, 3-dioxygenase
IFN	Interferon
Ig	Immunoglobulin

IGF	Insulin-like growth factor
IL	Interleukin
iNAMPT	Intracellular Nicotinamide phosphoribosyltransferase
JAK	Janus activated kinases
kDa	Kilo Dalton
LDH	Lactate dehydrogenase
LPS	Lipopolysaccharide
MAPK	Mitogen-activated protein kinase
MCP	Metacarpophalangeal
MHC	Major histocompatibility complex
MMP	Matrix metalloproteinase
mRNA	Messenger ribonucleic acid
MTP	Metatarsophalangeal
MTX	Methotrexate
MT-MMP	Membrane-type matrix metalloproteinase
NA	Nicotinic acid
NAD	Nicotinamide adenine dinucleotide
Nam	Nicotinamide
NAMPT	Nicotinamide phosphoribosyltransferase
NaMN	Nicotinic acid mononucleotide
NAPRT	Nicotinic Acid phosphoribosyltransferase
NF-κB	Nuclear factor kappa B
NIRF	Near-infrared fluorescence
NK	Natural killer
NMN	Nicotinamide mononucleotide
NMNAT	Nicotinamide mononucleotide adenylyltransferase
NO	Nitric oxide
NR	Nicotinamide riboside
OA	Osteoarthritis
OD	Optical density
OSM	Oncostatin M
PARP	Poly (ADP ribose) polymerase
PBEF	Pre B-cell colony-enhancing factor
PBS	Phosphate buffered saline
PCR	Polymerase chain reaction
PI3K	Phosphotidylinositol-3-kinase
PIP	Proximal interphalangeal
PG	Proteoglycan

PGE_2	Prostaglandin E_2
PRPP	Phosphoribosyl pyrophosphate
QPRT	Quinolinic acid phosphoribosyltransferase
RA	Rheumatoid arthritis
RASF	Rheumatoid arthritis synovial fibroblasts
RF	Rheumatoid factor
rfu	Relative fluorescent units
rh	Recombinant human
RNA	Ribonucleic acid
ROI	Region of interest
RQ	Relative quantity of gene expression
SCF	Stem Cell Factor
SDS-PAGE	Sodium dodecyl sulphate polyacrylamide gel electrophoresis
SIRT	Silent mating type information regulation 2 homolog
SNP	Single-nucleotide polymorphisms
STAT	Signal transducer and activator of transcription
TIMP	Tissue inhibitor of metalloproteinases
TGF	Transforming growth factor
TLR	Toll-like receptor
TMB	3,3',5,5'-tetramethylbenzidine
TNF	Tumour necrosis factor
VEGF	Vascular endothelial growth factor
qPCR	Quantitative polymerase chain reaction

Contents

Chapter 1: Introduction

Rheumatoid arthritis (RA) is a chronic, systemic inflammatory disease characterised by the activation and proliferation of synovial tissue, which is associated with progressive destruction of synovial joint articular cartilage and bone. Current therapies are focused on targeting factors that contribute to the inflammatory milieu, such as tumour necrosis factor alpha (TNFα). However, these biologic therapies are not curative, and so new therapeutic targets are continually sought. One such target, **NAMPT** (nicotinamide phosphoribosyltransferase), is a pleiotropic protein that was first characterised in 1994 (Samal et al., 1994) and shown to be upregulated in RA patients (Otero et al., 2006, Nowell et al., 2006). Originally named pre B-cell colony enhancing factor (PBEF), it is also found in the literature under a number of alternative names, including NaPRTase and visfatin. **The focus of the thesis is the role of NAMPT on articular cartilage catabolism in inflammatory arthritis.** In this introductory chapter I describe the structure of the synovial joint in health and disease (i.e. rheumatoid arthritis), with a particular focus on articular cartilage and control of its turnover by matrix metalloproteinases (MMPs; section 1.2.4). I then discuss what is currently known about the structure and function of NAMPT, and its soluble inhibitor, APO866, and the potential of NAMPT inhibition as a therapy in the treatment of RA (section 1.4.5). Finally, I delineate the objectives of this study and the specific aims of each experimental chapter (section 1.5).

1.1 The normal synovial joint

Dysregulation of NAMPT has been associated with numerous pathological disorders, including sepsis (Jia et al., 2004), atherosclerosis (Chung et al., 2009) and acute lung injury (Ye et al., 2005). This thesis will focus on the role of NAMPT in inflammatory joint disease pathogenesis, specifically the processes that contribute to destruction of articular cartilage within the synovial joint. Before describing these processes in depth, the tissues and cells that comprise a normal, healthy joint are identified.

1.1.1 Tissues of the normal joint

A synovial, or diarthrodial joint, consists of highly specialised tissues of bone, articular cartilage, synovial tissue, adipose tissue (the infrapatellar fat pad), ligaments, menisci and tendons. They are enclosed within a fibrous tissue capsule and bathed in synovial fluid. Synovial joints achieve movement at the point of contact between two opposing articulating bony surfaces that are lined with a smooth, durable layer of articular

cartilage. This articular cartilage, together with the menisci, absorbs shock and reduces friction during movement (figure 1.1).

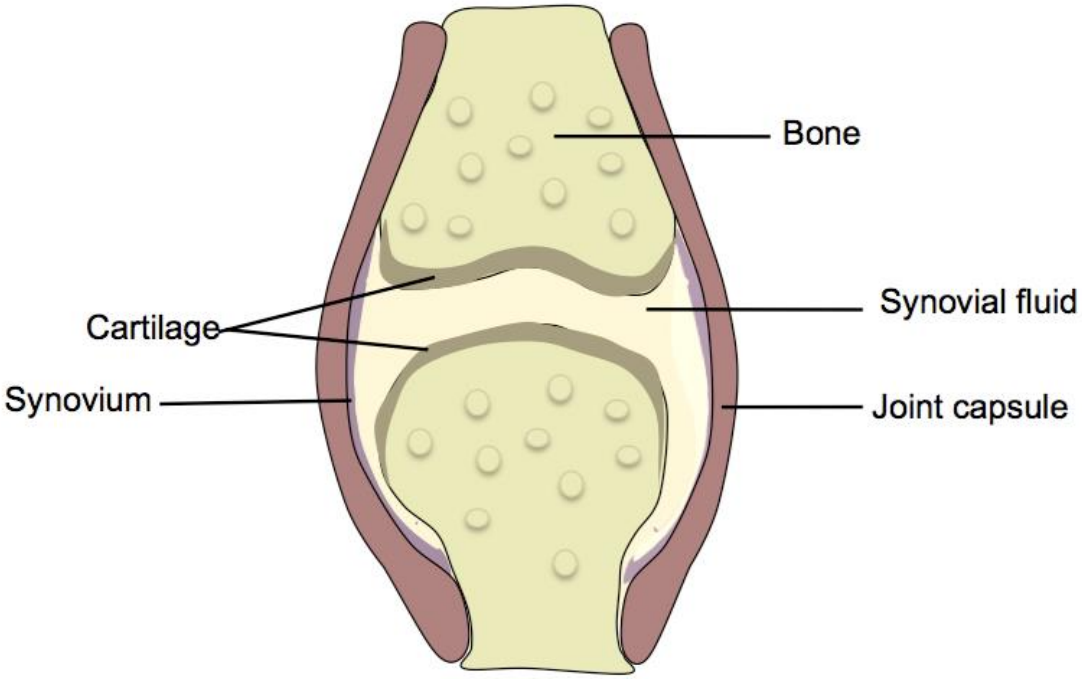

Figure 1.1 the diarthrodial joint

A schematic drawing of the structure of a healthy joint. The intimal layer of the synovium (shown in purple) is only 1-2 cells thick and remains separate from the cartilage and bone. The synovial fluid is clear of infiltrating cells, and cartilage provides a smooth articulating surface for the ends of the adjacent bones. Figure drawn from (Feldmann et al., 1996a).

1.1.1.1 Synovial membrane

The synovial membrane, also referred to as the synovium, lines the joint cavity. This membrane, normally 1-2 cells thick, produces synovial fluid, which lubricates the joint and provides nutrients for adjacent cartilage. The synovium contains a sub-intimal layer of fibrous or fatty tissue, and a thin intimal layer. The intimal layer is comprised of two cell types: fibroblasts and macrophages (MΦ). The synovium is highly vascular, with a dense network of small blood vessels beneath the intimal layer that provide nutrients for the synovium and adjacent cartilage (reviewed by Firestein et al., 2009).

1.1.1.2 Articular cartilage

The articulating joint surfaces are covered by hyaline-type cartilage. Articular cartilage is avascular with no lymphatic or nerve supply and contains only a single cell

type, the chondrocyte. Mature articular cartilage has a high matrix volume to cell ratio and is constantly being remodelled through the continuous synthesis and degradation of various extracellular matrix (ECM) components. The resident chondrocytes are pivotal regulators of these processes. Chondrocyte viability is therefore essential for adequate maintenance of the cartilage (Rowan, 2001).

Mature articular cartilage is both structurally and functionally heterogeneous. It consists of four distinct zones: i) superficial/tangential, ii) middle/transitional/intermediate, iii) deep/radial and iv) calcified cartilage. A tidemark separates the upper non-calcified tissue from the lower calcified cartilage. Beneath the calcified cartilage lies the subchondral bone plate. Each of the cartilage zones differs with respect to cell morphology and organisation, collagen fibre organisation and the biochemical composition of its ECM (figure 1.2; reviewed by Poole et al., 2001). Approximately 70-80% of articular cartilage consists of water (Rowan, 2001). The remainder of the tissue consists primarily of an insoluble fibrous protein called collagen and a highly glycosylated aggregating proteoglycan (PG), known as aggrecan. Collagen comprises two thirds of the dry weight of articular cartilage, and each of the distinct cartilage zones differs considerably in its collagen content and fibril organisation (Eyre et al., 2006). Type II collagen is the predominant collagen throughout articular cartilage, although collagen types I, III, VI, IX, XI, XII and XIV are also present in smaller amounts (Eyre, 2002, Eyre et al., 2006). Type II collagen consists of three polypeptide a1(II) chains arranged into a triple helix. These molecules pack together side-by-side forming banded fibrils with a periodicity of 67 nm (Revenko et al., 1994). Collagen fibrils in articular cartilage are heterofibrils that contain, in addition to the dominant collagen II, also types XI and IX collagens (Gelse et al., 2003) Collagen fibrils give cartilage its tensile strength and entrap many soluble molecules such as PGs, retaining them within the ECM (Otero and Goldring, 2007).

PGs are a family of glycosylated proteins that occur within the ECM, filling in the gaps of the collagen network, and occurring on cell surfaces. They are made up of a protein core with covalently linked, negatively charged, sulphated-glycosaminoglycans (s-GAGs). These are linear polysaccharide chains consisting of repeating disaccharide units (an amino sugar, N-acetylglucosamine or N-acetylgalactosamine, and an uronic acid sugar, glucuronic acid or iduronic acid). They include chondroitin sulphate, dermatan sulphate, keratan sulphate and heparan sulphate. As a family, the PGs vary considerably in terms of the size of their core proteins and the number and type of attached GAG chains. Although aggrecan is the principal PG of articular cartilage, the cartilage ECM comprises a number of other PGs, including decorin, biglycan, fibromodulin, perlecan, glypican and syndecan (reviewed by Knudson and Knudson, 2001).

Aggrecan is a large aggregating PG with a core protein consisting of three globular domains (G1, G2 & G3). The interglobular domain between G2 and G3 carries distinct chondroitin- and keratan sulphate-rich regions that give the molecule its distinctive 'bottlebrush' ultrastructural appearance (Watanabe et al., 1998). Aggrecan monomers are attached to hyaluronic acid, another unsulphated GAG, at the G1 domain by special link proteins, generating supramolecular aggregates that are confined by the collagen network. The high negative charge of the s-GAG within these aggregates attracts water, providing articular cartilage its viscoelastic properties and the ability to resist compressive impact loads (reviewed by Poole et al., 2001).

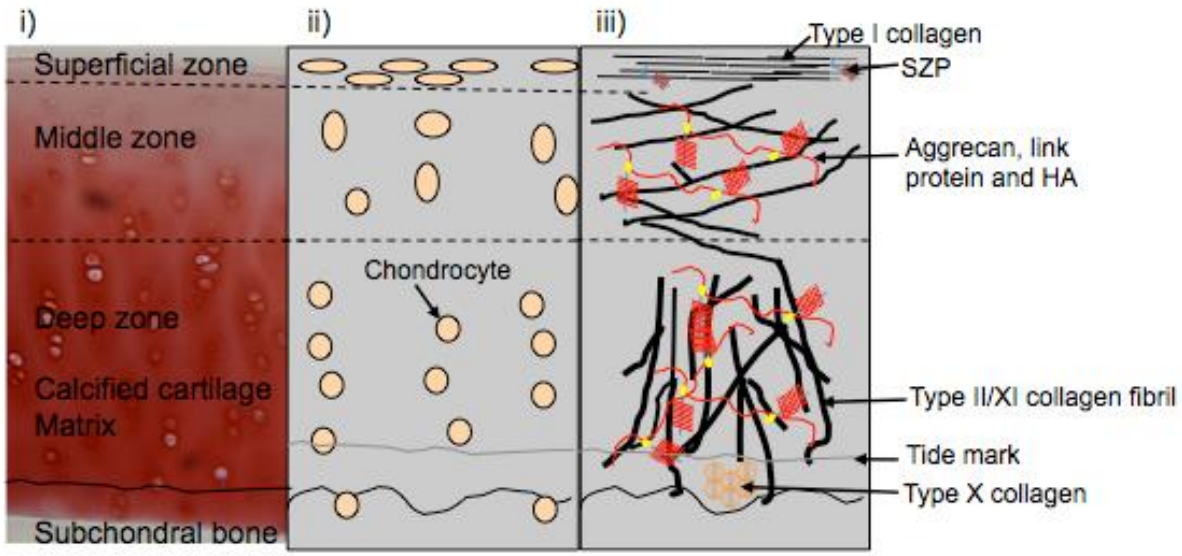

Figure 1.2 Zonal organisation of mature articular cartilage

A diagrammatic representation of the general structure of human articular cartilage, showing i) typical histology, ii) cellular morphology and organisation and iii) ECM composition and organisation. SZP, superficial zone protein; HA, hyaluronan. Compiled from (Poole et al., 2001).

1.1.1.3 Bone

Bone is a hard, dense connective tissue that is comprised of approximately 70% hydroxyapatite, an inorganic mineral compound. It also consists of 22% organic material, mainly type I collagen, and 8% water. Bone maintenance depends on the balance between bone formation by mesenchymal-derived osteoblasts, and bone resorption by haematopoietic osteoclasts. This process is known as remodelling or bone turnover, and is essential for development and growth, regulation of calcium homeostasis and to repair

micro-damage caused by everyday stress. Sub-chondral bone is also highly vascularised, and provides a conduit for nutrients from circulation for deeper zones of cartilage.

1.1.2 Cells of the normal synovial joint

The joint contains a number of different cell types of both mesenchymal and haematopoietic lineage. Many of the cells that make up the synovial joint are derived from precursor cells from the joint interzone, a thin mesenchymal cell layer believed to be critical for joint and articular cartilage development (Pacifici et al., 2006). Cells of mesenchymal origin include the articular chondrocytes, fibroblast-like synoviocytes, osteoblasts and osteocytes that are present within bone, adipocytes of the infra-patellar fat pad, and fibrochondrocytes of the meniscus. Outside the joint capsule, myocytes, tenocytes, and ligamentous cells occur within the supporting tissues of the joint. Cells of haematopoietic lineage include the macrophage-like osteoclasts and synoviocytes that populate bone and synovium respectively (Bartok and Firestein, 2010). This overview will focus on the cell types primarily involved in the degradative processes in RA (i.e. synovial cells and articular chondrocytes). Their specific involvement in the disease process, and the co-involvement of other invading cell types, is discussed further in section 1.2.2.

Fibroblast-like synoviocytes are non-vascular, non-epithelial cells that reside locally within both the intimal and sub-intimal layers of the synovium. They provide the joint cavity and the adjacent cartilage with nutritive plasma proteins and lubricating molecules such as hyaluronan, a long-chain sugar polymer that retains synovial fluid within the joint space (Edwards, 2000), and lubricin (superficial zone protein; SZP), which protects cartilage surfaces and inhibits synovial cell overgrowth (Rhee et al., 2005). Along with fibroblast-like synoviocytes, macrophage-like synoviocytes (MΦ) also comprise much of the intimal layer of the synovium. In normal tissue homeostasis, synovial MΦ are derived from CD34+ stem cells in the bone marrow, which differentiate into monocytes and circulate the peripheral blood. Upon entering specific tissues these monocytes differentiate further into different types of resident MΦ, including synovial MΦ. These mature cells remain localised within the synovial tissue until they senesce and die (Firestein et al., 2009). The monocyte/MΦ system is an integral part of the innate immune system, participating in the first-line response against infectious agents. They are responsible for removal of undesirable substances from the synovial fluid and contribute to the body's homeostasis by scavenging debris generated by physiological or pathological processes (Kinne et al., 2007).

Chondrocytes are the sole cell constituent of articular cartilage and are located within discrete lacunae within the cartilage ECM. Their size and morphology varies with

articular cartilage depth, ranging from small and discoidal at the articular surface to large and ovoid (i.e. hypertrophic) within the deep and calcified zones (see figure 1.2). The chondrocytes are responsible for the synthesis and turnover of the cartilage ECM. In each zone of the tissue, the chondrocytes synthesise and secrete unique matrix components (e.g. SZP in the surface zone and type X collagen in the calcified zone). Chondrocytes maintain a stable equilibrium between matrix synthesis and degradation in response to anti- and pro- inflammatory mediators. Anti-inflammatory mediators include transforming growth factor beta (TGFβ), whilst pro-inflammatory mediators include TNFα and interleukin (IL)-1 (Rowan, 2001). The latter are induced in response to mechanical stress, trauma or microbial insult (McInnes and Schett, 2007). If homeostasis is disrupted, then diseases of the tissue may occur.

1.2 Rheumatoid arthritis (RA)

Inflammatory arthritis is a term used to describe a number of conditions, including rheumatoid arthritis, ankylosing spondylitis, psoriatic arthritis and juvenile idiopathic arthritis. Of these, RA is the most common, affecting approximately 1% of the world's population and around 400,000 people within the UK. Onset generally occurs between the ages of 40-60, although it can potentially occur at any age. RA is most common in women, with 3-5 times more female sufferers compared to males (Walker, 2011). RA is a systemic, polyarticular autoimmune disease that causes chronic inflammation of the joints, leading to the progressive destruction of joint cartilage and bone. The condition was first described by Augustin Jacob Landré-Beauvais in 1800 (Landré-Beauvais, 2001), and the name rheumatoid arthritis was coined by Sir Alfred Garrod in 1859 (Garrod, 1892). In 1987 the American College of Rheumatology devised criteria for the classification of RA, based on symptoms ranging from morning stiffness and presence of rheumatoid factor in blood, to radiographic evidence of erosions and/or periarticular osteopenia (Arnett et al., 1988). However, these criteria were criticised for their lack of sensitivity, as diagnosis was largely based on late-stage features of disease. Therefore, in 2010, these criteria were superseded by a new classification system, which places more emphasis on serum markers and acute-phase reactants of disease (Aletaha et al., 2010); see Table 1.1). The aetiology of the disease is largely unknown; however, it is thought to be multi-factorial, with genetic and environmental factors playing a role.

Table 1.1 Classification criteria for Rheumatoid Arthritis

Criteria		Score
A. Joint involvement	1 large joint	0
	2-10 large joints	1
	1-3 small joints (with or without involvement of large joints)	2
	4-10 small joints (with or without involvement of large joints)	3
	>10 joints (at least 1 small joint)	5
B. Serology	Negative RF and negative ACPA	0
	Low-positive RF or low-positive ACPA	2
	High-positive RF or high-positive ACPA	3
C. Acute phase reactants	Normal CRP and normal ESR	0
	Abnormal CRP or abnormal ESR	1
D. Duration of symptoms	<6 weeks	0
	≥6 weeks	1

Classification criteria for the diagnosis of RA, as defined by the American College of Rheumatology (ACR) in 2010. A total score of 6 or more out of the listed criteria suggests a positive diagnosis of RA. RF, Rheumatoid factor; ACPA, anti-citrullinated protein antibody; CRP, C-reactive protein; ESR, erythrocyte sedimentation rate. Adapted from (Aletaha et al., 2010) .

1.2.1 Pathogenesis of RA

In RA the synovial intimal lining, normally only a thin layer of 1-2 cells, becomes thickened due to proliferation of macrophage-like and fibroblast-like synoviocytes. There is also a large degree of infiltration by inflammatory lymphocytes, macrophages and mast cells. A large number of neutrophils produced in the synovium rapidly transmigrate into the synovial fluid, which is produced in large quantities. All of these features contribute to significant joint swelling. Enhanced production of cytokines, along with autoantibodies such as rheumatoid factor (RF) and anti-citrullinated protein antibody (ACPA), maintain persistent chronic inflammation in RA tissue. Continuous inflammation of the synovium results in the growth of a large cellular mass called a pannus, derived from the Latin word meaning ‘cloth’, and the Greek word meaning ‘web’. This pannus covers and invades the articular cartilage and subchondral bone, causing erosions to occur through the secretion of catabolic mediators. This pannus formation is often described as a malignant mesenchymal transformation due to its aggressive and invasive behaviour (Burrage et al., 2006).

Secretion of these catabolic mediators from the proliferating pannus leads to a progressive loss of matrix proteins within the articular cartilage. The large PG aggrecan is amongst the first components of the cartilage ECM to be degraded. Cleavage of aggrecan monomers by aggrecanases known as A disintegrin and metalloproteinases with thrombospondin motifs (ADAMTSs) results in the loss of its GAG binding domains (Fosang et al., 2008); section 1.2.4.2). These PGs lose their GAG chains, which are essential for water retention within the cartilage ECM. As a result, they lose their ability to retain water, leading to a progressive weakening of the collagen fibre network. Loss of PG mainly occurs within the superficial zone of cartilage, although there is evidence of PG loss throughout the cartilage matrix, progressing from the surface to the deep zones. This is eventually accompanied by the enzymatic and biomechanical destruction of collagen. In contrast to PGs, which can be readily replaced once the catabolic stimulus is removed, collagen is more difficult to replace (Karsdal et al., 2008; Cawston and Young, 2010). All this results in a loss of tensile strength and increased friction of joints, leading to pain and decreased mobility in RA patients. The cells important in these processes are summarised in figure 1.3, and in the following sections.

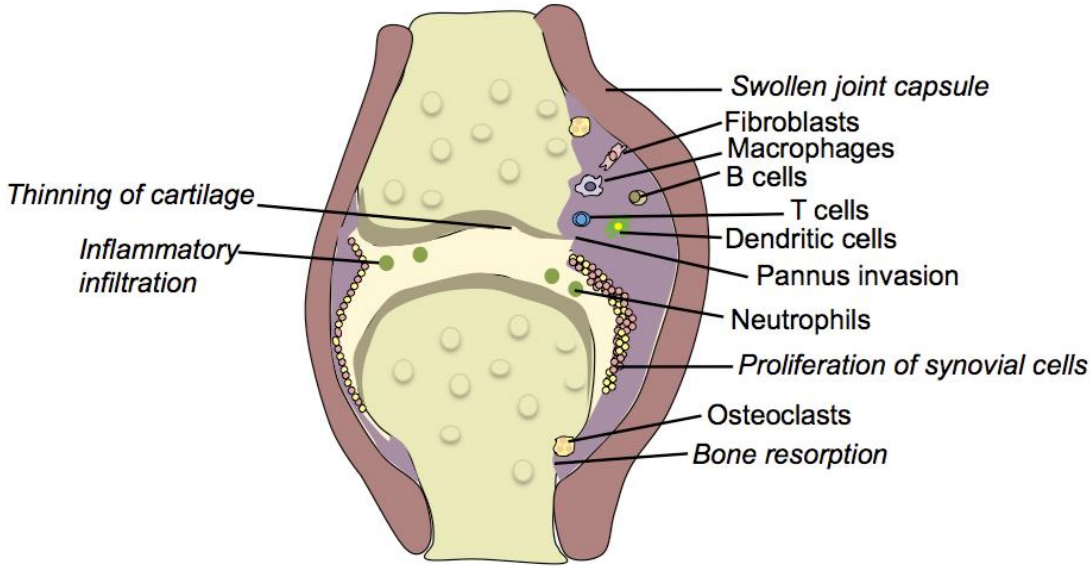

Figure 1.3 Processes and cells involved in joint destruction in RA

A diarthrodial joint, showing the appearance of a normal joint (left), compared with an inflamed diseased joint (right), Italicised writing indicates the processes involved in disease pathogenesis, whilst main cells associated with disease are also shown. Figure drawn from (Feldmann et al., 1996a).

1.2.2 Cells that propagate RA pathogenesis

Fibroblast-like synoviocytes (FLS) play a major role in RA disease pathogenesis. In RA, fibroblast cells become hyperproductive and phenotypically distinct from normal fibroblasts, leading to chronic persistent inflammation (Buckley et al., 2001). At a morphological level, these cells are more rounded, with large pale nuclei and prominent nucleoli compared to non-activated cells (Pap et al., 2000). Fassbender first described this altered phenotype in 1983 (Fassbender, 1983). FLS have an aggressive phenotype, and are capable of attaching to the articular cartilage surface and invading the ECM (Pap et al., 2000). These cells are more commonly referred to in the literature as rheumatoid arthritis synovial fibroblasts (RASFs), therefore the term RASFs will be used for the duration of the thesis. RASFs can be activated through stimulation by a number of soluble molecules, including cytokines, chemokines, growth factors, and bacterial products. The latter stimulate RASFs via highly conserved innate immune receptor

systems such as Toll-receptors (TLRs). RASFs can also be activated through cell-cell interactions with CD4+ T cells and MΦ. These stimuli cause activation of signalling pathways, leading to the induction of pro-inflammatory molecules via transcription factors such as NF-κB and AP-1. RASFs also produce vascular endothelial growth factor (VEGF), which promotes vascularisation of the synovium, and chemo-attractant proteins such as CXC chemokine ligand (CXCL) 8 and chemokine (C-C motif) ligand (CCL) 2, which increase accumulation of inflammatory cells into the synovium. Finally, RASF can also produce factors such as CXCL16, which induce CD4+ T cells. Thus, a exacerbatory cycle is established, contributing further to the inflammatory milieu (see (Müller-Ladner et al., 2007) and references therein).

Activated synovial macrophages (MΦ) also contribute greatly to the inflammatory environment. In RA there is increased plasticity in this differentiation process. Within the tissue, pro-inflammatory cytokines and growth factors may direct the differentiation of precursor monocytic cells, causing increased numbers of activated synovial MΦ, and also differentiation into dendritic cells (DCs), which are the major antigen-presenting and antigen-priming cells of the immune system. Activated MΦ have a clear activation status; they produce increased levels of cytokines, growth factors and chemokines, in addition to major histocompatibility complex (MHC) II proteins, C-reactive protein (CRP) and also MMPs -2 and -9 (Kinne et al., 2007). In response to inflammatory stimuli, synovial MΦ can produce yet more effector molecules to activate other MΦ in an autocrine fashion. This process is initiated through stimulation of TLRs by bacterial/viral components. They also engage in various cell-cell interactions, mainly with T cells, RASFs, endothelial cells and natural killer (NK) cells. These interactions cause activation of neighbouring cells, thus further perpetuating numbers of inflammatory cells present within the joint (Kinne et al., 2007).

In RA, proliferation of the synovium by RASFs and MΦ may eventually lead to pannus invasion of the neighbouring cartilage. Here, cells of the synovial pannus may produce excessive amounts of cartilage-degrading enzymes, causing dysregulation of cartilage homeostasis. This leads to substantial loss of PG within the superficial zone of cartilage, mainly at sites where the pannus has invaded the cartilage ECM. However, even in early stages of RA, PG loss can occur throughout the cartilage, indicating that chondrocytes themselves participate in degrading their own matrix (Otero and Goldring, 2007). This gives rise to what is called ‘inside-out’ degradation by resident chondrocytes, which coincides with the ‘outside-in’ enzymatic degradation caused by synoviocytes, thus creating a bidirectional attack (McInnes and Schett, 2007). This is supported by studies that have shown that cartilage destruction can occur uncoupled to joint inflammation (van den Berg, 1998). Furthermore, cytokines induce chondrocytes to produce nitric oxide (NO), which induces apoptosis and therefore loss of cell viability,

which may hinder the resynthesis of degraded matrix components (Otero and Goldring, 2007). All this contributes to gradual loss of the cartilage ECM within the RA joint.

Although activated synoviocytes play a requisite role in synovial joint inflammation, T cells also play a major role in RA disease pathogenesis. T cell aggregates are observed in the synovial sub lining layer of 50-60% of RA patients (Tak and Bresnihan, 2000). T cells can activate RASFs and MΦ through receptor-ligand interactions, triggering transcription factors such as NF-κB and AP-1, which in turn lead to upregulation and release of cytokines, growth factors and chemokines (Raza et al., 2005). Dendritic cells located near the intimal lining layer also play a pro-inflammatory and antigen-presenting role (Lutzky et al., 2007). B cells are also often observed in close contact with the inflamed synovial membrane, and can actively participate in the autoimmune process through interaction with T cells (Mauri and Ehrenstein, 2007). NK cells are also present within both the synovial lining layer and in the sub-synovial lining (Tak and Bresnihan, 2000). Mast cell subpopulations have been found to expand in RA synovial tissue, and may possibly be the main source of the disease-associated cytokine IL-17 within the RA synovium (Hueber et al., 2010). Finally, although not localised within the synovium, excessive numbers of neutrophils may be present within the synovial fluid. Collectively, these various cell types contribute to pro-inflammatory and pro-degradative processes (reviewed by Firestein et al., 2009).

1.2.3 Cytokines that regulate destructive processes in RA

Cytokines are low molecular weight proteins that act locally as intercellular mediators, with important roles in major biological processes. Cell surface receptor binding is the primary means by which cytokines mediate their effects upon cells. This ligand-induced activation is very efficient, meaning small quantities of cytokines can have extensive effects. During acute inflammation, cytokines play an immunomodulatory role, and are essential for resolving inflammation. However, in RA disturbance of the immune system leads to the persistence of cytokines within the sterile joint environment, promoting autoimmunity and driving chronic inflammation and tissue destruction (reviewed by Feghali and Wright, 1997). In the context of RA, cytokines are traditionally sub divided into those with pro-*inflammatory* effects and those with anti-*inflammatory* effects (Feldmann et al., 1996b); however, the situation is clearly more complex, as different cytokines can exert different effects depending upon their local microenvironment. Cytokines are implicated in each phase of disease pathogenesis in inflammatory joint diseases, from the promotion of autoimmunity in the pre articular phase (Raza et al., 2005), to the maintenance of chronic synovial inflammation, and eventually the destruction of the adjacent joint (McInnes and Schett, 2007). These processes are summarised in figure 1.4.

Numerous studies *in vitro* and *in vivo* suggest that the major cytokines involved in these processes are interleukin 1 beta (IL-1β) and TNFα, produced mainly by fibroblast- and macrophage-like synoviocytes (McInnes and Schett, 2007). In a systemic murine arthritis model, anti-TNFα treatment showed great efficacy shortly after disease onset, but had little effect in established disease. Anti-IL-1β ameliorated both early and full-blown disease (Joosten et al., 1996). This review will therefore explore these cytokines in depth, although other cytokines that are relevant to the RA disease process will also be discussed.

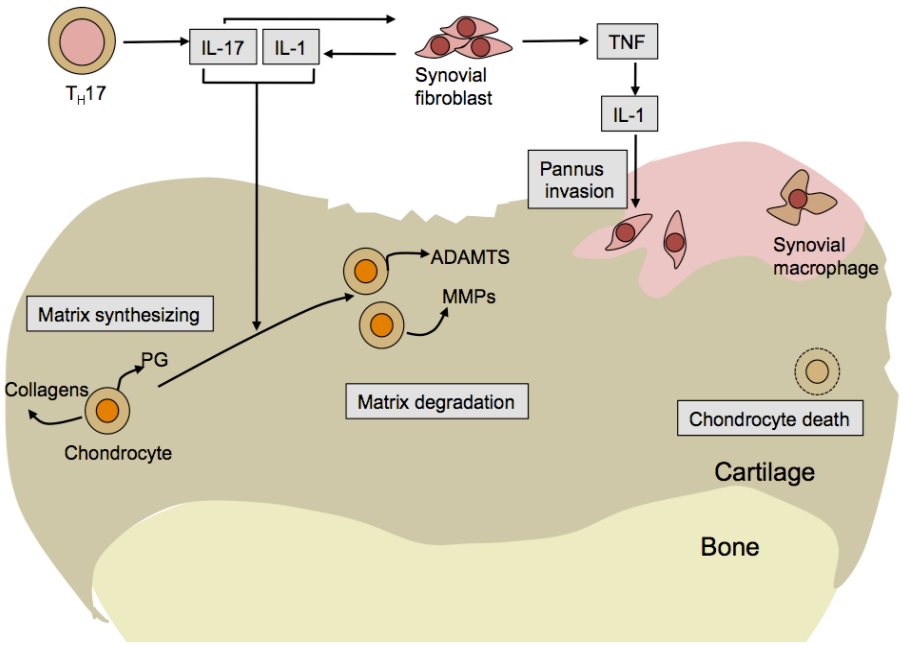

Figure 1.4 Cytokine interactions involved in cartilage destruction in RA Synoviocytes activated by cytokines such as IL-1 and IL-17. The upregulation of pro-inflammatory cytokines produced within the synovium and chondrocytes leads to an upregulation of cartilage-degrading enzymes, leading to matrix degradation. Chondrocyte death is another feature of cartilage damage, preventing replenishment of the degraded ECM. T_H17, T-helper type 17 cells; IL, Interleukin; TNFα, Tumour necrosis factor alpha; PG, proteoglycan; ADAMTS, a disintegrin metalloproteinases with thrombospondin motifs; MMPs, matrix metalloproteinases. Figure adapted from McInnes and Schett (2007).

Members of the IL-1 family of cytokines are pivotal in early and late stages of disease. This superfamily consists of 11 proteins, the most notable being IL-1α, IL-1β and IL-1 receptor antagonist (IL-1ra) (Dunn et al., 2001). The two isoforms IL-1α and IL-1β share low protein homology, but have comparable function and similar binding capacity to receptors. Produced predominantly by synovial MΦ, IL-1 is significantly elevated in the synovial fluid of RA patients compared to osteoarthritis (OA) patients (approximately 100 pg/ml and 30 pg/ml, respectively; (Westacott et al., 1990). It has long been established that IL-1 levels correlate with disease severity in RA patients (Eastgate et al., 1988). IL-1 promotes joint degradation by stimulating the production of MMPs and the inflammatory mediator Prostaglandin E_2 (PGE_2). Furthermore, it also inhibits the synthesis of new matrix proteins in cartilage through upregulation of NO (Järvinen et al., 1995).

Formally known as cachectin, TNFα is the best-known member of the TNF superfamily, a large group of cytokines involved in systemic inflammation. In contrast to IL-1β, TNFα levels are not elevated in the synovial fluid of RA patients compared to OA patients (Westacott et al., 1990). However, patients with early disease do exhibit high TNFα levels within synovial tissue samples, suggesting a role in disease onset (Tak and Bresnihan, 2000). Like IL-1β, TNFα stimulates pro-inflammatory cytokine release and PGE_2 production, and is also involved in chemokine induction and release, attracting leukocytes into the inflamed synovium (Brennan and McInnes, 2008).

The IL-6 family of cytokines are a group of pleiotropic regulators that use glycoprotein (gp)130 as a signal transducer. Members of the IL-6 family include leukemia-inhibitory factor (LIF), Oncostatin M (OSM), IL-11 and ciliary neurotrophic factor (CNTF) (Kishimoto et al., 1995). IL-6 is one of most highly elevated cytokines in RA, especially during acute disease (Houssiau et al., 1988). IL-6 cytokines facilitate the maturation and activation of B and T cells, MΦ, chondrocytes and osteoclasts (Brennan and McInnes, 2008). Along with TGFβ, they promote the differentiation of precursor cells into T_H17 cells, a key cell subset in inflammatory arthritis (McInnes and Schett, 2007).

Also of vital importance in RA pathogenesis is the IL-2 cytokine family, in particular IL-15. Produced by cells lining the synovium, it stimulates T cells to bind to MΦ and induce cytokine production, thus creating a self-perpetuating pro-inflammatory loop (Kinne et al., 2007). IL-17 is produced very early in the disease process by Th17 cells. It performs many functions, enhancing RASF cytokine and MMP release and leukocyte cytokine production, as well as downregulating GAG synthesis by chondrocytes (McInnes and Schett, 2007).

1.2.4 Proteinases involved in joint destruction in RA

Proteinases are essential for the completion of a range of biological processes, including development and apoptosis. Cytokines and growth factors stimulate the production of proteinases involved in normal ECM turnover. These proteolytic enzymes play major roles in the development of tissue lesions in RA, and are essential to pannus formation and invasion. Enzymes can be divided into two main categories: the intracellular proteinases, including aspartic, cysteine and threonine proteinases (refer to (Rengel et al., 2007) and references therein), and the extracellular proteinases, including serine and metalloproteinases (figure 1.5). Of these, the metalloproteinases are the most extensively investigated. These enzymes can be further sub-categorised into MMPs, A disintegrin and metalloproteinases (ADAMs; including those with additional thrombospondin motifs), serralysins, astracins and pappalysins (Rengel et al., 2007). Of these, MMPs and ADAMs, particularly those with additional thrombospondin motifs (see section 1.2.4.2), are considered to be the main enzymes responsible for the degradation of collagens and aggrecan, the large aggregating PG of cartilage (Firestein et al., 2009).

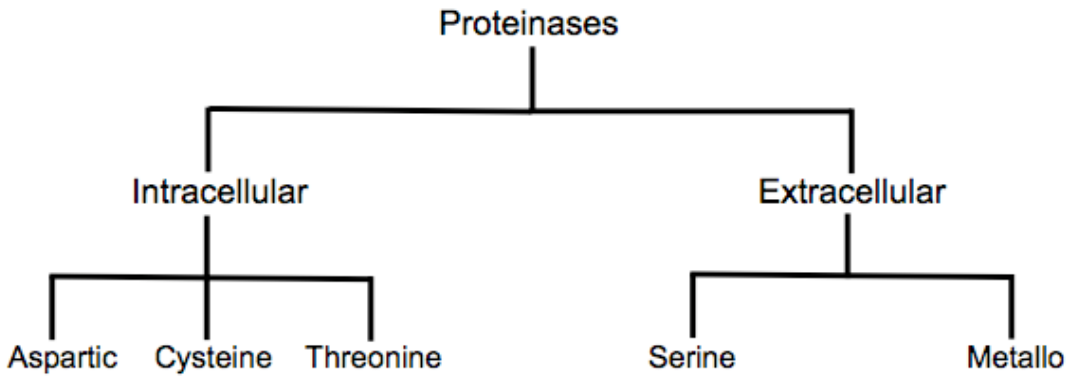

Figure 1.5 Classification of proteinases involved in ECM turnover

Schematic diagram showing the various classes of proteinases involved in ECM turnover. Compiled from (Rengel et al., 2007).

1.2.4.1 Matrix metalloproteinases

The MMPs are a group of zinc-dependent enzymes that collectively degrade all the components of the ECM. These proteins can be membrane bound or secreted extracellularly. The MMP family consists of collagenases, gelatinases, stromelysins and matrilisins, as summarised in Table 1.2. Although diverse in structure and biological

function, they all contain three shared domains; including a propeptide domain, a catalytic domain and hemopexin domain.

In healthy tissue, the proteolytic activities of MMPs are rigorously controlled to avoid inappropriate degradation of proteins. Firstly, MMPs are controlled at the transcriptional level, by the stimulating effects of cytokines and growth factors, which promote signalling cascades that lead to the transcription of MMPs (Nagase and Woessner, 1999). The production of MMPs as inactive proproteins (zymogens) is another important mechanism of regulation. The propeptide domain contains a “cysteine switch”, which keeps the catalytic domain inactive. Most MMPs are secreted from cells as inactive proproteins. Upon proteolytic removal of the cysteine residue, the catalytic domain is activated and MMPs are able to bind to and modify their substrates (Visse and Nagase, 2003). This proteolysis is often localised to pericellular pockets close to the cell membrane, limiting MMP activity to distinct regions (Firestein et al., 2009).

Finally, MMPs are also regulated by natural endogenous inhibitors known as tissue inhibitors of metalloproteinases (TIMPs). Like MMPs, expression of TIMPs is regulated during development and tissue remodelling. Four TIMPs have been identified in vertebrates, though only three are associated with the cartilage ECM (Table 1.2). All TIMPs inhibit all types of MMPs tested, with the exception of TIMP-1, which fails to inhibit MT1-MMP. TIMPs bind to MMPs in a 1:1 stoichiometry in order to exert their inhibitory effects (Visse and Nagase, 2003). In addition, TIMP-3 has been shown to inhibit ADAMs and ADAMTSs. In healthy tissue, a balance is maintained between MMPs and TIMPs, and thus matrix synthesis and degradation. Within the healthy joint, proteinases such as MMPs are involved in the catabolic aspect of normal tissue remodelling (Goldring, 2003). However, in RA an excess of MMP enzymes drives progressive joint damage. High levels of MMPs -1, -3, -8, and -9 are found in the synovial fluid of RA patients (Yoshihara et al., 2000, Tchetverikov et al., 2004). In particular, levels of MMPs -1 and -3 in the sera of RA patients correlate with disease activity (Green et al., 2003).

Table 1.2 MMPs and TIMPs in ECM degradation

	Name	ECM Substrates/target	Cell source/localisation	Inducers
	MMP-1 Interstitial collagenase-1	Collagens I-III, VII, X; gelatins; aggrecan; link protein; entactin; tenascin; perlecan	Fibroblasts; synovial cells; chondrocytes; MΦ, endothelial cells	Cytokines and growth factors (IL-1β, TNFα, VEGF); Chemical agents (LPS, EMMPRIN); Physical factors (heat shock, Ultra-violet rays
	MMP-8 collagenase-2	Collagens I-III; gelatins; aggrecan; link protein	Neutrophils, chondrocytes	TNFα; TPA; IL-1β
	MMP-13 collagenase-3	Collagens I-IV, IX, X, XIV; aggrecan; Fn; tenascin	Chondrocytes; MΦ; fibroblasts,	bFGF; TNFα; TGFβ
Gelatinases	MMP-2 gelatinase A	Gelatins; collagens IV, V, VII, XI; laminin; fibronectin; elastin; aggrecan; link protein	Fibroblasts; chondrocytes; mesangial cells; MΦ, endothelial cells	TGFβ; concanavalin A; EMMPRIN
	MMP-9 gelatinase B	Gelatins; collagens III, IV, V; aggrecan; elastin; entactin; link protein	Neutrophils; MΦ; chondrocytes; osteoclasts; trophoblasts; T lymphocytes	IL-1β; TNFα; EGF; TGFβ; TPA
Stromelysins	MMP-3 stromelysin-1	Aggrecan; decorin; gelatins; fibronectin; laminin; collagens III, IV, IX, X	Synovial cells; chondrocytes; fibroblasts	IL-1β; TNFα; EGF; LPS; concanavalin A; EMMPRIN
	MMP-10 stromelysin-2	Aggrecan; fibronectin; laminin; collagens III, IV, V; link protein	T lymphocytes	TPA; A23187; TGFβ; EGF
Matrilysins	MMP-7 matrilysin 1	Aggrecans; gelatins; fibronectin; laminin; elastin; entactin; collagen IV; tenascin; link protein	Chondrocytes; MΦ, mesangial cells; gland cells	IL-1β; TNFα; EGF; TPA; LPS
Membrane-type MMPs	MMP-14 MT1-MMP	Collagens I-III; gelatins; aggrecan; fibronectin; laminin; fibrin;	Chondrocytes; fibroblasts; synovial cells	Concanavalin A; TPA; bFGF; TNFα; IL-1α
Metalloprot-einase inhibitors	TIMP-1 TIMP-2 TIMP-3	MMPs (except MT-MMPs) MMPs MMPs; ADAMs; ADAMTSs	Connective tissue cells; Fibroblasts; MΦ Connective tissue cells; MΦ Fibroblasts; synovial cells	IL-1; IL-6; IL-11; TPA; TGFβ; TNFα; retinoic acid; LPS Progesterone, TGFβ, IGF-1, OSM

Classes of MMPs and MMP inhibitors associated with ECM degradation. MMPs highly expressed in RA are indicated in bold. bFGF, basic fibroblast growth factor; EGF, epidermal growth factor; TGF, transforming growth factor; EMMPRIN, extracellular matrix metalloproteinase inducer; TPA, 12-*O*-tetradecanoylphorbol-13-acetate (compiled from Firestein et al., 2009).

1.2.4.2 ADAMs

ADAMs are similar to MMPs, but also contain a unique disintegrin domain (Firestein et al., 2009). In particular, the ADAMTSs, which contain additional thrombospondin motifs, are significantly upregulated in RA. Pathologically relevant, ADAMTS-5 is expressed in the RA synovium. ADAMTS5 mainly degrades aggrecan, which along with type II collagen is a principle component of cartilage. (Vankemmelbeke et al., 2001). In contrast, ADAMTS4 can also cleave a number of other PGs including fibromodulin and decorin (Verma and Dalal, 2011).

1.2.5 Rheumatoid arthritis therapeutics

Inflammatory conditions like RA are a huge socioeconomic burden on society. As a consequence of the pain and disability caused by RA, the overall cost to the UK economy due to productivity losses is almost £8 billion annually, and NHS expenditure totals nearly £700 million per year (National Rheumatoid Arthritis Society, 2010). RA can be a devastating condition with a major impact on sufferers and their families. However, modern treatments have vastly improved disease prognosis. The costs of disease can be lowered with earlier intervention, which may slow the progression of disease and reduce the extent of joint damage. In newly diagnosed patients, a combination of drugs are administered as soon as possible; ideally within three months of onset of persistent symptoms. There are currently four distinct types of anti-rheumatic therapies available: NSAIDs, glucocorticoids, DMARDs and biologics.

Nonsteroidal anti-inflammatory drugs (NSAIDs) such as aspirin have also been used extensively as anti-inflammatory, antipyretic and analgesic agents. These drugs work by blocking the synthesis of prostaglandins, through inhibition of the enzymes involved in prostaglandin biosynthesis, Cyclooxygenase (COX)-1 and -2. Although widely used and highly beneficial, some patients can be at risk of developing gastrointestinal ulcerations. This is because whilst COX-2 expression is increased during inflammation, COX-1 is a constitutively expressed isoform essential for tissues not directly involved in inflammation, such as the gastroduodenal mucosa (Firestein et al., 2009).

Glucocorticoids such as the corticosteroid hormone cortisone have been in use since the 1950s. They work by acting on the glucocorticoid receptor, regulating the transcription of a variety of target genes, such as certain classes of cytokines. These treatments are considered some of the most effective anti-inflammatory and immunosuppressive substances around. However, they are associated with a wide array of potentially serious side effects, such as growth retardation and osteoporosis and so careful administration and monitoring is essential (Firestein et al., 2009).

Although the above therapies are effective, first line of treatment is usually a combination of disease-modifying anti-rheumatic drugs (DMARDs) (NICE, 2009). Of these, methotrexate (MTX) is one of the most frequently used since its introduction over 50 years ago. DMARDs not only decrease pain and inflammation, they also reduce or prevent joint damage. MTX is typically administered alone or in combination with other DMARDs such as sulfasalazine and hydroxychloroquine (Choy et al., 2005).

More recently, increased knowledge of the critical effector pathways in disease has led to the development of biologic DMARDs. The most widely-used biologic is infliximab, a chimeric antibody specific for human TNFα. Many patients with RA respond well to anti-TNFα treatment, with substantially reduced signs and symptoms of disease. Since the development of Infliximab, attention has turned to the utility of other pro-inflammatory cytokines as therapeutic targets. Some of these are summarised in Table 1.3. Many of these biologics fall within two categories: antibodies or antagonistic proteins. Pharmaceutical companies continually develop new compounds, and screen them for promising activity against a particular biological target that may be important in disease. Despite early success with these biologic therapies, further challenges remain. Blockade of TNFα is not curative, and not every patient is responsive to treatment. A recent meta-analysis showed that even the most efficacious biologic, certolizumab, only yielded a 20% improvement in ACR score (see Table 1.1) in 60% of patients (Mandema et al., 2011). It is thought patients with higher TNF levels in synovium prior to treatment generally respond better to anti-TNF therapies (Wijbrandts et al., 2008). Treatment safety is another concern, as the targeted cytokines also have essential roles in immunomodulation. For example, TNFα regulates host defences against mycobacterial infection (Bellofiore et al., 2009); therefore patients may be susceptible to new onset tuberculosis, or even reactivation of latent tuberculosis, as well as infection from other opportunistic pathogens (Rubbert-Roth, 2012).

For the reasons stated above, new pharmacological targets are continually being sought. In addition to therapies that target cytokines, a range of other possible targets have been explored, ranging from broad-spectrum B cell inhibitors, to specific inhibitors of proteolytic enzymes such as MMPs (Table 1.3). Despite early promise, MMP inhibitors have not been very successful, due to lack of efficacy and adverse side effects due to the inappropriate inhibition of MMPs not involved in disease processes. Clinical evaluation of these drugs is difficult and expensive, and large-scale trials have been terminated at great cost (Close, 2001).

Recently attention has returned to small molecule drugs as possible therapeutics for RA. Small molecule inhibitors are relatively cheap and easy to manufacture. These drugs can also be administered orally, compared to many biologics that need to be administered by injection or infusion (Sheridan, 2008). There is a vast array of potential inhibitors in the pipeline, including tyrosine kinase inhibitor CP-690550 (Tofacitinib citrate) and the extracellular signal-regulated kinase (ERK) inhibitor ARRY-162 (Waldburger and Firestein, 2009). If successful, small molecules could be used alone or in conjunction with the current mainstays of RA treatment.

Table 1.3 Targeted biologics for treatment of RA

Type		Agent(s)	Advantages	Disadvantages	Stage of development
Anti-cytokine antibodies	TNFα	Infliximab; Adalimumab	Validated clinical target; 70% efficacy	Infection risk; risk of increased malignancy	Widespread use
	IL-1	AMG 108 (anti IL-1β)	Plausible bioactivity; particular role in ECM degradation	Infection risk; limited efficacy in clinical trials	Licensed
	IL-6 receptor	Tocilizumab	Plausible bioactivity; good efficacy	May affect anti-inflammatory actions of IL-6	Licensed
	IL-15	AMG 714	Bioactivity *in vitro*; trends to efficacy	Possible disruption of host antiviral responses	Phase II clinical trials[1]
	IL-17	LY2439821	Plausible bioactivity; important role in rodent autoimmunity	Human biology requires clarification	Phase II clinical trials[2]
Soluble receptors	TNFα	Etanercept	Validated clinical target	Infection risk	Licensed
	IL-1	Anakinra (IL-1RA),	Plausible bioactivity; particular role in ECM degradation	Infection risk; cannot be used with TNF antagonists	Licensed
	IL-6	Soluble gp130	Efficacy in patients refractory to anti-TNF treatment	Infection risk	Pre-clinical phase
Cell-targeted	B cells	Rituximab	Enduring clinical response;	Intravenous only; possible immune toxicity	Licensed
	T cells	Abatement	Good efficacy; delays progression of structural damage	Cannot be used with TNF antagonists	Licensed
Signalling inhibitor	p38α	VX-745, BIRB 796	Promising target; well-tolerated	Limited efficacy	Phase I/II clinical trials[3]
MMP inhibitors	Collagenase inhibitor	Ro32-3555	Good results in animal models	Limited efficacy; adverse effects	Clinical trials terminated

Selected targeted biologics trialled and tested for the possible treatment of rheumatoid arthritis. IL-1RA, Interleukin 1 receptor antagonist; ECM, extracellular matrix. [1]Clinical Trial Identifier NCT00433875 [2]Identifier NCT00966875 [3]Identifier NCT00303563. Information compiled from Firestein et al., 2009; Brennan and McInnes, 2008; clinicaltrials.gov

1.3 NAMPT

NAMPT has received a great deal of attention in recent years as a potential target for the treatment of cancer (Holen et al., 2008), with the small-molecule NAMPT inhibitor APO866 exhibiting anti-angiogenic (inhibition of blood vessel growth) and anti-tumorigenic properties both *in vitro* (Wosikowski et al., 2002, Hasmann and Schemainda, 2003) and *in vivo* (Drevs et al., 2003), More recently, APO866 has been used to investigate the role of this protein in chronic disease progression in a murine arthritis model (Busso et al., 2008). This study suggested that NAMPT inhibition might have potential as a viable option for the treatment of RA. The next part of this chapter will provide a historical perspective of this protein.

1.3.1 Discovery of NAMPT

B-cell lymphogenesis within bone marrow cells is a tightly regulated process that requires several regulatory elements for each stage of activation, proliferation and differentiation. The early steps of B-cell development are controlled by IL-7, which acts synergistically with stem cell factor (SCF). Billips et al (1992) discovered that in addition to these two factors, pre-B-cell formation is dependent on the presence of S17 stromal cells, suggesting that a stromal-cell-derived molecule is involved in this early developmental step (Billips et al., 1992). Subsequent studies revealed that an uncharacterised cytokine was responsible (Dorshkind et al., 1992). In an attempt to discover new factors involved in the earliest events in B-cell development, Samal and colleagues (1994) screened activated human peripheral blood lymphocytes with a degenerate oligonucleotide probe designed to detect sequences similar to those present at the signal peptidase processing sites of numerous cytokines, including granulocyte macrophage-colony-stimulating factor (GM-CSF), IL-2, IL-1β, IL-6 and IL-3 (Samal et al., 1994). Clones with sequence homology or complements to the probe were isolated. From this screen, a novel cytokine-like gene was isolated and designated the name PBEF. Although PBEF alone did not enhance pre B cell formation in COS 7 cells, when added in conjunction with both IL-7 and SCF it caused a synergistic increase in pre-B cell colony formation (Samal et al., 1994).

The PBEF cDNA contained only one open reading frame of 1,470 bp (base pairs) encoding a polypeptide of 52 kDa (Samal et al., 1994). PBEF cDNA, as its encoded protein, shared no homology with any sequences present in the GenBank, EMBL or Swiss Protein databases at either the nucleotide or amino acid level, indicating the discovery of a novel factor. The presence of numerous message destabilising sequences (recognition signals for mRNA degradation processes) on the 3' untranslated region of the mRNA suggested that PBEF was a cytokine-like molecule. Through northern blot

analysis, three mRNA transcripts of 2.0, 2.4 and 4.0 kb were detected in human tissues, with the 2.4 kb transcript predominating (Samal et al., 1994). These transcripts are thought to arise due to alternative splicing of exons, or alternative polyadenylation sites. Recent annotation of the mRNA sequence suggests that there may be as many as 19 different mRNA variants of human PBEF, including 14 alternatively spliced variants and five unspliced forms. However, many of these variants have yet to be validated experimentally, and the physiological relevance of the variants is currently unknown. Current information on PBEF splice variants can be found using NCBI AceView (Thierry-Mieg and Thierry-Mieg, 2006).

Through northern blot analyses, PBEF was found to be expressed within the human heart, brain, placenta, lungs, liver, skeletal muscle, kidney and the pancreas (Samal et al., 1994). PBEF message is ubiquitously expressed in all tissues, with maximal expression occurring within the liver, muscle tissue (Samal et al., 1994) and immune cells (Friebe et al., 2011). The coding sequence of the PBEF gene is highly conserved, with orthologs found in prokaryotes (Martin et al., 2001) and also eukaryotes ranging from fish to Xenopus (Fujiki et al., 2000). Amino acid sequence alignment has revealed that the canine PBEF protein sequence is 96% identical to its human counterpart (McGlothlin et al., 2005), suggesting that the gene is evolutionarily highly conserved.

1.3.2 NAMPT and disease

It is clear from the literature that NAMPT is a ubiquitously expressed pleiotropic protein that is important for life. Attempts to create NAMPT knockouts in mice result in early embryonic lethality at embryonic day 10.5 (E10.5; (Fukuhara et al., 2005, Ognjanovic and Bryant-Greenwood, 2002), suggesting an essential role in cell metabolism. In normal tissues, NAMPT is very highly expressed in the liver, adipose tissue and peripheral blood leukocytes (summarised in figure 1.6). If NAMPT is expressed relative to the organ's metabolic activity, it is possible that organs that require NAMPT start to develop around E10.5; and therefore homozygous knockout embryos are not viable and are thus expelled. In contrast, NAMPT shows very low expression in brain tissue (Samal et al., 1994), suggesting that brain development is not affected by NAMPT deletion. NAMPT is constitutively expressed in human foetal membranes during pregnancy; however, it is overexpressed in the placenta during infection-induced pre-term labour (Ognjanovic and Bryant-Greenwood, 2002). Since its initial discovery, dysregulation of NAMPT has been continually implicated in a number of human diseases and conditions (summarised in figure 1.6).

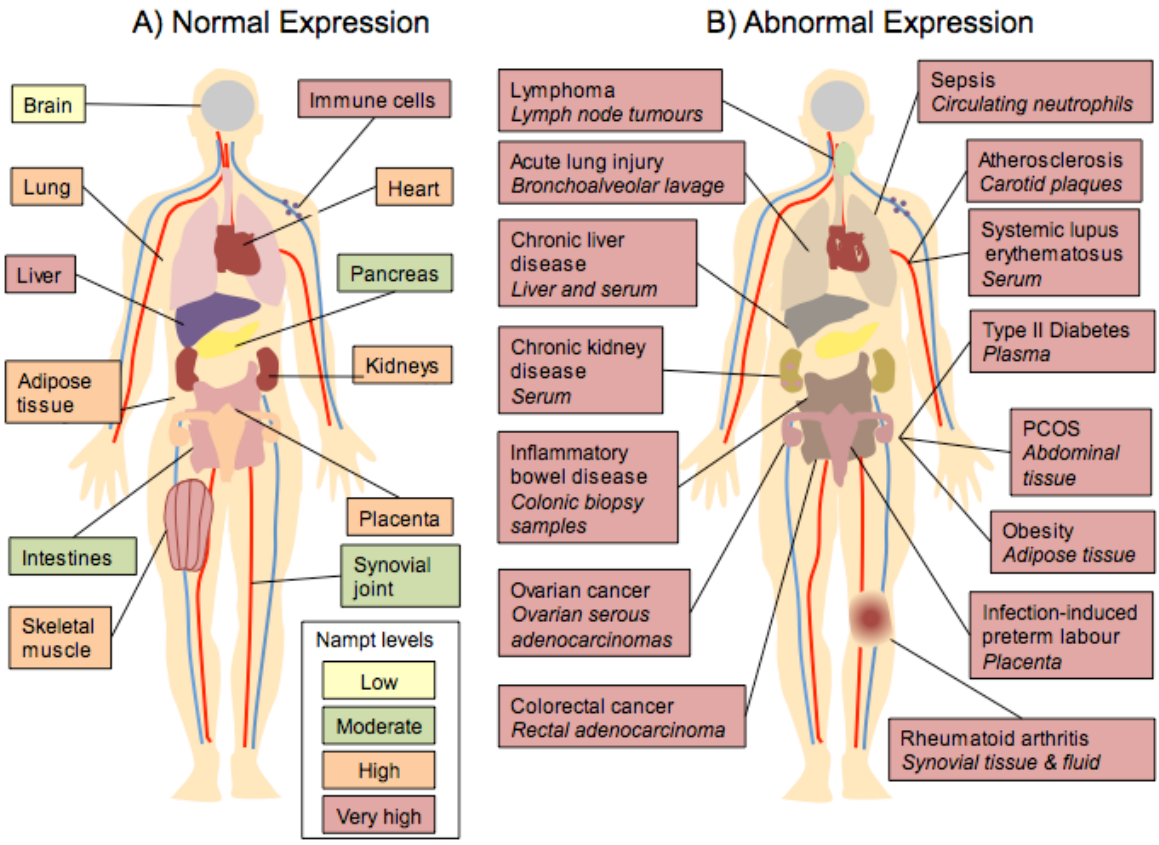

Figure 1.6 Expression and distribution of NAMPT in the human body

A) NAMPT is ubiquitously expressed in all tissues, though it is preferentially expressed in circulating leukocytes and the liver. Coloured boxes denote expression levels of NAMPT in cells and tissues, ranging from low (yellow) to very high (red). B) Pathological conditions where elevated NAMPT levels have been reported in the organ tissues and/or peripheral blood of patients. PCOS, Polycystic Ovary Syndrome.

Otero and colleagues (2006) published the first study linking NAMPT to RA, a chronic inflammatory syndrome characterised by swelling and stiffness of the joints. They investigated plasma levels of numerous adipokines in patients with RA and compared them with healthy controls, including leptin, adiponectin, NAMPT (called visfatin) and resistin. They reported a marked increase in levels of leptin, adiponectin and NAMPT in patients with RA, indicating NAMPT as one of the biomarkers of the disease (Otero et al., 2006). At the same time, Nowell et al (2006) found that levels of NAMPT were also elevated in the serum and synovial fluid of RA patients. Analysis of human RA synovial tissue confirmed that NAMPT was immunolocalised within the synovial membrane, adipose tissue and the subintimal lining of the synovial joint. Additionally, NAMPT was shown to be upregulated in fibroblast-like synoviocytes treated with IL-6 and its soluble receptor sIL-6R. Subsequently, RT-PCR analysis revealed that NAMPT regulation by IL-6 *trans*-signalling could by blocked by the inclusion of a STAT-3 inhibitor peptide. Based on these *in vitro* observations, wild type and IL-6 deficient mice were induced with

antigen-induced arthritis (AIA). Induction of AIA resulted in a 4-fold increase in NAMPT expression in wild-type mice, whilst little or no change was observed IL-6 deficient mice. Synovial STAT-1/3 activity was also impaired in the latter. This work demonstrated that STAT-3-dependent IL-6 trans-signalling regulates NAMPT expression, and that NAMPT is actively expressed during RA (Nowell et al., 2006).

Brentano and colleagues (2007) reported that increased levels of NAMPT in serum and synovial fluid were significantly correlated with the degree of inflammation and clinical disease severity in patients with RA. In RASFs, NAMPT was induced by TLR ligands and cytokines characteristically present in the joints of RA patients, including IL-1β, TNFα, TLR-4 ligand LPS, and TLR-2 ligand bLP (Brentano et al., 2007). The addition of NAMPT itself to RASFs activated NF-κB and AP-1, and induced IL-6 and CXCL8 protein, and NAMPT stimulation of RA monocytes caused an upregulation of IL-6 and TNFα. Similarly, Gosset et al (2008) found that IL-1β stimulated NAMPT synthesis in human articular chondrocytes. This was associated with excessive release of the catabolic mediator PGE_2, which in turn triggered the expression of MMPs and ADAMTSs; (Gosset et al., 2008).

NAMPT gene expression is elevated in synovial tissues, peripheral blood mononuclear cells (PBMC) and peripheral blood granulocytes (PBG) in patients with RA (Matsui et al., 2008). NAMPT is often described as an adipokine, a protein mediator secreted by fat cells (section 1.3.5). Rho and colleagues (2009) explored the effects of NAMPT, along with other adipokines, on radiographic joint damage in patients with RA. They compared serum concentrations of RA patients and non-diseased controls, and determined associations between adipokines and body mass index (BMI), CRP, IL-6 and TNFα and radiographic joint damage. They found that NAMPT levels were significantly higher in RA patients than controls, even after adjusting for BMI and inflammation. In addition to this, NAMPT concentrations were significantly and positively associated with the degree of radiological joint damage (Rho et al., 2009) suggesting that NAMPT is actively involved in degradative processes in RA.

Mesko and colleagues (2010) studied a database of 400 genes associated with RA, inflammatory bowel disease (IBD) and psoriasis. They identified 53 genes expressed in peripheral blood, which differed significantly between diseased and healthy individuals. Of these genes, NAMPT was identified as one of five genes that discriminate between samples from healthy controls and patients with chronic inflammatory diseases; highlighting NAMPT as a universal marker of chronic inflammation (Mesko et al., 2010). These data, combined with observations within our group, establish NAMPT as a pro-inflammatory and pro-degradative mediator of joint inflammation in RA. However, the possible mechanisms by which NAMPT exerts these effects are as yet to be resolved.

1.3.3 Cytokine-like properties of NAMPT

Ognjanovic and colleagues (2001) performed *in silico* analysis of the PBEF nucleotide sequence, combined with primer extension analyses of RNA extracted from a human amniotic epithelial cell line. They discovered that the gene for PBEF spans a length of 34.7 kb on the long arm of chromosome 7, and incorporates 11 exons and 10 introns, which encode 491 amino acids (Ognjanovic et al., 2001). The PBEF gene has both proximal and distal promoters upstream of the translation initiation codon, suggesting that the gene may be differentially expressed in different tissues. The 1.4 kb proximal promoter is GC[1] rich (60% GC), with a particularly G+C rich segment spanning the first 500 bp upstream of the major transcription initiation site. This segment contains several transcription initiation sites for numerous regulatory elements including NF (nuclear factor)-1 and AP (activator protein)-1. In contrast, the 1.6 kb distal promoter has more AT bases (60% AT), and several canonical TATA and CAAT boxes about 2 kb upstream from the transcription initiation site. The distal promoter shares many regulatory elements with the proximal promoter, including an NF-κB binding site, a regulatory element associated with inflammation (figure 1.7) (Ognjanovic et al., 2001).

Since these initial studies, evidence of more functions of PBEF have been uncovered. Jia and colleagues (2004) found that PBEF is expressed in neutrophils and monocytes in response to inflammatory stimuli such as LPS, TNFα and IL-1β stimulation. Neutrophils have a key role in normal immune homeostasis, and are constitutively apoptotic cells with a limited lifespan of 5-6 hours *in vivo*. However, in response to inflammatory stimuli apoptosis is delayed. Blocking PBEF translation with an antisense oligonucleotide blocked inhibition of apoptosis in activated neutrophils, suggesting a requisite role for PBEF in the delayed neutrophil apoptosis observed in clinical and experimental sepsis (Jia et al., 2004).

Ye and colleagues (2005) discovered that the PBEF gene is polymorphic, detecting two single-nucleotide polymorphisms (SNPs). The T-1001G SNP was found within in the proximal promoter region, and the C-1543T SNP was found in the distal promoter (Ye et al., 2005). Since this observation, yet more SNPs have been uncovered in the PBEF gene. According to the dbSNP NCBI database (Sherry et al., 2001), there are currently 620 reported SNPs in the human PBEF gene, although the functional consequences of many of these SNPs are currently unknown. This polymorphic nature, coupled with the presence of transcription factor binding sites within promoter regions,

[1] Referring to amino acid base content. G= Guanine, T= Thymine, C= Cytosine, A= Adenine

are characteristics PBEF shares with many innate immunity genes (Lazarus et al., 2002). These data suggest a role for PBEF in innate and adaptive immunity, functioning as a secreted cytokine. A number of pathways have been implicated in these processes. Studies in $CD14^+$ monocytes suggested that PBEF upregulates a number of cytokines through p38 and MEK1 pathways (Moschen et al., 2007). PBEF also exhibits angiogenic actions in vascular endothelial cells via the activation of ERK 1/2 (Kim et al., 2007). Similar findings have been observed in human umbilical vein endothelial cells (HUVECs), with PBEF-mediated upregulation of VEGF dependent on the mitogen-activated protein kinase (MAPK)/ERK, phosphatidylinositol 3-kinase (PI3K)/Akt, and VEGF/VEGF type-II receptor (VEGFR2) signalling cascades (Adya et al., 2008). PBEF was also found to activate NF-κB and AP-1 signalling pathways in fibroblasts (Brentano et al., 2007). Finally, extracellular PBEF was found to block macrophage apoptosis through activation of an IL-6/STAT3 signalling pathway (Li et al., 2008b). This body of evidence suggests that PBEF plays an active role in numerous signalling pathways.

Despite this evidence, two early observations have raised questions about this putative cytokine-like role. Firstly, the 5' flanking region of the gene lacks the classical sequence motif GPuGPuTTPyCAPy[2] (Ognjanovic et al., 2001). This sequence, found in many haematopoietic cytokines including IL-2, IL-3, C-SF (colony-stimulating factor) and GM-CSF, may be important for the coordinated activation of these factors (Zhang et al., 2011). However, the chemokine CXCL8 also lacks this sequence, so it may not be a prerequisite for all cytokines (Nemeth et al., 2000). Secondly, PBEF mRNA transcripts do not contain cytokine-specific secretion sequences, as predicted using von Heijne's (-3,-1) principle (von Heijne, 1986). This suggests it is not secreted in the same manner as other cytokines. Despite these observations PBEF appears to exert cytokine-like activity in response to pro-inflammatory mediators. Using FLAG-tagged versions of PBEF in conjunction with FLAG-tagged intracellular and extracellular control proteins (Dhfr-FLAG and Ppl-FLAG respectively), Revollo et al (2007) showed that PBEF is actively secreted from adipocytes, and not merely released as a result of cell lysis or death. The addition of brefeldin A (an inhibitor of Golgi-ER mediated protein secretion) had no effect on PBEF levels in cell culture supernatants, indicating that PBEF release is not mediated by an ER-Golgi-dependent pathway (Revollo et al., 2007b). Studies in 3T3-L1 preadipocytes reinforced these findings, and also ruled out release of PBEF through microvesicle secretion (Tanaka et al., 2007). All these data suggest that PBEF is released from cells through a non-classical secretory pathway, as originally determined by Samal and colleagues (1994) with von Heijne's principle (Samal et al.,

[2] G= Guanine, T= Thymine, C= Cytosine, A= Adenine, Pu= Purine base, Py= Pyrimidine base

1994, von Heijne, 1986). To date, PBEF has been detected in the culture medium of numerous cell types, including lymphocytes (Samal et al., 1994), neutrophils (Jia et al., 2004), HepG2 cells (Garten et al., 2009), and murine 3T3-L1 adipocytes (Tanaka et al., 2007, Revollo et al., 2007b).

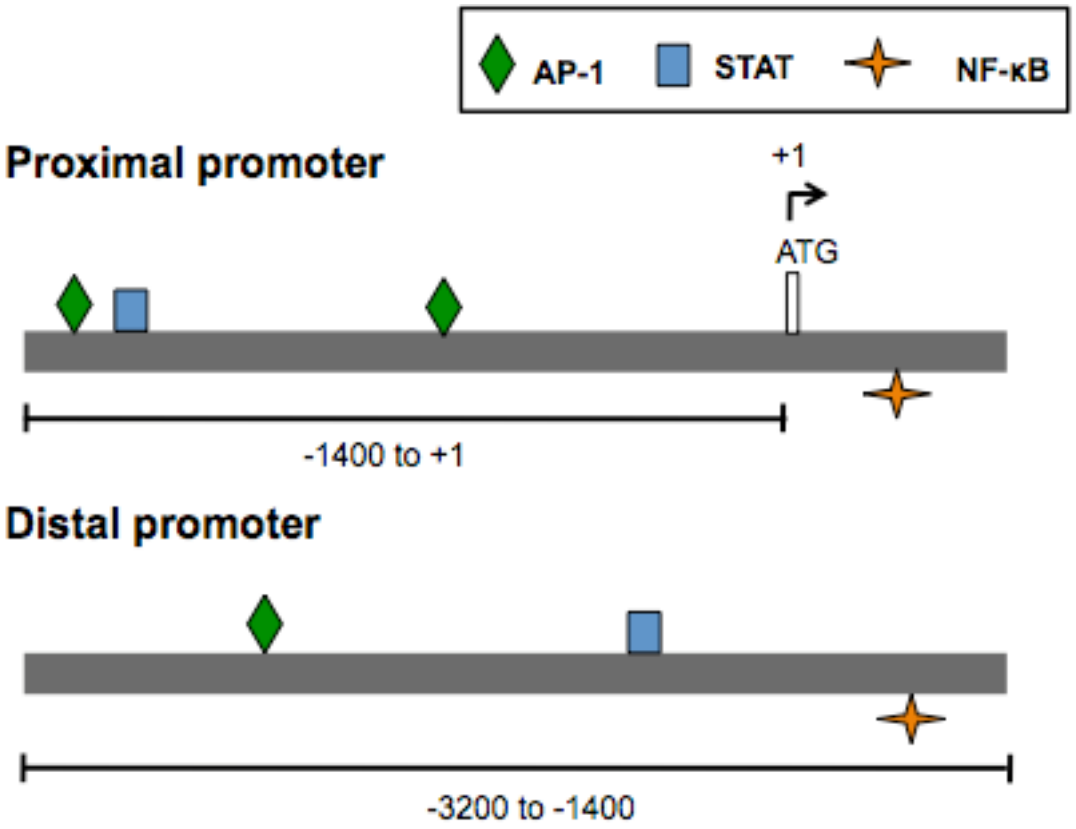

Figure 1.7 Genomic organisation of NAMPT/PBEF/Visfatin

A simplified schematic representation of proximal and distal promoters upstream of the NAMPT gene, showing a selection of regulatory elements present. Adapted from (Luk et al., 2008).

1.3.4 Enzymatic activity of NAMPT

As studies into its cytokine-like properties continued, another vital function of PBEF was being uncovered. In 2001, Martin and colleagues were attempting to identify a factor that enabled some bacterial species to grow in the absence of nicotinamide adenine dinucleotide (NAD^+). NAD^+ is a coenzyme found in all living cells that plays a pivotal role in a variety of biochemical and biological processes. In mammals, intracellular NAD^+ is mainly synthesised via three distinct metabolic pathways (figure 1.8). In many bacterial species, NAD^+ is synthesised via the *de novo* pathway, which involves the essential amino acid tryptophan. In addition to this, NAD^+ can also be synthesised either by nicotinic acid (NA) or nicotinamide (NAm) via two analogous pathways known as the salvage pathways, the former of which is also referred to as the "Preiss-Handler" pathway (Martin et al., 2001). More recently, nicotinamide riboside (NR) was identified as an additional NAD^+ precursor in eukaryotes (Bieganowski and Brenner, 2004).

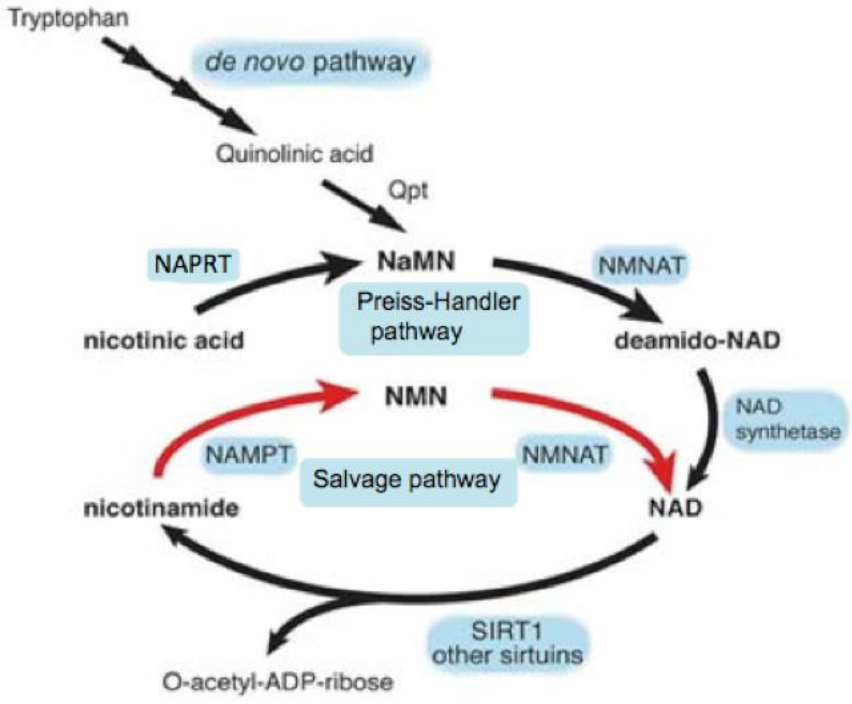

Figure 1.8 The mammalian NAD^+ biosynthesis pathways

QPRT, quinolinic acid phosphoribosyltransferase; NAPRT, nicotinic acid phosphoribosyltransferase; NaMN, nicotinic acid mononucleotide; NMNAT, Nicotinamide mononucleotide adenylyltransferase; NAMPT, nicotinamide phosphoribosyltransferase; NMN, nicotinamide mononucleotide; NAD, nicotinamide adenine dinucleotide; SIRT1, Silent mating type information regulation 2 homolog1. Adapted from (Imai and Kiess, 2009).

Although the *de novo* pathway is the predominant pathway for NAD^+ biosynthesis in bacteria, some species can use NAm as a precursor for NAD^+, and are thus classified as NAD^+-independent. Through cloning, sequence analysis and characterisation of a plasmid-encoded gene, Martin and colleagues (2001) characterised a gene in *Haemophilus ducreyi* that could confer NAD^+-independence when transformed into NAD^+-dependent species, allowing them to utilise NAm as a precursor for NAD^+. The gene, designated *nadV*, shared significant homology with the human PBEF sequence, in addition to other previously unidentified genes in NAD^+-independent bacterial species (Martin et al., 2001).

Previously, little was known about the enzyme involved in the conversion of NAm, which had been designated nicotinamide mononucleotide pyrophosphorylase (Dietrich et al., 1966, Powanda et al., 1969). On the basis of the work by Martin *et al* (2001), Rongvaux and colleagues (2002) hypothesised that murine PBEF is a NAMPT which incorporates NAm and 5-phosphoribosyl-1-pyrophosphate (PRPP) to produce nicotinamide mononucleotide (NMN). To test this, they measured the formation of radioactive NMN in mouse liver cytoplasmic extracts containing [^{14}C]NAm as a substrate. They detected high levels of NAMPT enzymatic activity, which was strongly abrogated by the addition of an anti-PBEF polyclonal antibody. The role of NAMPT was further confirmed by cloning the murine PBEF gene into *nadV*-deficient NAD^+-dependent *Pasteurellaceae*. Bacteria containing the cloned gene acquired the ability to grow in the presence of NAm, indicating that the gene allowed the utilisation of NAm as a precursor for NAD^+ biosynthesis (Rongvaux et al., 2002). In the same study, splenic T cells were stimulated *in vitro* and cell extracts and culture supernatants were analysed for PBEF protein levels by enzyme-linked immunosorbent assay (ELISA). In contrast to expected findings, PBEF was not actively secreted upon cellular activation, remaining as a cytoplasmic protein (Rongvaux et al., 2002). This suggests that in T-cells, release of PBEF upon activation-induced cell death is the mechanism for homeostatic control of lymphocyte responses (Rongvaux et al., 2002). The Human Genome Organisation Gene Nomenclature Committee (HGNC) has since approved Nicotinamide phosphoribosyltransferase (NAMPT) as the official gene name for PBEF. Therefore for the duration of this thesis PBEF will be referred to as NAMPT. This enzymatic role for NAMPT occurs intracellularly, and so intracellular NAMPT is often referred to as iNAMPT. The proposed NAMPT signalling molecule is often referred to as extracellular (e)NAMPT (Imai, 2009).

Revollo et al (2004) explored the enzymatic role of iNAMPT further by studying its kinetics in NAD^+ biosynthesis, along with nicotinamide mononucleotide adenylyltransferase (NMNAT), which directly synthesises iNAMPT product NMN into NAD^+ (figure 1.8). Using murine his-tagged recombinant proteins, they reconstituted the

NAD^+ biosynthesis pathway and developed an enzyme-coupled fluorometric assay *in vitro* (Revollo et al., 2007b). The group discovered that iNAMPT, not NMNAT, was the rate-limiting enzyme in the pathway. They also found that no NAD^+ was generated in the absence of iNAMPT substrates Nam or PRPP, confirming that the NAMPT pathway is the predominant pathway in most mammalian tissues (Revollo et al., 2004). The few exceptions to this are the brain and the liver, which primarily synthesise NAD^+ via the *de novo* pathway (Bogan and Brenner, 2008).

Following on from this work, Van der Veer (2005) found that vascular smooth muscle cells (SMCs) overexpressing iNAMPT had a significantly higher intracellular NAD^+ content and enhanced cell survival when compared to control cells, providing further evidence that iNAMPT is a regulator of NAD^+-dependent reactions in cells (Van Der Veer et al., 2005). Furthermore, $NAD^{`+}$-dependent histone deacetylates (HDACs, also known as sirtuins) were required for SMC maturation, suggesting that NAD^+ levels are a key determinant of SMC behaviour (Van Der Veer et al., 2005).

1.3.5 Insulin mimetic activity of NAMPT

In 2005 yet another function of NAMPT was proposed. Fukuhara and colleagues detected a cDNA fragment that was more abundantly expressed in visceral fat than subcutaneous fat (Fukuhara et al., 2005). Sequencing revealed that this fragment corresponded to the NAMPT gene. Further analysis revealed that the NAMPT protein was secreted by visceral fat in humans and mice. The authors named it visfatin (a name still commonly used throughout the scientific literature) and described it as an adipokine, a protein mediator secreted by fat cells. From two female patients they found that levels of NAMPT/visfatin were predominantly higher in visceral fat compared to subcutaneous fat. They also reported that high doses of NAMPT/visfatin lowered plasma glucose levels in both insulin-resistant and insulin-deficient mice. Finally, they claimed that NAMPT had insulin mimetic effects, engaging and activating insulin signalling through the insulin receptor (IR), but in a manner distinct from insulin (Fukuhara et al., 2005).

These findings had a high impact, prompting increased interest in NAMPT and its implications in metabolic syndrome. They also raised the possibility that NAMPT could be a useful target for the development of drug therapies for diabetes. Chen et al (2006) reported elevated plasma levels of NAMPT in patients with Type 2 diabetes mellitus, suggesting a role in the pathogenesis of this condition (Chen et al., 2006). Xie and colleagues (2007) also reported insulin mimetic effects of NAMPT in cultured osteoclasts, resulting in increased glucose uptake in these cells (Xie et al., 2007).

However, other groups failed to replicate these findings and started to dispute the integrity of the research. Berndt and colleagues (2005) could find no evidence that

NAMPT was predominantly expressed in visceral fat compared to subcutaneous fat, in some cases finding greater amounts of NAMPT in the latter (Berndt et al., 2005). They also failed to observe a correlation between NAMPT plasma concentrations and parameters of insulin sensitivity (Berndt et al., 2005). Upon investigation of the laboratory by the Committee for Research Integrity (CRI), it was recommended that the entire paper should be retracted, although the authors continue to stand by their observations (Fukuhara et al., 2007).

1.3.6 Crystal structure of NAMPT

In 2006 the three dimensional structure of mammalian NAMPT was resolved individually by different groups. The crystal structure of murine NAMPT was elucidated by Wang and colleagues, alone and in combination with its substrate NMN (Wang et al., 2006). Meanwhile Kim et al (2006) resolved the crystal structure of rat NAMPT (Kim et al., 2006). Both groups reported that the NAMPT monomer consists of 491 residues that form 22 β-strands and 15 α-helices arranged into three structural domains (figure 1.9). Analyses of human and murine NAMPT 3D structures were performed by Khan et al (2006), who showed that NAMPT protein has a low sequence identity with other phosphoribosyltransferase enzymes. However, its tertiary structure is similar to nicotinic acid phosphoribosyltransferase (NAPRT) from *Thermoplasma acidophilum*, the enzyme that catalyses the conversion of NA into nicotinic acid mononucleotide (NaMN). NAMPT protein also shares some common features with *Mycobacterium tuberculosis* quinolinic acid phosphoribosyltransferase (QPRT), which converts quinolinic acid to NaMN. On the basis of these similarities, NAMPT has been designated a type II phosphoribosyltransferase. However, there are important conformational differences between the three enzymes. NAMPT is the largest of the three, constituting 100 more amino acid residues than NAPRT, with QPRT being smaller still. There are also notable differences in the composition of their residues, which impact greatly on both the structure and orientation of their active sites (Khan et al., 2006).

NAMPT is homodimeric in solution, with its product NMN bound near the top of the central β-sheet in domain B. Two active sites lie at the interface of the dimer, suggesting that dimerisation is required for catalytic activity of the NAMPT enzyme. Revollo et al (2007) confirmed this by showing that mutation of Ser199 and Ser200 residues, essential for symmetrical dimer formation, decreased NAMPT enzymatic activity (Revollo et al., 2007b). NAMPT contains an acidic residue that specifies Nam as a substrate, excluding alternative negatively charged substrates. NAMPT was also shown to undergo autophosphorylation of histidine residues, hydrolysing adenosine triphosphate (ATP) to increase its enzymatic activity. This autophosphorylation is thought to enhance enzymatic activity through the generation of additional negative charge,

which may promote cleavage of pyrophosphate from PRPP, enhancing the formation of NMN. Mutation of the residue His247, an important residue in autophosphorylation, either significantly decreases or abolishes NAMPT enzymatic activity (Wang et al., 2006).

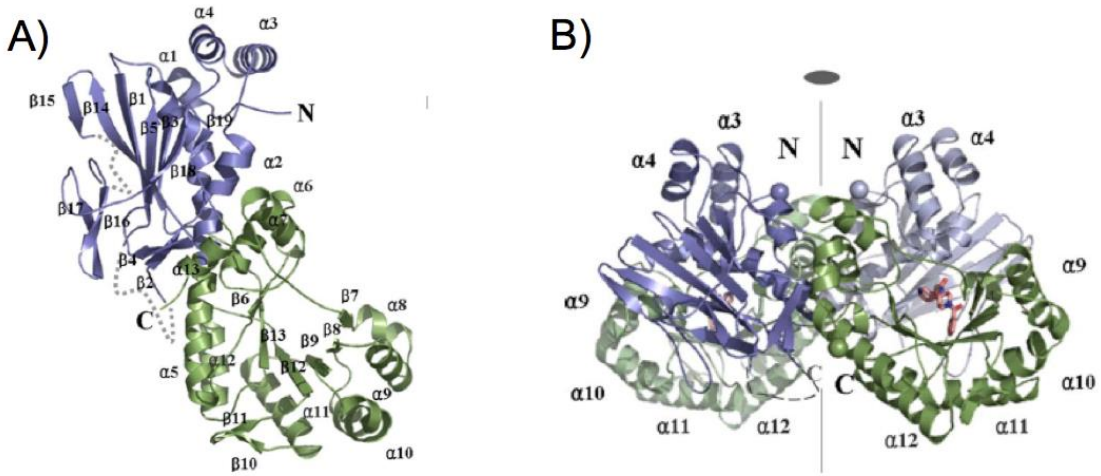

Figure 1.9 Crystal structure of PBEF/NAMPT/Visfatin

A) A schematic ribbon diagram of the overall fold of the PBEF monomer. The first domain in shown in blue, and the second domain is in green. B) The PBEF dimer, with the second monomer shown in pale blue and green. Two APO866 (PBEF inhibitor) molecules are shown in red. Taken from (Kim et al., 2006).

1.4 APO866

Due to its association with the degree of disease inflammation and clinical disease activity (Rho et al., 2009), NAMPT has been identified as a possible therapeutic target for the development of new RA drugs (Brentano et al., 2007). Preliminary studies have demonstrated that suppressing NAMPT with a highly specific small molecule inhibitor named APO866 limits the effects of RA in a murine collagen-induced arthritis model. This effect was seen when treatment was administered before the appearance of arthritis, and also in established disease (Busso et al., 2008). In fact, *in vivo* studies indicated that APO866 had comparable efficacy to anti-TNF treatment (Busso et al., 2008) and Nowell et al; unpublished). Therefore the last part of this review will provide a historical perspective on APO866, including its interactions with NAMPT and the findings of work involving this molecule.

1.4.1 Discovery of APO866

Angiogenesis is the process involving the growth of new blood vessels from pre-existing vessels. In normal tissues this is a vital process in growth, development and wound healing. However, excessive angiogenesis is associated with tumour formation. In 2003 researchers working for Fujisawa Deutschland GMBH developed a number of different compounds with the aim of inhibiting/reducing angiogenesis. One such compound was (E)-N-[4-(1-benzoylpiperidin-4-yl) butyl]-3-(pyridin-3-yl) acrylamide, which was designated FK866 (Beidermann et al., 2003). Since its development this compound has been in the possession of a number of different pharmaceutical companies. In 2005 the Fujisawa Pharmaceutical Co., Ltd merged with Yamanouchi Pharmaceutical Co., Ltd to form Astellas Pharma GmbH. In October 2005 Swiss biopharmaceutical company Apoxis SA acquired exclusive worldwide development and marketing rights to the drug and renamed it APO866, although it is still often referred to in some literature by its former names FK866 and WK175 (Apoxis, 2005). Finally, in 2007 Apoxis was acquired by TopoTarget, which has continued to initiate clinical studies of APO866 in order to understand its biologic effects.

1.4.2 Assigning *in vitro* functionality of APO866

Wosikowski et al (2002) published the first study of APO866 *in vitro*. In a screen of novel anti-tumour agents, they discovered that APO866 had distinct characteristics to conventional chemotherapies: it induced apoptosis in cells, with no DNA-damaging effects which can lead to genomic instability and generation of resistant tumour phenotypes (Wosikowski et al., 2002). They stimulated a human monocytic cell line (THP-1) with APO866 for four days, and found that this agent caused a time and dose-dependent decrease in cell metabolic activity, as determined by a cell proliferation assay.

They also observed a concurrent increase in the proportion of apoptotic cells. They discovered that it exerted these effects by interfering with NAD^+ biosynthesis, resulting in decreased cellular NAD^+ content (Wosikowski et al., 2002). Prolonged incubation of cells with APO866 altered mitochondrial membrane potential. This disruption of mitochondrial function led to activation of caspase 3, which is a crucial event in the final degradation phase of apoptosis. These data suggest that depletion of intracellular NAD^+ is a trigger that initiates the apoptotic cascade, resulting in an anti-tumour effect (Wosikowski et al., 2002).

In 2003 Hasmann and Schemainda explored the pro-apoptotic effects of APO866 further in human liver carcinoma (HepG2) cells. Like Wosikowski et al (2002), they observed that APO866 decreased metabolic activity and cell number, whilst increasing the proportion of non-viable cells. These effects were observed along with a concurrent decrease in intracellular NAD^+. They sought to determine which NAD^+ biosynthesis pathway APO866 was involved in, using radiolabelled NAD^+ precursors Nam and NA. APO866 caused rapid inhibition of Nam-mediated NAD^+ production, with no discernible effect on NA-mediated NAD^+ levels. Additionally, no accumulation of radiolabelled NMN was observed; suggesting that NAMPT and not the downstream enzyme NMNAT was the target for APO866 (Hasmann and Schemainda, 2003).

1.4.3 Molecular basis of APO866 inhibition of NAMPT activity

In 2006 groups working on the crystal structure of NAMPT co-crystallised it with APO866, as well as its reaction product NMN, in order to determine the molecular basis of NAMPT enzymatic activity and inhibition (Kim et al., 2006, Khan et al., 2006). NAMPT is a dimer in solution, and is only active in this dimeric form. APO666 is tightly bound in a tunnel at the interface of this dimer. It competes directly with Nam, and therefore acts as a competitive inhibitor of NAMPT activity (figure 1.10). This inhibition is highly specific to NAMPT, as the structurally similar NAPRT does not contain a tunnel at its dimer surface, which is the molecular basis for APO866 inhibition. Mutations of the NAMPT binding site abolished inhibition by APO866 (Khan et al., 2006).

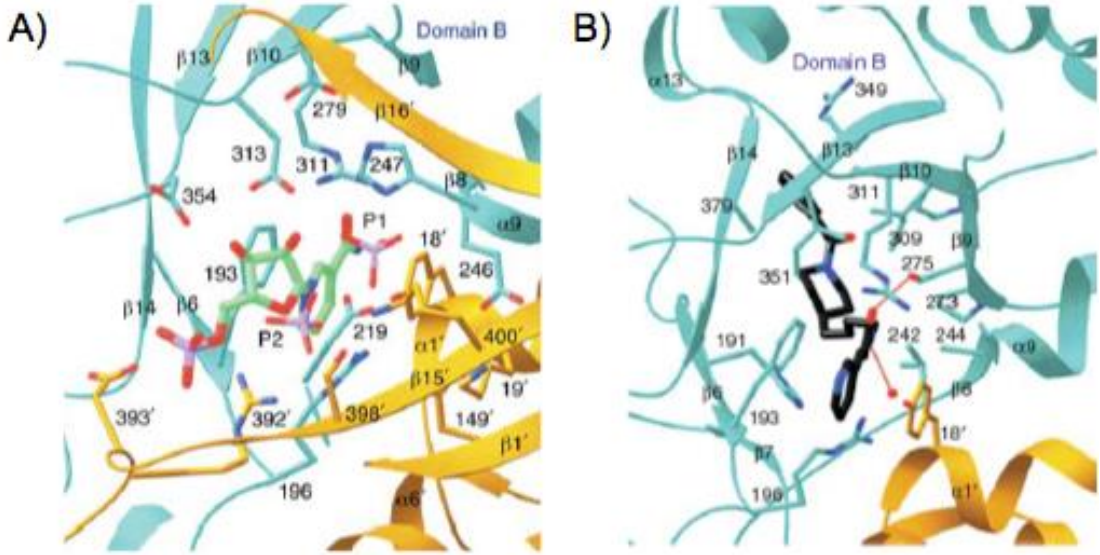

Figure 1.10 The molecular basis of NAMPT inhibition by APO866

A) Ribbon diagram of the NAMPT dimer (in cyan and gold) co-crystallised with NMN (shown in green and red). B) Interaction of NAMPT dimer with APO866 (shown in black). Images adapted from (Hasmann and Schemainda, 2003).

1.4.4 Assessing impact of APO866 *in vivo*

Once the anti-tumour effects of APO866 were established, Drevs and colleagues (2003) set out to investigate the anti-tumour, anti-metastatic and anti-angiogenic potency of this agent in a murine renal cell carcinoma model (RENCA) (Drevs et al., 2003). This was achieved by inoculating mice with RENCA tumour cells to initiate tumour growth, before treating orally with various doses of APO866. Mice were sacrificed on day 21 and analysed for primary tumour weight and volume, lung metastases and tumour vessel density. It was found that doses of ≥10 mg/kg showed significant anti-tumour and non-significant anti-metastatic activity on RENCA primary tumours, with all doses resulting in anti-angiogenic activity (Drevs et al., 2003). In a subsequent study the metabolic effects of APO866 were investigated in a mouse mammary carcinoma model *in vivo*. Groups of mice were given two different dosages of the drug, administered by intra-peritoneal (i.p.) injection. The lower dosage treatment resulted in retarded tumour growth compared to controls, whilst the higher dose also caused reduced mammary carcinoma tumour radiation sensitivity. Histological annexin staining of APO866-treated tumours also showed evidence of apoptosis compared with controls (Muruganandham et al., 2005).

Although most interest in APO866 is focused on its potential as an anti-cancer agent, it is now emerging that APO866 may also be useful in inflammatory and autoimmune diseases. Busso et al found that APO866 treatment reduced intracellular

NAD^+ levels and pro-inflammatory cytokine secretion by inflammatory cells *in vitro*. *In vivo*, animals with collagen-induced arthritis (CIA) were treated with APO866 by i.p. Injection, resulting in reduced disease severity, comparable to anti-TNFα drug etanercept. They observed that APO866 caused a reduction in circulating TNFα levels during endotoxemia in mice (Busso et al., 2008). In light of these findings, the Nowell research group have further investigated the *in vivo* efficacy of APO866 in CIA animals with the use of osmotic minipumps. Early findings suggest that APO866 ameliorates disease in treated animals in a time and dose-dependent manner.

1.4.5 Clinical studies involving APO866

Preclinical studies in rats and monkeys showed that lymphocytes are most sensitive to APO866, resulting in lymphocytopenia and reticulocytopenia (Holen et al., 2002). Following on from these findings Holen et al (2008) carried out an open-label Phase I clinical trial (Holen et al., 2008). Patients with solid tumour malignancies were given escalating doses of APO866 as continuous 96 hour infusions. The group aimed to determine dose-limiting toxicities of APO866, in addition to its pharmacokinetics, efficacy and effect on VEGF levels. VEGF is an important signalling protein in vasculogenesis and angiogenesis, which can contribute to disease when over expressed by providing a blood supply to solid tumours. APO866 was generally well tolerated, although some patients suffered from a drop in platelet levels, but recovered quickly at the end of the study. Plasma VEGF levels appeared to drop, but due to the small sample size this effect was not significant. None-the-less, a few patients showed improvement. Although APO866 has potential as a single agent, it may work best if administered in combination with other anti-tumour agents (Holen et al., 2008). TopoTarget subsequently initiated a Phase II study to determine the efficacy and safety of 3 cycles of APO866 for the treatment of advanced cutaneous melanoma (Topotarget, 2009b), as well as a Phase I/II study for the treatment of B-Chronic Lymphocytic Leukaemia (B-CLL) (Topotarget, 2009a). These studies have recently been completed, and a third Phase II study on APO866 in cutaneous T cell lymphoma (CTCL) is currently underway (Topotarget, 2011).

1.5 Summary and Thesis aims

NAMPT is a relatively newly characterised pleiotropic protein. Since its discovery in 1994 it has been implicated in a variety of important cellular processes, and has garnered increased interest in the last decade for its role in NAD^+ biosynthesis, and its association with a host of diseases, including inflammatory arthritis.

The overall hypothesis of this thesis is as follows:

Overexpression of NAMPT in the synovial joint propagates cartilage destruction during inflammatory arthritis.

It is anticipated that the results of this thesis will further our knowledge of the role of NAMPT in the disease pathology of RA and may lead to the development of novel therapeutics aimed at suppressing its activity in driving pathology. In addition, this knowledge may potentially be applied to other chronic conditions such as inflammatory bowel disease or chronic kidney disease. The specific aims of the individual experimental chapters are outlined below:

- To determine the effect of exogenous (e)NAMPT on catabolic proteinases *in vitro.*
- To determine the effect of NAMPT inhibition on catabolic proteinases *in vivo.*
- To determine the effect of iNAMPT inhibition on articular cartilage *ex vivo.*
- To investigate how intracellular (i)NAMPT is regulated in RASFs *in vitro.*

Chapter 2: Materials and methods

2.1 Cell and tissue culture experiments

Unless otherwise stated, all cell and tissue culture reagents were purchased from Gibco, Life Technologies Ltd. In chapter 3, the human recombinant extracellular NAMPT (eNAMPT) used was purchased from Enzo Life Sciences Ltd, Exeter, UK. The lyophilised protein was reconstituted in sterile phosphate-buffered saline (PBS) to produce a stock solution which was aliquoted and stored at -20°C, as recommended by the manufacturer. All cytokines used throughout this thesis were purchased from R&D Systems, Abingdon UK (Cat no: 201-LB, 210-TA, 295-OM; IL-1β, TNFα and OSM, respectively). Lyophilised cytokines were reconstituted in sterile PBS containing 0.1% bovine serum albumin (BSA) to a stock concentration of 10 µg/ml, and were aliquoted and stored at -20°C until required. Cytokines were used at working concentrations ranging from 1-20 ng/ml, depending on the model system. Concentrations of 1-10 ng/ml of cytokine were typically applied to monolayer cultures of RASFs (Brentano et al., 2007, Niederer et al., 2011) and chondrocytes (Gosset et al., 2008, Hong et al., 2011). In cartilage *ex vivo* culture (section 2.1.5), cytokine concentrations up to 20 ng/ml were used, as per previously published work (Sondergaard et al., 2006, Karsdal et al., 2008). NAMPT inhibitor APO866 (provided by TopoTarget A/S, Denmark) was stored in a 10 mg/ml solution in 60% propylene glycol. For each stimulation assay, APO866 was diluted to a working concentration in Dulbecco's modified Eagle's medium (DMEM) prior to use. Concentrations ranging from 0.01 nM to 100 nM were used, as previously described (Busso et al., 2008, Nahimana et al., 2009). Beta NMN and NA (both available from Sigma-Aldrich Ltd, Dorset, UK) were dissolved in deionised water (dH_2O) at a stock concentration of 10 mg/ml, aliquoted and stored at -20°C until required. These NAD^+ precursors were used at a working concentration of 100 µM, as this is within the range of concentrations typically applied to cells in previous studies (Busso et al., 2008, Van Gool et al., 2009).

2.1.1 Monolayer tissue culture

2.1.1.1 Cell passage

All cells used in this thesis were cultured as monolayers, in medium supplemented with 10% heat-inactivated foetal bovine serum (FBS), and 100 U/100 µg per ml Penicillin-Streptomycin (Penstrep). For cell passage, culture medium was removed and cells were washed twice in 10 ml sterile PBS, in order to remove residual FBS that may inhibit trypsinisation. PBS was aspirated, and 0.25% Trypsin-ethylenediaminetetraacetic acid (EDTA) was added. Cells were incubated at 37°C for 5-10 minutes with frequent agitation until all cells had been seen to detach from the flask

under an inverted microscope. Trypsin activity was quenched by the addition of an equal volume of fresh culture medium with 10% FBS. The cell suspension was centrifuged at 400 x g for 5 minutes, and the resulting pellet was resuspended in fresh culture medium. Cells were seeded at a density of approximately $3x10^4$ cells/ml and incubated in new culture flasks at a volume of 15 ml in a T75 flask, and 30 ml in a T175 flask. Cells were then grown at 37°C in a humidified atmosphere containing 5% CO_2. Culture medium was changed twice weekly.

2.1.1.2 Freezing and resuscitating cells

Prior to freezing, cells were washed twice in PBS and trypsinised as described in the previous section. A small (<100 µl) aliquot of cell suspension was taken for determination of cell number. A series of dilutions of the cell aliquot (1:5, 1:10, 1:20) were made, and a 10 µl aliquot of cell suspension was pipetted onto a bright line haemocytometer and covered with a clean glass coverslip (Sigma-Aldrich Ltd, Dorset, UK). The cells were counted in 5 grids (figure 2.1) and the total number of cells in the sample was calculated as follows:

Number of cells= average grid count x 10^4 x dilution x total volume

If cell numbers exceeded 50 per grid, then a more diluted cell suspension was used, until an appropriate count was obtained. The remaining cell suspension was centrifuged at 400 x g for 5 minutes. The cell pellet was reconstituted in FBS containing 10% dimethyl sulfoxide (DMSO; Sigma-Aldrich Ltd, Dorset, UK) as a cryoprotectant, at a concentration of $3x10^4$ cells/ml according to European Collection of Cell Culture (ECACC) recommendations. Cell suspensions were mixed thoroughly and aliquoted into 1 ml Cryo™ cryovials (Greiner Bio-One Ltd, UK). Vials were labelled and stored at -80°C in a “Mr. Frosty” freezing container to gently cool at 1°C per minute (Nalgene, Thermo Fisher Scientific, Denmark) overnight, before being transferred into liquid nitrogen (LN_2) dewars for long-term storage.

To revive frozen cell stocks, 5 ml of fresh culture medium with 10% FBS was prepared, sterilised with a 0.22 µm filter, and pre-warmed in a 37°C water bath. Cryovials of cells were carefully removed from LN_2 storage. Vials were sprayed with 70% (v/v) ethanol and opened partially under sterile laminar flow in a Class II cabinet to permit the release of pressure caused by excess LN_2. Vials were resealed and thawed rapidly in a 37°C water bath until only a few ice crystals remained. The thawed suspension of cells was quickly added to the pre-warmed culture medium. Cells were counted, before being transferred to a T25 tissue culture flask. Cells were maintained in culture as described in section 2.1.1.1, and used as needed.

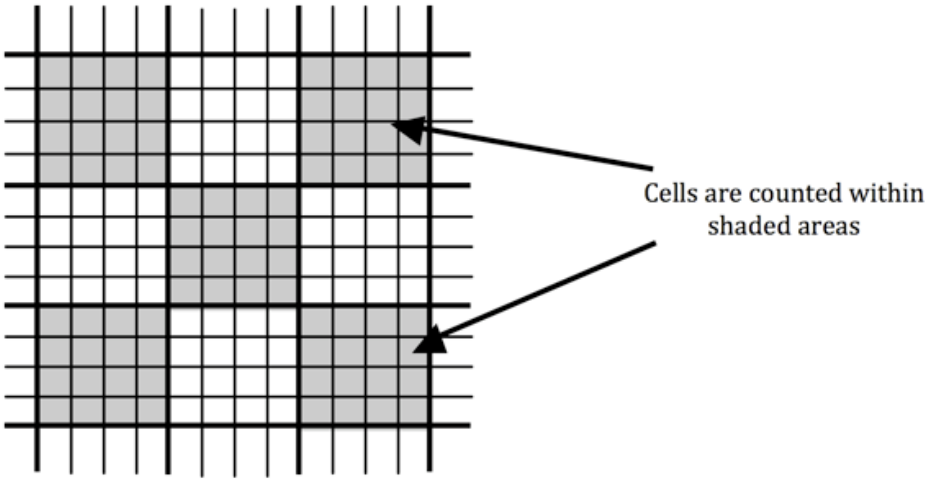

Figure 2.1 Haemocytometer grid for cell counts

Shaded regions show where cells are counted. Cells positioned on the right hand or bottom boundary lines were also counted.

2.1.2 Human primary cells and cell lines

Human RA joint cells, namely articular chondrocytes and synovial fibroblasts, were extracted from an elbow joint, acquired with ethical approval from an RA patient undergoing joint replacement surgery. The joint was stored at 4°C in sterile DMEM culture medium prior to digestion. Dissection equipment was sterilised prior to use by autoclaving at 121°C for 30 minutes. The entire chondrocyte extraction procedure was carried out in a Class II Safety cabinet. Throughout the dissection procedure, equipment was routinely sterilised by exposure to alcohol flame.

2.1.2.1 Human primary articular chondrocytes (HACs)

Cartilage was removed from the entire articulating surface of the elbow joint using a sterile scalpel, and finely diced to enable efficient dissociation of chondrocytes from the cartilage ECM. Cartilage shavings were placed into a sterile tube containing chondrocyte-specific culture medium comprising DMEM supplemented with the following: 100 U/100 µg per ml Penstrep, 10% (v/v) FBS, 100 mM HEPES, 1 mM sodium pyruvate (all from Gibco, Life Technologies Ltd, Paisley, UK), 0.1 mM ascorbic acid, and 5 mM glucose (both Sigma-Aldrich, Dorset, UK).

Once all the articular cartilage was harvested, the medium was removed and replaced with chondrocyte culture medium containing 5% FBS and 70 units/ml pronase from *Streptomyces griseus* (Roche Diagnostics Ltd, West Sussex, UK). Articular cartilage was incubated in the pronase solution with gentle agitation for 1 hour at 37°C,

5% CO_2. Pronase medium was then removed and replaced with chondrocyte culture medium containing 5% FBS and 300 units/ml collagenase Type I from *Clostridium histolyticum* (Gibco, Life Technologies Ltd, Paisley, UK). Collagenase digestion was carried out for 3 hours at 37°C 5% CO_2, with gentle agitation. Prior to the digestion procedure, both pronase and collagenase solutions were sterilised by filtration with a 0.22 µm Millex-GP syringe driven filter (Millipore Ltd, Watford, UK). The resulting suspension was passed through a 40 µm cell strainer (BD Biosciences, Oxford, UK) to remove any undigested material. An equal volume of serum-free DMEM plus supplements was added to quench the collagenase, and the suspension was centrifuged at 400 x g for 5 minutes. The supernatant was aspirated, and the cell pellet was reconstituted in 1 ml serum-free DMEM. A 100 µl aliquot of cell suspension was taken to determine cell number (see section 2.1.12). Finally, chondrocytes were seeded onto tissue culture plates at a seeding density of 6000 cells/cm^2, and cell stimulations were performed as described in section 5.2.1.

2.1.2.2 Human RA synovial fibroblasts

Under sterile conditions, synovial tissue was finely diced to maximise its surface area for digestion. Tissue was added to a sterile tube containing a 1:1 mixture of DMEM and Nutrient Mixture F-12 (DMEM:F-12) containing 100U/100 µg/ml Penstrep, 5% heat-inactivated FBS, and 1 mg/ml Collagenase Type I. The tissue was digested in the collagenase solution at 37°C, 5% CO_2 with mechanical agitation, for 2 hours, or until the synovial tissue was fully digested. The resulting suspension was passed through a cell strainer to remove any undigested material. This filtrate was centrifuged at 400 x g for 5 minutes, and the resulting pellet was washed once in DMEM:F-12, and centrifuged once more. Finally, the washed pellet was resuspended in 5 ml DMEM:F-12 containing 10% FBS and transferred to a T25 tissue culture flask. Cells were cultured overnight, and non-adherent cells were removed by changing the culture medium. Medium was changed twice weekly until confluence was achieved. In order to produce a uniform cell population, primary cells (passage 0) were passaged and used at passage 3 and beyond. This was to ensure a homogeneous population free of contaminating macrophage-like synoviocytes, and also to expand the number of proliferating cells (Neumann et al., 2010). Passage was carried out when cells reached 80% confluency (see section 2.1.1.1). Cell stimulations were performed as described in section 6.2.

2.1.2.3 Human foetal foreskin fibroblasts

Two sources of human foetal foreskin fibroblasts (HFFF2) were used for *in vitro* experiments. One batch was obtained in-house, whilst another batch was purchased from ECACC. At time of purchase, the cells were at passage 14, and used up to (but not exceeding) passage 20. Cells were seeded at a density of $3x10^4$ cells/ml, and cultured

in a monolayer in tissue culture flasks containing DMEM supplemented with 10% FBS, and 100 U/100 µg per ml Penstrep. Cells were grown in a humidified atmosphere, at 37°C, 5% CO_2, and culture medium was changed twice weekly. Cells were cultured and passaged (section 2.1.1.1). For stimulation assays, cells were trypsinised and passaged onto 6-well tissue culture plates. Refer to section 3.2 for details of individual experiments using HFFF2 cells.

2.1.3 ELISA of culture supernatants

Tissue culture supernatants were thawed and analysed for the presence of natural MMP-1, MMP-3, TIMP-1, CCL2 and CXCL8 released from cells using an ELISA (figure 2.2). Commercial kits were purchased from R&D Systems, Abingdon UK and performed as per manufacturer's instructions. The general ELISA protocol is described below, and details of individual assays given in Table 2.1.

Firstly, the capture antibody supplied within the kit was reconstituted with 1 ml sterile PBS to make a stock solution. This stock was subsequently diluted further to a suitable working concentration recommended by the protocol, and 100 µl of capture antibody was added to each individual well of a 96-well Immulon 4HBX flat-bottomed microtitre plate (Fisher Scientific, UK). The plate was sealed and incubated overnight at 4°C. Wells were aspirated and washed three times with a wash buffer solution containing 0.05% Tween® 20 (Sigma-Aldrich Ltd, Dorset, UK) in PBS, ensuring complete removal of liquid at each step for good ELISA performance. This was achieved by forcefully blotting plates onto tissue paper. The plate was then blocked for 1 hour with the addition of 200 µl 5% BSA (Affymetrix Ltd, High Wycombe, UK) in PBS. The aspiration/wash step was repeated before the addition of 100 µl of the samples to be tested, or serial dilutions of the standard provided. Samples and standards were diluted in a reagent diluent consisting of 1% BSA in PBS. Samples and standards were plated in duplicate. The plate was sealed and incubated 2 hours at room temperature. The aspiration/wash step was repeated, and 100 µl of the provided detection antibody (diluted to a working concentration in reagent diluent) was added to wells, and the plate was incubated for a further 2 hours. After another wash step, 100 µl of a working dilution of streptavidin-horseradish peroxidase (HRP; diluted in reagent diluent) was added to each well. The plate was covered and incubated for 20 minutes at room temperature, away from direct light. Finally, the plate was aspirated and washed again, before the addition of 100 µl SureBlue TMB (3,3',5,5'-tetramethylbenzidine) Microwell Peroxidase (Insight Biotechnology Ltd, UK) for 20 minutes, or until a sufficient colorimetric change had occurred. The reaction was terminated by the addition of 50 µl of a stop solution containing 1M sulphuric acid (H_2SO_4). The plate was read in a microplate reader set to 450 nm with a wavelength correction of 540 nm. The standard values were used to

generate a line of best fit, which was used to extrapolate protein titres in culture supernatants.

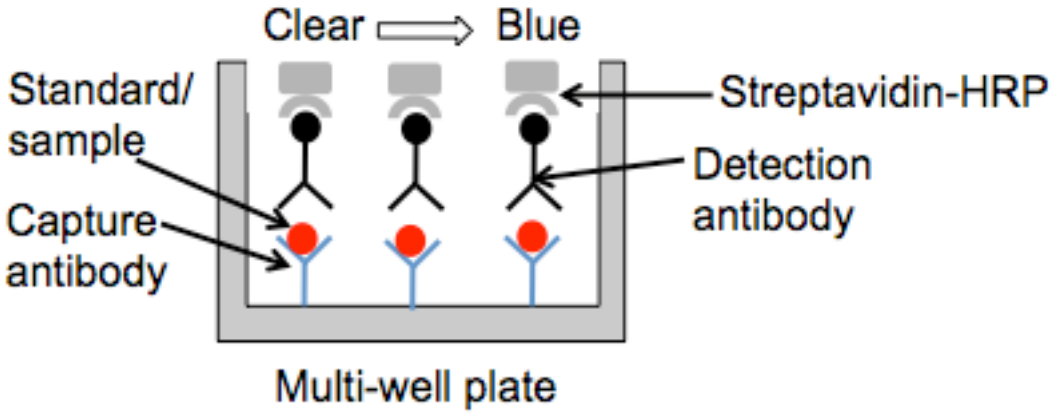

Figure 2.2 Enzyme-linked immunosorbent assay (ELISA)

The ELISA technique is used to quantify the amount of a protein of interest within a sample/solution. Firstly, the protein (antigen) in solution is affixed to the surface of the plate by a capture antibody, and then a specific detection antibody is applied over the surface, which binds with the standard/sample. Then, streptavidin attached to the enzyme horseradish peroxidase (HRP) is applied. Finally a TMB solution (a substrate for HRP) is applied, which results in a colorimetric change upon cleavage of the substrate by HRP. Between each step, the plate is washed with a mild detergent solution (e.g. PBS-TWEEN®) to remove any unbound proteins.

Table 2.1 Antibody concentrations and standards for human ELISA assays

ELISA assay	Capture antibody	Top standard concentration	Detection antibody
Human MMP-1 Cat no: DY901	Goat anti-human MMP-1 (Working solution: 2 µg/ml)	10,000 pg/ml	Biotinylated goat anti-human MMP-1 (100 ng/ml)
Human MMP-3 Cat no: DY513	Goat anti-human MMP-3 (0.8 µg/ml)	2,000 pg/ml	Biotinylated goat anti-human MMP-3 (100 ng/ml)
Human TIMP-1 Cat no: DY970	Mouse anti-human TIMP-1 (2 µg/ml)	2,000 pg/ml	Biotinylated goat anti-human TIMP-1 (50 ng/ml)
Human CCL2/MCP-1 Cat no: DY279	Mouse anti-human CCL2 (1 µg/ml)	1,000 pg/ml	Biotinylated goat anti-human CCL2 (100 ng/ml)
Human CXCL8/IL-8 Cat no: DY208	Mouse anti-human CXCL8 (4 µg/ml)	2,000 pg/ml	Biotinylated goat anti-human CXCL8 (20 ng/ml)

2.1.4 Quantification of NAD+

NAD^+ was quantified using both an in-house assay and a commercial kit, both based upon previously published NAD+ cycling assays (Hinz et al., 1973, Szabo, 1996, Ying et al., 2001). In essence they are based on the ability of NADH (the reduced form of NAD^+) to reduce thiazolyl blue tetrazolium bromide (MTT) to purple-coloured formazan. This results in a change in absorbance that can be detected spectrophotometrically. The resulting absorbance readings are proportional to NAD^+ levels within the sample (figure 2.3).

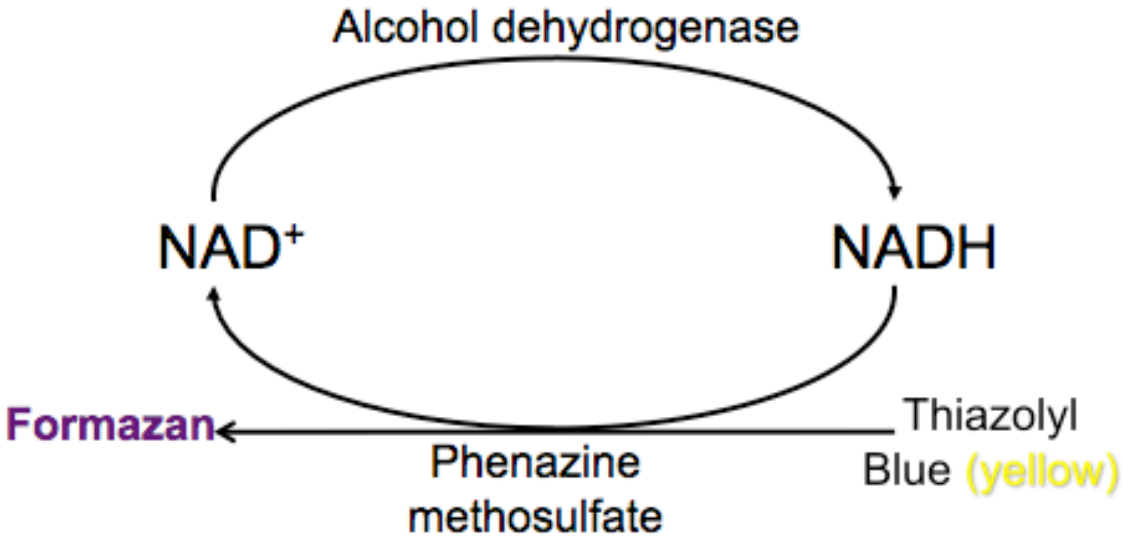

Figure 2.3 Principles of in-house NAD^+ detection assay

Samples extracted from actively-dividing human RASFs were tested for intracellular NAD^+ using a colourimetric detection assay. NAD^+ is rapidly reduced to form NADH by enzymatic cycling with alcohol dehydrogenase. In turn, NADH reduces MTT to purple-coloured formazan through the intermediation of electron carrier phenazine methosulfate.

2.1.4.1 In-house NAD^+ assay

All reagents for the in-house assay, unless otherwise stated, were purchased from Sigma-Aldrich Ltd. Firstly, medium was aspirated from cell monolayer cultures on 6-well plates, and cells were washed once in PBS. Cells were then treated with 750 µl 0.5 N ice-cold perchloric acid ($HClO_4$), to rapidly extract the metabolites of interest, and scraped at 4°C with a cell scraper. The solution was subsequently neutralised by the addition of 120 µl 3 M KOH/125 mM Gly-Gly buffer, pH 7.4. The cell solutions were mixed by pipetting and transferred to 1.5 ml microcentrifuge tubes. The mixtures were centrifuged at 10,000 x g for 2 minutes at 4°C. Finally, supernatants were collected and stored at -20°C for use in the NAD^+ cycling assay.

For the cycling assay, 25 µl of each sample was added in duplicate to a flat-bottomed 96-well plate. A standard solution of NAD^+ was prepared and diluted serially from a top standard of 30 µg/ml to 0.47 µg/ml and plated in duplicate. A cycling buffer (100 µl per reaction) was prepared fresh immediately prior to each assay, and consisted of the following: 0.1 mM MTT, 0.9 mM phenazine methosulfate, 13 units/ml alcohol dehydrogenase, 100 mM nicotinamide and 5.7% (v/v) ethanol in 61 nM Gly-Gly buffer. Nicotinamide was added to ensure complete recovery of the pyridine nucleotides within the extracts (Zerez et al., 1987), whilst the other components were needed for cycling to occur (figure 2.3). Upon addition of the cycling buffer, plates were covered and incubated

at room temperature for 10 minutes, and absorbance was read at OD_{595nm}. Standard OD values were plotted on a Michaelis menton non-linear regression curve using GraphPad Prism version 4.0a, and sample NAD^+ values were extrapolated from the curve.

2.1.4.2 Commercial NAD^+ assay

Intracellular NAD^+ levels were also quantified with a commercially-available NAD/NADH Assay Kit (Abcam®, Cambridge UK). The kit was used as per manufacturer's instructions. Firstly, cells were scraped and a small aliquot of the resulting suspension was taken to obtain a cell count, whilst the rest of the cell suspension was pelleted at 400 x g for 5 minutes. The supernatant was removed and 1 ml of ice- cold PBS was added, and cells were pelleted again at 400 x g for 5 minutes at 4°C. The PBS was removed and replaced with 400 µl of NAD/NADH extraction buffer and cells were extracted by two freeze/thaw cycles (20 minutes on dry ice, then 10 minutes at room temperature). Extractions were vortexed for 10 seconds and then centrifuged at 20,000 x g for 5 minutes. The supernatants were transferred to 10 kDa molecular weight cut-off filters (Millipore Ltd, Watford, UK) and centrifuged at 20,000 x g until the buffer had passed through the filters. Finally, samples were kept on ice and assayed immediately.

For the assay, 10 µl of a 1 nmol/µl standard was diluted with 990 µl NADH/NAD extraction buffer to generate a 10 pmol/µl standard NADH. Varying quantities of the standard were added in duplicate to wells of a 96-well plate, and diluted further with extraction buffer to generate 0, 20, 40, 60, 80 and 100 pmol/well standards. To detect total NADt (total NADH and NAD^+), 50 µl of extracted samples were transferred into the 96-well plate in duplicate. To detect NADH, an additional 200 µl of extracted samples were heated to 60°C for 30 minutes to decompose NAD^+, before cooling on ice. These NAD^+ decomposed samples were transferred to the 96-well plate in duplicate along with NADt extracted samples.

Once standards and samples were plated, a NAD^+ cycling mix was prepared with 100 µl cycling buffer mix and 2 µl NAD^+ cycling enzyme mix per reaction, and 100 µl was added to each well. Wells were mixed and the plate incubated at room temperature for 5 minutes to convert NAD^+ to NADH, before adding 10 µl NADH developer into each well. The reaction continued to develop for 1-4 hours before the absorbance was read at an optical density of 450 nm in a FLUOstar Optima plate reader (BMG Labtech Ltd, Aylesbury, UK). Once the plate was read, sample readings were applied to a NADH standard curve and amounts of NADt and NADH in the samples were calculated. The concentration of NAD^+ was determined as follows:

NAD^+ = Total NADH - NADH.

NAD^+ yields were normalised to cell count and expressed as pmol/10^6 cells.

2.1.5 Bovine tissue culture

2.1.5.1 Bovine articular cartilage preparation and culture

Articular cartilage was obtained from the metacarpophalangeal /metatarsophalangeal (MCP/MTP; hock) joints of freshly slaughtered 7-day old calves from F. Drury and Sons Ltd (Swindon, UK). Immature bovine cartilage was used for all *ex vivo* culture studies, as it is thicker and easier to harvest than articular cartilage from mature joints, and has a greater abundance of chondrocytes (Stockwell, 1971). In preparation for tissue culture, hocks were cleaned thoroughly with tap water, soap and a brush, and sprayed with 70% ethanol and microSol 3+ (Anachem Ltd, UK). Skin was removed using a non-sterile number 3 scalpel handle with number 10 surgical blade**.** A chainmail glove was worn on the other hand to safeguard against injury whilst cutting the tissue. Once skin was removed, both ends of the hind limb were covered with sterile rubber gloves or foil and the surface sprayed once again with 70% ethanol and microSol 3+. Once the joints had been prepared for dissection under sterile conditions, all further work was carried out in a Class I tissue culture cabinet using aseptic technique. All utensils used for cartilage extraction were sterilised prior to use by autoclaving at 121°C for 30 minutes. To obtain full-depth cartilage explants of a consistent size and weight (76 ± 1.8 mg), articular cartilage cores were taken using a 6 mm biopsy punch. The explants were released from the subchondral bone with the aid of a scalpel, ensuring that the cores contained the full-depth of cartilage, including the basal calcified cartilage tissue. Throughout the procedure scalpel blades and other surgical utensils were routinely washed in 70% ethanol, followed by a wash in sterile PBS, to reduce the risk of contamination. Cartilage explants were weighed and then immersed in prepared culture medium consisting of DMEM supplemented with 100 U/100 µg/ml Penstrep, and 50 µg/ml gentamicin (all from Gibco, Life Technologies Ltd, Paisley, UK). For each experiment, three explants were rapidly fixed in 4% paraformaldehyde solution to serve as time zero (T_0) experimental controls, and processed for histology (see section 2.3.1).

Full-depth cartilage explants were pre-incubated in culture medium containing 5% heat-inactivated FBS (Gibco Life Technologies Ltd, Paisley, UK) at 37°C in 5% CO_2 for 72 hours to enable the cartilage to equilibrate prior to *ex vivo* culture. During this period, media were refreshed every 24 hours. Cartilage explants were then washed twice in sterile PBS, weighed individually and aseptically, before culturing in experimental medium (figure 2.4). Each explant was placed individually into a well of a 48-well plate. Unless otherwise stated, three explants were used for each experimental condition (n=3). Cultures were maintained for the required number of days, with medium change every 48 hours, including culture medium supplemented with IL-1ß. This continual cytokine assault was carried out to mimic the chronic inflammatory environment within

the RA joint, comparable to that performed in related studies (Sondergaard et al., 2006, Karsdal et al., 2008, Wang et al., 2009a). Tissue was processed for papain digestion (see below) or histology (section 2.3.1), and culture media were collected and stored at -20°C until required.

Cartilage was papain digested for dimethylmethylene blue (DMMB) analysis (refer to section 2.1.5.2) using the following method. Cartilage was placed into a stock buffer (0.05 M sodium acetate, 0.025 M Na_2EDTA, pH 5.6) containing 5 mM Cysteine-HCl and 1 unit of papain suspension from *papaya latex* per ml of buffer (all reagents purchased from Sigma-Aldrich). 1 ml of buffer was used per 100 mg cartilage to be digested. Cartilage samples in buffer were then incubated at 65°C for 18 hours, with occasional mixing. Once digestion was completed, samples were boiled for 15 minutes, and then left to cool at room temperature. Finally, samples were stored at -20°C until needed.

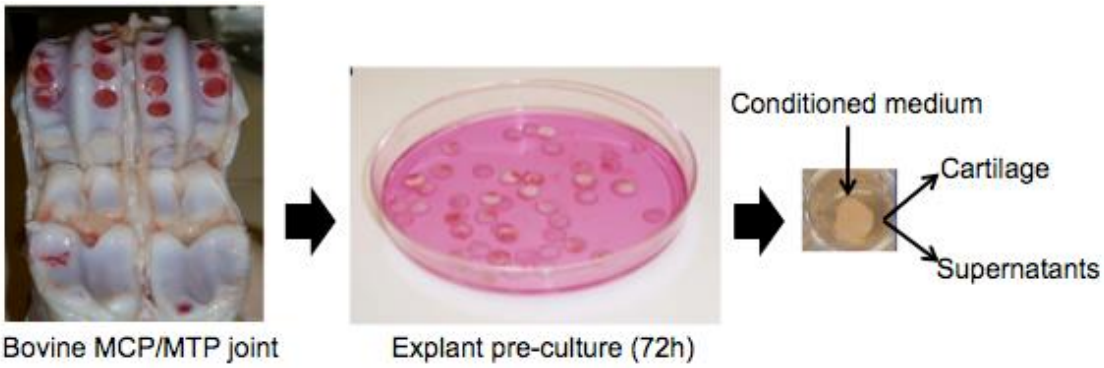

Figure 2.4 Cartilage explants in *ex vivo* culture system

Cartilage explants taken from the bovine MCP/MTP joint using a biopsy punch were prepared for *ex vivo* culture in supplemented medium. Both cartilage and explant supernatants were analysed to assess cartilage integrity.

2.1.5.2 DMMB assay

A colorimetric assay was used to quantify levels of s-GAG in culture supernatants and cartilage extracts as described previously (Farndale et al., 1986). Within the cartilage ECM, degradative enzymes such as MMPs and ADAMTSs can cleave PGs such as aggrecan resulting in a loss of s-GAG (refer to section 1.2.4) which is detectable in the culture supernatant of explant cultures (figure 2.5). The DMMB assay is based on the ability of s-GAGs to bind to 1,9-dimethylmethylene blue, which results in a shift in its absorption spectrum. Total GAG remaining in the tissue was also analysed using the DMMB assay, following papain extraction (section 2.1.5.1).

A solution of 1,9-dimethylmethylene blue was prepared by dissolving 32 mg DMMB in 20 ml absolute ethanol overnight, and making up to 2 L with 59 ml 1M NaOH, 7 ml 98% formic acid and MilliQ water. The solution was stirred and the absorbance readings at 525 nm and 592 nm were checked. Absorbance readings of 0.3 and 1.4 respectively suggested that the dye was sufficiently dissolved and the solution was stored at room temperature ready for use. Standard curve solutions were prepared fresh for each set of assays using Chondroitin Sulphate C from shark cartilage (Sigma-Aldrich Ltd, Dorset, UK). Solutions of 0, 10, 20, 30 and 40 µg/ml in DMEM were prepared and 40 µl plated in triplicate into wells of a flat-bottomed 96-well microtitre plate (Nunc, Thermo Scientific, UK). Samples were plated in duplicate at a volume of 40 µl at 1:10 and 1:100 dilutions respectively. Using a multi-channel pipette, 200 µl of DMMB solution was added to all wells and plates were read immediately at 525 nm using the FLUOstar Omega microplate reader (BMG Labtech Ltd, Aylesbury, UK). From the standard curve the concentrations of total s-GAG in µg/ml were determined, and values were subsequently adjusted for explant wet weight (µg/ml per mg of cartilage). Samples outside the dynamic range (i.e. greater than 40 µg/ml) were adjusted for concentration accordingly and re-analysed.

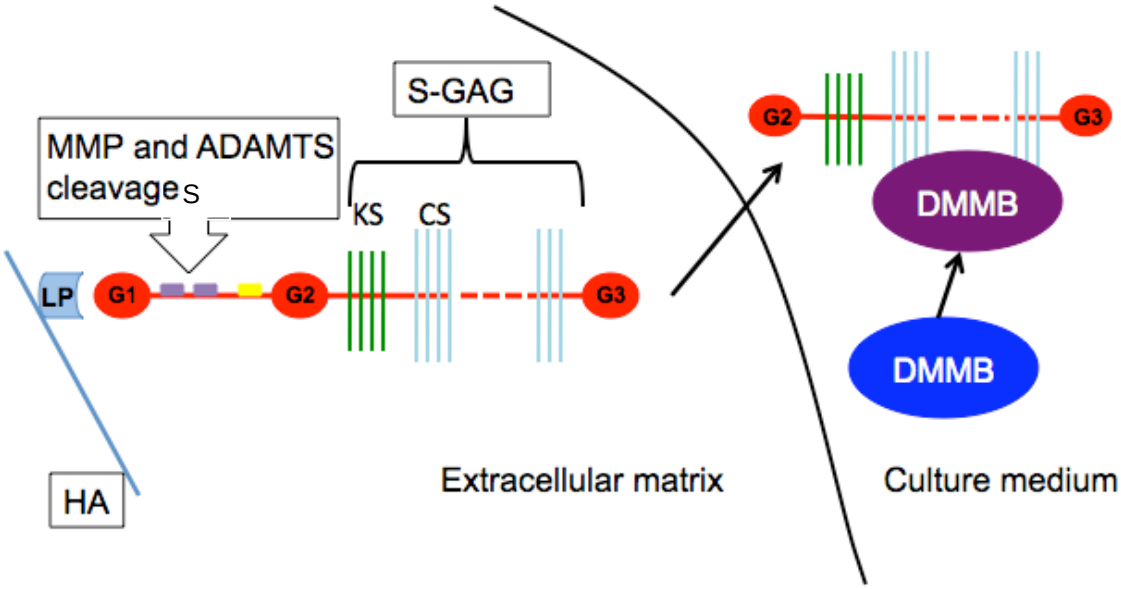

Figure 2.5 Principles of DMMB s-GAG detection assay

Sulphated GAGs are cleaved from the aggrecan core protein by matrix-degrading enzymes such as MMPs and ADAMTSs, and released from the cartilage ECM into the surrounding culture media. The amount of s-GAG release can be detected using DMMB, a heterochromatic dye that rapidly changes colour upon binding to s-GAG. HA, hyaluronan; LP, link protein; KS, keratan sulphate; CS, chondroitin sulphate; G1, 2, 3, globular domains.

2.1.5.3 Gelatin zymography

Explant culture supernatants from *ex vivo* studies were analysed for MMP expression and activity using gelatin zymography (figure 2.6). The technique used was based upon a protocol devised by Leber and colleagues (Leber and Balkwill, 1997). Firstly, a 7.5% sodium dodecyl sulphate-polyacrylamide (SDS-PAGE) resolving gel containing 1 mg/ml gelatin was prepared (Table 2.2). Commercially-available premixed buffers were used whenever possible for ease of use and consistency. The gel mixture was mixed by pipetting to avoid the addition of oxygen (which inhibits the polymerisation process), before casting in a Bio-Rad mini-PROTEAN casting system (Bio-Rad Laboratories Ltd, Hertfordshire, UK). The resolving gel was overlaid with dH_20, to ensure the interface between the stacking and resolving gels was smooth and level. Once the resolving gel had set, the water was poured away and a stacking gel (prepared as in Table 2.3) was overlaid and set using a 10-well comb insert to enable sample loading. This facilitates stacking of the samples and ensures they run evenly down the resolving gel (Schagger, 2006).

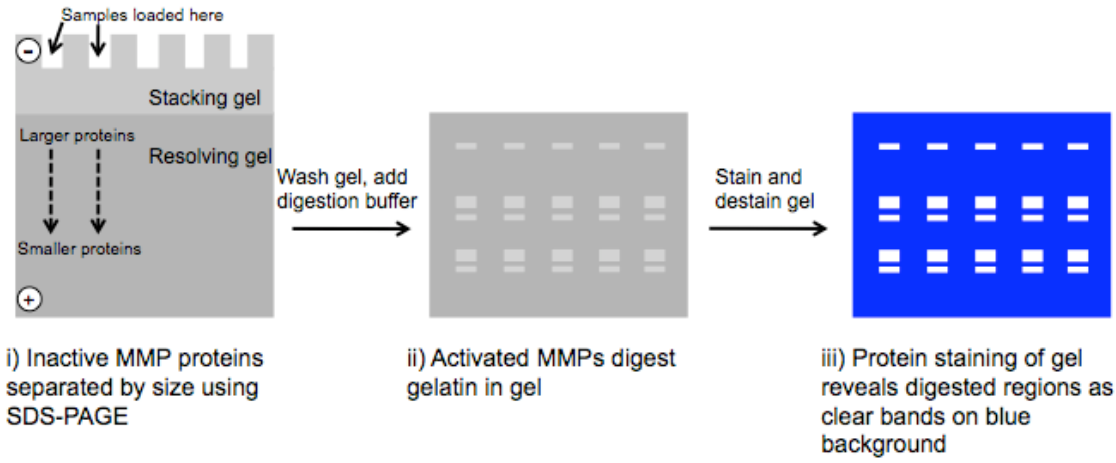

Figure 2.6 Principles of gelatin zymography

Samples are loaded onto an SDS-PAGE gel and proteins within the samples are separated on the basis of size by running through a resolving gel containing gelatin. Gels are washed in detergent to remove SDS, thus allowing enzyme renaturation, and a digestion buffer containing $CaCl_2$ activates enzymes in the gel, enabling them to digest the gelatin embedded within the gel. Staining the gelatin with coomassie blue reveals areas of zymogen activity.

Table 2.2 Reagents and suppliers for 10 ml 7.5% gelatin SDS-PAGE resolving gel.

Ingredient	Volume	Supplier
Acrylamide/bis-acrylamide 40% solution (cat no: A7168)	1.875 ml	Sigma-Aldrich Ltd, Dorset, UK
4x Protogel resolving buffer (1.5 M Tris-HCl, 0.4% (w/v) SDS, pH 8.8) (cat no: EC-892)	2.5 ml	National Diagnostics UK, Yorkshire, UK
dH_2O	5.515 ml	n/a
50 mg/ml solution Type B gelatin from bovine skin, dissolved in dH_2O (cat no: G9382)	200 µl	Sigma-Aldrich Ltd, Dorset, UK
10% Ammonium persulphate (APS), dissolved in dH_2O (cat no: A3678)	100 µl	Sigma-Aldrich Ltd, Dorset, UK
N,N,N′,N′-Tetramethylethylenediamine (Temed) (cat no: T9381)	10 µl	Sigma-Aldrich Ltd, Dorset, UK

Table 2.3 Reagents and suppliers for 5 ml 4% SDS-PAGE stacking gel

Ingredient	Volume	Supplier
Acrylamide/bis-acrylamide 40% solution	0.65 ml	Sigma-Aldrich Ltd, Dorset, UK
Protogel stacking buffer (0.5 M Tris-HCl, 0.4% (w/v) SDS, pH 6.8 (cat no: EC-893)	1.25 ml	National Diagnostics UK, Yorkshire, UK
dH_2O	3.05 ml	n/a
10% Ammonium persulphate (APS)	25 µl	Sigma-Aldrich Ltd, Dorset, UK
N,N,N′,N′-Tetramethylethylenediamine (Temed)	5 µl	Sigma-Aldrich Ltd, Dorset, UK

Cast gels were placed into the Mini-PROTEAN tetra electrophoresis module along with a 1X solution of running buffer comprising 25 mM Tris, 192 mM glycine, 0.1% (w/v) SDS, pH 8.3. Explant culture supernatants were thawed, and 10 µl of each sample was mixed with 5 µl of a non-reducing sample buffer containing 0.5 M Tris-HCl, 10% (v/v) glycerol, 10% SDS and 0.05% (w/v) bromophenol Blue (all from Sigma-Aldrich Ltd, Dorset, UK). The resulting mixtures were carefully loaded into wells of the stacking gel. The gels were run at 150 V and 20 mA per gel for 2 hours, or until the dye front had run to the bottom of the gel.

Gels were carefully removed from between the glass casting plates, and washed three times in 2.5% Triton X-100 solution (Sigma-Aldrich Ltd, Dorset, UK) for 15 minutes, to ensure the complete exchange of SDS with Triton X-100. Gels were then incubated for 18 hours at 37°C in a digestion buffer containing 100 mM $CaCl_2$. Following this, gels were washed briefly in dH_2O and stained for 1 hour in a solution containing 10% acetic acid, 45% methanol (Fisher Scientific) and 0.25% (w/v) Coomassie Brilliant Blue R (Cat no: B0149; Sigma-Aldrich). Finally, gels were destained in a solution of 10% acetic acid and 45% methanol, until clear bands were visible on a blue background (figure 2.7).

Gels were scanned using the Kodak FX Pro Imaging system. UV epi-illumination images were taken against a white background, captured using an exposure time of 1 second, F-stop 2.51. Images were analysed using the Carestream Molecular Imaging software v 5.3.2 (Carestream Health UK Ltd, Herts, UK). Band boundaries incorporated regions of pro and active MMP-2 or MMP-9. Background was corrected, and identified bands were quantified for net intensity.

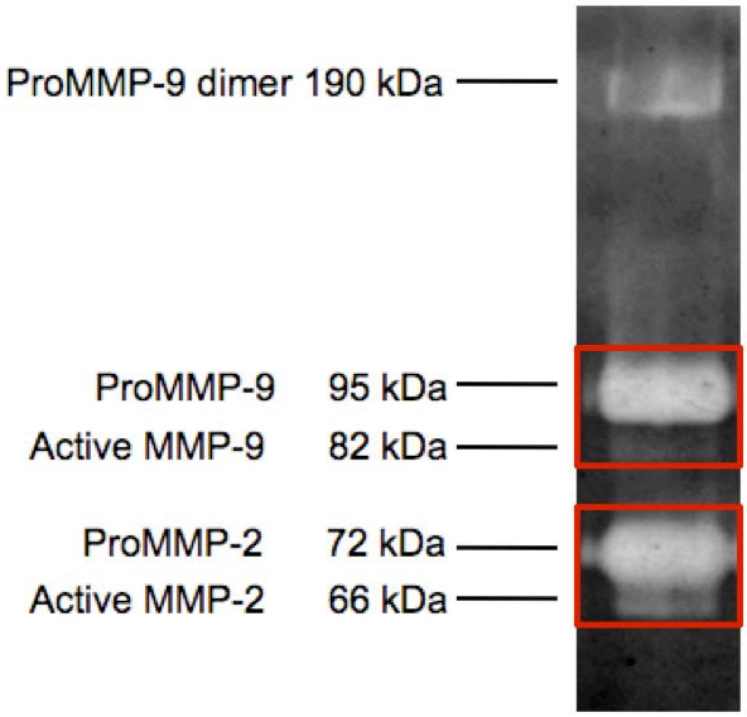

Figure 2.7 A representative gelatin zymogram

A lane from a zymogram demonstrating a typical banding pattern revealed following digestion and staining of gelatin gels. The bands detected and their molecular weights are shown. Red squares indicate regions of interest used to determine total MMP-9 and MMP-2.

2.1.5.4 Histological assessment of PG depletion

Fixed articular cartilage explants were placed into tissue processing/embedding cassettes (Simport Scientific, QC, Canada), sandwiched between foam pads to secure them within their cassettes, and processed overnight for histology (section 2.3.1). Full-depth serial sections (7 µm thick) were cut so that all zones of the articular cartilage were evident, and stained with Safranin O/Fast green.

Bovine cartilage explant sections were digitally scanned and examined for the degree of Safranin O staining retention. A percentage of PG loss was estimated from the proportion of Safranin O to Fast Green. Explant sections with full retention of Safranin O staining and no visible Fast Green staining were scored 0 % PG loss. Conversely, sections exhibiting no visible Safranin O staining were deemed to have complete (100%) PG loss (figure 2.8). Explant images were also analysed using the Leica QWin V3 digital processing software (Leica Microsystems Ltd, Bucks, UK). A macro program was designed to automatically detect regions of the image containing Safranin O staining (figure 2.9). The proportion of staining in the entire image was calculated as a percentage, and from this, PG loss was determined.

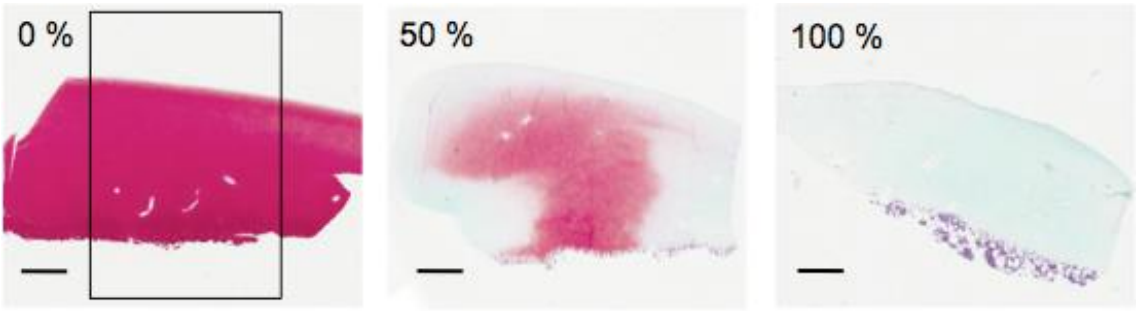

Figure 2.8 Histological assessment of proteoglycan depletion

Representative cartilage histological sections stained with Safranin O/Fast Green, exhibiting 0%, 50% and 100% proteoglycan loss. The rectangle indicates the region the of explant section studied for qualitative analysis, Scale bars indicate 500 µm.

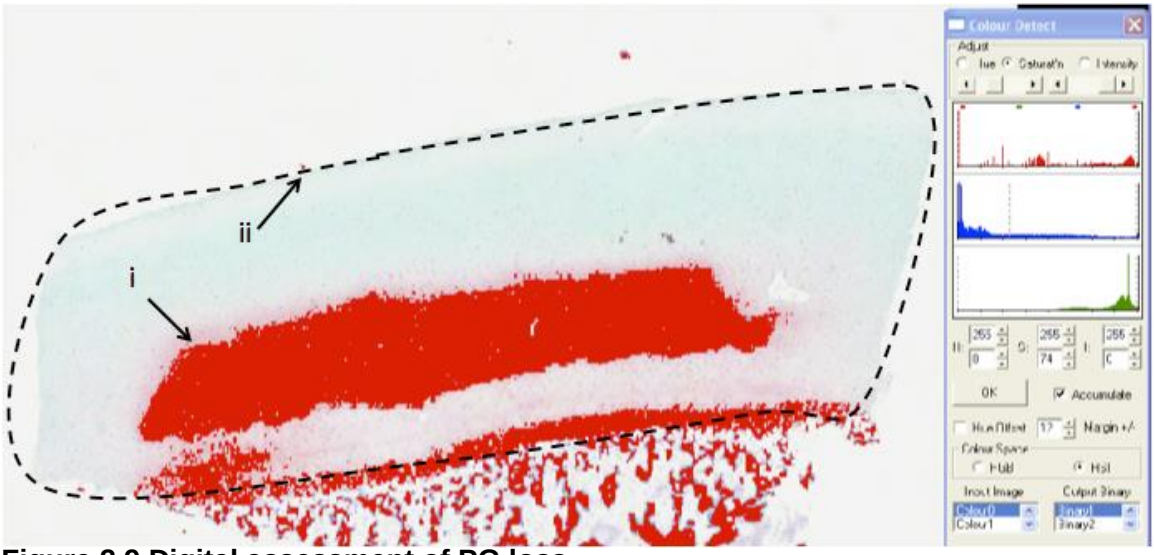

Figure 2.9 Digital assessment of PG loss

Imaging software was used to highlight regions containing staining of a certain hue (i), and the proportion of staining was determined within a defined region of interest (ii). Regions containing sub-chondral bone were excluded from the analyses.

2.1.6 Cell viability assays

In this thesis, two methods of determining cell viability were performed: the MTT assay and the LDH assay (see below). The MTT assay is a well-established technique that is widely used to analyse cell viability in monolayer culture (Cree et al., 2011). However, this method requires that all cells are lysed in order to quantify cytotoxicity, making it unsuitable for monitoring explant cell viability over time. Cell viability was therefore monitored in explants using the commercially-available LDH membrane integrity assay. In contrast to the MTT assay, the LDH assay measures leakage of components into the culture medium, making it applicable to longitudinal analyses of cell viability.

2.1.6.1 MTT cell viability assay

The MTT assay is based on the ability of mitochondrial dehydrogenase within living cells to cleave the tetrazolium rings of pale yellow thiazolyl blue tetrazolium bromide (MTT), to form purple formazan crystals (see figure 2.10). These crystals, impermeable to cell membranes, accumulate within healthy cells. Lysing cells with the addition of a detergent causes release and subsequent solubilisation of the formazan product. This colorimetric change can be used to determine the proportion of surviving cells within a culture dish.

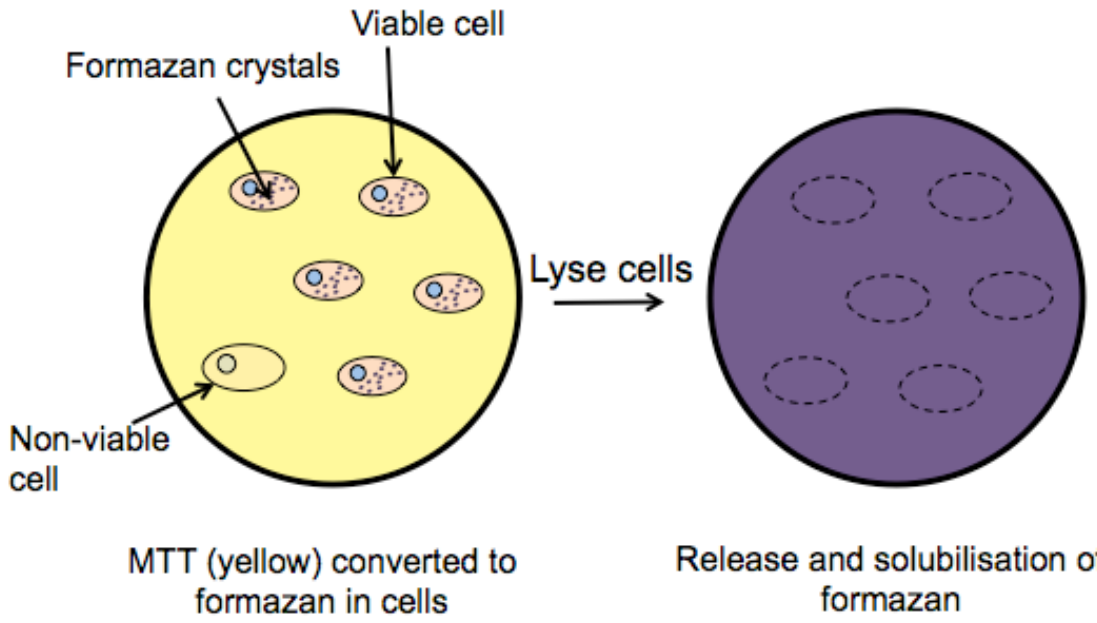

Figure 2.10 The MTT viability assay

Cells in a tissue culture dish convert pale yellow MTT into purple formazan crystals that accumulate within the cytoplasm. Non-viable cells do not create and accumulate formazan. Lysing the cells liberates the crystals, and the resulting formazan product is reflective of the proportion of viable cells within the culture dish.

For the MTT assay, medium was removed from monolayer culture and replaced with 500 µl DMEM containing 1 mg/ml thiazolyl blue tetrazolium bromide (MTT; Cat no M2128; Sigma UK). Cells were incubated for 4 hours at 37°C, 5% CO_2 to allow the MTT to be incorporated into cells and converted to formazan. Medium was removed and tissue culture plates were blotted onto tissue to remove excess MTT solution. Cells were lysed by the addition of 500 µl DMSO to each well. The resulting solutions were mixed thoroughly and added in duplicate to a flat-bottomed 96-well microtitre plate (100 µl per well) and the plate was read at 540/570 nm. A 100 µl aliquot of DMSO served as a blank control. Every OD value obtained was calculated relative to an untreated control well.

2.1.6.2 LDH membrane integrity assay

Cell viability is often defined based on the integrity of the cell membrane; therefore the measurement of leakage of components from the cytoplasm into the surrounding culture medium is a widely-accepted method for estimating viability. The CytoTox-ONE™ Homogenous Membrane integrity assay (Cat no: G7890; Promega UK, Southampton, UK) is a well-established method for measuring the release of LDH from damaged cells within the cartilage ECM. LDH is readily released from chondrocytes

(Peters et al., 2011), and its enzymatic activity is such that its conversion of lactate to pyruvate can be easily coupled with the generation of a fluorescent product called resofurin (figure 2.11). This technique has been successfully applied to cartilage explants in previous studies (Ailland et al., 2003, Hoffler et al., 2006, Devkota and Weinhold, 2010).

The assay was performed as per manufacturer's instructions. Prior to the assay, explant culture supernatants to be tested were thawed and equilibrated to room temperature. A reagent mix was prepared by the addition of 11 ml of a supplied assay buffer to a lyophilised substrate mix. The resulting CytoTox-ONE™ reagent mix was left to equilibrate to room temperature. Test samples (100 µl per well) were added in duplicate to wells of an opaque-walled 96-well plate. In addition to test samples, the following controls were added in triplicate: a medium control (containing DMEM:F12 only) and a maximum LDH release control. For explants, maximum LDH control samples were made by the addition of a lysis solution (9% (w/v) Triton™ X-100 in dH2O) to explants in culture medium. Explants were incubated for 48 hours, before supernatants were removed and stored at -20°C for use in the LDH assay. For LDH analyses of cell monolayer cultures, the lysis solution was added to cells and left for 5 minutes, or until all cells had been lysed and had released the maximal potential amount of LDH into the surrounding culture medium.

Once all controls and samples had been plated, an equal volume of CytoTox-ONE™ reagent mix was added to each well, and the plate was protected from light and left to shake at 500 rpm for 10 minutes at room temperature. At the end of the incubation period, 50 µl of a supplied stop solution was added to each well, as recommended within the protocol to ensure consistency. Finally, fluorescence was measured using a FLUOstar Optima fluorescent plate reader (BMG Labtech Ltd, Aylesbury, UK) with excitation wavelength 560 nm and an emission wavelength of 590 nm. The average fluorescence values (rfu) of the background (culture medium) were subtracted from all the fluorescence values of the experimental and maximum LDH wells. From the resulting fluorescence readings, the percent cytotoxicity for each given treatment was determined as follows:

Percent cytoxicity = 100 x (Experimental sample / Maximum LDH release)

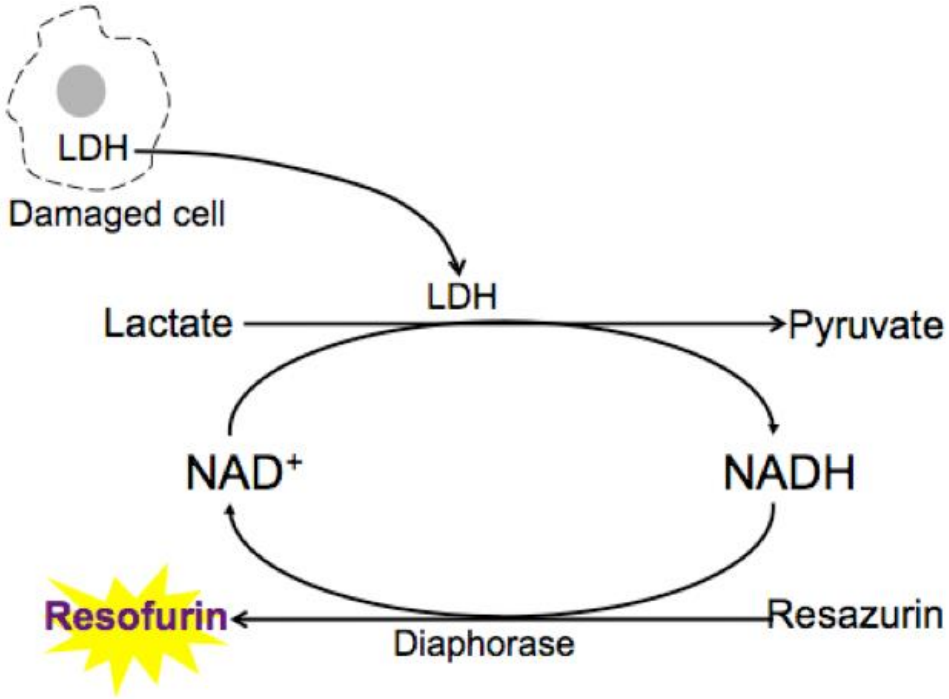

Figure 2.11 Principles of LDH membrane integrity assay

Schematic demonstrating how LDH released from damaged/leaky cells reacts with the substrates lactate, NAD^+ and resazurin in the presence of the oxidoreductase enzyme diaphorase. The generation of the fluorescent product resofurin is proportional to the amount of LDH.

2.2 *In vivo* experiments

2.2.1 Collagen-induced arthritis

Experimental arthritis was performed in accordance with the Home Office approved project licence (PPL-30/2361). Aged 7-8 week old DBA-1 mice were immunised intradermally (i.d.) at day 0 with 100 µl 1 mg/ml of type II collagen from chick sternal cartilage (Sigma-Aldrich Ltd, Dorset, UK) dissolved overnight in 10 mM acetic acid and emulsified in Freund's complete adjuvant (FCA). FCA was made by grinding 100 mg *Mycobacterium Tuberculosis* H37Ra (BD Biosciences, Oxford, UK) to a fine powder using a pestle and mortar, and mixing with a 10 ml vial of Freund's incomplete adjuvant (Sigma-Aldrich Ltd, Dorset, UK). Once prepared, 2.5 ml of the FCA was combined with 2.5 ml of the dissolved collagen and mixed until an emulsion was formed. Once induced, the immune response to collagen was boosted 21 days later (day 21) with a second intradermal injection of type II collagen in FCA. If no clinical signs of arthritis were observed by day 25, animals were each given a single intra-peritoneal (i.p.)

injection of 20 μg LPS dissolved in 100 μl of PBS to potentiate the onset of disease (Caccese et al., 1992), as outlined in the project licence. Experiments were performed using 3-10 mice per study. Limbs were removed for analyses and either placed in fixative (for use in histology), or snap-frozen on dry ice and stored at -80^{o}C (for use in quantitative PCR). In one experiment blood was taken for sera analyses (see section 2.2.1.4).

2.2.1.1 Clinical score and paw diameter

Animals were observed at least twice a week from day 21 for the development or arthritis. Arthritis was scored in each animal in a blinded manner using an established subjective clinical score: 0, normal; 1, mild/moderate erythema and swelling; 2, severe erythema and swelling affecting entire paw or joint; 3, up to three joints affected by arthritis; 4, greater than three joints affected by arthritis; 5, deformed paw or joint with ankylosis. Each paw was graded 0-5 and the total score for each mouse determined to give the clinical score. Any animal with a paw score of 5 in any one paw or a combined clinical score exceeding 14 was removed from the experiment and humanely killed, as outlined within the project licence. Hind paw ankle swelling was measured using a modified POCO 2T spring caliper gauge (Kroeplin Längenmesstechnik, Germany). In addition to clinical score and paw diameter, individual weights of the animals were monitored. Animals exhibiting >20% weight loss in two consecutive weigh-ins (compared to weight at the onset of arthritis) were removed from the experiment and humanely sacrificed.

2.2.1.2 Radiology

High power x-ray images of hind and front paws were carried out using a Kodak FX Pro *in vivo* imaging system and Kodak Molecular Imaging software. Images were captured using an exposure time of 60 seconds at 35KVP, f-stop 4, Field of view (FOV) 80 mm. Radiological damage was scored in each limb in a blinded manner, based on a comprehensive scoring system validated by both a clinical Rheumatologist and an Orthopaedic Registrar (Smale *et al*, unpublished). In the forefoot, 2nd-4th proximal interphalangeal joints (PIPs) were scored for visible soft tissue swelling, based on the ratio of soft tissue to bone (scored 0-2 per joint, figure 2.12A[i]). The 1st-5th MCPs were assessed for erosion, osteopenia and periosteal reaction, and each scored 0 (no evidence) or 1 (evidence) for each parameter (figure 2.12A[ii]). The base of the 1st metatarsal in the hind paw (figure 2.12A[iii]) and the 5th metatarsal in the fore paw (figure 2.13B[i]) were scored for erosion, osteopenia and periosteal reaction, with each parameter scoring 0 (no evidence) or 1 (evidence). In the midfoot the 2nd distal tarsal (hind paw, figure 2.12A[iv]) or the 3rd distal tarsal (front paw, figure 2.12B[ii]) were scored for joint space loss and osteopenia, with each parameter scoring 0 (no evidence) or 1 (evidence). Finally, in the hindfoot hind paws were scored for joint space loss between

the fibulare and 4th and 5th distal tarsals and intermedium and centrale (figure 2.12A[v]). The front paws were scored similarly for joint space loss between the radial epiphysis and fused radiale and intermedium (figure 2.12B[iii]). The bones surrounding each of these joint lines were also scored for osteopenia. Each parameter was scored 0 (no evidence) or 1 (evidence). The maximum total radiology score obtainable with the above system is 30 and 28 for hind and front paws, respectively.

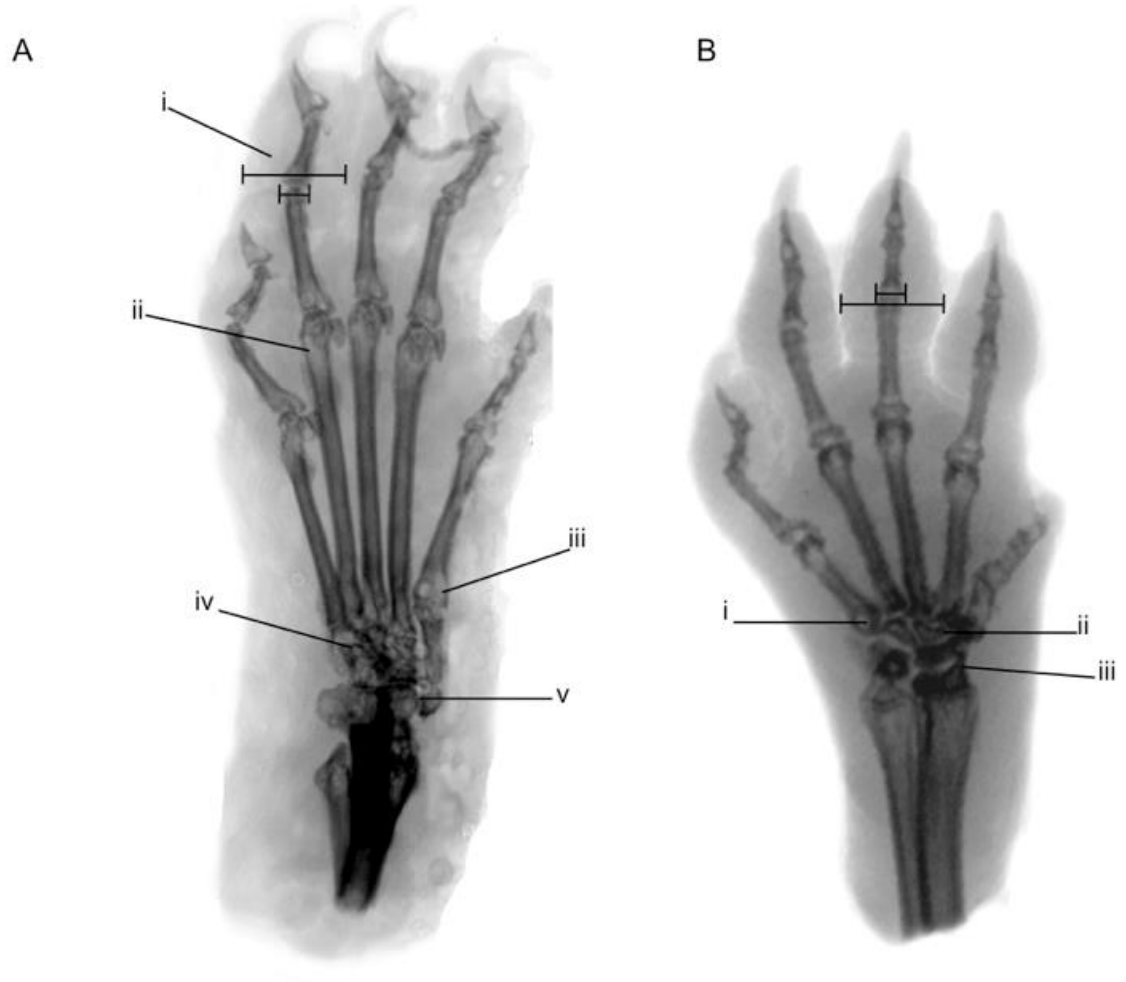

Figure 2.12 High power radiographic images

X-ray of a hind paw (A) and a front paw (B) from an arthritic animal, with the main features used for scoring indicated. A: [i] Proximal interphalangeal joints, showing how the extent of soft tissue swelling is determined; [ii] The 4th metacarpophalangeal joint; [iii] The base of the 1st metatarsal; [iv] The 2nd distal tarsal and [v] The loss of joint space between the fibulare and 4th and 5th distal tarsals and intermedium and centrale. B: [i] The base of the 5th metatarsal; [ii] The 3rd distal tarsal; [iii] Radial epiphysis and fused radiale and intermedium.

2.2.1.3 Histopathology

The bases of the hind limbs were slit with a scalpel blade prior to tissue processing, to aid in the penetration of fixative. Limbs were then placed in tissue processing/embedding cassettes (Simport Scientific, QC, Canada), fixed in neutral formal buffered saline (NFBS) and decalcified with formic acid at 4˚C for 48 hours. An X-ray was performed on joints as in section 2.2.1.2 to determine whether tissue was completely decalcified. Tissue was then processed as described in section 2.3.1 before processing the tissue overnight. Mid-coronal serial sections (7 µm thickness) were sectioned and stained with Safranin-O/Fast Green (section 2.3.1).

Histology sections were scored according to an adaptation of an established scoring method (Nowell et al., 2003). Firstly, inflammatory cells within the synovial tissue were scored as follows: 0, normal adipose tissue with no inflammatory infiltrate; 1, focal inflammatory infiltrate and adiposity hardly affected; 2, random inflammatory infiltrate equalling adiposity; 3, inflammatory infiltrate dominating the tissue; 4, substantial infiltrate with severe loss of adiposity; 5, ablation of adiposity due to infiltrate (figure 2.13A). Secondly, synovial exudate was scored as follows: 0, normal; 1, evidence of inflammatory cells in space; 2, moderate numbers of inflammatory cells in space, possibly evidence of fibrin deposits; 3, substantial numbers of inflammatory cells with large fibrin deposits (figure 2.13B). Finally, articular cartilage/subchondral bone erosion was scored as follows: 0, no cartilage erosion and retention of Safranin O staining; 1, some loss of Safranin O staining from superficial zone of cartilage; 2, substantial loss of Safranin O staining and some erosion; 3, extensive loss of Safranin O staining with severe erosion (figure 2.13C). Forefoot histology (comprising the MCP joints) and mid/hindfoot histology (including the bones of the midfoot) were scored separately, and the mean scores calculated for each parameter. The maximum total histology score available is 11.

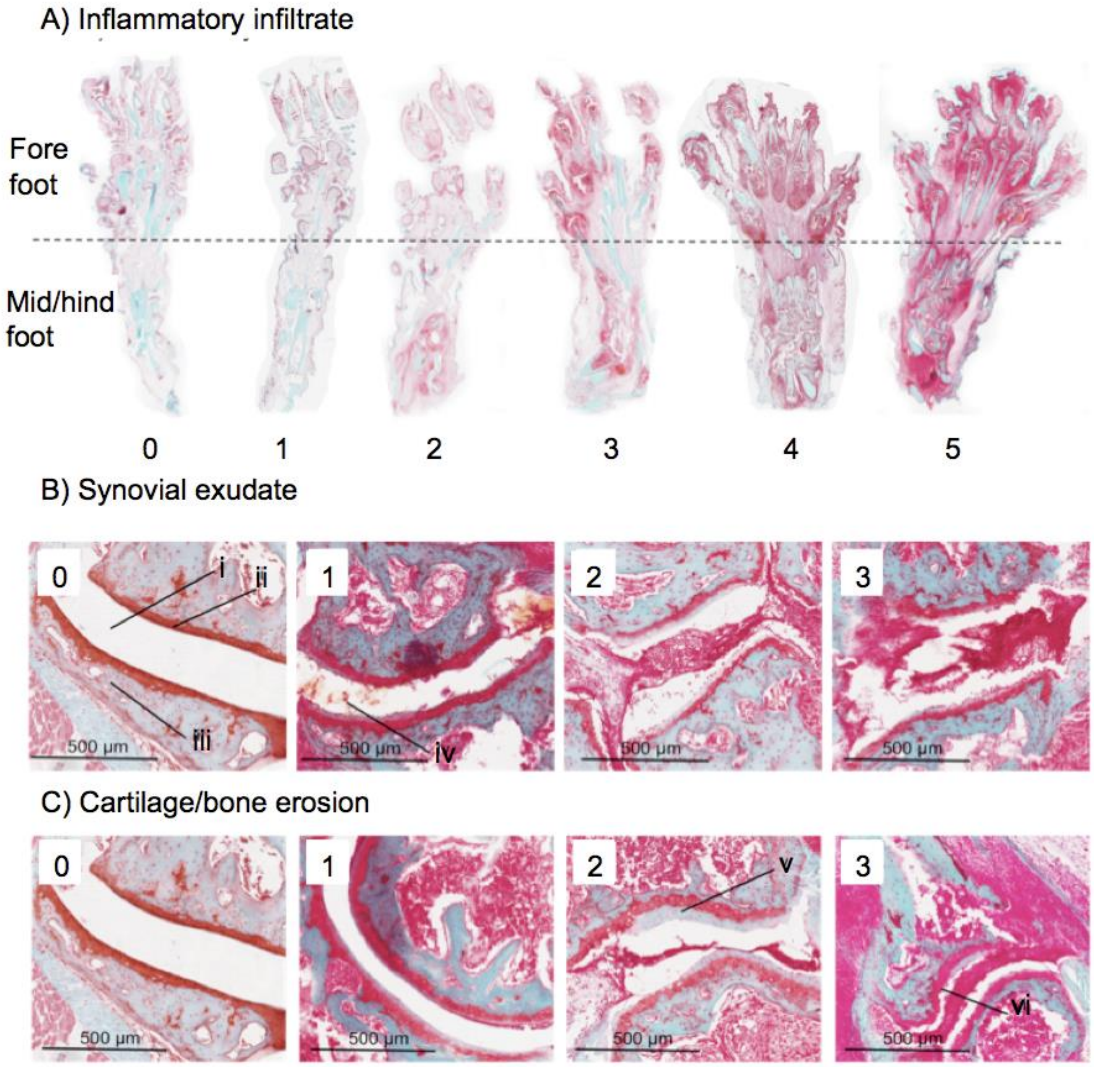

Figure 2.13 Histology scoring system

A) Representative Scanscope images of hind paw histological sections, showing the progression of infiltrate score from 0-5. Forefoot and hindfoot regions were scored separately. B) High power images of joints of the midfoot, showing progress of extent of synovial exudate, from 0-3. [i] joint space; [ii] cartilage; [ii] sub-chondral bone; [iv] evidence of synovial exudate in the joint space. C) High power images demonstrating the progression of joint erosion from 0-3. [v] proteoglycan loss from cartilage; [vi] evidence of cartilage erosion.

2.2.1.4 Serum analysis

Sera samples taken from mice were tested by ELISA for the presence of collagen type II (CII)-specific IgG2a, a marker of the antibody response to collagen. All blood sampling was taken when animals were sedated under anaesthetic nose cone. Approximately 100 µl of blood was taken from mice by removing less than 5mm of the tail tip using a sterile surgical scalpel blade. If blood was to be retaken, the blood clot formed from the previous tail tip bleed was removed. Blood was collected using a Microvette® CB 300 capillary tube (Sarstedt Ltd, Leicester, UK). Blood collected in capillary tubes was left at room temperature to clot and centrifuged for 10,000 x g for 5 minutes, or until the serum was separated from the plasma. Sera were aliquoted into sterile 1.5 ml microcentrifuge tubes and stored at -70°C until needed.

An ELISA was carried out as in section 2.1.3, with the following modifications. A 96-well Immulon 4HBX flat-bottomed microtitre plate (Fisher Scientific, UK) was coated with 5 µg/ml solution of chick type II collagen (dissolved in acetic acid) in PBS overnight at 4ºC, and blocked with 5% (w/v) bovine serum albumin (BSA) in PBS at room temperature for 1 hour. Mouse serum was diluted in 1% (w/v) BSA in PBS serially diluted down the plate (dilution range: 1:20 to 1:2560), and incubated for 2 hours at room temperature. CII-IgG2a was detected with 0.25 µg/ml biotin-conjugated rat anti-mouse IgG2a (Southern Biotech, Alabama, US) in 1% (w/v) BSA in PBS and incubated for 2 hours at room temperature followed by Ready to Use Streptavidin-HRP (Vector Laboratories Ltd, Peterborough, UK) for 30 minutes and SureBlue™ TMB (Insight Biotechnology Ltd, UK). The substrate reaction was stopped with 2M H_2SO_4 and when a colorimetric change was detected, absorbances were read at OD_{450nm} using a FLUOstar Optima plate reader (BMG Labtech Ltd, Aylesbury, UK).

2.2.2 *In vivo* imaging with MMPSense fluorescent probes

To monitor MMP activity *in vivo*, animals with established disease were injected with protease activatable fluorescent *in vivo* imaging agents; MMPSense680 or MMPSense750. MMPSense680 works by enzymatic cleavage of the peptide fluor from its quencher, resulting in fluorescence (figure 2.14). MMPSense750 FAST is similar, but contains a pharmacokinetic modifier designed to effect rapid accumulation and activation in target tissues (figure 2.14) which, according to the manufacturer, confers an improved pharmacokinetic profile and earlier imaging time points than MMPSense680 (Groves et al., 2010).

The MMPSense agents (Perkin Elmer, MA) are activated by a number of MMPs including MMP-2, -3, -9 and -13 (see figure 2.15 for activation profiles).

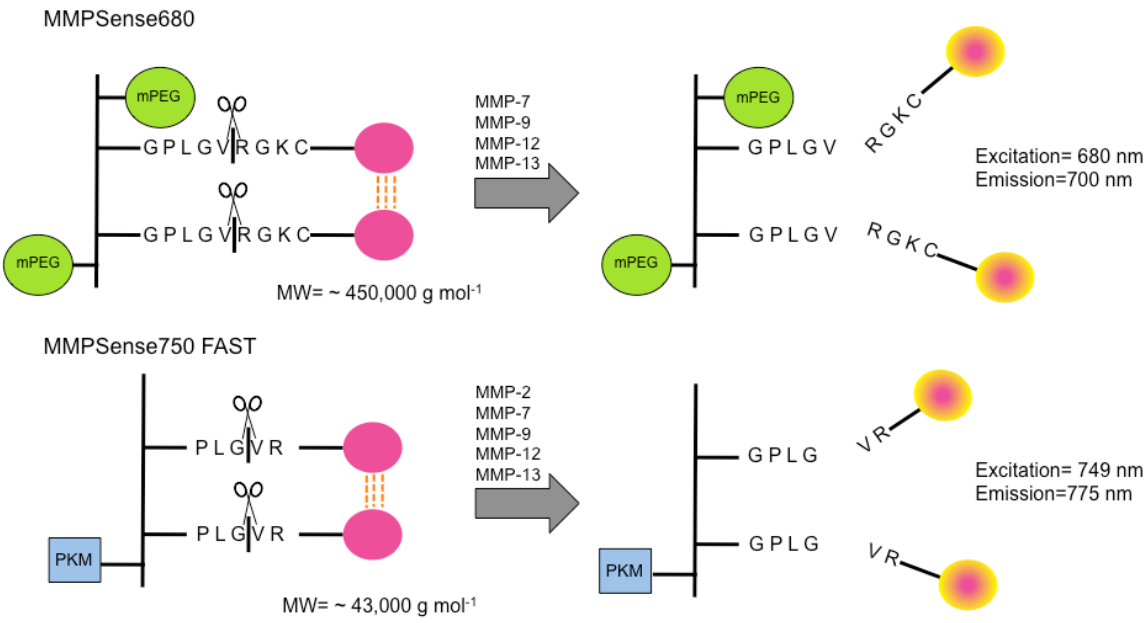

Figure 2.14 MMPSense680 and MMPSense750 FAST probe activation

Schematic showing how MMPSense probes are activated. MMPSense680 consists of a poly-L-lysine backbone to which methoxy polyethylene glycols (mPEGs) are attached for reduced immunogenicity and increased half-life. The peptide sequence (GPLGVRGKC) used to link the autoquenched fluorochromes (pink circles) to the backbone molecule is cleaved by a panel of MMPs, resulting in the activation of fluorochromes (orange circles). MMPSense750 is activated in a similar fashion, but cleavage specificity is conferred by the peptide sequence PLGVR. The backbone contains an unspecified pharmacokinetic modifier (PKM) and has a lower molecular weight than MMPSense680, allowing MMPSense750 FAST to rapidly accumulate and fluoresce in tissue.

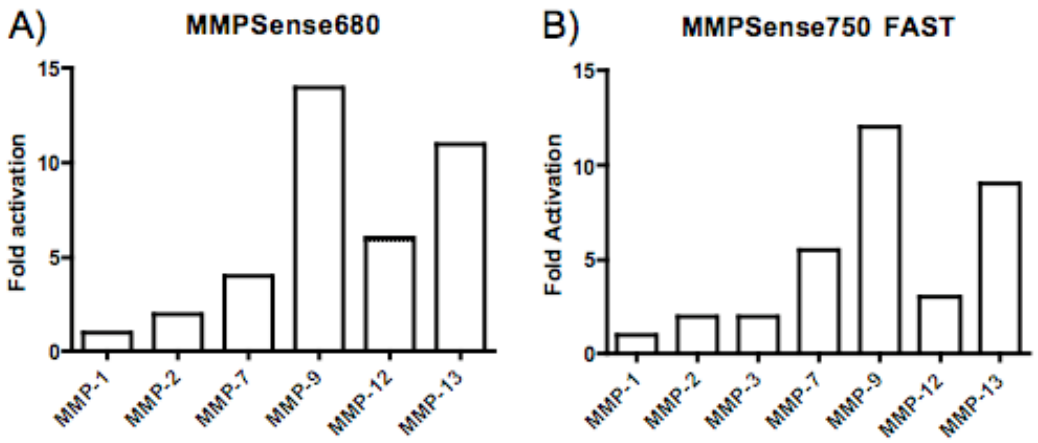

Figure 2.15 Biochemical profile of the activatable MMPSense agents

Fold activation of A) MMPSense680 and B) MMPSense750 FAST fluorescence produced as a result of cleavage by different MMPs *in vitro*. Fold activation was determined by dividing the fluorescence released after complete cleavage with the enzyme to the fluorescence of the probe only. Images adapted from (Kossodo et al., 2010) and (Groves et al., 2010).

2.2.2.1 Preparation and administration of fluorescent probes

The MMPSense680 preparation comprised a solution of 20 nmol in 1.5 ml PBS. MMPSense750 FAST was delivered in a dry solid form, and was reconstituted with PBS to make a 7 nM solution. Upon reconstitution the vial was protected from light and stored at 4°C until further use, for up to 10 days.

The imaging agents were left to equilibrate at room temperature prior to use. In preparation for i.v. injections, animals were placed in a warming chamber at 37°C for 15-20 minutes to dilate the tail veins. Mice were then anaesthetised using the inhalational agent isoflurane, and were placed in a restraining device whilst under anaesthetic nose cone. Once the imaging agent was ready, it was loaded into a Monoject™ 29 gauge Insulin syringe (Covidien, MA). These syringes were used to ensure less of the probe solution was lost within the syringe (i.e. less “dead space”). Animals were injected i.v. with 2 nmol of the probe solution, the recommended dose for an adult (~25 gram) mouse. Immediately post-injection, the mice were placed back into the warming chamber until they had recovered from the anaesthesia and showed no signs of distress.

2.2.2.2 MMPSense680 imaging and region of interest analysis

For MMPSense680 imaging, mice were anaesthetised and imaged in the prone position, 24 hours post-injection using the Kodak FX Pro *in vivo* Imaging system. Animals were imaged every 24 hours thereafter until the experimental end-point. Fluorescent images were captured using an exposure time of 30 seconds at excitation 630 nm, emission 700 nm, f-stop 4. Radiographic images of the animals were captured using an exposure time of 30 seconds at 35KVP, f-stop 4, and field of view 11.7 cm.

Analysis of MMPSense680 fluorescent images was carried out using KODAK software version 5.0.0.40 (Carestream Health UK Ltd, Herts, UK). The fluorescent signal was converted to a pseudocolour scale and overlaid onto the radiographic image (figure 2.16). Regions of interest (i.e. areas showing high levels of fluorescent intensity) were highlighted using a free form region of interest (ROI) analysis tool (figure 2.16), and the net intensity of fluorescence was calculated for all individual limbs using the Kodak Molecular Imaging software. The net intensity is the sum of the background-subtracted pixel values within the ROI. This parameter was chosen for ROI analyses because it was the only parameter that corrected for ROI area size, allowing the signal intensity of front paws to be compared alongside hind paws.

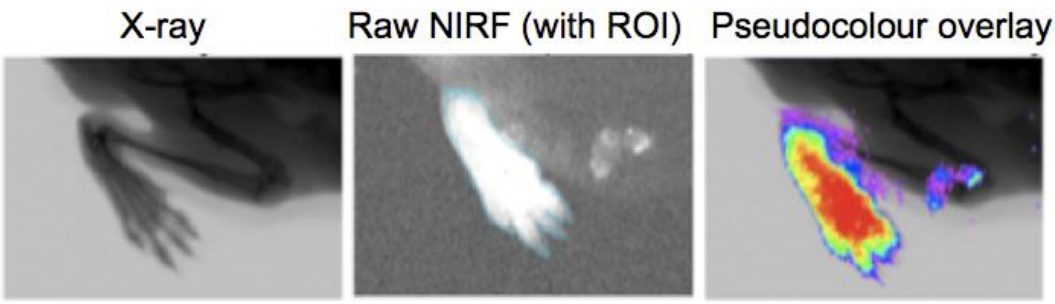

Figure 2.16 ROI analysis with the Kodak molecular imaging software

Panel showing an X-ray image of a hind paw, and its corresponding fluorescence image. Areas of high fluorescence were isolated with a free-form tool (blue line) and analysed for net fluorescence intensity. A pseudocolour overlay image could be obtained to visualise localisation and intensity of fluorescence.

2.2.2.3 MMPSense750 FAST imaging and region of interest analysis

For imaging MMPSense750 FAST, mice were anaesthetised and imaged in the prone position using the Xenogen IVIS 200 (Caliper Life Sciences, Runcorn, UK). This machine was used, to accommodate the emission and excitation filters required for the MMPSense750 imaging probe. Animals were imaged every 24 hours thereafter until the experimental end-point. Fluorescent images were captured using an exposure time of 1 second at excitation 750 nm, emission 810 nm, f-stop 1, field of view 13.2 cm.

Analysis of fluorescent images obtained was carried out using Living Image® 2.50.2 software (Caliper Life Sciences Ltd, Cheshire, UK). Rectangular ROIs of a fixed dimension (front paws: w=1.1 x h=1.1 cm, hind paws: w= 1.9 x h=1.1 cm) were selected and fluorescent efficiency quantified for each ROI. Fluorescence efficiency is a display of the fluorescence emission range normalised to the incident excitation intensity. This eliminates the variable excitation light from the measurement, enabling a more quantitative comparison of fluorescence signal.

2.2.3 Subcutaneous administration of APO866 via minipump

In this study, animals were treated with APO866 by continual infusion by osmotic minipump 20 days post disease initiation. Preliminary studies within the group showed that the APO866 applied in this manner up to 0.08 mg/kg/h was a well-tolerated dose with no adverse effects on mice (figure 2.17). The range of doses chosen was based on the maximum tolerated dose in humans (0.126 mg/m^2/h) (Holen et al., 2008). The

equivalent dose in mice was calculated as 0.04 mg/kg/h, determined using an established dose translation formula (Reagan-Shaw et al., 2008). Alzet 1002 mini-osmotic pumps (Durect Corp, CA) were chosen for APO866 administration, as they allowed for a continuous infusion of APO866 at a rate of 0.25 µl/h for up to 14 days (figure 2.18).

2.2.3.1 Minipump Filling and Priming

Preparation of minipumps was carried out in a Class II tissue culture cabinet under aseptic conditions. The APO866 treatment solution was prepared by mixing 64 µl APO866 with 36 µl sterile saline per animal, vortexing well and loading 100 µl of the resulting solution into each minipump using a blunt-tipped 27 gauge filling tube (supplied with the minipump), ensuring that no air bubbles were introduced into the reservoir. The vehicle treatment solution (propylene glycol in saline) was prepared and loaded the same way. The minipump flow moderators were replaced and the filled pumps were primed in saline at 37 °C overnight to allow them to begin operation prior to implantation.

2.2.3.2 Minipump implantation

Pre-primed minipumps were implanted subcutaneously posterior to the scapulae of experimental animals. Implantation was carried out under complete aseptic conditions with autoclaved dissection instruments, including scissors, two hemostats and fine forceps. For subcutaneous placement, mice under anaesthesia were shaved and the implantation site was sterilised with povidone-iodine solution. Using fine scissors, a small incision was made in the skin between the scapulae, and a hemostat was used to spread the subcutaneous connective tissues apart, forming a small pocket. The pump was inserted into the pocket with the flow moderator pointing away from the incision. The skin incision was then closed up using fine forceps, hemostats and three to four sutures. All instruments were sprayed with 70% ethanol between procedures. Animals were placed into a warming chamber onto vet bedding immediately after the implantation procedure, and observed regularly to ensure sufficient recovery from the procedure.

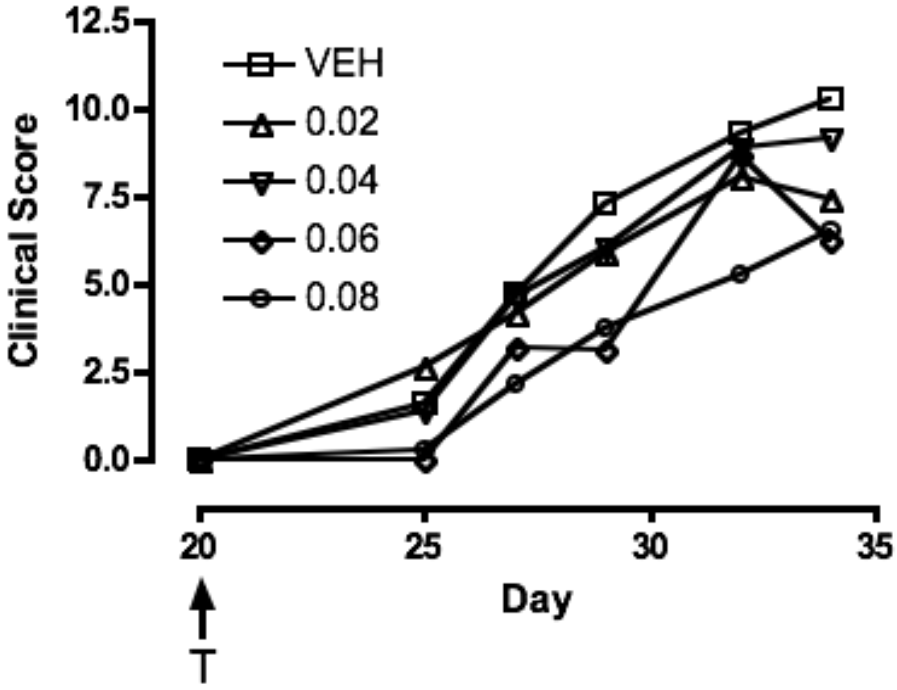

Figure 2.17 CIA clinical scores from preliminary minipump studies

In a previous study by Mari Nowell, DBA-1 mice (n=4 animals per group) were treated prior to the onset of disease with minipumps containing 0-0.08 mg/kg/h APO866. Data points represent the mean combined clinical scores of animals in each treatment group. T=treatment initiation at 20 days post induction.

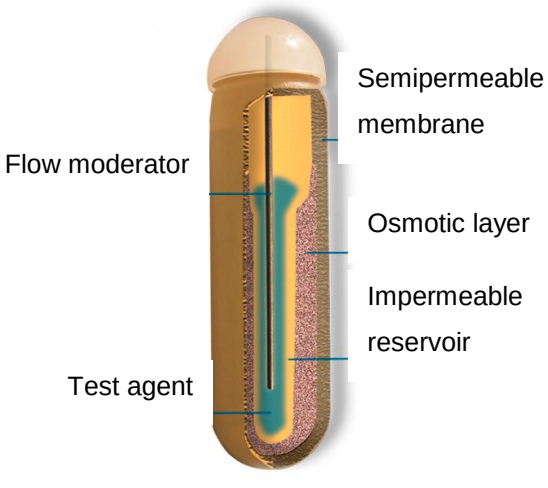

Figure 2.18 Cross section of an osmotic minipump

Image taken from the Alzet® resources web page (http://www.alzet.com/resources/index.html).

2.3 General Tissue processing methods

2.3.1 Histology

2.3.1.1 Processing into wax

Unless otherwise stated, all stains and reagents used for histological analyses were purchased from Sigma-Aldrich Ltd, Dorset, UK. Tissue was processed into wax using a Thermo Shandon Citadel 2000. This machine dehydrates samples by transferring them through baths of progressively more concentrated ethanol, followed by replacement with xylene, before impregnation in paraffin wax at 60°C to facilitate sectioning. Tissue was embedded in paraffin blocks, using a Shandon Histocenter, and 7 µm sections taken using a Surgipath Microtome. Sections were mounted onto HistoBond® adhesion slides (VWR International Ltd, West Sussex, UK), and excess wax removed by overnight incubation at 60°C.

2.3.1.2 Safranin-O Fast Green section staining

Mounted sections were dewaxed in xylene and rehydrated through a descending gradient of industrial methylated spirits (100%, 90%, 70% IMS) to water. Tissue sections were then stained in 0.02% (w/v) aqueous fast green for 3 minutes, washed briefly in 1% (v/v) acetic acid and stained in 0.1% (w/v) aqueous Safranin O for 5 minutes. Sections were then dehydrated and mounted with coverslips using DPX mountant (Sigma-Aldrich Ltd, Dorset, UK). Slides were scanned using an Aperio Scanscope CS system and images acquired using ImageScope imaging software.

2.3.2 Real-time quantitative PCR analyses

2.3.2.1 Ribonucleic acid (RNA) preparation

Whole joint RNA was prepared from murine front paws by grinding under liquid nitrogen using a pestle and mortar. The ground tissue was rapidly transferred to cooled microcentrifuge tubes and kept on dry ice. For each individual paw, 1 ml of TRI Reagent was added to the tissue and each mixture transferred to a Qiashredder (Qiagen Ltd, West Sussex, UK) and centrifuged for 17,000 x g for 2 minutes to filter out any insoluble debris and reduce the viscosity of the homogenate. For cell monolayer cultures, cells were lysed directly on the tissue culture plates by the addition of TRI reagent (1 ml per 10 cm^2 of plate surface area). All cell/tissue homogenates were transferred to 1.5 ml microcentrifuge tubes for RNA extraction.

RNA was extracted from cell/tissue homogenates as recommended in the TRI Reagent manufacturer's protocol. Firstly, each homogenate was incubated at room temperature for 5 minutes for the complete dissociation of nucleoprotein complexes. Then 0.2 ml of chloroform was added to each 1 ml sample, tubes were shaken for 15

seconds and incubated at room temperature for a further 3 minutes. For phase separation, the samples were centrifuged at 12,000 x g for 15 minutes at 2-8°C. Centrifugation caused samples to separate into three distinct phases: a lower red, phenol-chloroform phase, an interphase, and a colourless upper aqueous phase. The RNA-containing aqueous phase was transferred to a fresh tube, and mixed with 0.5 ml of isopropyl alcohol to precipitate the RNA. Samples were incubated for 10 minutes at room temperature before centrifugation at 12,000 x g for 10 minutes at 2-8°C. The RNA pellets were then washed by adding 1 ml of 75% ethanol and centrifuged at 7500 x g for 5 minutes at 2-8°C. The pellets were air-dried and each re-dissolved in 20 µl of RNase-free water. Finally, samples were heated to 55°C for 10 minutes to ensure the complete dissolution of RNA. RNA concentration was determined by measurement of the optical density at 260 and 280 nm using a NanoDrop-1000 spectrophotometer (Fisher Thermo, USA). A selection of samples was run in an Agilent 2100 Bioanalyzer (Agilent Technologies Ltd, Berkshire, UK), for quantification and quality control of the extracted RNA samples.

Total RNA from each sample was DNase-treated using RQ1 RNase-Free DNase (Promega UK, Southampton, UK). A digestion reaction was set up for each sample containing 3 µg total RNA, RQ1 RNase-free DNase 10X reaction buffer, and RQ1 RNase-Free DNase (1 unit/µg of total RNA), to a total volume of 10 µl. Sample tubes were incubated at 37˚C for 30 minutes, before the addition of 1 µl of RQ1 DNase Stop solution to terminate the reaction, followed by incubation at 65˚C for 10 minutes to inactivate the DNase enzyme. DNase-treated RNA was immediately reverse transcribed into cDNA, or stored at -80°C until needed.

2.3.2.2 Complementary DNA (cDNA) synthesis

DNase-treated RNA samples were reverse transcribed into cDNA using a Precision nanoScript™ Reverse Transcription kit (PrimerDesign Ltd, Southampton, UK). For each sample, 2 µg of RNA template was added to a sterile RNase-free microcentrifuge tube along with 1 µl of a 1:1 mixture of Oligo-dT and random nonamer primers, and RNase/DNase-free water to a final volume of 10 µl. This priming strategy was used for optimum cDNA yield (Primerdesign, 2011). Samples were heated to 65˚C for 5 minutes to melt the secondary structure within the template and allow primers to anneal, and then immediately cooled in an ice water bath to prevent secondary structures reforming. Next, a reaction mix containing the following components was added to each of the annealed primer/templates: 2 µl nanoScript 10X buffer, 1 µl 10 mM dNTP mix, 2 µl 100 mM DTT, 4 µl RNase/DNase-free water and 1 µl nanoScript RT enzyme (enzyme units not disclosed). A separate reaction tube was set up containing an additional 1 µl of water in place of the nanoScript enzyme as a “minus RT” control. Samples were mixed

by briefly vortexing followed by a pulse spin, and incubated at room temperature for 5 minutes before incubating at 55˚C for 20 minutes for the reverse transcription reaction to occur. Finally, the reaction was heat inactivated by incubation at 75˚C for 15 minutes. The cDNA samples were stored at -20°C until further use.

2.3.2.3 Primer design and synthesis

Most primer assays used in quantitative real-time polymerase chain reactions (qPCR) were SYBR green based detection assays; with the exception of murine MMP-3 and MMP-13, which were TaqMan® primer/probed based assays (purchased from Applied Biosystems). Details of murine and human primers used in this thesis are listed in Tables 2.4 and 2.5, respectively. With the exception of SIRT1, all SYBR green primer assays were designed and synthesised by Primerdesign Ltd, and upon arrival were reconstituted with RNase/DNase-free water and stored at -80°C. The SIRT1 gene was designed in- house by the following method. Firstly, the target gene was studied in the ENSEMBL genome browser (http://www.ensembl.org/index.html) for details of alternative transcripts/splice variants. Primers were targeted specifically against the gene of interest, and when possible primers were designed to span exon-exon junctions, to avoid amplification of contaminating genomic DNA in cDNA samples. Primers were designed using open-source software, Primer3 version 0.4.0. (http://frodo.wi.mit.edu/). The source sequence for the gene of interest was pasted into the input box, and square brackets were used to highlight preferred regions for the primers to target. Primer product sizes were limited to 50-150 bases in length, as shorter amplicons allow for faster more efficient reactions, and increased consistency of results (Rozen and Skaletsky, 2000). The Primer3 search was run and the output contained numerous forward and reverse primer pairs. Candidate primer pairs were entered into Primer-BLAST (http://www.ncbi.nlm.nih.gov/tools/primer-blast/), to check the specificity of primers against a library of genomic DNA sequences. Finally, the Sigma-Aldrich DNA Calculator (http://www.sigma-genosys.com/calc/DNACalc.asp) was used to determine if the chosen primers were likely to form secondary structures, or 3’ self-complementary primer-dimers. Custom oligonucleotides were purchased from Sigma-Aldrich UK and were reconstituted in RNase/DNase-free water to a stock concentration of 100 µM. From this stock, aliquots containing a mixture of forward and reverse primers (6 µM each) were made ready for use in qPCR reactions.

Table 2.4 Gene names and sequences of murine primers used in real-time PCR reactions

Primer and primer type	Gene name	Gene symbol	Sequence accession number	Primer Sequences	Amplicon length
MMP-1a (SYBR green)	*Mus musculus* matrix metallo-peptidase 1a (Interstitial collagenase 1)	Mmp1a	NM_032006	Sense-TAAACTACACACCATATTTGCCAAA Antisense-CAATATCGCCTTCCTCCTCAAA	123
MMP-3 (TaqMan®)	*Mus musculus* matrix metallo-peptidase 3 (Stromelysin)	Mmp3	NM_010809	Not disclosed	N.D.
MMP-9 (SYBR green)	*Mus musculus* matrix metallo-peptidase 9 (type IV collagenase)	Mmp9	NM_013599	Sense-TGATGCTATTGCTGAGATCCAG Antisense-CCTGTAATGGGCTTCCTCTATG	92
MMP-13 (TaqMan®)	*Mus musculus* matrix metallo-peptidase 13 (Interstitial collagenase 3)	Mmp13	NM_008607	Not disclosed	N.D.

Table 2.5 Gene names and sequences of human primers used in real-time PCR reactions

Primer	Gene name	Gene symbol	Sequence accession number	Primer sequences	Amplicon length
NAPRT	*Homo sapiens* nicotinate phosphoribosyltransferase	NAPRT1	NM_145201	Sense- GTGGTGCTGTCCGAGAGG Antisense- GGAAAAGTGAGTGATTCGTGTTG	111
NAMPT	*Homo sapiens* nicotinamide phosphoribosyltransferase	NAMPT	NM_005746	Sense- TTCCCACTACTCCAGCCTAAG Antisense- TTTGTGTAAAGGGCAGGTTAATAAA	94
IDO	*Homo sapiens* indoleamine 2,3-dioxygenase	IDO1	NM_002164	Sense-CAGTCCGTGAGTTTGTCCTTT Antisense- CAGGAATCAGGATGTACTTAGTCA	129
QPRT	*Homo sapiens* quinolinate phosphoribosyltransferase	QPRT	NM_014298	Sense- CCCCAGCCCTTGATTTCTCC Antisense- GGTGTCATCCTCTTCCGGTTTA	93
MMP-1	*Homo sapiens* matrix metallopeptidase 1 (interstitial collagenase)	MMP1	NM_002421	Sense- GCACTGAGAAAGAAGACAAAGG Antisense- CTAAGTCCACATCTTGCTCTTG	127
MMP-3	*Homo sapiens* matrix metallopeptidase 3 (Stromelysin 1, progelatinase)	MMP3	NM_002422	Sense- ATCATGAACAATGGACAAAGGATAC Antisense- AGTGTTGGCTGAGTGAAAGAG	101
SIRT1	*Homo sapiens* sirtuin 1, transcript variant 1	SIRT1	NM_012238	Sense- CCGGATTTGAAGAATGTTGG Antisense- AGCGCCATGGAAAATGTAAC	174

2.3.2.4 qPCR

qPCR was performed with the ABI Prism 7900HT instrument (Applied Biosystems, Life Technologies Ltd, Paisley, UK). Each qPCR reaction consisted of the following: 1 µl primer or primer/probe mix (working concentration 300 nM in a 20 µl reaction), 10 µl PrimerDesign 2X Precision™ Mastermix (PrimerDesign Ltd, Southampton, UK), 4 µl RNase/DNase-free water and 5 µl (5 ng/ µl) cDNA template. Of this mix, 15 µl was pipetted into each well of a MicroAmp® Optical 96-well Reaction Plate (Applied Biosystems, Life Technologies Ltd, Paisley, UK) according to the plate set up. Finally, 5 µl of cDNA diluted to a concentration of 5 ng/ml (based on the concentration of RNA used in the reaction) was added to wells according to the experimental plate set up. The plate was sealed using MicroAmp® adhesion film and centrifuged at 12,000 x g for 1 minute to bring contents to the bottom of the wells. The plate was placed into the 7900HT Fast Real-Time PCR System and Sequence Detection System Software (SDS version 2.3; Applied Biosystems) was used to set the required cycling conditions and detectors for each reaction plate.

All reactions were performed under the following cycling conditions: an enzyme activation step at 95˚C for 10 minutes, followed by 50 cycles of 95˚C for 15 seconds (denaturation step) and 60˚C for 60 seconds (data collection step). As SYBR green binds non-specifically to all double-stranded DNA sequences, an additional dissociation step analysis was performed to determine the specificity of the primers and detect the presence of any primer dimers. This involved heating samples to 95˚C for 15 seconds, cooling to 65˚C for 15 seconds, before a slow ramp to 95˚C. At a specific melting point (T_m), the amplicons dissociated causing the release of the SYBR green fluorophore. The resulting change in fluorescence was plotted as a derivative dissociation curve of rate of change as a function of temperature (for example see figure 2.19). Fluorogenic data were collected through the FAM and SYBR channels for TaqMan® and SYBR green probes respectively. Assays were performed in duplicate, and the following control wells were included: -RT control (wells where the equivalent concentration is added minus the reverse transcription step) and a –cDNA control (wells where the cDNA is replaced with RNase/DNase-free water).

Upon completion of the real-time PCR run, the resulting data were saved as a .SDS file. For SYBR green runs, the SDS v2.3 software was used to determine the threshold value (C_T) from the resulting amplification plots of the different primers. The C_T value is the fractional cycle number at which the fluorescence passes the threshold. The threshold level was set to be above the baseline, but sufficiently low to be within the exponential growth region of the amplification curve. For TaqMan® reactions, RQ

Manager Version 1.2.1 was used to set the thresholds and determine C_T values of TaqMan® primer/probe amplification plots. Once the C_T values for both, the reference gene(s) and gene(s) of interest, had been determined, the resulting data were exported as a Microsoft Excel spreadsheet (.xls) file for further analysis (see section 2.3.2.6).

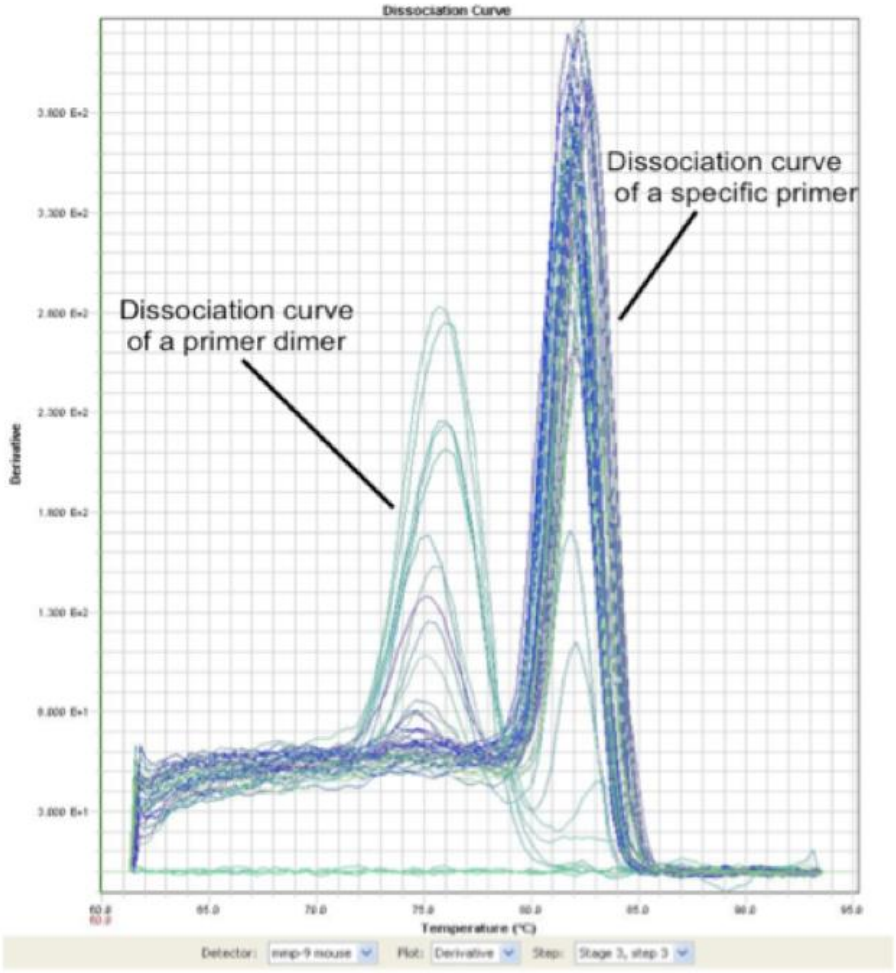

Figure 2.19 Dissociation curve of SYBR green amplicon

Using SDS v2.3 software, a dissociation curve of change in fluorescence (expressed as a derivative) was plotted against temperature. In this graph the specific primer product has a T_m of 82.5°C. A second smaller peak has a T_m of 75°C characteristic of a primer dimer. Any samples containing primer dimers were omitted from the analysis, as they were likely to contain low copy numbers of the target gene. If primer dimer formation proved a persistent problem, then redesigning the primer was necessary. Image adapted from SDS software output.

2.3.2.5 Reference gene selection

For accurate gene quantification, it is essential to normalise qPCR data to a reference gene that is unaffected by experimental conditions. Reference gene expression levels are likely to vary between tissue origin, as well as between healthy and diseased tissue (Vandesompele et al., 2002). For this reason, prior to performing qPCR experiments, candidate reference genes were tested for their suitability for each given experimental scenario. This was achieved using geNorm™ reference gene selection kits (Primerdesign Ltd, Southampton, UK), comprising of a panel of candidate reference gene primers which can be tested for expression stability on a selection of cDNA samples. A mouse geNorm™ kit was used to determine the most stably expressed reference gene in cDNA samples from murine paws, whilst the equivalent human geNorm™ kit was used to determine the best candidate reference gene for real-time PCR reactions using human chondrocyte and RASF cDNA samples.

For each geNorm analysis, a random assortment of six cDNA samples and six candidate reference targets were assessed. The cDNA samples chosen were randomly selected samples from cells or tissues subject to different experimental treatments. The analyses were carried out as outlined in the manufacturer's protocol. Firstly, the lyophilised primer and probe mixes were each reconstituted in 220 µl RNase- free water. Next, each re-suspended primer was used to create a real-time PCR master mix as follows (per one reaction): 1 µl primer/probe (creating a working concentration of 300 nM per 20 µl reaction); 10 µl PrimerDesign 2X Precision™ Mastermix; 4 µl RNase- free water. The following cycling conditions were applied: enzyme activation (95˚C for 10 minutes), followed by 50 cycles of 95˚C for 15 seconds, 50˚C for 30 seconds and 72˚C for 15 seconds. All geNorm kits were primer/probe based assays, so an additional dissociation step was not required. Upon completion of the real-time PCR run, the resulting data were saved as .SDS files. RQ Manager Version 1.2.1 was used to set the thresholds and determine C_T values of the primer/probe amplification plots. The resulting data were exported as Microsoft Excel spreadsheets and analysed using qbasePLUS data software (Biogazelle, Belgium Version 1.5).

For murine tissue, 18S rRNA gene was found to have the greatest expression stability in whole joint tissue and so was used in all subsequent qPCR reactions (figure 2.20). The genes for 18S rRNA, UBC and Beta-actin were found to be the most stably expressed candidate reference genes in human chondrocytes (figure 2.21A). Similarly, the genes for 18S rRNA, GAPDH and Beta-actin were found to be the most stably expressed candidate reference genes in RASFs (figure 2.21B).

The cDNA samples were analysed for these reference genes, and a specific normalisation factor was calculated by taking the geometric mean of the C_T values of these genes, as recommended in the literature (Hellemans et al., 2007; Vandesompele et al., 2002).

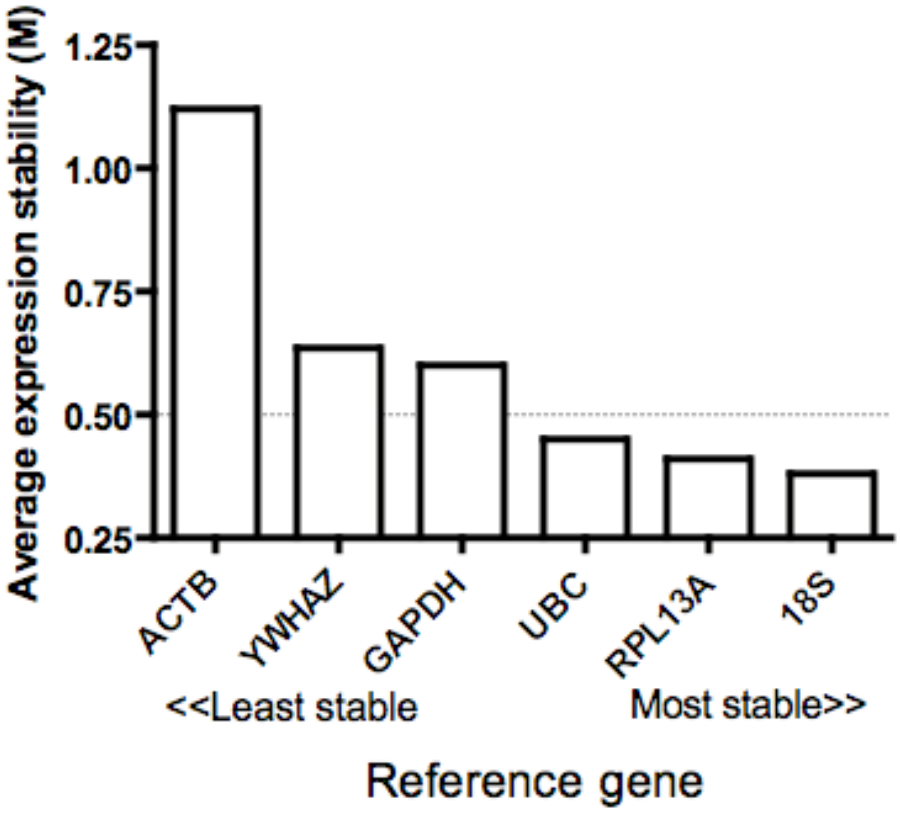

Figure 2.20 Reference gene selection for murine front paw qPCR analysis Complementary DNA (cDNA) samples of murine front paws from different treatment groups were run in a qPCR reaction with a panel of reference genes to determine average expression stability, expressed as geNormM-values (average pairwise variation of a gene with all other reference genes). ACTB, *Mus musculus* actin beta cytoplasmic mRNA; YWHAZ, *Mus musculus* phospholipase A2 mRNA; GAPDH, *Mus musculus* glyceraldehude-3-phosphate dehydrogenase mRNA; UBC, *Mus musculus* ubiquitin C mRNA; RPL13A, *Mus musculus* ribosomal protein L13a mRNA; 18S, *Mus musculus* 18S rRNA gene.

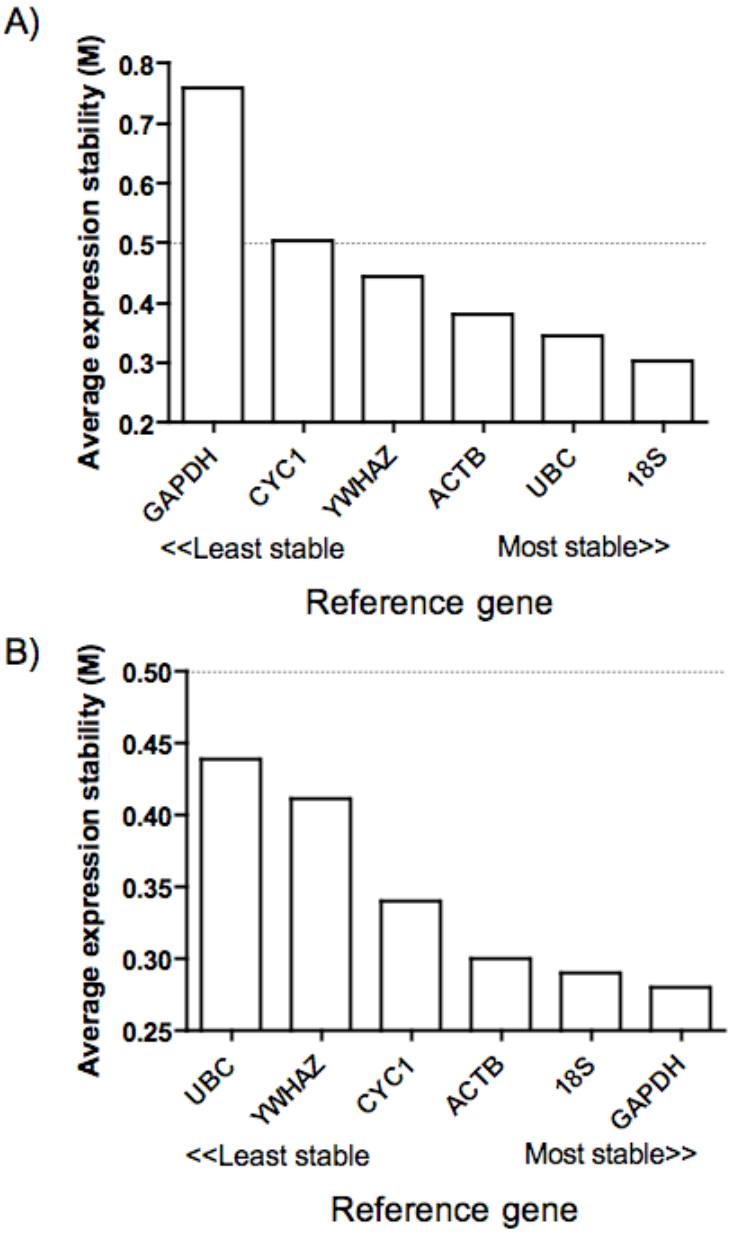

Figure 2.21 Reference gene selection for human qPCR analysis

Complementary DNA (cDNA) from a random selection of human A) chondrocyte and B) RASF samples were run in a qPCR reaction with a panel of reference genes to determine the most stably expressed reference genes. Average expression stability, expressed as geNorm M (average pairwise variation of a gene with all other reference genes). Reference genes with GeNorm M values ≤ 0.5 (denoted by the dotted line on the Y-axis) are considered stably expressed. GAPDH= *Homo sapiens* glyceraldehyde-3-phosphate dehydrogenase mRNA, CYC1= *Homo sapiens* cytochrome c-1 mRNA, YWHAZ= *Homo sapiens* phospolipase A2 mRNA, ACTB= *Homo sapiens* actin beta mRNA, UBC= *Homo sapiens* ubiquitin C mRNA, 18S= *Homo sapiens* 18S rRNA gene.

2.3.2.6 Relative quantification (RQ) analyses

From the raw C_T values, ΔC_T (delta C_T) was calculated by subtracting the C_T of the target gene (e.g. NAMPT) from the C_T of the reference gene (Beta-actin) for each sample:

$$\Delta C_T = C_{T(target)} - C_{T(reference)}$$

Next, the $\Delta\Delta C_T$ values were determined by subtracting the ΔC_T values of treated samples (e.g. IL-1β stimulated) from those of untreated samples (e.g. medium controls):

$$\Delta\Delta C_T = C_{T(treated)} - C_{T(untreated)}$$

Once the $\Delta\Delta C_T$ was determined for every individual sample, the Relative Quantity of gene expression (RQ) was determined using the comparative C_T method:

$$RQ = 2^{-\Delta\Delta Ct}$$

RQ determines the change in expression of a target nucleic acid sequence relative to the same sequence in an untreated control.

2.4 Statistical analyses

All data acquired were processed using Microsoft® Excel 2008 for Mac. Graphs were generated and statistical analyses performed using GraphPad Prism Version 4.0a. Prior to performing statistical tests, all data were tested for normality using the Kolmogorov-Smirnov normality test. If the data did not meet the assumption for normality, then non-parametric analyses were carried out. Details of both types of test are described below. All data points were graphically presented with mean ± standard error of the mean (S.E.M). All data were expressed as P-values. Values of $P \geq 0.05$ were considered not significant, $P < 0.05$ were considered significant, and $P < 0.01$ considered highly significant. In this thesis, the term *experimental replicates* is used when one biological sample (e.g. a cDNA sample or culture supernatant) is analysed multiple times. The term *biological replicates* refers to when different samples (e.g. different cell sources) are used for different replicates.

2.4.1 Parametric tests

Student's unpaired two-tailed t-tests with 95% confidence intervals were performed to determine differences between two treatment groups at a single time point. Welch's T-test was used in cases where variances were found to be unequal between data sets, as determined by F-tests.

One-way analysis of variance (ANOVA) was performed to compare the means of two or more treatment groups, such as for time course and dose response analyses upon

stimulation of cells or tissues (e.g. with eNAMPT or IL-1β). Bonferroni post-tests were used to perform a pair-wise comparison of the various treatment groups. These analyses were also performed to test different treatment groups at a single time point, for example the effect of eNAMPT in the presence of absence of APO866.

Two-way ANOVA analyses with no repeat measures were used to determine the interaction between treatment groups over time, for example in experiments looking at the effects of APO866 in explants longitudinally. Bonferroni post-tests were used to compare mean values from different treatment groups for each time point.

Pearson's Correlation coefficient, two-tailed with 95% confidence intervals (CI), was used to determine relationships between two different variables (e.g. histology score vs. fluorescence) at a single time point. Significant deviation from zero (P-value) and the Pearson r correlation coefficient (r value) were reported for each correlation analysis. Graphs were presented with a line of best fit drawn to show the relationship between the two variables.

2.4.2 Non parametric tests

If the dataset was not normally distributed, then for the comparison of two treatment groups, Mann-Whitney *U* test used to determine whether the two groups were significantly different.

For comparisons of more than two treatment groups of non-parametric data, Kruskal-Wallis analyses with Dunns post-tests were performed to compare the medians of the different treatment groups.

Spearman's Rank correlation coefficient was used to determine non-parametric relationships between two different variables.

2.4.3 Power analyses

G*Power version 2 was used to perform *A priori* power analyses on datasets where appropriate (Erdfelder et al., 1996). These analyses were performed for *in vivo* studies, in order to determine the sample sizes required to obtain a yield significant difference between variables or treatment groups.

Chapter 3: Exogenous NAMPT and catabolic protease production *in vitro*

3.1 Introduction

In this first experimental chapter, the principle aim was to investigate the effects of eNAMPT on the production of mediators of the early degradative and inflammatory processes in human fibroblasts. In this introduction, I describe the role of fibroblasts in these processes, through the production of MMPs and TIMPs. I then summarise current knowledge of eNAMPT signalling and its role in MMP production, and what is currently known about APO866 and its specificity for eNAMPT.

3.1.1 Fibroblasts as a model for matrix remodelling

RASFs exhibit an activated destructive phenotype that is markedly altered from those of a normal synovial joint. RASFs taken from RA patients have been used extensively to study processes in established disease. However, this chapter aimed to study the effect of eNAMPT on early initiation of pro-degradative and pro-inflammatory mediators of disease. A caveat of using RASFs is that the altered phenotype they possess does not reflect the cell types present within a naïve (i.e. healthy) joint. However, whilst RASFs can be easily obtained from surgical waste of patients undergoing joint replacement surgery, synovial fibroblasts from healthy joints are not as easily obtainable. For this reason, human fibroblast cell lines such as the HFFF2 cell line are useful models for studying early inflammatory processes in naïve cells. As a well characterised, homogeneous cell line, they confer certain advantages over RASFs, which are subject to great variability, as patients may be in different stages of disease, or taking different therapeutics. In addition, the HFFF2 cell line proliferate rapidly and are resilient and amenable to processes such as transfection (McFarlane et al., 2011).

3.1.2 MMPs and TIMPs in cartilage catabolism in RA

Normal fibroblasts help chondrocytes to maintain articular cartilage through the secretion of factors involved in both matrix deposition and matrix degradation (Konttinen et al., 2000). The balance of MMPs and their endogenous inhibitors (TIMPs) is crucial for maintenance of articular cartilage (figure 3.1.1). Of all the different classes of MMPs and TIMPs present within the synovial joint, the ratio of MMP-3 to TIMP-1 is one of the most important in RA disease pathogenesis. MMP-3 plays a vital role in the initiation of joint damage, through the activation of the collagenase MMP-1 (Van Meurs et al., 1999a). Although there are four TIMPs in vertebrates, all of which are capable of inhibiting MMP-3, immunolocalisation studies of synovial samples have shown that

TIMP-1 is the principle inhibitory factor within these tissues (Hembry et al., 1995). Therefore, levels of MMP-3 and TIMP-1 were assessed in this chapter.

Under normal physiological conditions, MMP gene expression is relatively low in synoviocytes. TIMPs are of a lower molecular weight than MMPs; with TIMP-1 and MMP-3 approximately 28 and 54 kDa in size, respectively. Because of this, TIMPs are normally present in molar excess (Cunnane et al., 2001). However, in RA MMPs are upregulated in molar excess of endogenous TIMPs. This local imbalance between proteinases and inhibitors is believed to play a central role in the destruction of articular cartilage (reviewed by Rowan, 2001). Analyses of levels of MMPs and TIMPs in the serum, show that concentration ratios of TIMP-1:MMP-3 are lower in RA patients (6.6) compared with those with undifferentiated disease (12.1). Additionally, higher molar ratios correlated with high metalloproteinase activity (Cunnane et al., 2001). In all the studies conducted, MMP-3 is consistently the most abundant in RA synovial fluid, present at concentrations ranging from 22-110 µg/ml (Yoshihara et al., 2000).

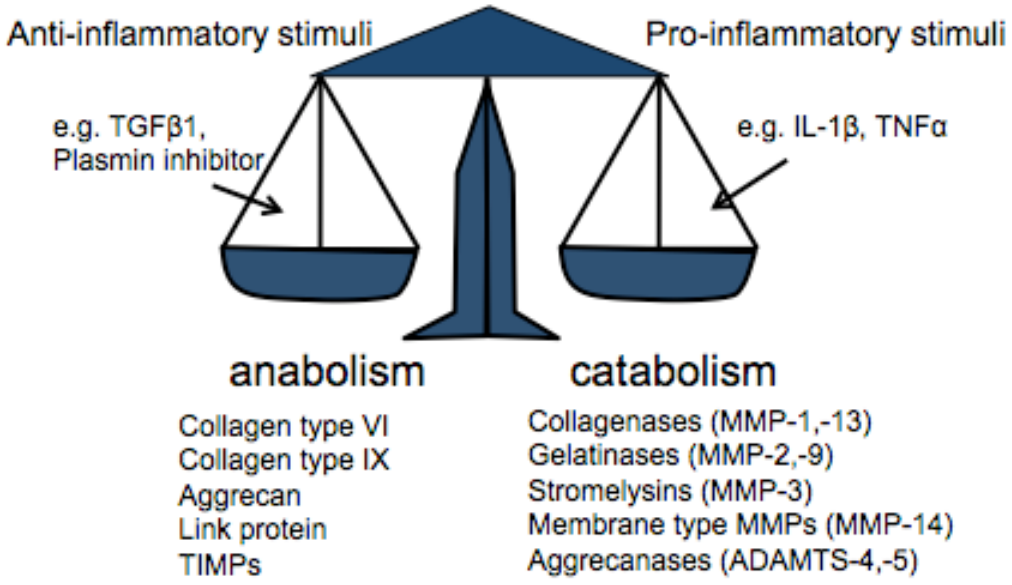

Figure 3.1.1 The role of synovial fibroblasts in cartilage matrix turnover

In normal tissue, synovial fibroblasts help chondrocytes maintain articular cartilage. They are stimulated by both anti- and pro-inflammatory stimuli, via a variety of cell-surface receptors, resulting in activation of gene transcription. Synthesis and secretion of matrix components and TIMPs is balanced with pro-degradative enzymes such as MMPs. TGFβ1, Transforming growth factor beta 1; TIMP, Tissue inhibitor of metalloproteinases; MMP, matrix metalloproteinases; ADAMTS, A disintegrin and metalloproteinase with thrombospondin motifs. Image adapted from (Aigner et al., 2006).

3.1.3 Extracellular NAMPT activity in disease processes

Recent work has shown a distinct correlation between circulating eNAMPT levels and markers of cartilage destruction in the sera and synovial fluid of arthritis patients (Duan et al., 2011). In addition, eNAMPT levels have been associated with DAS 28 score in RA patients, which is the measure of the number of tender or swollen joints (Brentano et al., 2007). Otero and colleagues were the first to report enhanced eNAMPT levels in the plasma of RA patients, with mean levels in RA patients (100.35 ng/ml) significantly greater than eNAMPT levels in non-arthritic controls (89.56 ng/ml) (Otero et al., 2006). Similar observations have been reported in synovial fluid samples (Nowell et al., 2006). Although eNAMPT is also detectable in the synovial fluid of osteoarthritis patients (mean concentration 64 ng/ml), levels are elevated in RA patients (150 ng/ml) (Nowell et al., 2006). However, although eNAMPT levels were shown to be higher in RA patients, these studies did not address whether this difference in eNAMPT levels is biologically relevant.

Since these studies, there has been considerable interest in the role of circulating eNAMPT in this condition. In disease, numerous cells actively secrete eNAMPT, including synovial fibroblast-like cells (Brentano et al., 2007). Previous studies suggest that eNAMPT is released from cells via a non-classical secretory pathway (Revollo et al., 2007b, Tanaka et al., 2007). The eNAMPT protein induces MMP-1 and MMP-3 gene expression in RASFs (Brentano et al., 2007), as well as MMP-9 mRNA levels in human THP-1 monocytes (Dahl et al., 2007) and MMP-3 and -13 mRNA and protein in murine chondrocytes (Gosset et al., 2008); suggesting a role for eNAMPT in the upregulation of MMP gene expression from cells within the synovial joint. However, these studies have mainly focussed on mRNA expression. Moreover, none have assessed the levels of TIMP protein levels in relation to MMP levels in the presence of eNAMPT.

As well as inducing mediators of cartilage catabolism, eNAMPT has been implicated in the production of inflammatory mediators. Overexpression of eNAMPT has been shown to augment TNFα induced CXCL8 secretion five-fold in human pulmonary epithelial cells (Li et al., 2008a). In a separate study, the addition of eNAMPT protein caused a 20-fold induction of CCL2 secretion in human endothelial cells (Adya et al., 2009).

3.1.4 APO866 and its inhibition of eNAMPT

APO866 is a potent and specific inhibitor of eNAMPT, binding in a tunnel at the interface of the NAMPT dimer and competing with the nicotinamide substrate for the active site (Khan et al., 2006). Previous studies have shown that APO866 added to cells in combination with eNAMPT inhibits eNAMPT induced NF-κB activation and inducible nitric oxide synthase (iNOS) induction in human aortic smooth muscle cells (Romacho

et al., 2009), and also eNAMPT induced PGE_2 release in human chondrocytes (Jacques et al., 2012).

In the context of MMP expression, Fan and colleagues (2011) found that APO866 blocked eNAMPT-mediated induction of MMP-9 four-fold in human macrophages. APO866 also inhibited extracellular matrix metalloproteinase inducer, EMMPRIN, in human macrophages (Fan et al., 2011). To date, the effect of eNAMPT inhibitor APO866 on MMP and TIMP production has yet to be investigated in fibroblasts, which are a major source of MMPs within the RA synovial joint. Use of APO866 within in a fibroblast cell line will provide novel insights into the role of eNAMPT in the induction of degradative processes in naïve cells.

3.1.5 Chapter aims

The role of eNAMPT has not yet been studied in the context of early degradative processes. Additionally, it is not fully established whether APO866 can inhibit the effects of this protein *in vitro*. Therefore, the specific objectives of this chapter were as follows:

- Determine the effect of NAMPT antagonist APO866 on eNAMPT-mediated MMP-3 and TIMP-1 release.
- Determine the effect of exogenous (e)NAMPT protein on MMP-3 and TIMP-1 secretion in a human fibroblast cell line (HFFF2).

3.2 Materials and methods

All experiments in this chapter were carried out on a human foetal foreskin fibroblast cell line (HFFF2) and cultured as described in section 2.1.2.3. Cells were cultured in 6-well plates to 80-90% confluency, before being washed twice with sterile PBS and starved in serum-free DMEM medium for 48 hours. Cells were then washed again before the addition of the medium containing supplements. Details of stimulation assays are given below.

Firstly, in order to assess the effect of APO866 on HFFF2 cell viability, serum-starved cells were washed and treated with serum-free DMEM supplemented with 0-100 nM APO866 for 24 hours, before culture media was removed and cell viability assayed by MTT assay (section 2.1.6.1). To assess the inhibitory effect of APO866 on eNAMPT stimulated cells, HFFF2 cells were washed, before pre-incubation with either untreated serum-free DMEM, or DMEM containing 10 nM APO866 (provided by TopoTarget A/S, Denmark). Cells were pre-incubated with APO866 for 1 hour, before the addition of 200 ng/ml eNAMPT. In order to demonstrate specificity of APO866, cells were also cultured as shown above, but with the addition of 2.5 ng/ml IL-1β in the presence or absence of 10 nM APO866. Finally, a dose response of eNAMPT stimulation was performed. Serum-starved HFFF2 cells were incubated with serum-free DMEM containing 0-400 ng/ml of human recombinant eNAMPT overnight (18-24 hours). Cell culture supernatants were collected and stored at -80°C for analysis of protein levels by ELISA (section 2.1.3). Levels of MMP-3, TIMP-1, CCL2 and CXCL8 were determined.

3.3 Results

3.3.1 APO866 did not affect HFFF2 cell viability

Firstly, an MTT assay was performed as described in section 2.1.6.1. The purpose of this assay was to determine a suitable working concentration of APO866 for use in inhibitory studies. Concentrations assayed ranged from 0-100 nM, based on published *in vitro* studies performed in other cell lines (Busso et al., 2008, Van Gool et al., 2009). APO866 had no significant effect on cell viability relative to an untreated medium control, even at concentrations of 100 nM APO866 (P=0.727, figure 3.3.1), and upon extending the time course up to 24 hours. All subsequent experiments in this chapter were performed with 10 nM APO866. This dose was previously shown to abrogate MMP-9 protein levels four-fold in monocytes stimulated with 200 ng/ml eNAMPT (Fan et al., 2011).

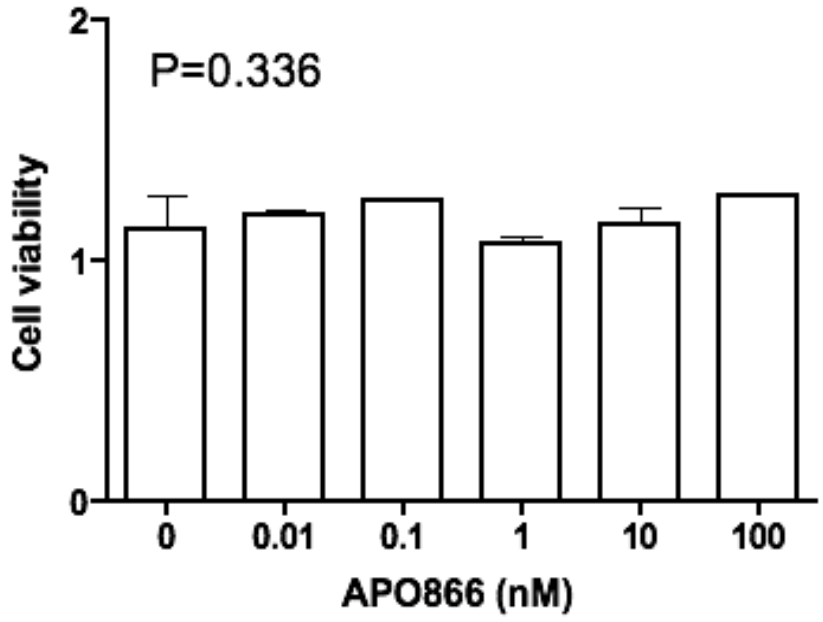

Figure 3.3.1 MTT assay to assess viability of APO866-treated cells

HFFF2 (one cell source, n=3 experimental replicates per condition) were incubated with escalating doses of APO866 for 24 hours (section 3.2). Cells were subsequently analysed for viability using an MTT assay. The viability of treated cells was determined by calculating the amount of formazan product relative to non-treated control wells. Error bars depict standard error of the mean (S.E.M). Kruskal-Wallis tests with Dunn's multiple comparison post-test analyses were performed to determine the significance levels between treatment groups. The experiment was performed using a single HFFF2 cell line. MTT, thiazolyl blue tetrazolium bromide.

3.3.2 APO866 inhibits eNAMPT, but not IL-1β-induced MMP-3 in HFFF2 cells

HFFF2 cells were cultured with or without 200 ng/ml eNAMPT in the presence or absence of 10 nM APO866. This particular concentration of eNAMPT was chosen, as it is physiologically relevant, and was shown to induce MMP gene expression and protein levels in previous studies (Brentano et al., 2007, Fan et al., 2011). The addition of 200 ng/ml eNAMPT resulted in a 2.5-fold increase in MMP-3 concentration compared to the unstimulated control (mean ± S.E.M, 2.09 ± 0.93 ng/ml and 5.38 ± 2.99 ng/ml, unstimulated control and eNAMPT stimulated, respectively; figure 3.3.2A). However, this was not statistically significant (P=0.1568).Co-incubation of eNAMPT with 10nM APO866 significantly lowered levels of MMP-3 compared to cells stimulated with eNAMPT alone (P=0.0467).

TIMP-1 was not affected by the addition of 200 ng/ml of eNAMPT compared to the unstimulated control (0.99 ± 0.65 ng/ml (unstimulated), 0.88 ± 0.53 ng/ml (eNAMPT); (P=0.8153; figure 3.3.2B). The addition of both eNAMPT and APO866 also had no effect on TIMP-1 release compared to eNAMPT alone (P=0.9014).

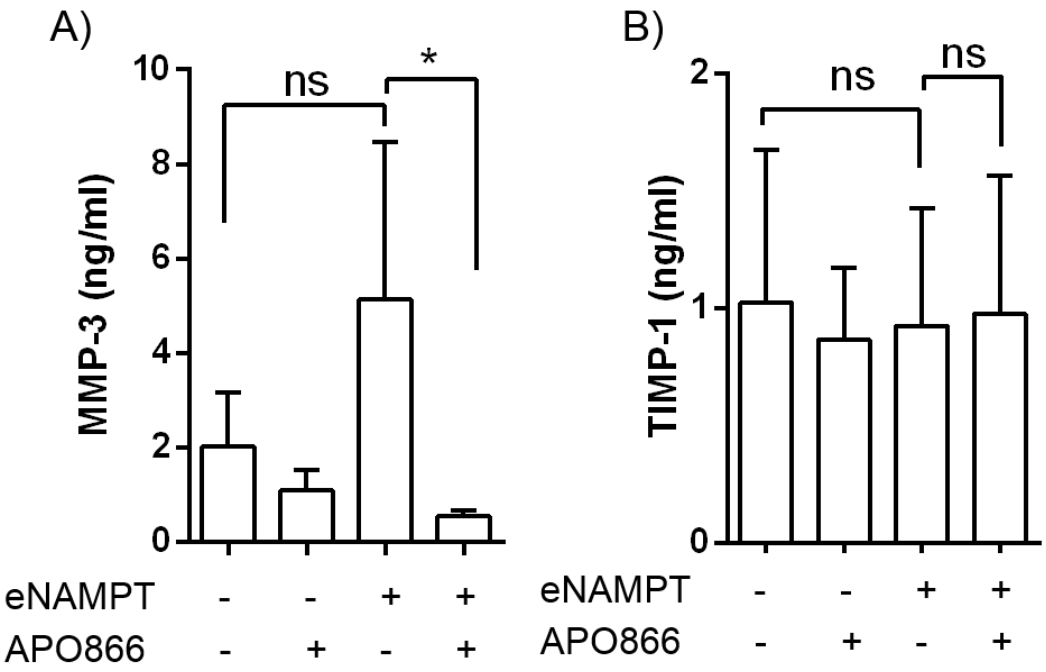

Figure 3.3.2 Effect of eNAMPT and APO866 on MMP-3 and TIMP-1 concentration

HFFF2 (n=4 experimental replicates) were stimulated with 200ng/ml eNAMPT for 18 hours, in the presence or absence of 10 nM APO866, and cell culture supernatants were assayed in duplicate for A) MMP-3 and B) TIMP-1 levels. Error bars depict standard error of the mean (S.E.M). Significance levels between means of the different treatment groups were determined using a two-tailed unpaired t test. *=P≤0.05, ns=not significant (P>0.05).

To determine whether APO866 inhibition of MMP-3 was specific to eNAMPT incubated cells, HFFF2 cells were stimulated with 2.5 ng/ml IL-1β, alone or in combination with 10 nM APO866.IL-1β caused a (7-fold) significant increase in MMP-3 production (P=0.036; figure 3.3.3A). The addition of APO866 had no significant effect on MMP-3 production in IL-1β stimulated cells (P=0.997).

Overall, TIMP-1 levels were not significantly different between IL-1β incubation (P=0.8539). Like eNAMPT, IL-1β had no stimulatory effect on TIMP-1, with protein levels comparable to values observed in unstimulated medium controls (P=0.776; figure 3.3.3B).

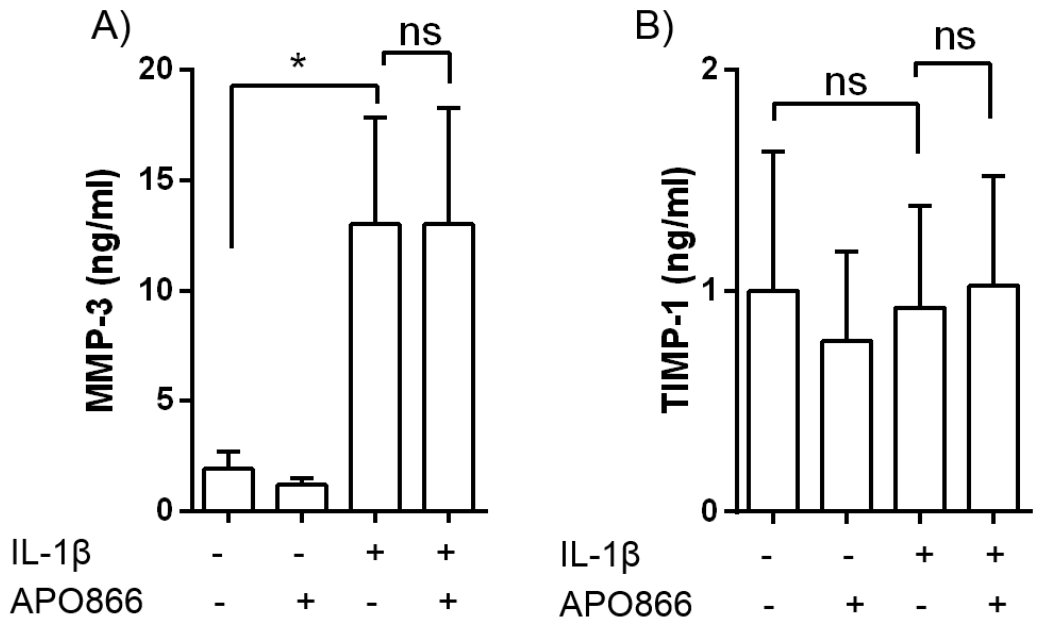

Figure 3.3.3 Effect of APO866 on IL-1β-induced MMP-3 and TIMP-1 concentration

HFFF2 cells (n=6 experimental replicates) were stimulated with 2.5 ng/ml IL-1β for 18 hours, in the presence or absence of 10 nM APO866, and cell culture supernatants were assayed in duplicate for A) MMP-3 and B) TIMP-1 levels. Error bars depict standard error of the mean (S.E.M). Significance levels between means of the different treatment groups were determined using a two-tailed unpaired t test. *=P≤0.05, ns=not significant (P>0.05).

3.3.3 eNAMPT caused a dose-dependent increase in MMP-3 production in HFFF2 cells

The addition of eNAMPT for 18 hours caused a significant dose-dependent increase in MMP-3 release in human fibroblasts (P=0.0237; figure 3.3.4A). In contrast, these same culture supernatants showed no significant change in TIMP-1 protein levels, even when stimulated with 400 ng/ml eNAMPT (P=0.715; figure 4.3.1B).

Although eNAMPT caused a dose-dependent effect on MMP-3, it was observed that the mean MMP-3 concentration from cells stimulated with 200 ng/ml eNAMPT was a third of that seen when the equivalent dose was used in an earlier experiment (figure 3.3.2). For this reason, the stability of eNAMPT in response to consecutive freeze-thaw cycles was questioned in the following section.

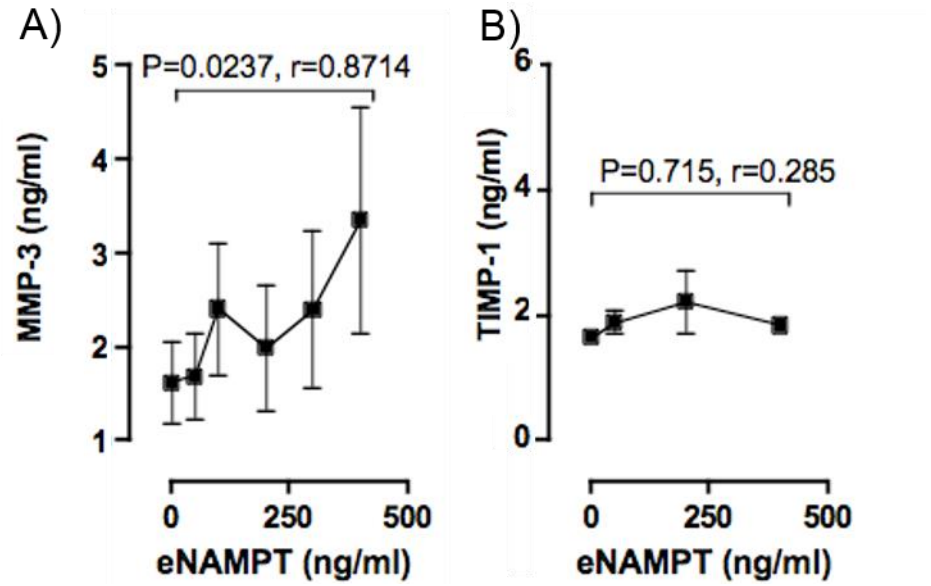

Figure 3.3.4 Dose effect of eNAMPT on MMP-3 and TIMP-1 concentration

HFFF2 (n=4 experimental replicates) were stimulated with eNAMPT (0-400 ng/ml) for 18 hours and A) MMP-3 and B) TIMP-1 levels in culture supernatants were assayed in duplicate by ELISA. Error bars depict standard error of the mean (S.E.M). Pearson's correlation coefficient was used to determine the relationship between eNAMPT concentration and resulting MMP-3 and TIMP-1 concentrations.

3.3.4 eNAMPT activity was affected by freeze/thaw cycles

The effect of eNAMPT on MMP-3 production diminished over time. The eNAMPT concentration-dependent production of MMP-3 in HFFF2 cells was repeated in cells of the same passage but using two different batches of eNAMPT. The parallel studies compared eNAMPT that had been subjected to one freeze/thaw cycle, versus freshly-reconstituted reagent. Freshly-reconstituted eNAMPT was more potent with regards to MMP-3 production than the batch that had been previously frozen (figure 3.3.5).

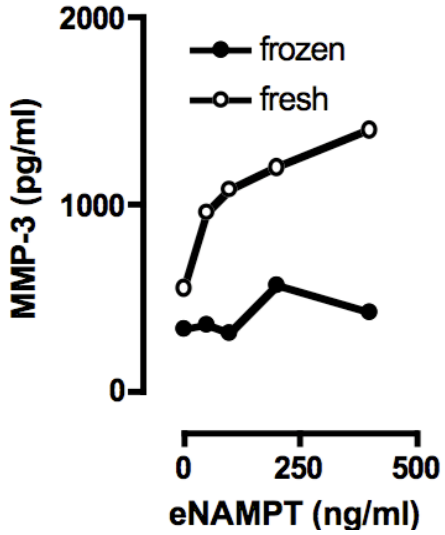

Figure 3.3.5 Effect of freeze-thaw on eNAMPT activity

Representative plots of MMP-3 production using either fresh or frozen eNAMPT preparations (n=1 experimental replicate per eNAMPT batch, assayed in duplicate by ELISA). The experiments were performed in parallel with the same source of HFFF2 cells.

3.3.5 Cellular response to eNAMPT decreased over time and between batches

In addition to the quality of the eNAMPT protein, an additional factor considered was the effect of cell passage on responsiveness to eNAMPT. A study in RASFs showed that cells at passage 7-8 differed greatly from cells at passage 2-4, with over 10% of genes differentially expressed (Neumann et al., 2010). To see whether HFFF2 cells were likewise affected, MMP-3 values obtained were plotted against the passage of the cells used. Comparisons of MMP-3 values obtained in individual experimental replicates showed that cells of a higher passage (>15) were less responsive to eNAMPT stimulation compared with stimulations carried out in cells of an earlier passage (figure 3.3.6A). Passage number also affected levels of MMP-3 from untreated medium control cells, with cells of a higher passage also exhibiting lower basal levels of MMP-3 (figure 3.3.6B).

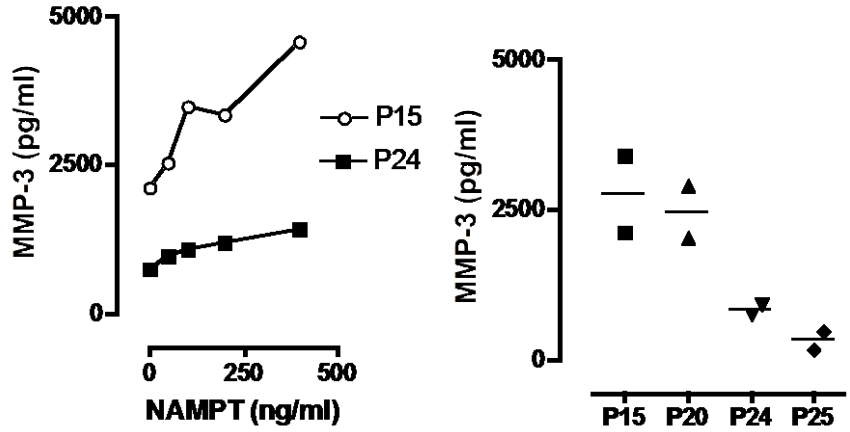

Figure 3.3.6 Effect of passage on MMP-3 production

A) HFFF2 cells (n=1 experimental replicate per passage source) were stimulated with 200 ng/ml eNAMPT. Culture supernatants were plated in duplicate and assayed for MMP-3 levels, which were plotted by cell passage number. B) Basal MMP-3 concentration from culture supernatants of untreated HFFF2 (n=2 experimental replicates presented per passage number). P= cell passage.

3.3.6 eNAMPT causes a dose-dependent increase in CCL2 and CXCL8 release in HFFF2 cells

Extracellular NAMPT has been previously shown to induce levels of release of both chemokine C-C motif-ligand 2 (CCL2) and CXC motif-ligand 8 (CXCL8), two chemokines involved in leukocyte recruitment (Li et al., 2008a, Adya et al., 2009). Therefore, cell culture supernatants previously assayed for MMP-3 and TIMP-1 were also assayed for release of these chemokines to determine whether the variability in MMP-3 levels due to eNAMPT reagent (figure 3.3.5) or cell passage (figure 3.3.6) applied to other proteins, or was restricted to MMP-3.

Incubation with 400 ng/ml eNAMPT induced a dose-dependent induction of CCL2 compared with untreated control cells (P=0.001; figure 3.3.7A). Culture supernatants of cells treated with both eNAMPT and APO866 had significantly lower levels of CCL2 compared with those stimulated with eNAMPT alone (P=0.0407; figure 3.3.7C). The addition of eNAMPT had a dose-dependent effect on CXLC8 production (P=0.0148; figure 3.3.4B), with a dose of 400 ng/ml eNAMPT inducing CXCL8 75-fold. Although 200 ng/ml eNAMPT did not significantly induce CXLC8 compared with the control (P=0.1886), co-incubation of eNAMPT with APO866 significantly attenuated CXCL8 production (P=0.0406; figure 3.3.7D). Overall, the same reduction in potency was apparent from CCL2 and CXCL8 values, reiterating that eNAMPT reagent and cell passage were factors in experimental variability.

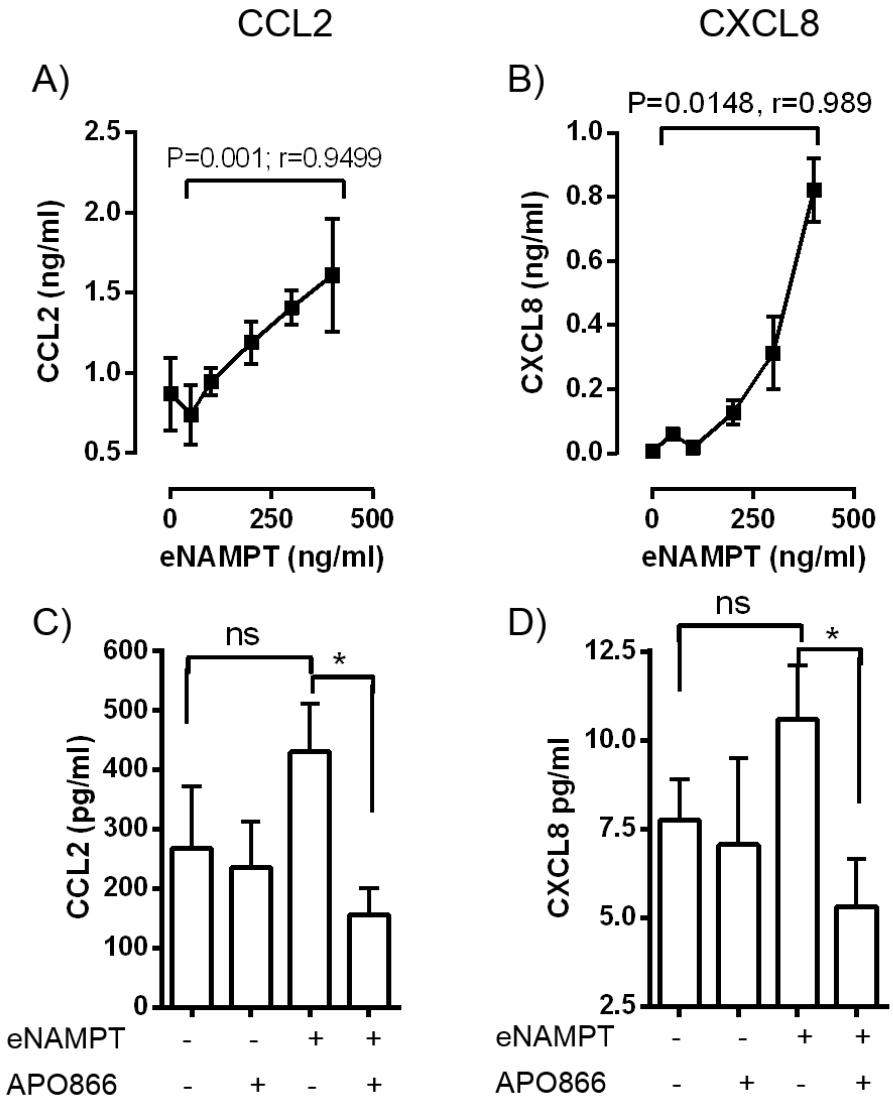

Figure 3.3.7 Effect of eNAMPT on chemokine release in HFFF2 cells

HFFF2 cells (one cell source, n=4 experimental replicates) were stimulated with eNAMPT (0-400 ng/ml) for 18 hours, and A) CCL2 and B) CXCL8 levels assayed in duplicate by ELISA. Pearson's correlation coefficient was used to determine the effect of eNAMPT concentration on subsequent MMP-3 concentration. In a separate experiment, HFFF2 cells (n=6 experimental replicates) were stimulated with 200 ng/ml eNAMPT for 18 hours, in the presence or absence of 10 nM APO866, and cell culture supernatants were assayed for C) CCL2 and D) CXCL8 by ELISA. Each point represents the mean value for each concentration, with error bars depicting standard error of the mean (S.E.M). Significance levels between means of the different treatment groups were determined using a two-tailed unpaired t test. *=P≤0.05, ns=not significant (P>0.05).

3.4 Discussion

3.4.1 eNAMPT causes a dose-dependent increase in MMP-3 release

Previous studies have shown that the mean level of NAMPT detected in synovial fluid in RA patients is 150 ng/ml (Nowell et al., 2006). Similar titres have also been detected in circulating plasma (Otero et al., 2006) and sera (Brentano et al., 2007) of RA patients. Therefore, the concentrations used in these *in vitro* studies are comparable to those seen in patients. The initial aim was to determine whether the stimuli used are capable of eliciting a pro-degradative effect in a naïve cell line. The addition of eNAMPT caused a statistically non-significant dose-dependent increase in MMP-3 release from HFFF2 cells. Induction of MMP-3 mRNA and protein has been previously reported in immature mouse articular chondrocytes (Gosset et al., 2008), and Brentano and colleagues (2007), reported that down-regulating eNAMPT expression using RNA interference causes a significant down-regulation of basal MMP-3 gene expression in synovial fibroblasts (Brentano et al., 2007). Despite this, IL-1β remains the more potent inducer of MMP-3, with mean values of 13 ng/ml compared with 4.7 ng/ml seen for eNAMPT incubation (figures 3.3.2 and 3.3.3).

3.4.2 eNAMPT does not stimulate production of TIMP-1

In addition to regulation at the level of transcription, MMPs are controlled at the protein level by TIMPs. Therefore, the effect of eNAMPT on the release of MMP inhibitor, TIMP-1, was also determined. The addition of eNAMPT did not induce TIMP-1 protein in HFFF2 cells, despite the apparent induction of MMP-3. This is different to previous findings in HUVECs, which showed that eNAMPT attenuates TIMP-1 and TIMP-2 gene expression after 4 hours of stimulation (Adya et al., 2008). This discrepancy may be due to the timings of the supernatant harvest. HUVECs show a significant drop in expression of TIMP-1 and -2 mRNA after 4 hours, and TIMP-1 and -2 protein after 24 hours. One possible explanation is that at the time point used in this current study eNAMPT had not had enough time to exert an effect on TIMP-1 levels. Alternatively, it may be the case that cells were not sufficiently affected by the addition of eNAMPT. Likewise to eNAMPT, IL-1β had no discernible effect on TIMP-1 levels in our study. It may be that whilst IL-1β can induce TIMP-1 in certain cell types (Wilczynska et al., 2006), this may not be true for fibroblasts. Adya and colleagues used VEGF as a positive control for MMP upregulation and TIMP downregulation in HUVECs. Therefore, future studies involving eNAMPT control of MMP/TIMP expression could utilise VEGF for this purpose.

3.4.3 APO866 inhibits eNAMPT-induced, but not IL-1β-induced MMP-3 release

Pre-incubation of cells with the NAMPT inhibitor APO866 appeared to inhibit the induction of MMP-3 by eNAMPT. APO866 inhibition was not attributed to cell death, as an MTT viability assay showed that 24 hours of exposure to 100 nM APO866 does not exert a cytotoxic effect in HFFF2 cells (figure 3.3.1). In addition, IL-1β-mediated MMP-3 release was not inhibited by APO866, suggesting APO866 is a potent and highly specific inhibitor of eNAMPT. Studies in RASFs show that IL-1β induces NAMPT mRNA expression (Brentano et al., 2007). If APO866 does inhibit IL-1β-induced iNAMPT activity, the downstream effect of this iNAMPT inhibition on MMP expression could be masked by the other, possibly overwhelming, cellular changes that occur in response to IL-1β. However, this apparent inhibitory effect by APO866 should be interpreted with caution, as eNAMPT itself did not significantly enhance MMP-3 production in this particular experiment.

An inhibitory effect of APO866 on eNAMPT-induced MMP activity has been previously reported in THP-1 derived macrophages, with APO866 inhibiting eNAMPT-stimulation of both EMMPRIN and MMP-9 (Fan et al., 2011). It is possible that APO866 may inhibit eNAMPT enzymatic activity outside of the cell inhibiting the conversion of nicotinamide from the culture medium into NMN. This NMN may either be subsequently taken up by cells, or bind to a surface receptor to activate signalling pathways, resulting in the production of MMP-3. This idea is reinforced by the fact that NMN causes eNAMPT mimetic effects in vascular smooth muscle cells (Wang et al., 2009b), human aortic smooth muscle cells (Romacho et al., 2009), human THP-1 derived macrophages (Fan et al., 2011), and murine chondrocytes (Jacques et al., 2012). The effects of exogenous NMN on human fibroblasts were not determined in this chapter, as the above findings had not been published at the time of carrying out these experiments. However, the effect of NMN on MMP expression and release in fibroblasts should be considered in future experiments.

Despite evidence from previous studies (Wang et al., 2009b), it remains to be seen exactly how NMN may exert these eNAMPT mimetic effects. If cells actively take up NMN, it could work to increase cellular NAD^+ pools, which may in turn affect the stability or phosphorylation of various signalling molecules. For example, increased NAD^+ availability may increase activity of SIRT1, which has been shown to interact with and deacetylate the RelA/p65 subunit of NF-κB (Yeung et al., 2004). However, even if NMN does function this way, there is still the issue of whether or not eNAMPT can produce this compound extracellularly. A recent study in mouse plasma has shown that although eNAMPT is enzymatically active, it is incapable of forming NMN extracellularly,

due to a requirement for ATP and PRPP, which are lacking in extracellular spaces (Hara et al., 2011).

Some groups propose that eNAMPT engages with a putative receptor to exert an immunomodulatory role (Brentano et al., 2007, Moschen et al., 2009). APO866 binding may cause a slight conformational change to eNAMPT, potentially affecting its capacity to bind to cell surface receptors. Khan and colleagues reported such a change in the Tyr240 and Tyr18' residues of the murine NAMPT molecule upon binding with APO866 (Khan et al., 2006). In addition, Kim *et al* (2006) found that the conformation of the NAMPT/APO866 complex differed from the structure of unbound NAMPT by 2.46 Å (angstrom) (Kim et al., 2006). Whether this change is sufficient to impact upon possible receptor/ligand interactions remains to be seen. Further work needs to be done to determine the relative contributions of iNAMPT and eNAMPT on MMP release in fibroblasts. For example, stimulation of cells with eNAMPT, in conjunction with inhibitors of transcription factors activated by eNAMPT, may determine if downstream effects on MMP release are comparable to the effects of iNAMPT inhibition.

3.4.4 NAMPT activity is diminished following repeated freeze-thaw cycles

The results of initial experimental replicates demonstrated a stimulatory effect on MMP-3 release at concentrations exceeding 50 ng/ml, although this effect was less apparent in subsequent experimental repeats. The initial stimulation assays involving eNAMPT showed very strong dose-dependent induction of MMP-3. Significant changes in MMP production upon eNAMPT stimulation became diminished in each successive experiment, with later observations showing no induction of MMP-3 by eNAMPT at all. A number of tests were performed to determine the source of these inconsistencies, which ranged from assessing the effect of cell passage, to comparing two different HFFF2 cell sources, as well as both fresh and frozen aliquots of the eNAMPT protein.

The results of these tests suggest that activity of the eNAMPT protein became reduced during prolonged periods of storage, even when kept at -80°C. There are few published reports of eNAMPT protein added to cells *in vitro* compared with other cytokines. Therefore, information regarding the storage and use of eNAMPT is somewhat limited. It was eventually determined that lyophilised eNAMPT, reconstituted and added directly to cells, induced MMP-3 release more strongly than aliquots of protein that had been used from frozen stocks (figure 3.3.5). Therefore, recombinant eNAMPT protein should be handled with great care and consideration and used fresh whenever possible, to ensure its activity is retained.

There have been both recorded and anecdotal reports that the NAMPT protein lacks stability (Lin et al., 1972, Rongvaux et al., 2002). Lin and colleagues reported

extreme lability of enzymatic activity of the NAMPT enzyme[3] in total extracts of recombinant protein purified from rat erythrocyte, with the paper citing pH and the presence (or absence) of ATP as possible effectors of enzymatic activity (Lin et al., 1972). More recently, Rongvaux's group (2002) found that the purified recombinant NAMPT protein consistently expressed very weak enzymatic activity, therefore they used a complementation test in a prokaryotic host to demonstrate the activity of NAMPT (Rongvaux et al., 2002). However, it is noteworthy that both these studies looked specifically at the enzymatic functions of NAMPT, and not its reported signalling role.

3.4.5 eNAMPT activity is lost over successive passage in HFFF2 cells

If eNAMPT signalling is responsible for induction of MMP-3, a possible explanation for a drop in this activity is through loss of the eNAMPT receptor, which might arise from successive cell passage or through serum withdrawal. For example, expression of the TNF superfamily member death receptor 3 (DR3) in monocytic cell lines has been shown to drop gradually when cultured for prolonged periods of time (Wang, E.C.; personal communication). A similar effect has been reported in a human breast adenocarcinoma cell line, where late passage cells become less responsive to TGFβ than earlier passage cells. This was attributed to lower levels of TGFβ receptor type II (TGFBR2) in late passage cells (Ko et al., 1998). Similarly, early passage bone marrow mesenchymal stem cells (BMSCs) display a unique set of chemokine receptors that are lost in culture-expanded BMSCs of later passage (Honczarenko et al., 2006). In RASFs, expression of cytokine receptors including insulin-like growth factor 1 receptor (IGF-R1) are altered as a result of successive passage and freezing (Neumann et al., 2010). Therefore, it may be that the HFFF2 cell line is affected in a similar manner.

Another possibility is that the growth phase of cells in culture has an effect on receptor expression. This has been shown for a diverse range of receptors, including the transferrin receptor (Musgrove et al., 1984), CXC chemokine receptor 3 (CXCR3) (Romagnani et al., 2001), and thyroid hormone receptor β (Maruvada et al., 2004), with most showing maximal receptor expression at the G2/M phase. It is possible that cell growth may have become arrested in this current study, possibly due to over-confluency of monolayer cultures, or prolonged serum starvation.

The addition or withdrawal of serum may have an effect on cytokine receptor dynamics. In our laboratory, we traditionally serum starve all our cells for 48 hours prior to cytokine stimulation to ensure that no serum effects could alter the results. Upon a

[3] Originally designated the name nicotinamide mononucleotide pyrophosphorylase in this paper

review of the literature, it was apparent that many groups stimulate with eNAMPT protein *in vitro* in the presence of serum (Brentano et al., 2007, Dahl et al., 2007), or may only starve cells for a maximum period of 24 hours (Gosset et al., 2008, Jacques et al., 2012), sometimes in the presence of low (<0.3%) serum (Wang et al., 2009b, Romacho et al., 2009, Fan et al., 2011). Low serum and limited serum withdrawal may therefore be required in future studies to help retain cellular response to eNAMPT. Another possibility is that there may be a cofactor present in serum required by eNAMPT to induce its effects upon cells.

3.4.6 Basal MMP-3 levels diminished over time

Initially, the amount of MMP-3 and TIMP-1 present in HFFF2 cells appeared consistent with basal levels previously seen in RASFs (Noss et al., 2011, Fearon et al., 2006). However, as experiments continued, a drop in basal expression of MMP-3 was observed over time. Low MMP-3 detection levels in culture supernatants may be partially attributed to problems with the ELISA kits used (e.g. problems with quality of antibody aliquots), although this is unlikely. It is likely that this drop in basal MMP-3 production is a reflection of loss of viability over repeated passage of cells.

3.4.7 Summary

The data herein confirm that IL-1β causes a significant effect on MMP-3 protein levels in HFFF2 culture supernatants. Initial studies suggested a dose-dependent effect on MMP-3 release by eNAMPT. However, problems with reproducibility mean these findings are inconclusive and further investigation is warranted. To improve experimental reproducibility, future studies should carefully consider: (1) the preparation and biological shelf-life of eNAMPT; ideally using fresh batches whenever possible; (2) the replicative history of the cell culture under scrutiny, thus utilising cells that have undergone a minimum number of population doublings, and (3) the potential importance of serum in the cellular response to eNAMPT. Addition of eNAMPT does not affect production of TIMP-1; suggesting eNAMPT activity may contribute to a local imbalance of MMPs and TIMPs that occurs in the synovium during RA pathogenesis.

The data indicate that APO866 may inhibit eNAMPT-mediated MMP-3 release in HFFF2 cells. Further studies are needed to establish whether APO866 is capable of blocking eNAMPT activity in RASFs and other synovial cells, and to elucidate the role of exogenous NMN in these processes. Drawing from information gathered in this chapter and reports in the literature, the potential roles of eNAMPT in MMP regulation are summarised in the schematic shown in figure 3.4.1.

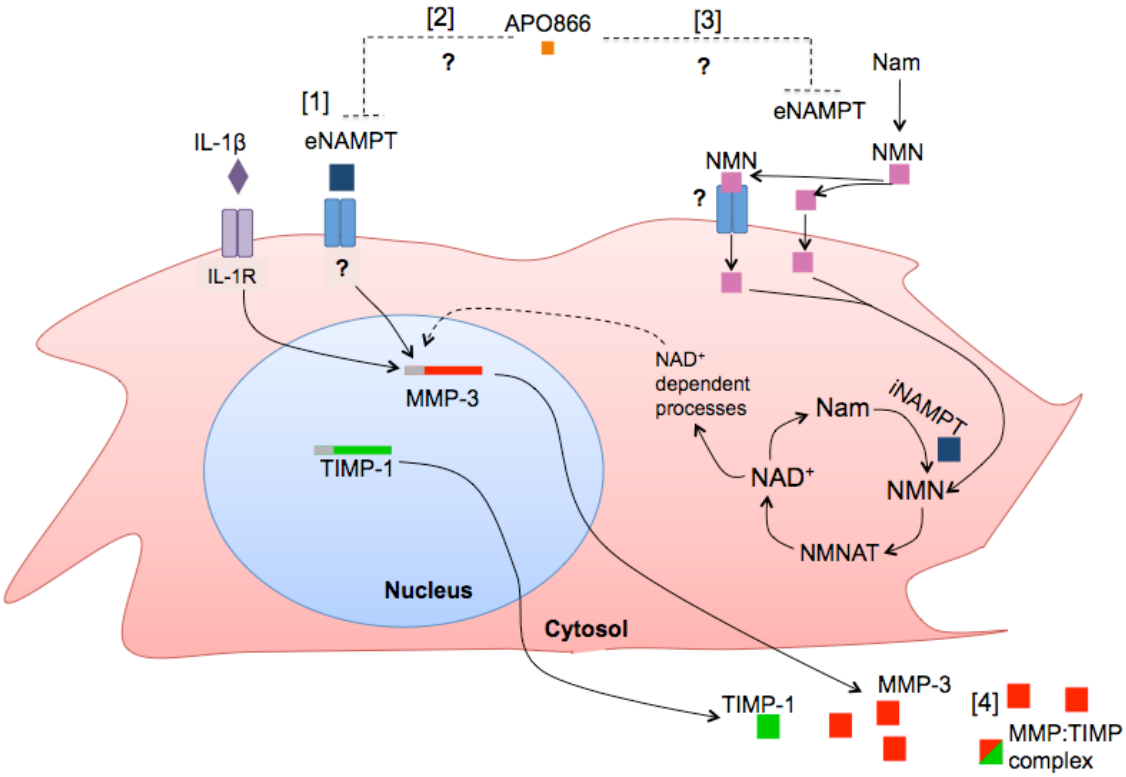

Figure 3.4.1 Proposed functions of eNAMPT in HFFF2 cells

[1] Similarly to IL-1β, eNAMPT is believed to act as an extracellular signalling ligand, inducing signalling cascades that result in the upregulation of MMP-3. APO866 inhibits eNAMPT mediated MMP-3 release. This could be via two mechanisms: [2] by interacting with and inhibiting eNAMPT binding to its receptor, or [3] reducing the eNAMPT enzymatic product NMN. NMN may itself signal as a secondary metabolite, or be taken up by the cell to promote intracellular NAD^+, and NAD^+-dependent factors. [4] TIMP-1 expression is not altered by either the addition of IL-1β or eNAMPT, thereby contributing to a local imbalance of MMP:TIMP ratios.

Chapter 4: The effect of NAMPT inhibition on catabolic protease production *in vivo*

4.1 Introduction

The main aim of this chapter was to assess the bioactivity of NAMPT antagonist APO866 *in vivo* in the collagen-induced arthritis (CIA) model. The effects of APO866 on in situ MMP production and cartilage pathology were measured as primary outcomes. This brief introduction summarises the advantages of the CIA model over alternative animal models, and how it can be utilised to assess early disease processes within the synovial joint. As detection of MMP activity was a priority in this chapter, fluorescence probes activated by MMP enzymatic activity are introduced as to detect protease activity in live CIA mice.

4.1.1 Animal models of arthritis

Animal models of inflammatory arthritis have been used extensively in research to study disease pathogenesis and for the evaluation of therapeutic agents. These models are relatively easy to perform with good reproducibility of data. One such model is the CIA model. Although originally established in the rat (Trentham et al., 1977), the murine CIA model is now used routinely as the benchmark to evaluate therapeutic entities with potential application in rheumatoid arthritis. The model involves immunisation of mice with CII, usually bovine or from chicken sternal cartilage. This results in a T- and B- cell response to autologous CII and thus disease manifestation. The CIA shares many histopathological features in common with RA (Table 4.1.1). Additionally, as CII (the target tissue of RA) is a major component of cartilage, this is a useful model for the study of cartilage degradation. Cartilage breakdown is measurable in CIA using subjective histological scoring systems. Histological evidence of cartilage degradation has been detected in joint tissues using proteoglycan stains such as Safranin O (Griffiths et al., 1995), hematoxylin and eosin (H&E) (Konda et al., 2010) and toluidine blue (Ishikawa et al., 2005). A recent study showed that MMP-derived collagen degradation-quantified by newly-developed ELISAs for collagen breakdown products is significantly increased in sera of CIA animals compared with control animals (Siebuhr et al., 2012). Upon injection of collagen in Freund's complete adjuvant, disease onset typically occurs in most animals between 21-25 days after the first injection. However, an injection of LPS can potentiate disease in animals when onset is slow (Caccese et al., 1992).

Table 4.1.1 Comparison of disease features of RA and CIA.

Disease feature	RA	CIA	References
Immune complex	Yes	Yes	(van den Berg, 2009)
MHC association	Yes	Yes	(Wooley et al., 1983)
T cell role	Yes	Yes	(Joosten et al., 1996)
Cartilage autoimmunity	Yes	Yes	(Trentham et al., 1977)
Synovitis	Yes	Yes	(Trentham et al., 1977)
Cartilage and bone erosion	Yes	Yes	(Trentham et al., 1977)
Periosteal reaction	No	Yes	(van den Berg, 2009)

4.1.2 Assessment of disease severity mice with collagen-induced arthritis

Established disease in the murine CIA model is traditionally monitored with a subjective scoring system, in conjunction with measurement of hind paw swelling using a caliper gauge (Brand et al., 2007). At the experimental end point, analyses may be carried out for the presence of autoantibodies or other serological markers of disease (reviewed by Mota et al., 2009). Histological examination can provide additional information pertaining to inflammatory infiltrate and cartilage erosion. Traditionally, serial sections of fixed tissue are taken from the sagittal plane, usually of the knee joint or the calcaneus region (Joosten et al., 1996). A commonly used staining regimen is haematoxylin and eosin (H&E) staining, which is used mainly for the examination of inflammatory infiltrate and exudate. Safranin O, Toluidine blue and Alcian blue are all commonly used stains for assessing the degree of proteoglycan depletion from the cartilage surface. More recently, researchers have started to image animals radiographically using systems such as the Faxitron M20, and have devised scoring systems to assess parameters such as bone erosion (Seeuws et al., 2010). Such techniques may confer advantages over subjective scoring systems, as software can perform quantitative analyses of images.

4.1.3 Assessment of MMP activity *in vivo*

As with RA, MMP production is greatly enhanced in the CIA model, particularly MMP-3 (Seeuws et al., 2010). However, whilst MMP titres have been determined in RA patient samples, there are relatively few published studies investigating MMP levels in the CIA model. Studies in RA sera and synovial fluid have shown enhanced levels of a number of MMPs in disease, including MMPs -1, -3, and -9 (Yoshihara et al., 2000, Cunnane et al., 2001, Tchetverikov et al., 2004). Of these, MMP-3 is the most abundant, with concentrations in synovial fluid often exceeding 100 µg/ml (Yoshihara et al., 2000). Also of interest is the collagenase, MMP-13. This MMP, which is preferentially produced by chondrocytes, is present at very low levels in normal tissues but is greatly induced by cytokine stimulation (Konttinen et al., 1999).

Traditionally, MMP activity within the CIA model has been monitored using various approaches, including: zymography of spleen cell supernatants (Chen et al., 2004, Shen et al., 2007), ELISA analysis of sera (Seeuws et al., 2010) or immunohistochemistry (IHC) with the use of antibodies which recognise C-terminal neopitopes in the aggrecan core protein (Van Meurs et al., 1999b). These neopitopes are generated by activity of MMPs -1, 2, -3, -7, -8 and -9 (Hughes et al., 1995). However, these methods have their drawbacks: they can be time-consuming, and often require optimisation. Additionally, results may not be easily reproducible between laboratories and many of these techniques are carried out at the experimental end-point when much of the proteolytic degradation of cartilage has already occurred.

In vivo imaging using near-infrared fluorophore (NIRF)-labelled imaging probes offers a way of studying markers of cartilage degradation, such as enhanced MMP activity, both longitudinally and non-invasively. Most commercially-available agents are activatable, meaning they are optically silent in their native (quenched) state, but fluoresce brightly upon enzyme-mediated release of their fluorochrome. Commercially-available probes can be targeted to particular areas of interest, or distributed passively through blood vessels. Although these probes have been shown to work in preliminary studies on arthritis models (Kossodo et al., 2010), there is currently little published work involving *in vivo* detection of MMP activity. Notable against this dearth of information is a study of transient cerebral ischemia in mice (Liu et al., 2011), and an analysis of MMP activity in human femoral condyles (Jones et al., 2012). To date, MMP activatable probes have not been used within murine arthritis models.

4.1.4 Assessing treatment efficacy in CIA

The CIA model has been used in efficacy studies of a range of RA treatments, including anti-IL-1β (Joosten et al., 1999), anti-TNFα (Mukherjee et al., 2003), and anti-IL-6 (Fujimoto et al., 2008) therapies. Our group discovered that when administered in established disease, doses of 0.08 mg/kg/h and 0.12 mg/kg/h APO866 had a significant impact on clinical scores, reflected in reductions in synovial inflammation and bone erosion. APO866 efficacy was further improved if administered as a prophylactic, i.e. prior to the onset of disease. Real-time PCR analyses also showed reduced expression of MMPs -3 and -13 in this animal model (unpublished data). Busso and colleagues studied the effects of APO866 in early onset CIA (Busso et al., 2008). In this experiment, CIA animals were treated with 2, 5 or 10 mg/kg APO866 twice daily, via the intraperitoneal route. APO866 treatment ameliorated disease severity and decreased proinflammatory cytokine secretion in affected joints. Studies in our group have investigated the efficacy of APO866 administered via minipump. An osmotic pump

containing the drug is implanted into animals subcutaneously, allowing continual dosing with less researcher intervention. The doses used in our lab were calculated based on the maximum tolerated dose determined in human trials (Holen et al., 2008).

Activatable fluorescent agents may enable researchers to study the efficacy of potential therapeutics in the live animal, to supplement traditional end-point analyses. Similar longitudinal studies have already been carried out in the CIA and Zymosan models, looking at the effects of MTX (Wunder et al., 2004) and dexamethasone (Caglic et al., 2011) on cysteine protease-activated fluorescence. Cysteine proteases are primarily involved in intracellular protein turnover, though at least some of them are believed to be involved in numerous pathologies, including RA (Caglic et al., 2011). The authors found that treatment with MTX and dexamethasone significantly decreased fluorescence signal in paws compared to the untreated CIA mouse (Wunder et al., 2004, Caglic et al., 2011). It is possible that fluorescent agents could be used to assess the efficacy of APO866 treatment *in vivo*.

4.1.5 Chapter aims

The main aim of this chapter was to assess the bioactivity of NAMPT antagonist APO866 *in vivo* in the collagen-induced arthritis (CIA) model, with particular emphasis on its effects on MMP expression and activity, and cartilage integrity. The specific objectives of this chapter were to:

- Induce murine collagen-induced arthritis in a reproducible manner and assess disease severity using a combination of established techniques.
- Develop and establish *in vivo* imaging protocols for the longitudinal assessment of MMP enzymatic activity in live mice (i.e. imaging on more than one occasion).
- Evaluate *in vivo* MMP activity against clinical scores, radiology, histopathology and MMP mRNA expression
- Assess the treatment efficacy of NAMPT antagonist, APO866 using *in vivo* imaging protocols and established techniques.

4.2. Materials and methods

4.2.1 CIA induction and imaging protocol in the MMPSense680 evaluation study

In this proof-of-concept study, six male DBA-1 animals (Harlan) were started on the collagen-induced arthritis protocol (section 2.2.1). Animals were observed at least twice a week for clinical signs of arthritis after the administration of the second intradermal injection of collagen on day 21, (section 2.2.1.1). All animals developed arthritis by day 26 (figure 4.2.1A). Three of the animals were humanely killed by day 31 of the experiment, as their clinical scores exceeded the severity limits specified in the legislative authority specified in our project licence (see timeline; figure 4.2.1B).

On day 33, the three remaining animals were each injected with 2 nmol of MMPSense680 probe (section 2.2.2.1). Imaging and region-of-interest (ROI) analyses were performed as described in section 2.2.2.2. Probing and imaging had been postponed up until this point, to coincide with the arrival of an *in vivo* imaging expert from Advanced Molecular Vision (AMV; Lincolnshire, UK), who facilitated the imaging and ROI analyses. Animals were imaged in the Kodak FX Pro 24 hours after probe administration. Fluorescence images were captured at emission 630nm after excitation at 700 nm quickly followed by whole body X-ray images. In order to assess fluorescence signal drop off, animals were imaged daily, up until day 36, when the animals were killed.

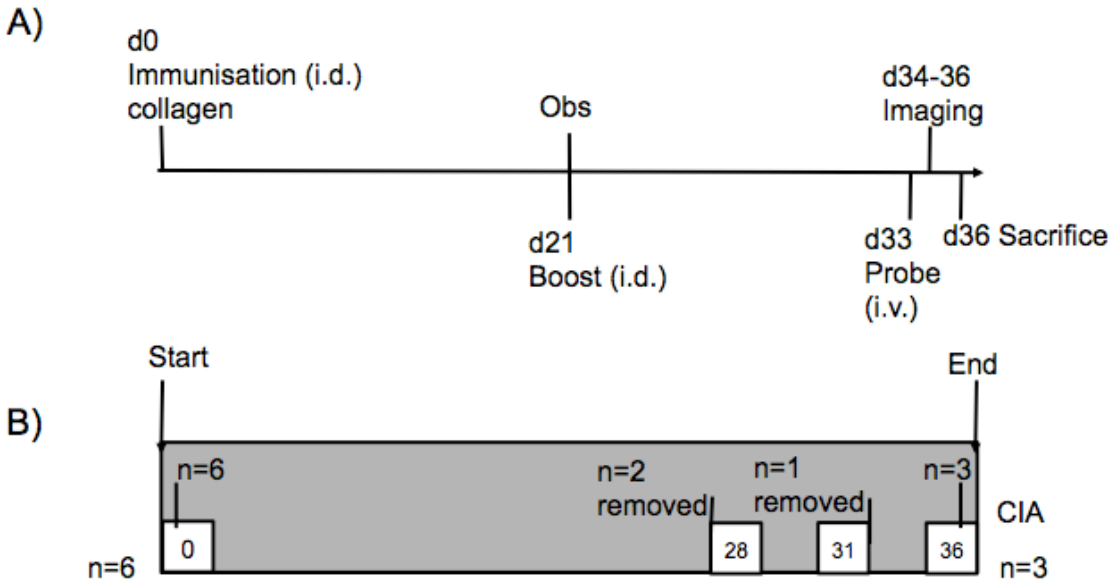

Figure 4.2.1 Experimental timeline of the MMPSense680 evaluation study

Six animals were used in this study. All six were immunised with collagen at days 0 and 21. From day 21 onwards, animals were observed at least twice a week. By day 33, three animals were removed from the experiment; the three remaining animals were injected (i.v) with MMPSense680 and imaging commenced daily until the experimental endpoint at day 36. B) Three animals had to be removed from the experiment on days 28 and 31. i.d., Intradermal; i.v., Intravenous; Obs, observation.

4.2.2 CIA induction and imaging protocol in the MMPSense 750 FAST evaluation study

In separate experiments, an alternative activatable fluorescent agent (MMPSense750 FAST, PerkinElmer) was used. MMPSense750 FAST was also tested with a view to assess its applicability, in longitudinal studies, for measuring MMP activity in actively inflamed joints of mice with CIA. Since this was also a proof-of-concept study, and for ethical reasons, only a small number of mice were used (three female DBA-1 mice from an in-house colony). CIA was induced in only two mice. A third non-immunised mouse was used as the age-matched control for the experiment. In this experiment only one of the immunised mice demonstrated clinical signs of arthritis at day 27 whilst the remaining immunised mouse, uncharacteristically, developed CIA on day 34. No animals were removed from the study for ethical reasons and all remained experimental until endpoint (see timeline; figure 4.2.2).

At the first clinical sign of arthritis (day 27), the one arthritic animal and the naïve control were injected intravenously with 2 nmol MMPSense750 FAST (section 2.2.2.1).

Probe solution was protected from light and stored at 4°C until further use. Animals were imaged using the Xenogen IVIS 200 imager, and ROI analyses performed (section 2.2.2.2). The remaining immunised mouse was also imaged and served as “no-probe” control for the experiment. It was used as a reference to determine endogenous background levels of fluorescence in an age-matched mouse. In order to measure any potential reduction in fluorescence signal over time; both mice were imaged daily until day 34. The day 34 fluorescence reading for each mouse provided the background for the next stage of the experiment. Both mice (with CIA) were injected with 2 nmol MMPSense750 FAST probe, re-imaged and sacrificed 6 hours later. Background fluorescence values were subtracted from the values acquired 6 hours after injection of the probe. MMP-specific fluorescent activity was calculated using the equation (below) where T is time (in hours) after injection of probe:

MMP fluorescence (T_x) = probe fluorescence (T_x) - pre-probe fluorescence (T_0)

Figure 4.2.2 Experimental timeline of the MMPSense750 evaluation study

Three animals were used in this study. Two animals were immunised with collagen at days 0 and 21. One animal was not immunised and acted as a naïve control. From day 21 onwards animals were observed at least twice a week. One CIA with arthritis and one naïve were injected (i.v) with MMPSense750 on day 27. All animals were imaged daily until day 34. All animals were probed with MMPSense 750 and subsequently imaged once more on day 34, before sacrifice at the experimental endpoint. i.d., Intradermal; i.v., Intravenous; Obs, observation.

4.2.3 CIA induction and MMPSense 750 imaging protocol in the APO866 treatment study

From the first two experiments, the MMPSense750 imaging agent was chosen for the final larger study, due to the ease of use of the Xenogen imaging system. Twelve male DBA-1 animals (Harlan) were purchased for this study. CIA was induced in ten

mice and two mice were used as naïve age-matched (non-immunised) controls. Two of the CIA immunised animals had to be removed from the experiment on days 21 and 23 prior to administration of probe or treatment. The first animal was killed as it showed signs of distress. The second animal died two days later, possibly due to anaesthesia sequelae. As no clinical signs of arthritis were seen in the remaining eight animals by day 25, mice were treated with a single i.p. injection of LPS, as described in section 2.2.1, in order to increase the rapidity and uniformity of disease. By day 27, six out of the eight remaining immunised mice showed clinical signs of arthritis (see timeline; figure 4.2.3A).

On day 27, all remaining immunised mice (n=6 with arthritis and n=2 no arthritis) and non-immunised controls (n=2 naïve) were injected with MMPSense750 FAST. All mice were imaged 24 hours post-injection (day 28) and every 24 hours thereafter until experimental endpoint (see section 2.2.2.3). Immediately after the imaging protocol was completed, CIA immunised animals (n=8) were assessed for arthritis. The mice were then divided into two treatment groups (n=4 per group) that were matched in arthritis severity (determined by clinical score). One group was implanted with an osmotic minipump set to release vehicle (propylene glycol in saline, section 2.2.3.1). The second group was implanted with osmotic minipumps set to release APO866 dissolved in sterile saline at a rate of 0.08 mg/kg/h. One mouse in each group showed no signs of arthritis (clinical score=0) at day 28 or until experimental end point (day 32). The non-immunised controls (n=2) received no treatment (figure 4.3.2B).

The day 32 fluorescence reading, when minimal fluorescence from the initial MMPSense750 FAST probe injection was detected, was taken as background. Mice were injected with one further dose of MMPSense750 FAST probe (2 nmol). The mice were re-imaged 24 hours after this 2nd injection, then killed and tissue harvested for subsequent analyses (section 4.2.4). MMPSense750 FAST fluorescence values were corrected for background fluorescence as described in section 4.2.3.

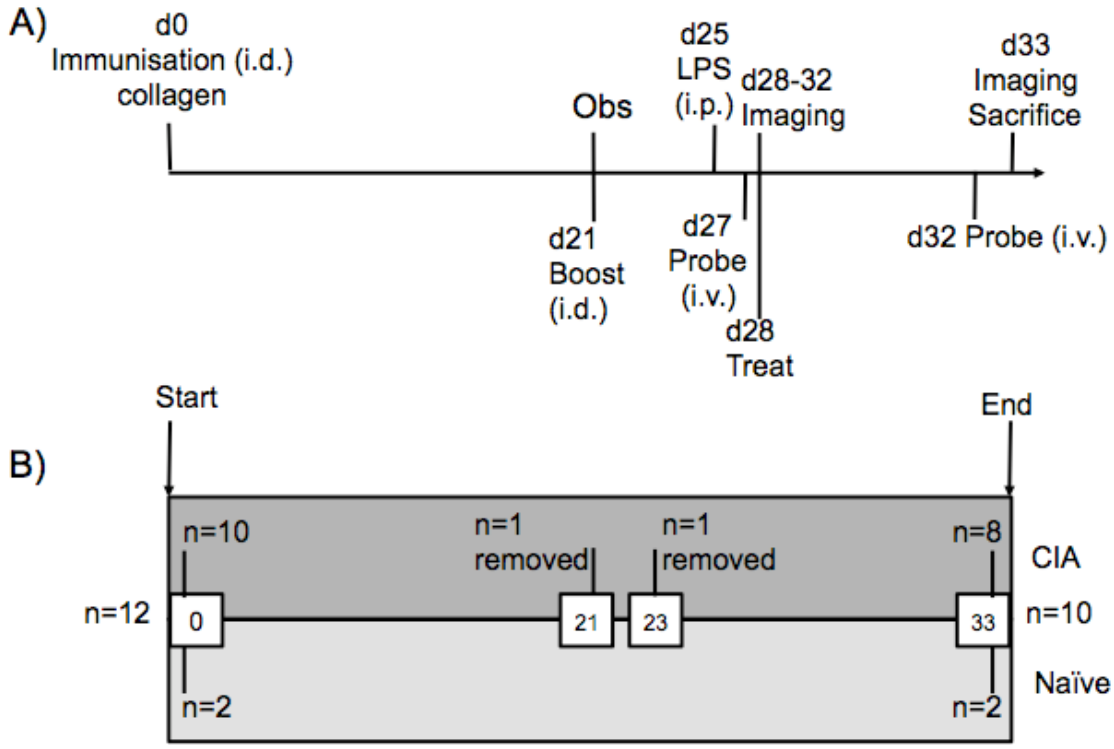

Figure 4.2.3 Experimental timeline of MMPSense750 APO866 treatment study

Twelve animals were used in this study. Ten animals were immunised with collagen at days 0 and 21. Two animals were not immunised and acted as a naïve controls. From day 21 onwards, animals were observed at least twice a week. On day 25, immunised animals were given a single i.p injection of LPS. On day 27, all animals were injected (i.v) with MMPSense750. On day 28, CIA animals were arranged into groups and treated by osmotic minipump. Naïve control animals were not treated with minipumps. Imaging continued daily until day 32, when animals were re-probed and re-imaged, prior to sacrifice at the experimental end point on day 33. B) Two animals had to be removed from the CIA experimental group on days 21 & 23. i.d., Intradermal; i.p, intra-peritoneal; LPS, Lipopolysaccharide; i.v., Intravenous; Obs, observation.

4.2.4 Post-mortem analyses

Hind limbs were removed and analysed by radiology (sections 2.2.1.2) and histopathology (section 2.2.1.3). Fore limbs were removed and analysed by radiology and qPCR (section 2.3.2). MMPs -1a, -3, -9 and -13 were analysed by qPCR because their expression is elevated in the RA synovium (Konttinen et al., 1999), (refer to Table 1.2). In addition, MMPs -9 and -13 preferentially cleave and activate the MMPSense probes (refer to figures 2.15 and 2.16 in materials and methods).

4.3 Results

The findings of the three individual experiments are presented in turn; the two MMP probe evaluation studies and the MMPSense750 APO866 treatment study. Arthritis induction data, clinical scores, *in vivo* imaging and mRNA analysis are presented. In addition, cDNA samples extracted from archived paws were analysed by qPCR to determine the dose-dependent effect of APO866 upon MMP expression in the joint. Finally, data were combined to determine the relationship between MMP activity (as determined by *in vivo* imaging) and other disease parameters.

4.3.1 MMPSense680 evaluation study

4.3.1.1 Animals in MMPSense680 evaluation study developed arthritis

For the initial study, six animals were immunised at day 0, and again at day 21, as described in section 4.2.1. By day 21, one animal displayed swelling in a front paw, and by day 26 all six animals had established arthritis (figure 4.3.1A), as apparent by a change in clinical score (figure 4.3.1C) and paw diameter (figure 4.3.1D). Paw diameters started to noticeably increase by day 26, and peaked at day 28, before subsiding. Weights of the animals dropped gradually in line with the rise in arthritis severity (figure 4.3.1E), which was attributed to impaired feeding as a result of decreased mobility (Griffiths et al., 1995). Loose pellets were distributed in the cage to counter this effect. Three of the mice were sacrificed prior to starting the imaging schedule because their combined clinical score exceeded the maximum (14) allowed within the project licence; one on day 28 and two on day 31 (figure 4.3.1B). The three remaining animals were used to trial the MMPSense680 probe.

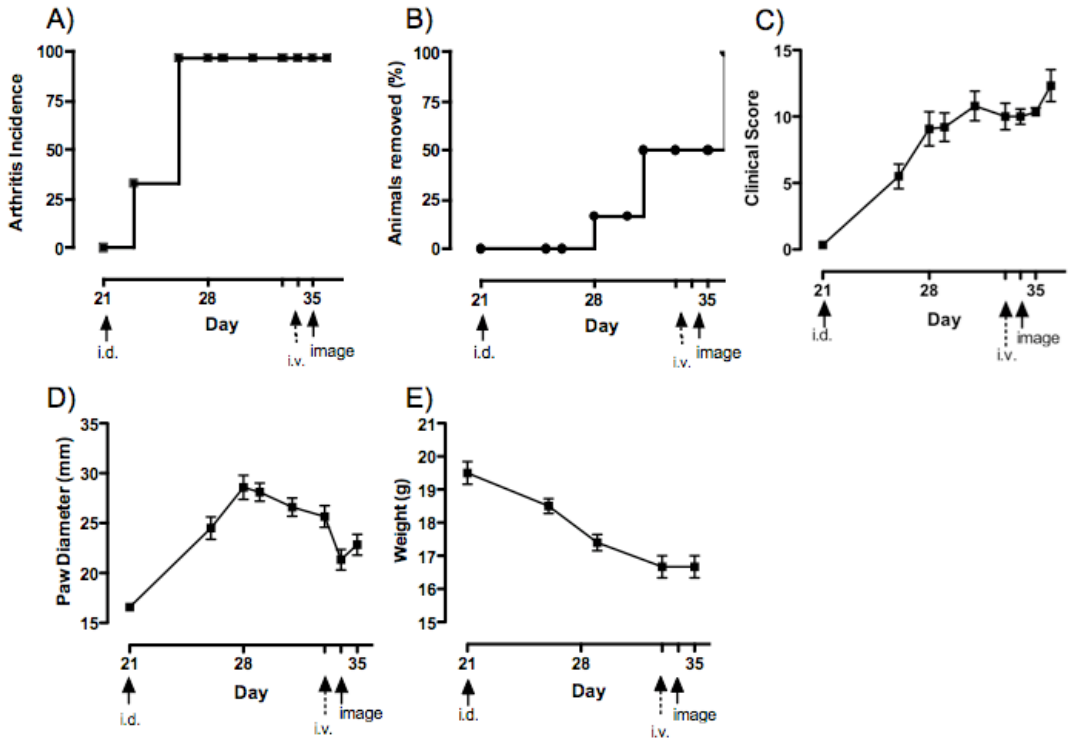

Figure 4.3.1 Arthritis incidence and survival in MMPSense680 evaluation study

N=6 animals were induced with CIA. A) Arthritis incidence in study group. B) Percentage of animals removed from the study; by day 31, three animals remained in the study. Animals were monitored for: C) clinical score, D) paw diameter and E) body weight. Data points Data plotted as mean ± standard error of the mean (S.E.M). i.d., intradermal booster injection of collagen; i.v., intravenous injection of MMPSense680

4.3.1.2 MMPSense680 probe was detected in arthritic limbs

Imaging data was first collected on day 34. The affected limbs fluoresced brightly, with swollen paws exhibiting visibly greater fluorescence than paws with milder swelling (figure 4.3.2). Although care was taken to ensure no probe was injected into the tail subcutaneously, tails also fluoresced slightly. The net intensity values were determined for each imaging time point and plotted over time for front and hind paws (figure 4.3.3). Although there was a clear signal drop-off for all limbs, particularly between 24-48 hours post-injection, fluorescence was still readily detectable by the experimental endpoint, particularly within the hind limbs.

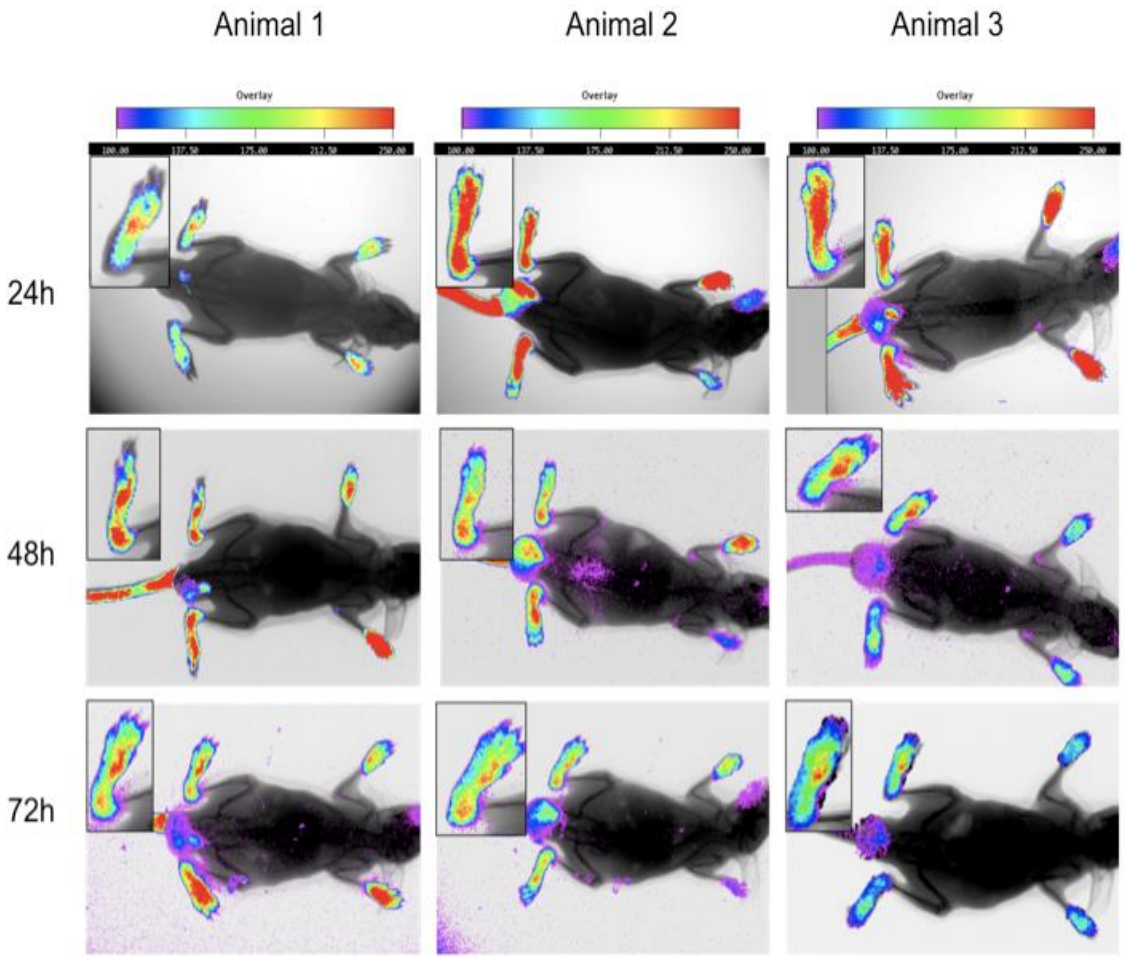

Figure 4.3.2 Detection of MMPSense680 fluorescence

Panel shows X-ray images of the three CIA animals, with fluorescent intensity shown as a pseudocolour overlay using the KODAK FX Pro imaging system. Whole animal images were taken on day 34 (24 hours post-injection) and every 24 hours thereafter. Boxes within each image depict high power hind paw images. Intensity scale [minimum=100, maximum=250 relative fluorescent units (rfu)].

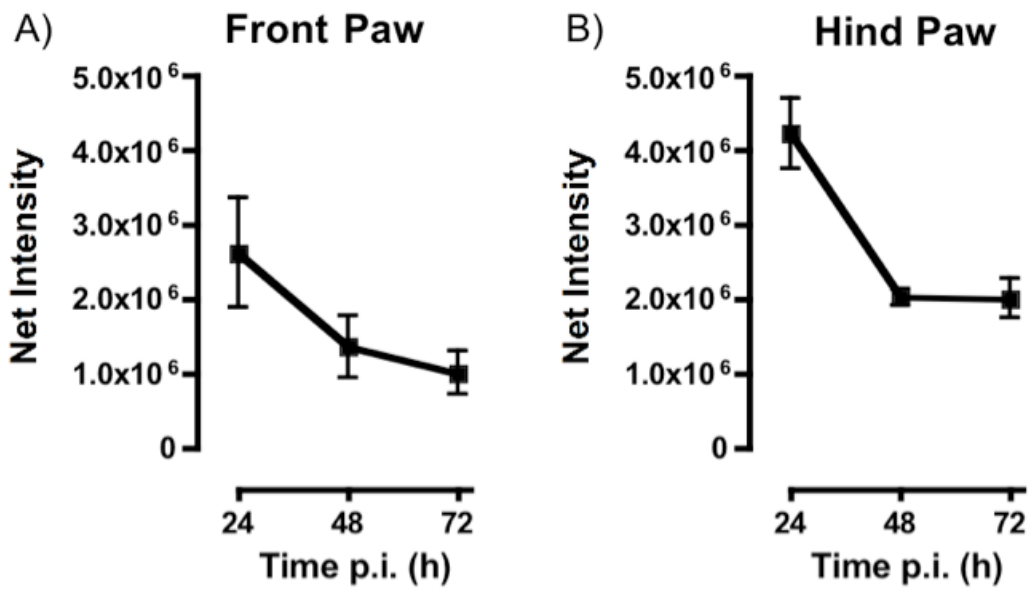

Figure 4.3.3 MMPSense680 fluorescent signal drop off

Net intensity readings (rfu) of each individual limb (n=3 animals, n=6 limbs) were taken every 24 hours until the experimental endpoint, using the KODAK FX Pro. A) Front paw readings taken at 24, 48 and 72 hours post-injection, at which point the experiment was terminated B) Hind paw readings. Data plotted as mean ± standard error of the mean (S.E.M) net intensity value (n=3 animals, n=6 limbs).

4.3.1.3 MMPSense680 fluorescence intensity correlated with clinical score

The net intensity values of the individual limbs taken 24 hours after probe administration (day 34) were plotted against respective paw diameter and clinical score values observed on that day. Net fluorescence intensity significantly correlated with clinical score (P=0.0027 r=0.9828; figure 4.3.4A). *A priori* (prospective) power analysis confirms that a sample size of n=10 limbs would have been sufficient to yield a significant (P≤0.05) correlation between net fluorescence intensity and clinical score. Net intensity correlated positively but not significantly with paw diameter (P=0.1302 r=0.688; figure 4.3.4B). *A priori* power analysis suggests a sample size of n=14 limbs would be required to yield a significant (P≤0.05) correlation between net fluorescence intensity and paw diameter.

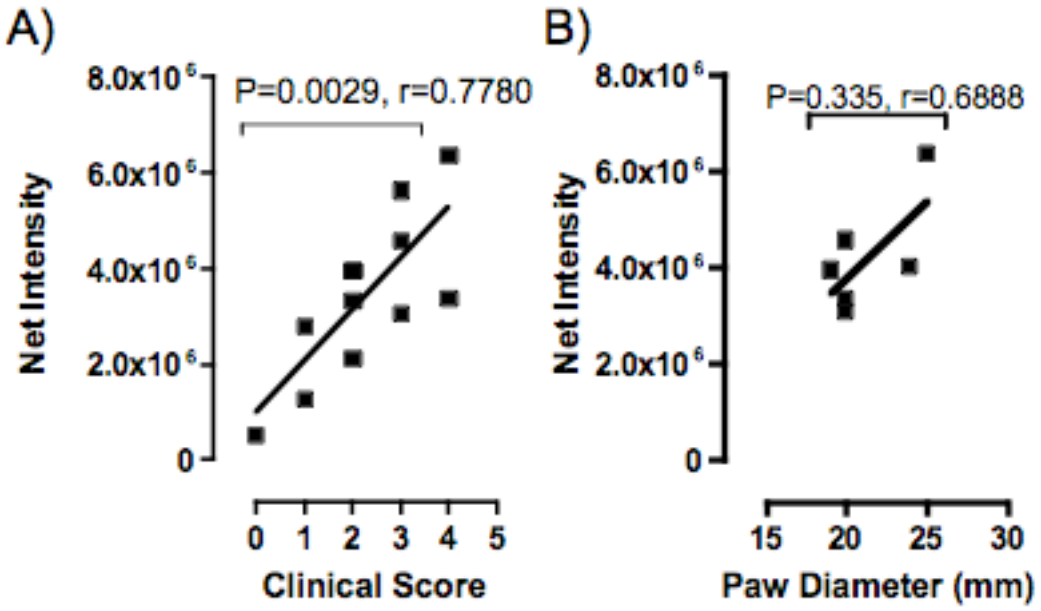

Figure 4.3.4 Comparing MMPSense680 fluorescence with arthritis index

An ROI analysis tool was used to determine the net fluorescent intensity of each individual limb. A) Correlation of clinical scores of front and hind limbs at day 34 with their respective net intensity values (three animals, n=12 limbs). B) Correlation of paw diameter of hind limbs at day 34 with their respective net intensity values (three animals, n=6 limbs). Correlation was determined using Pearson's Correlation coefficient. *A priori* power analysis was used to determine the sample size required to reject the null hypothesis of no significant correlation between the two variables based on the effect size (R-value).

4.3.1.4 MMPSense680 fluorescence was localised in areas of radiological and histological damage

All animals were sacrificed on day 36, hind limbs were harvested and high power x-ray images taken (see section 2.2.1.2). X-ray images showed evidence of soft tissue swelling in the hind paws, as well as signs of osteopenia, erosion (i.e. loss of continuity of cortical bone), and periosteal reaction (figure 4.3.5B[i]-[iii]), particularly within the MCP joints. It was noted that areas of radiological damage coincided with areas of greater MMPSense680 fluorescence intensity (figure 4.3.5A). Once x-rayed, hind paws were processed, fixed and sectioned for histological analyses as described in section 2.3.1. Histological staining showed evidence of inflammatory infiltrate, sub-synovial exudate and loss of cartilage integrity, as evidenced by loss of continuity of Safranin O staining of the joint surface (figure 4.3.5C[iv]-[vi]). Histological damage was particularly evident around the bones of the mid-foot and the individual MCP joints.

Correlation analyses were carried out to determine the association between MMPSense680 fluorescence intensity and radiology and histology scores. In all cases the sample size (n=6 limbs) was insufficient to infer a positive association between the variables. *A priori* power analyses based on r-value determined a sample size of 13 limbs would be required for a positive association between net intensity and radiology score ($P=0.2517$, $r=0.5562$; figure 4.3.5D). The associations between MMPSense680 fluorescence with histological ($P=0.4806$, $r=0.3621$; figure 4.3.5E) and cartilage erosion scores ($P=0.3335$, $r=0.4815$; figure 4.3.5F) were weak. The sample size was too small for accurate statistical interpretation ($n>40$ limbs required).

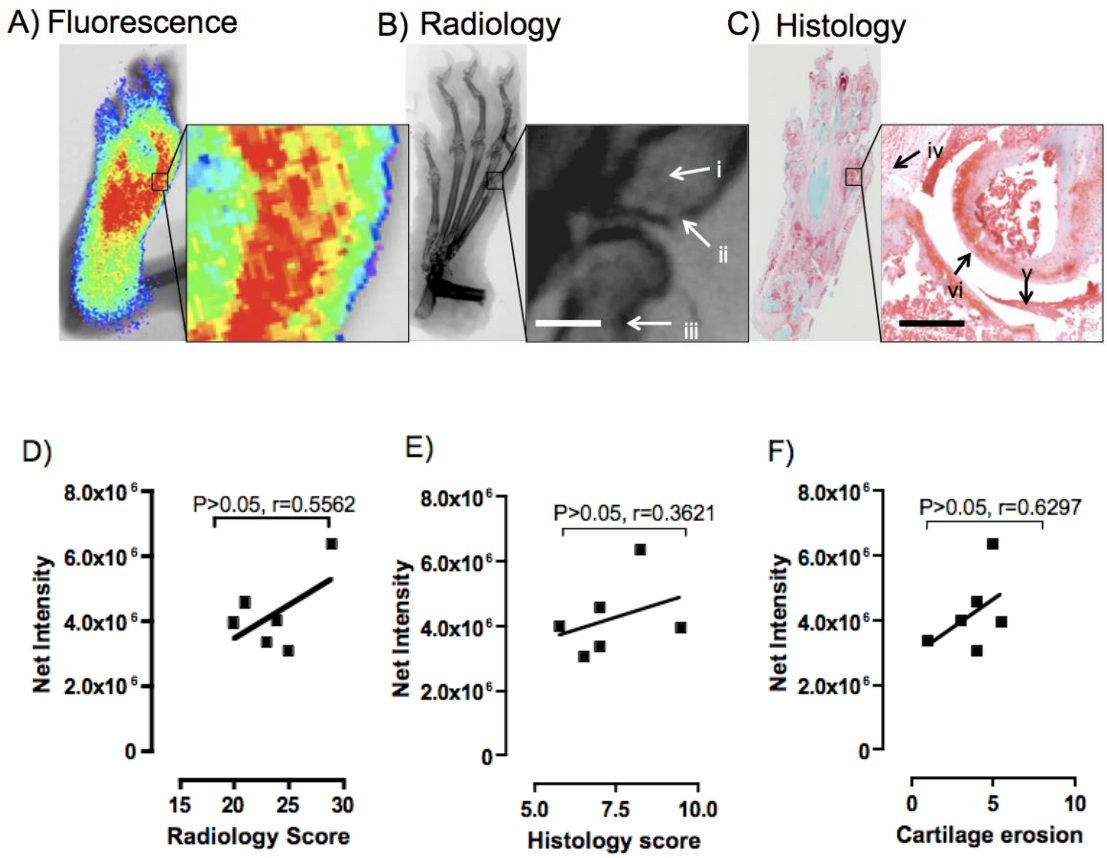

Figure 4.3.5 Comparison of MMPSense680 fluorescence distribution with radiological and histological disease parameters

A) A hind paw of a live animal imaged at day 34 (24 hours post-injection with MMPSense680), using the KODAK *in vivo* FX Pro. B) The same hind limb immediately after sacrifice (day 36), x-rayed at high power exhibiting: i) osteopenia ii) erosions iii) periosteal reaction. Tissues were fixed and processed, and 7 µm sections mounted and stained with Safranin O and fast green. C) High power image of an MCP joint, exhibiting: iv) inflammatory infiltrate v) sub-synovial exudate vi) cartilage degradation. Scale bars represent 500 µm. Fluorescence net intensity values of individual hind paws from day 34 (three animals, n=6 limbs) were related to their respective radiology scores and histology scores, and correlation determined using Pearson's correlation coefficient. Net intensities were related to D) radiology, E) histology and F) cartilage erosion scores. *A priori* power analysis used to determine the sample size required to yield a significant correlation between the two variables indicated sample sizes of >10 paws would be required.

4.3.1.5 MMPSense680 activity did not correlate with MMP mRNA expression

Gene expression levels of MMPs -1a, -3, -9 and -13 (figure 4.3.6A-D) from extracted cDNA of homogenised front paws did not significantly correlate with MMPSense680 fluorescence intensity readings from day 34. In fact, in some cases brightly-fluorescing limbs yielded relatively low levels of MMP gene expression. *A priori* power analyses indicate much larger sample sizes would be needed to yield a significant effect; therefore MMP enzymatic activity (as assessed by MMPSense680 fluorescence) cannot be meaningfully related to MMP gene expression in this experiment.

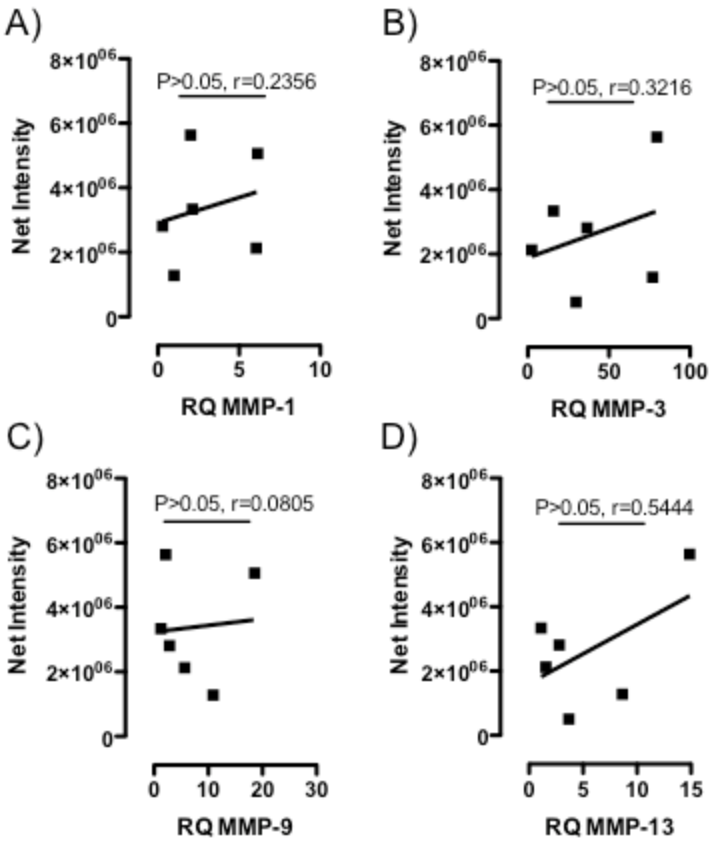

Figure 4.3.6 Relating MMPSense680 probe intensity to MMP mRNA

Whole front paws (three animals, n=2 limbs per animal) from day of sacrifice (day 36) were homogenised for qPCR analysis. Relative quantity of gene expression (RQ) was determined by analysing cDNA samples in duplicate and relating ΔC_T values of arthritic animals to those of a naïve control animal (n=2 limbs). Individual RQ readings for A) MMP-1a, B) MMP-3, C) MMP-9, and D) MMP-13 were correlated to the respective net intensity of their front paws 24 hours post-injection (day 34). Correlation analysis was carried out using Pearson's Correlation coefficient. *A priori* power analysis was used to determine the sample size required to reject the null hypothesis of no significant correlation between the two variables based on the effect size (r-value).

4.3.2 MMPSense750 FAST evaluation study

The first study stood as a preliminary proof-of-principle study of the MMPSense 680 probe. The second study was initiated to test the applicability of an alternative fluorescent probe, MMPSense750 FAST. Two female DBA-1 mice were immunised at day 0, and again at day 21, as described in section 4.2.2. A third DBA-1 mouse served as a naïve control. Clinical signs of arthritis were first observed in one mouse at day 24, but the other animal remained unaffected until day 34, when it presented with swelling in the proximal interphalangeal (PIP) joint (figure 4.3.7A). Clinical scores and paw diameters increased in the arthritic animal from day 24 (figure 4.3.7B). Paw diameter increased in comparison to the naïve control, with swelling peaking at day 29 before falling slightly in subsequent observations (figure 4.3.7C). As with the initial study, disease severity was accompanied by a loss in weight (figure 4.3.7D). Weight loss did not exceed the 20% limit specified in the project licence.

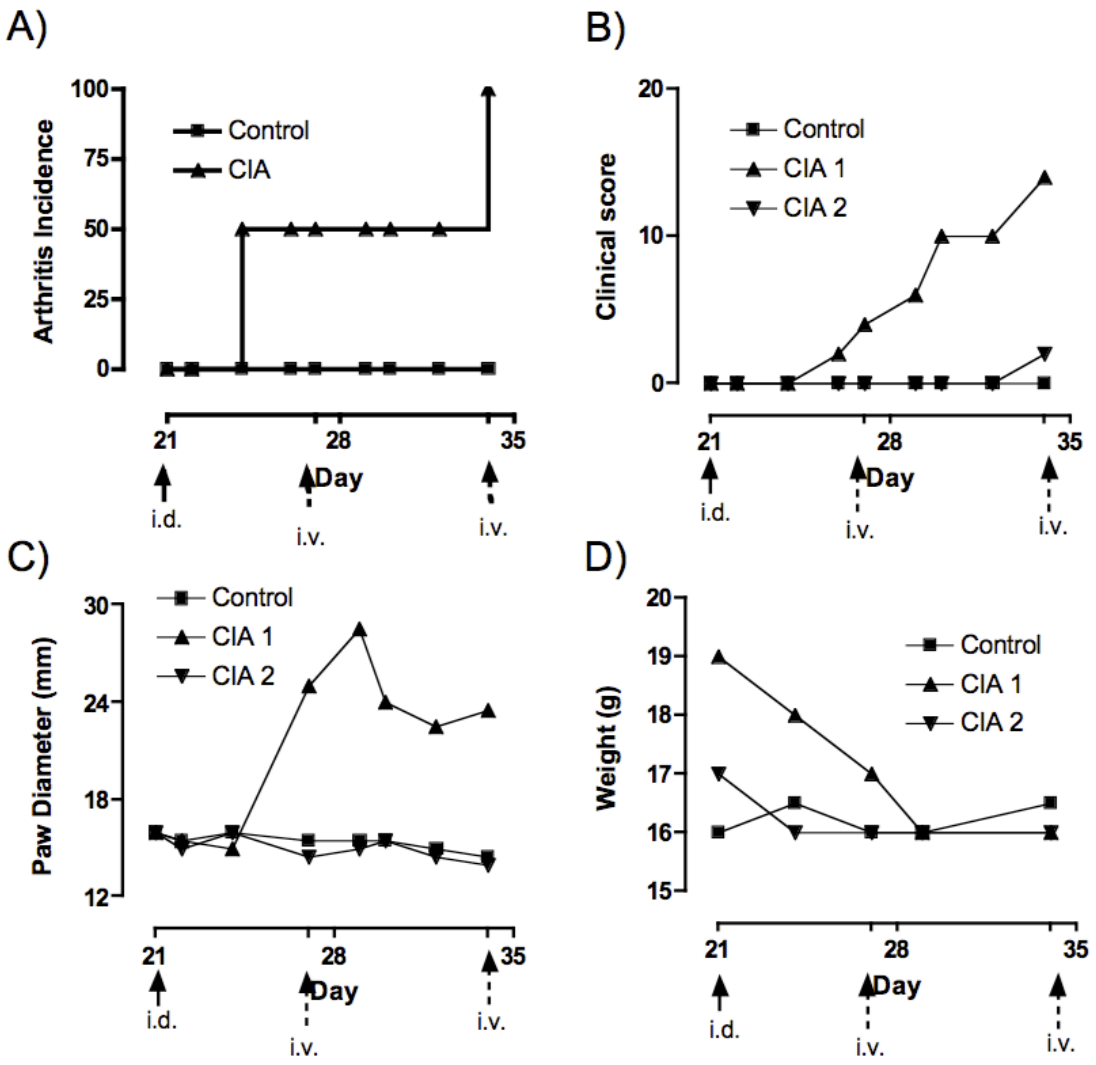

Figure 4.3.7 Experimental arthritis in the MMPSense750 evaluation study

The two CIA animals (labelled CIA 1 and CIA 2) and the naïve control were observed at least twice weekly from the day of the second i.d. (day 21). Animals were monitored for: A) arthritis incidence, B) clinical score, C) paw diameter and D) body weight. i.d., intradermal booster injection of collagen; i.v., intravenous injections of MMPSense750 probe; CIA, Collagen-induced arthritis animal.

4.3.2.1 MMPSense750 fluorescence was enhanced in arthritis compared with a naïve control

An i.v. injection of MMPSense750 was to be administered in animals at the first clinical sign of arthritis; in one CIA immunised animal, this occurred day 27. The entire volume (70 µl) of the probe was successfully injected into the tail vein of this mouse and the naïve control. The second CIA mouse was not injected with the probe until day 34, as there were no signs of disease until this time (explained further in section 4.3.2.3). Imaging was carried out immediately upon injection of the probe (0h) and every 24 hours thereafter, using the Xenogen IVIS 200, as detailed in section 2.2.2.3. Analysis of whole animal fluorescent overlays showed that the limbs fluoresced strongly, particularly the hind paws, up to 120h post-injection (figure 4.3.8). MMP fluorescence was considerably more intense in the arthritic mouse than in the naïve mouse, as evident from the pseudocolour display. MMPSense fluorescence was apparent at the injection site in the base of the tail for all both of the mice injected with the probe.

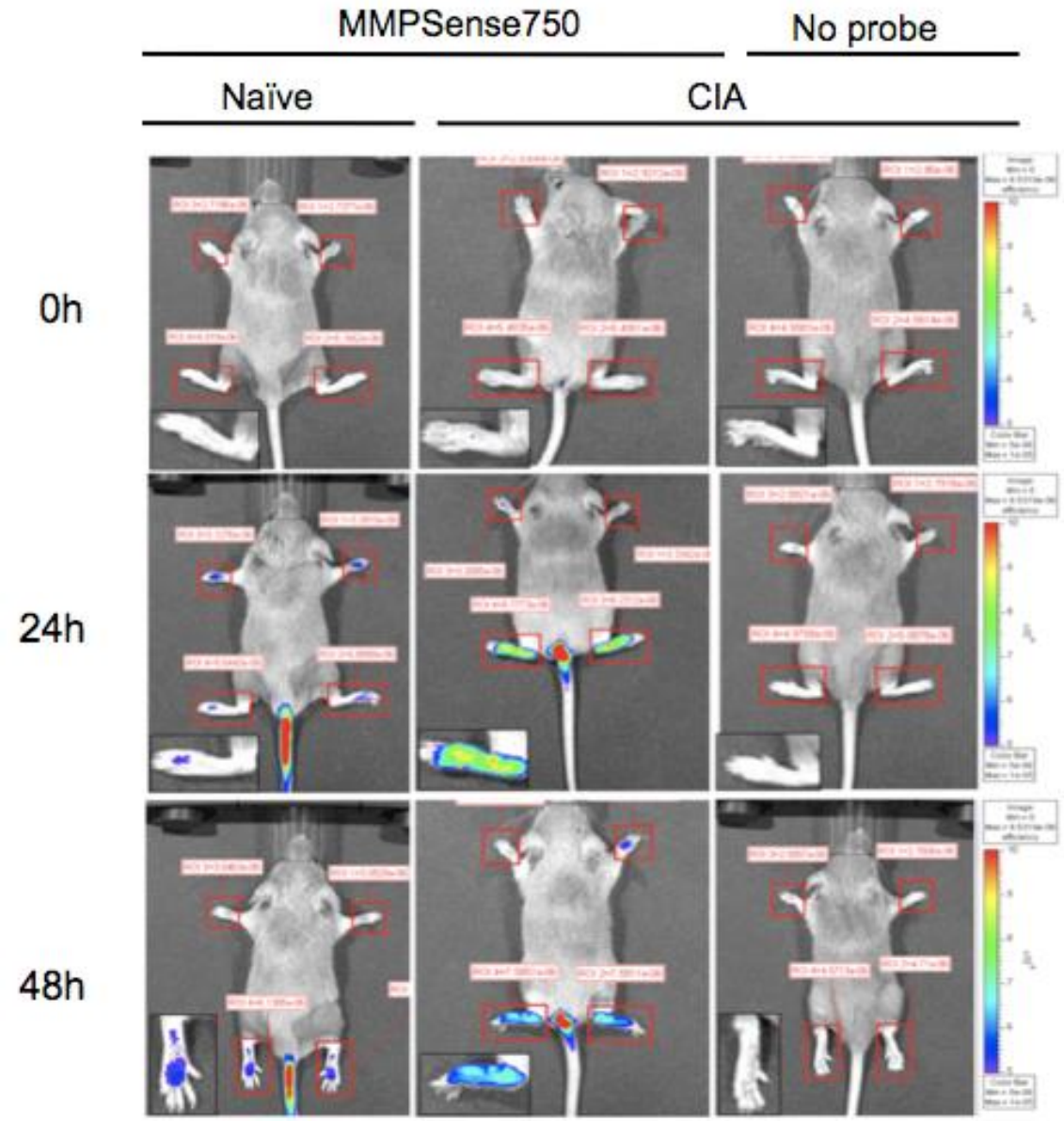

Figure 4.3.8 Detection of MMPSense750 Fast

Panel shows photographic images of the three mice, with fluorescent intensity shown as a pseudocolour overlay using the Xenogen IVIS 200 imaging system. Two mice were administered MMPSense750 FAST, the naïve control (CON) and the one mouse with clinical signs of arthritis (middle column). The other CIA mouse did not receive MMPSense750 FAST (no probe). Whole animal images were taken on day 27 (immediately after probe administration and every 24 hours thereafter up to 120h post-injection (time course continued overleaf). Boxes within each image depict high power hind paw images. Red boxes show the ROIs used in the analysis. Intensity scale (minimum=5 x 10^{-6}, maximum=1.0 x10^{-5} units).

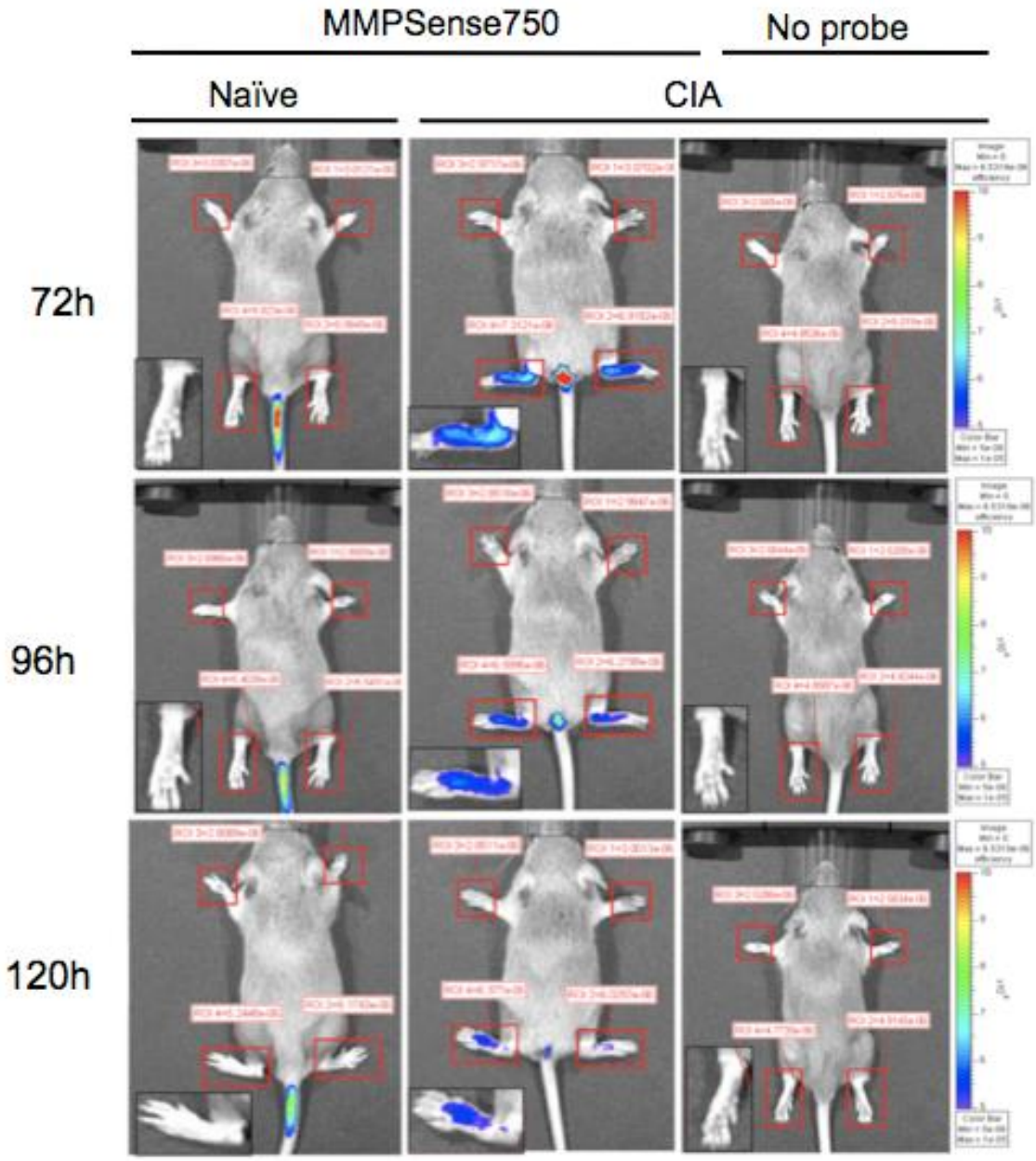

Figure 4.3.8 (continued from previous page): Detection of MMPSense750 Fast

4.3.2.2 MMPSense750 fluorescence was still detectable five days post-injection

Fluorescence efficiency was monitored daily from day 27 to 32 to determine signal drop-off. Although the MMPSense750 probe was not completely cleared by day 32 (120h post-injection), fluorescence in the arthritic mouse had fallen close to those of the naïve (non-arthritic) control in both front paws (figure 4.3.9A) and hind paws (figure 4.3.9B). In contrast to hind paws, there was negligible difference in front paw fluorescence between naïve and CIA mice (mean efficiency values 2.75×10^{-6} and 2.93×10^{-6}, naïve and CIA, respectively), indicating that fluorescence was not as enhanced in these tissues compared with hind paws.

The results obtained from experiments with MMPSense680 were compared against the data acquired for MMPSense750. The drop in MMPSense750 versus MMPSense680 fluorescence efficiency over the first 72 hours post injection was plotted (figure 4.3.10). These data show the half-life of the MMPSense750 probe was 57.2 hours (front paws) and 61.3 hours (hind paws) compared against 1.3 hours (front paws) and 3.6 hours (hind paws) for MMPSense680. These data contradict the manufacturer's guide, which claim a half-life of 5 hours for the MMPSense750 probe (Groves et al., 2010).

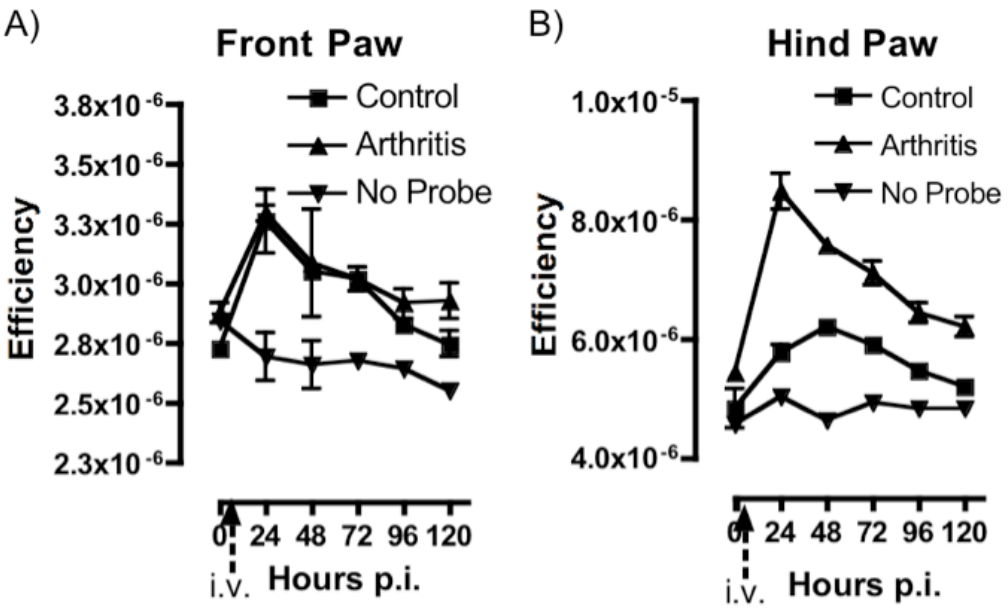

Figure 4.3.9 MMPSense750 FAST signal drop off

Mice (n=2 limbs per animal) were imaged on day 27 (0h), prior to injection of MMPSense750 using the XENOGEN IVIS 200. Mice were then imaged 24 hours post-injection, and every 24 hours thereafter, up until 120 hours post-injection (day 32). The no probe mouse was CIA immunised but with no clinical signs of disease. Raw fluorescence values (four per animal) were determined at every time point using ROI analysis. A) Drop in efficiency values in front paws by 120 hours. B) Hind paw efficiency values from 0-120 hours. Data points were graphically presented with mean ± standard error of the mean (S.E.M). Values here are raw values obtained from ROI software, not corrected for background autofluorescence.

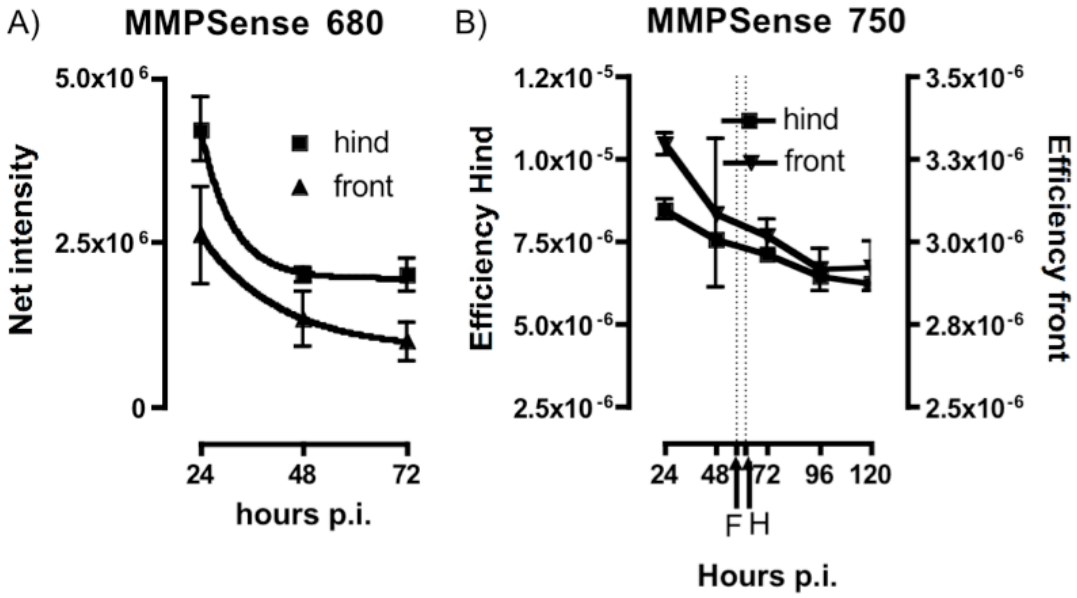

Figure 4.3.10 Comparison of MMPSense680 and MMPSense750 probe clearance

Raw fluorescence values from arthritic mice were taken from each time point up until 72 hours post-injection to determine which probe had the fastest rate of clearance. From these raw values a percentage drop/rise in fluorescence relative to the first imaging time point (24 hours p.i.) was determined for each subsequent time point. A) MMPsense680 free-form ROI net intensity values using KODAK MI software. Rate of decay from 24 hours p.i. was calculated using one-phase exponential decay (Prism) and determined using non-linear regression analyses (three mice, n=6 front and hind limbs). Front paws: half-life=1.26 hours, K=0.06 units/h, hind paws: half-life=3.59 hours, K=0.19 units/h. B) MMPSense750 efficiency values using the IVIS 200 system with ROI analysis of a fixed dimension around the limb. Fluorescence from the first imaging time point 24 hours p.i. (one mouse, n=2 front and hind limbs). The plateau values taken from the no-probe control were used to accurately determine half-life. Front paws: half-life=57.24 hours, K=0.012 units/h, hind paws: half-life=61.3 hours, K=0.011 units/h. F= half-life of front paws, H= half-life of hind paws.

4.3.2.3 MMP fluorescence signal differed in early and advanced disease

On day 34, the second CIA immunised mouse had begun to exhibit very early clinical signs of arthritis (i.e. a swollen PIP joint, and clinical score of 1). This mouse was injected with MMPSense probe, as well as the first CIA mouse and the naïve control. For this part of the experiment, this former 'no probe control' was subsequently referred to as an early arthritis (EA) animal. The other CIA mouse, whose clinical score on day 34 was 14, was referred to as the advanced arthritis (AA) animal. Six hours post-injection, the early arthritis animal exhibited a small area of enhanced fluorescence, which was localised to the single proximal interphalangeal (PIP) joint in the left hind paw (figure 4.3.11). The front paws remained unaffected, and showed no evidence of fluorescence. In contrast, the mouse with advanced arthritis demonstrated a large degree of fluorescence in all limbs (figure 4.3.11). Although MMPSense750 fluorescence had reduced in intensity in the naïve and advance arthritis animal from the previous injection administered on day 27, a small amount of residual fluorescence remained, which was taken into account in the analysis. Overall, these data reiterate the sensitivity of the MMPSense probes, and how *in situ* MMP activity is a good reflection of the disease state of the animal.

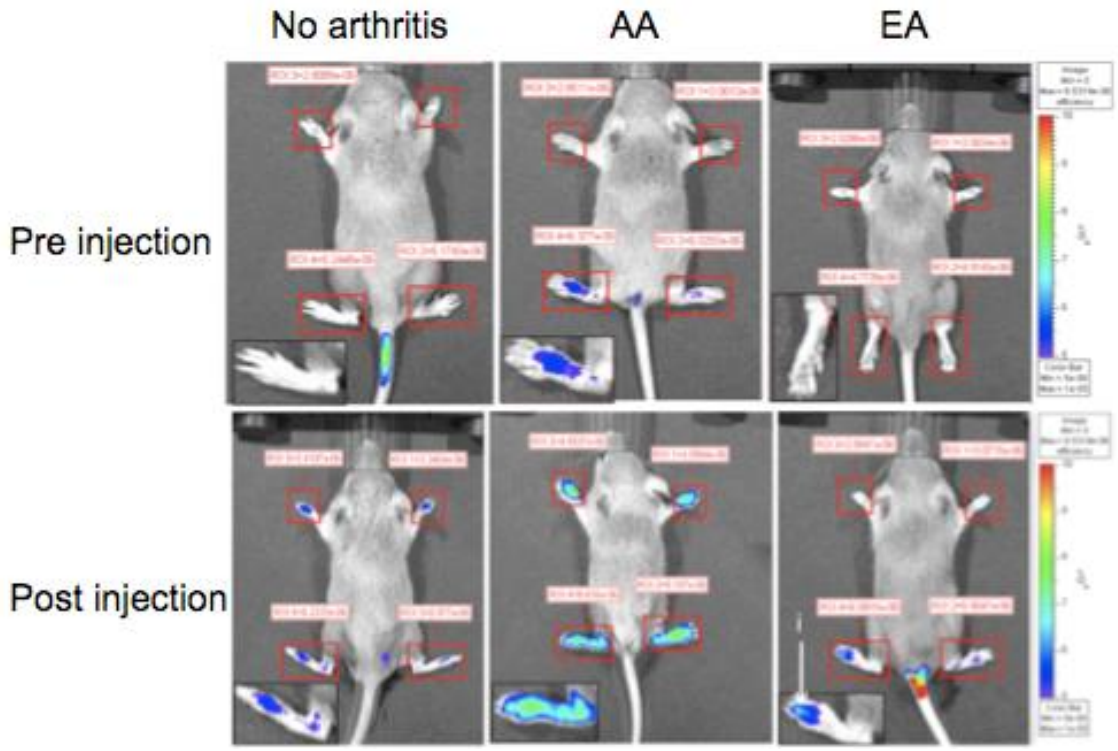

Figure 4.3.11 MMPSense750 FAST fluorescence images on day 34

Panel shows photographic images of the three mice, with fluorescent intensity shown as a pseudocolour overlay using the Xenogen IVIS 200 imaging system. All animals were administered MMPSense750 FAST: the naive control (CON), the mouse with advanced arthritis (AA), and the mouse with early arthritis (EA). Whole animal images were all taken on days 34 and 35, immediately before probe administration (top panel) and 24 hours post-injection (bottom panel). Boxes within each image depict high power hind paw images. i) High power magnification of early arthritic hind paw, showing enhanced fluorescence in one of the proximal interphalangeal joints (PIPJ). Red boxes show the ROIs used in the analysis. Intensity scale (minimum=5.0 x 10^{-6}, maximum=1.0 x10^{-5} units.

4.3.2.4 Early signs of arthritis were detectible in radiological and histological examination

The three experimental animals (described above) were sacrificed at day 34.Their hind paws were X-rayed and scored (section 2.2.1.2). The hind paws from the naïve and early arthritis mice (CIA onset day 34) exhibited no signs of radiological damage. In contrast, the hind paws of the mouse with advanced arthritis (CIA onset day 24) showed signs of osteopenia and erosions around the cortical bone (figure 4.3.12). This was reflected in the radiology scores obtained (figure 4.3.12D). Due to the small sample size, no statistical analyses were performed on these data.

Hind paws were then processed for histological analyses (section 2.3.1). The advanced arthritis animal had evidence of inflammatory infiltrate and signs of cartilage erosion (figure 4.3.13). This was in contrast to the naïve control (figure 4.3.13A), which showed no evidence of damage. One paw from the mouse with early arthritis showed some evidence of disease, with a high number of inflammatory cells localised around one of the proximal interphalangeal (PIP) joints and no other pathology (figure 4.3.13C). These differences were reflected in the histological (figure 4.3.13D) and cartilage erosion scores (figure 4.3.13E).

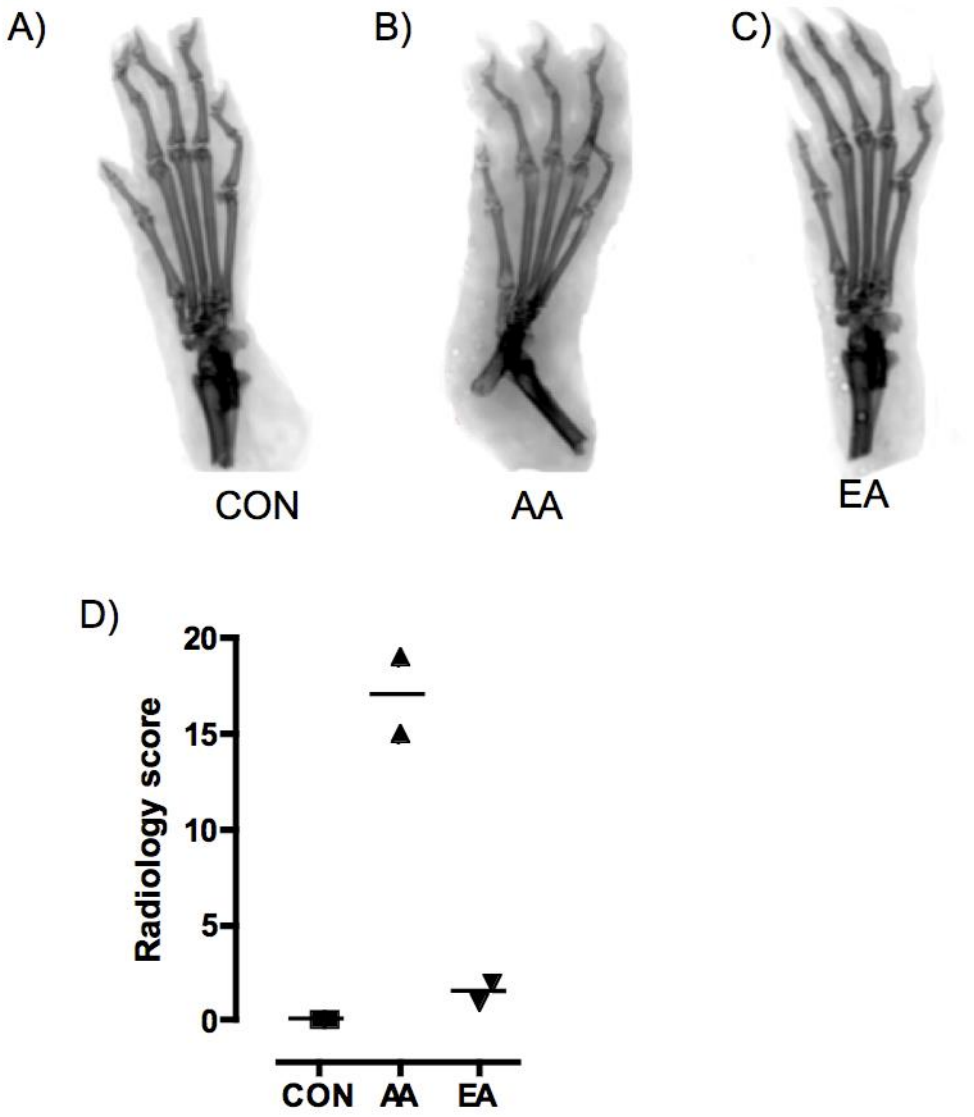

Figure 4.3.12 Comparison of radiographic images of hind paws

Representative hind paw images taken at time of sacrifice (day 34), from A) naive control mouse, B) mouse with advanced arthritis (AA) and C) mouse in the early stages of disease (EA). D) Radiology scores obtained from each mouse (n=2 limbs per mouse).

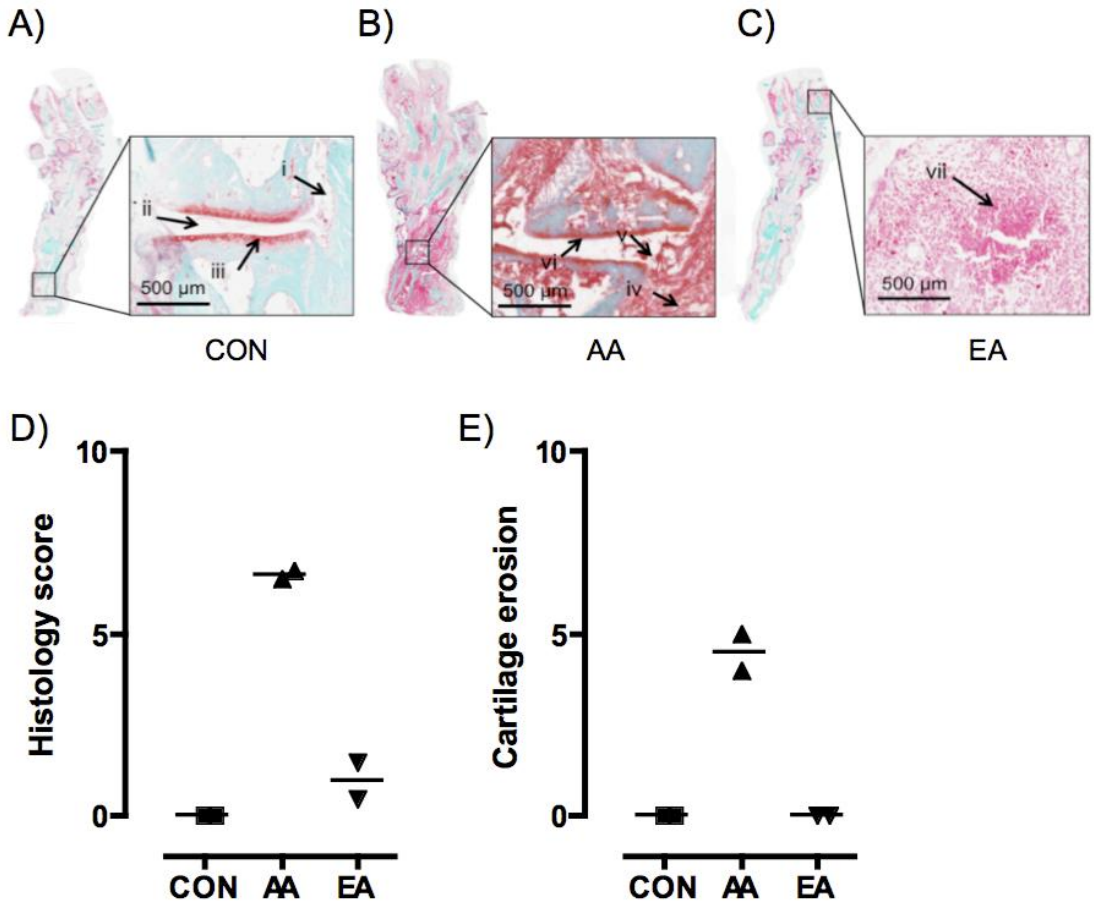

Figure 4.3.13 Histological assessment of disease

A) A representative hind paw of the naïve control mouse (CON). Boxed area: High power magnification of the hind-foot region from a normal tissue section showing i) normal adipose tissue, ii) no synovial exudate, and iii) normal healthy cartilage. B) Histological image of a mouse with advanced arthritis (AA) Boxed area: High power magnification of the diseased hind-foot region contains substantial iv) synovial infiltrate, v) exudate and vi) some loss of continuity of Safranin O staining, indicating early signs of cartilage erosion. C) High paw from early arthritis (EA) mouse. Boxed area: swollen proximal interphalangeal joint. D) Histology and E) Cartilage erosion scores taken from each mouse (n=2 limbs for each).

4.3.3 MMPSense750 APO866 treatment study

The final *in vivo* imaging experiment involved the use of MMPSense750 FAST as a tool to monitor changes in MMP activity resulting from inhibiting NAMPT (using APO866) in animals with established CIA.

By day 27, 75% arthritis incidence was achieved in CIA animals (figure 4.3.14A). Of all the surviving immunised animals, two did not develop arthritis. Data from these animals are not presented in the main analyses, but are presented separately in section 4.3.3.8. During the course of the experiment, two animals were removed from the study, leaving eight immunised animals and the two naïve control mice (figure 4.3.14B).

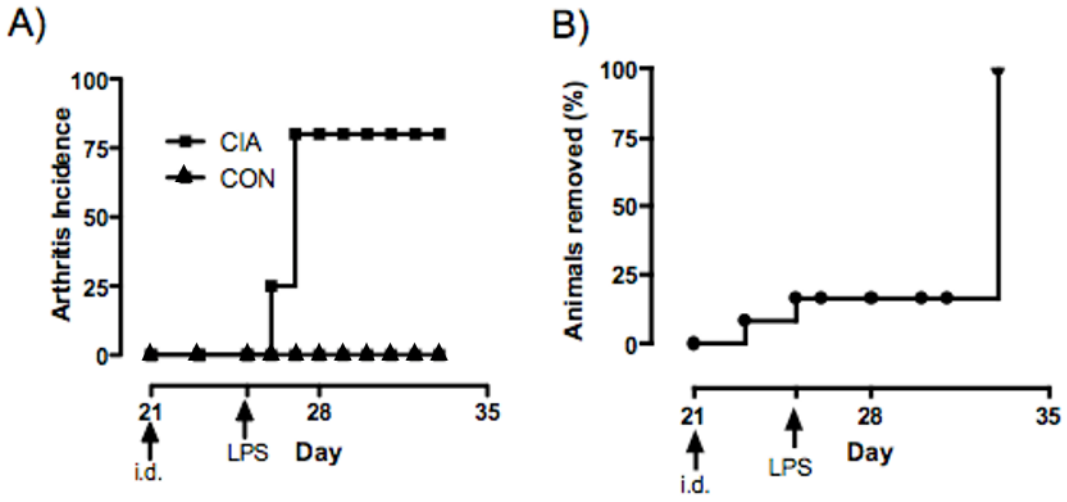

Figure 4.3.14 Experimental arthritis in MMPSense750 APO866 treatment study

A) Arthritis incidence graph of animals immunised with collagen (n=10 animals; CIA) compared to naïve controls (n=2 animals; CON). B) Percentage of animals removed from analysis throughout the course of the study. i.d., intradermal booster injection of collagen; LPS, injection of lipopolysaccharide.

4.3.3.1 CIA animals were evenly distributed into groups prior to minipump treatment based on clinical score

CIA animals showed signs of arthritis at day 28. However, scores were varied and there were no significant differences in front or hind paw clinical scores between CIA and control animals (P<0.0001 for both front and hind paws, figures 4.3.15A and B, respectively). Hind paws of CIA animals were markedly swollen compared with control animals, as determined by a significant increase in paw diameter (P=0077; figure 4.3.15C). No front paw measurements were taken, as this is not easily measurable by caliper. The two animals that did not develop disease were each placed into the VEH and APO groups, in the event that they may develop disease at a later date. However, this did not happen and therefore analyses of these animals have been kept separate and the data are presented in section 4.3.3.8.

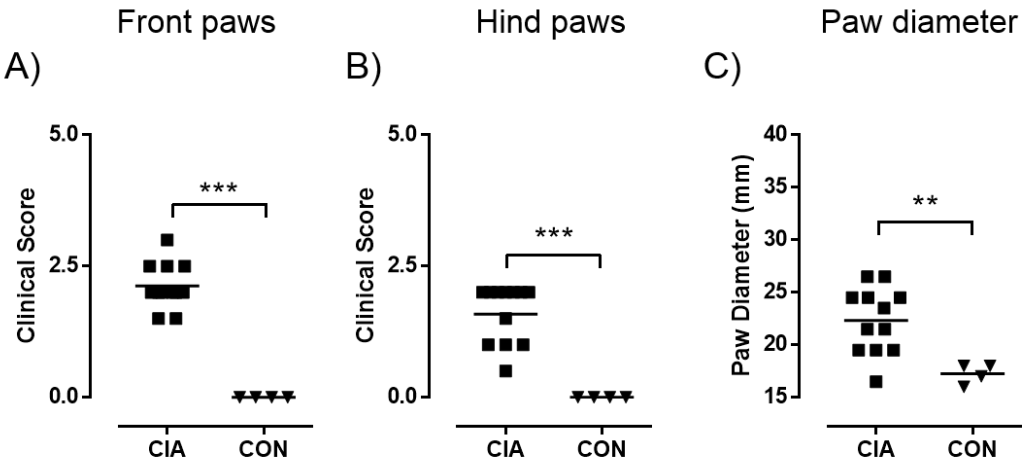

Figure 4.3.15 Clinical assessment of disease on day 28 (pre-treatment)

Prior to treatment, collagen-immunised animals (CIA; six animals, n=12 limbs) were scored and compared to naïve control animals (CON; two animals, n=4 limbs). Immunised animals with no signs of arthritis were excluded from this analysis. A) Front paw clinical score observations at day 28. B) Hind paw clinical score observations. C) Hind paw diameters measured on day 28. Lines on graph represent the mean values. Significant differences between means were determined using a two-tailed unpaired t test. **=P≤0.01, ***=P≤0.0001.

4.3.3.2 MMPSense750 fluorescence was consistent in CIA animals prior to treatment

MMPSense750 probe was administered to all animals on day 27 and imaging occurred 24 hours later (i.e. day 28). As with the previous MMPSense750 study, the extent and intensity of fluorescence in both front and hind paws was noticeably greater in CIA animals compared to the naïve controls (figure 4.3.16). The CIA-immunised animals with no clinical signs of arthritis are presented elsewhere (figure 4.3.27). The increase in fluorescence was reflected in the ROI analyses, which showed significantly greater efficiency values in animals with established arthritis compared to the naïve controls. This was evident in both front paws ($P<0.0001$; figure 4.3.17A) and hind paws ($P<0.0001$; figure 4.3.17B); as confirmed by Dunn's post-test analyses. All immunised animals were placed were then divided into VEH or APO treatment groups (n=4 per group), matched in arthritis severity (determined by clinical score).

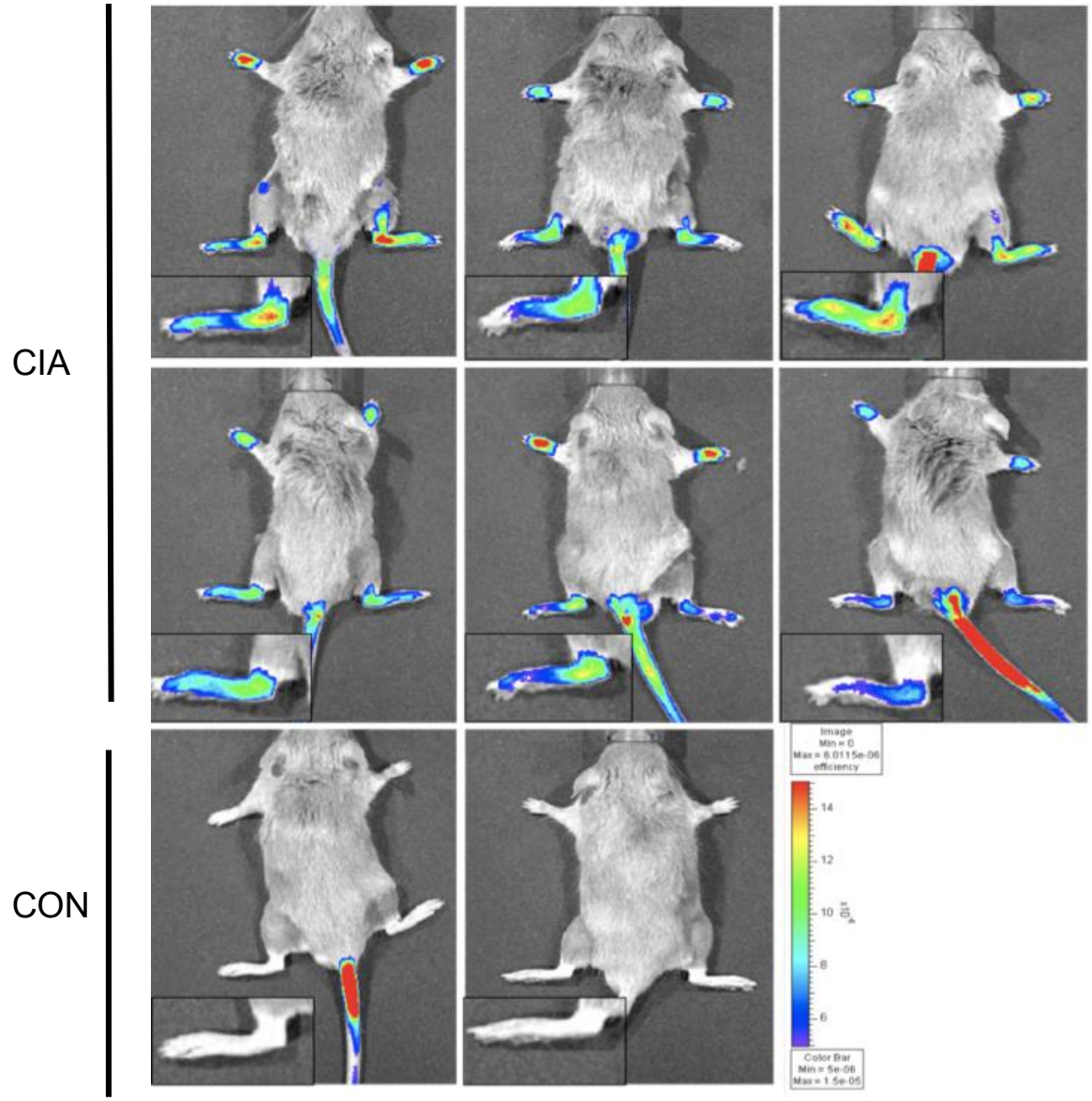

Figure 4.3.16 Fluorescence intensity on day 28

Panel shows photographic images of the six animals with established arthritis (CIA) and two naïve control (CON) animals, with fluorescent intensity shown as a pseudocolour overlay using the Xenogen IVIS 200 imaging system. All animals were administered MMPSense750 FAST on day 27 and whole animal images were taken on day 28, immediately before minipumps were inserted. Boxes within each image depict high power hind paw images. Intensity scale (minimum=5.0 x 10^{-6}, maximum=1.0 x10^{-5} units).

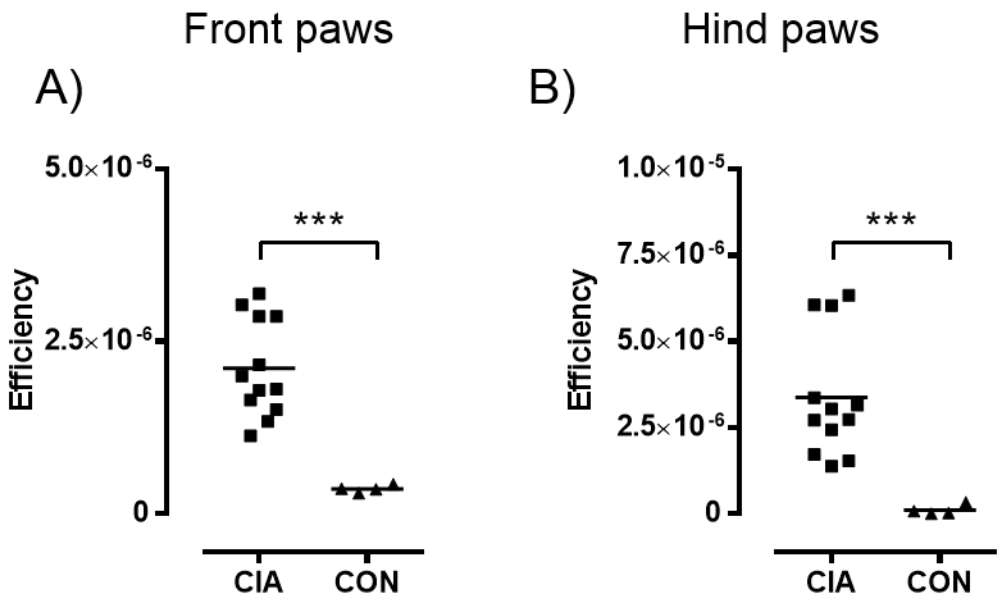

Figure 4.3.17 Fluorescence efficiency values on day 28

Individual front and hind paw efficiency readings taken 24 hours after probe administration and immediately before minipumps were inserted (i.e. day 28). Values were corrected for background autofluorescence and arranged by treatment group. A) Front paw fluorescence efficiency values of animals with established arthritis (CIA; six animals, n=12 limbs) and naïve control (CON) group (two animals, n=4 limbs). B) Hind paw fluorescence efficiency. Significant differences between means were determined using a two-tailed unpaired t test. ***=P≤0.0001.

4.3.3.3 Clinical scores were significantly enhanced in vehicle, but not APO866-treated CIA animals, four days post-treatment

After four days after the commencement of treatment with 0.08 mg/kg/h APO866 treatment (day 32), mean clinical scores were compared with those of vehicle animals. Although median clinical scores were generally lower in APO866-treated animals, this difference was not statistically significant compared with the vehicle controls. This was the case for both front paws and hind paws (P=0.0937 and P=0.00839; front and hinds paws, respectively; figures 4.3.18A and B). However, hind paw swelling in general was significantly attenuated in APO866-treated animals compared with vehicle controls (P=0.0307; figure 4.3.18C). This suggests that after four days of treatment, APO866 is beginning to attenuate paw swelling.

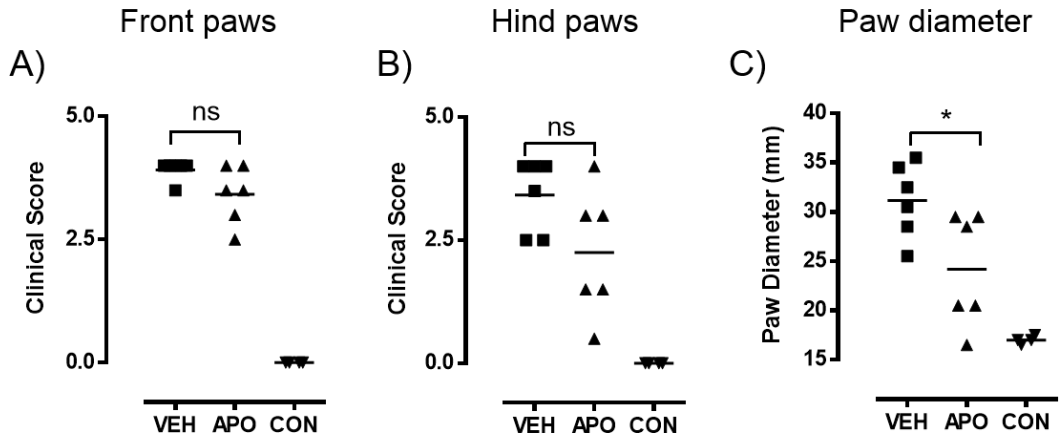

Figure 4.3.18 Clinical assessment of disease on day 32 (post-treatment)

Clinical scores of animals in the vehicle (VEH) group (three animals, n=6 limbs), 0.08 mg/kg/h APO866 (APO) group (three animals, n=6 limbs) and naïve control (CON) group (two animals, n=4 limbs), four days after the commencement of treatment (day 32). A) Front paw clinical score observations at day 32. B) Hind paw clinical score observations C) Hind paw diameters measured on day 32. Lines on graph represent the mean values. Significant differences between means were determined using a two-tailed unpaired t test.*=P≤0.05, ns=not significant (P>0.05).

4.3.3.4 MMPSense750 fluorescence was significantly enhanced in vehicle, but not APO866-treated CIA animals

On day 32, animals were imaged and fluorescence detected. From observation of the fluorescence images alone, the extent and intensity of MMP fluorescence had increased in all CIA mice over the treatment period. However, fluorescence in APO mice appeared visibly attenuated compared to vehicle-treated animals (figure 4.3.19). These observations were supported by ROI analyses, which showed that front paw fluorescence readings were significantly higher in the vehicle treated mice compared with animals treated with APO866 (P=0.0021; figure 4.3.20A). This was also the case with hind paw readings (P=0.0096; figure 4.3.20B). These data indicate that MMP enzymatic activity was dampened in the limbs of animals treated with APO866.

The changes in MMPSense fluorescence efficiency over time in the different treatment groups were also monitored (figure 4.3.21). From days 28 to 32, fluorescence efficiency readings from VEH animal front paws increased, though this was not statistically significant (P=0.0564; figure 4.3.21A). However, hind paw fluorescence values were significantly elevated by over 90% throughout the treatment period (P=0.0089; figure 4.3.21B). In the APO group, MMPSense fluorescence was significantly elevated over the treatment period in front paws (P=0.0211; figure 4.3.21C), but not in hind paws (P=0.7793; figure 4.3.21D). In fact, in some instances fluorescence efficiency in these animals decreased. This resulted in an overall drop of 12.1% in fluorescence efficiency between pre- and post-treatment values. Finally, fluorescence in naïve controls remained largely unchanged in all paws (P=0.9538 and P=0.0511; figures 4.3.21E-F; front paws and hind paws, respectively). Overall, these data show that although APO866 treatment did not halt the progression of disease in CIA mice, it did slow it down somewhat, compared with treatment with a vehicle control.

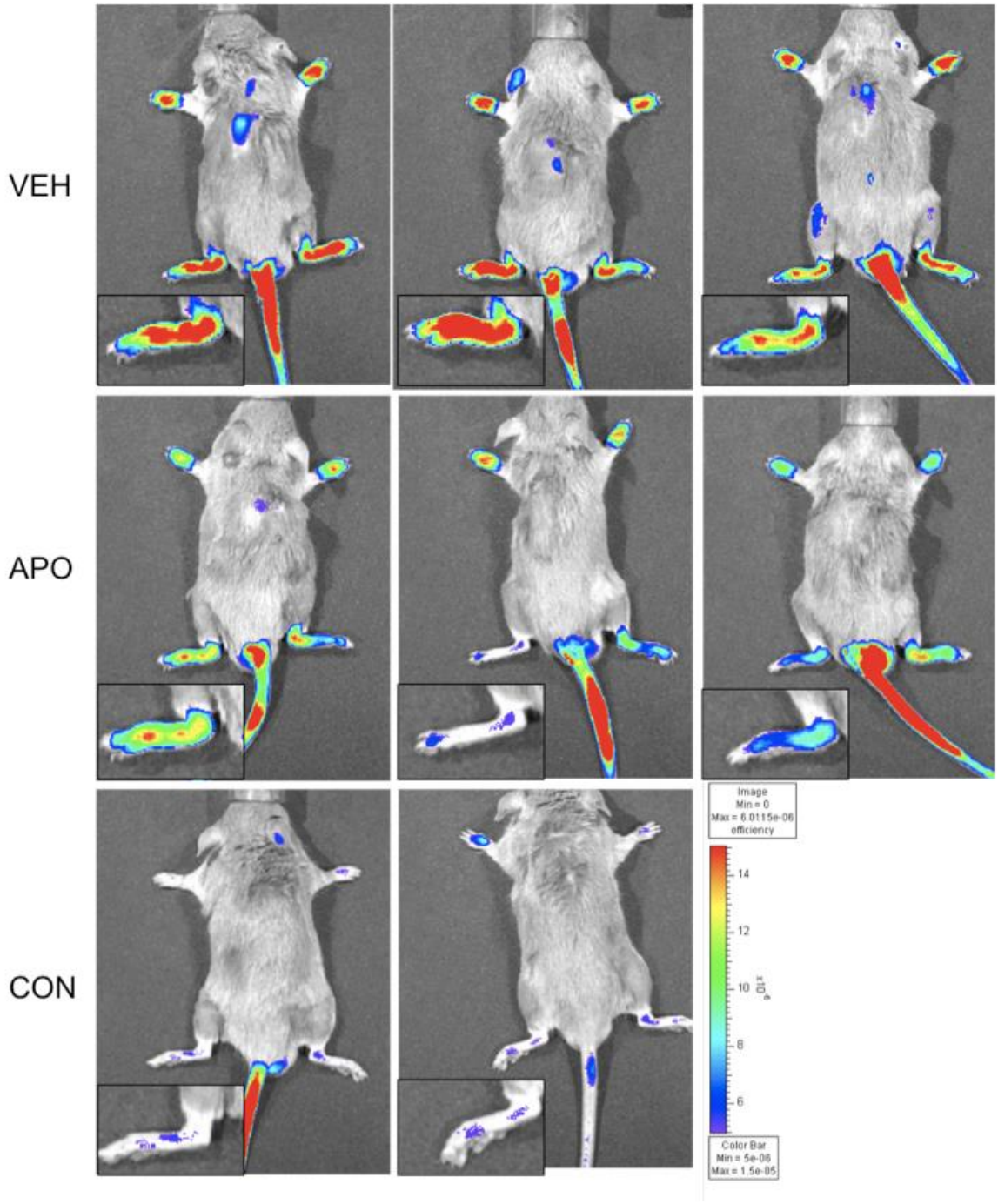

Figure 4.3.19 Fluorescence intensity on day 32 (post-treatment)

Panel shows photographic images of the six animals with established arthritis (VEH and APO groups) and two naïve control (CON) animals, with fluorescent intensity shown as a pseudocolour overlay using the Xenogen IVIS 200 imaging system. All animals were administered MMPSense750 FAST on day 32 and whole animal images taken 6 hours later and 4 days after minipumps were inserted, administering vehicle alone (VEH) or 0.08 mg/kg/h APO866 (APO). Boxes within each image depict high power hind paw images. Intensity scale minimum=5.0 x 10^{-6}, maximum=1.0 x10^{-5} units.

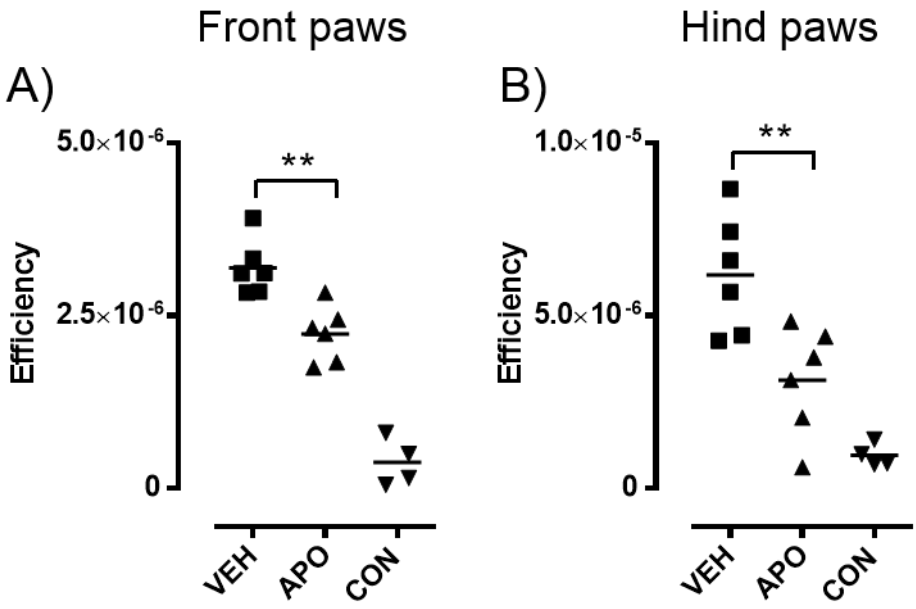

Figure 4.3.20 Fluorescence efficiency values on day 32 (Post-treatment)

Individual front and hind paw efficiency readings taken 6 hours after probe administration (on day 32) and 4 days after minipumps were inserted, administering vehicle alone (VEH) or 0.08 mg/kg/h APO866 (APO). Values were corrected for background autofluorescence and arranged by treatment group. A) Front paw fluorescence efficiency values of animals in the vehicle (VEH) group (three animals, n=6 limbs), APO866 (APO) group (three animals, n=6 limbs) and naïve control (CON) group (two animals, n=4 limbs). B) Hind paw fluorescence efficiency. Significant differences between means were determined using a two-tailed unpaired t test.**=P≤0.01, ns=not significant.

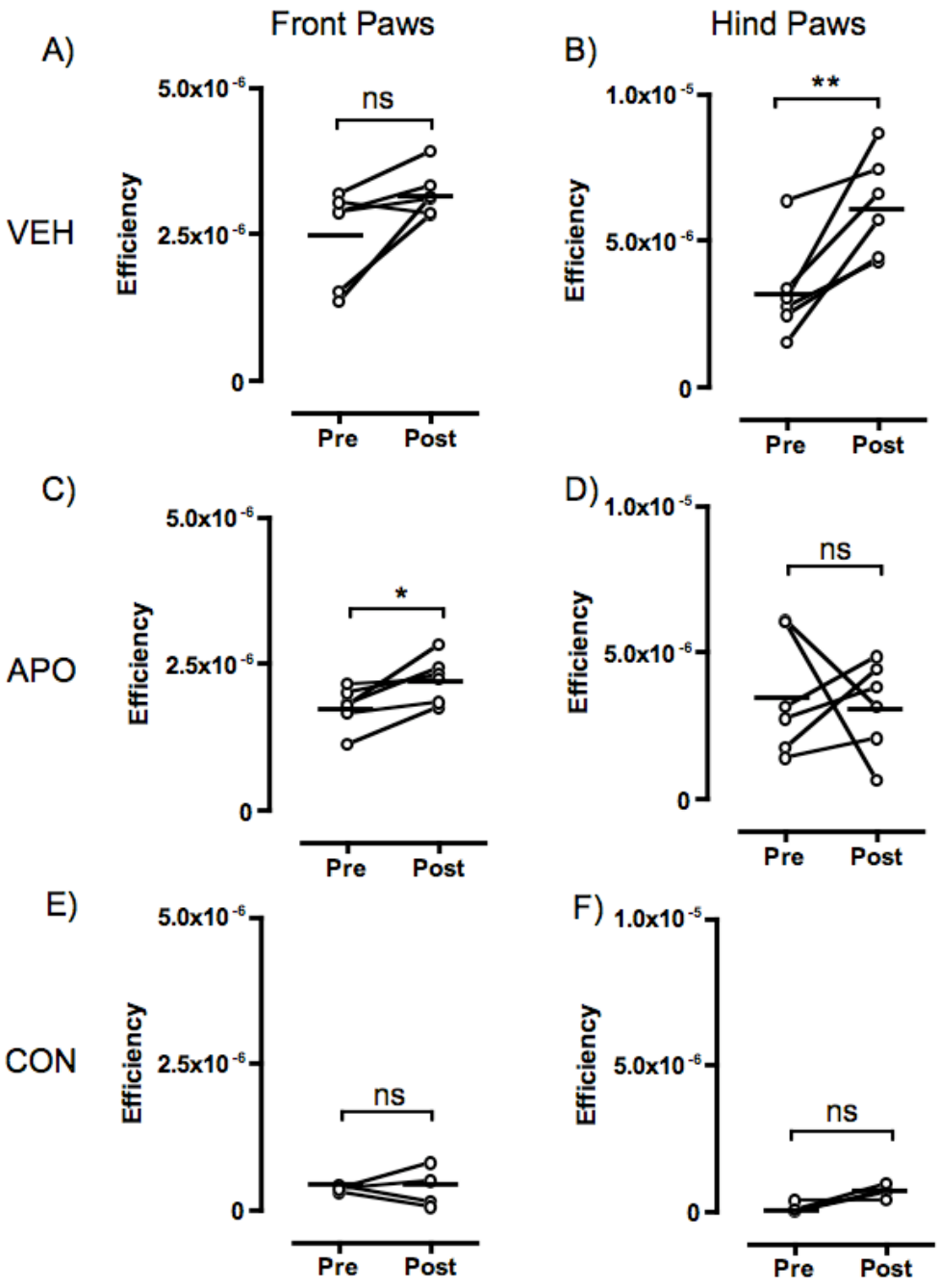

Figure 4.3.21 Changes in fluorescent efficiency pre- and post- APO866 treatment

Vertical 'before and after' graphs show the changes in fluorescence efficiency readings in the vehicle (VEH) group (three animals, n=6 limbs), APO866 (APO) group (three animals, n=6 limbs) and naïve control (CON) group (n=4 limbs), pre-treatment (pre: day 28) and post-treatment (post: day 32). Values were corrected for background fluorescence. Horizontal lines on graphs represent the mean values. Significant differences between means were determined using a two-tailed paired t test. *=P≤0.05, **=P≤0.01, ns=not significant (P>0.05).

4.3.3.5 Radiology, histology and cartilage erosion scores were not attenuated after 5 days of APO866 treatment

Overall, paw radiology scores in both VEH and APO treatment groups were significantly greater than those of the naïve controls (figure 4.3.24). APO866 radiology scores appeared attenuated compared to the vehicle treatment group; however, this difference was not statistically significant (P=0.1872 and P=0.061; front paws and hind paws, respectively.

Low power images of histological sections from each hind paw were scored in a blinded manner for pathological changes (figure 4.3.24). There was a visible attenuation in degree of infiltrate in APO866-treated animals compared with the vehicle control (4.3.24A). Vehicle and APO866-treated animals both exhibited extensive histological damage compared with naïve controls. However, there was no significant difference in histological score between APO and VEH groups (P=0.495). Likewise, cartilage erosion scores did not differ between the two treatment groups (P=0.668; figure 4.3.24C). Collectively, these data imply that the APO866 treatment was insufficient to completely halt the progression of disease.

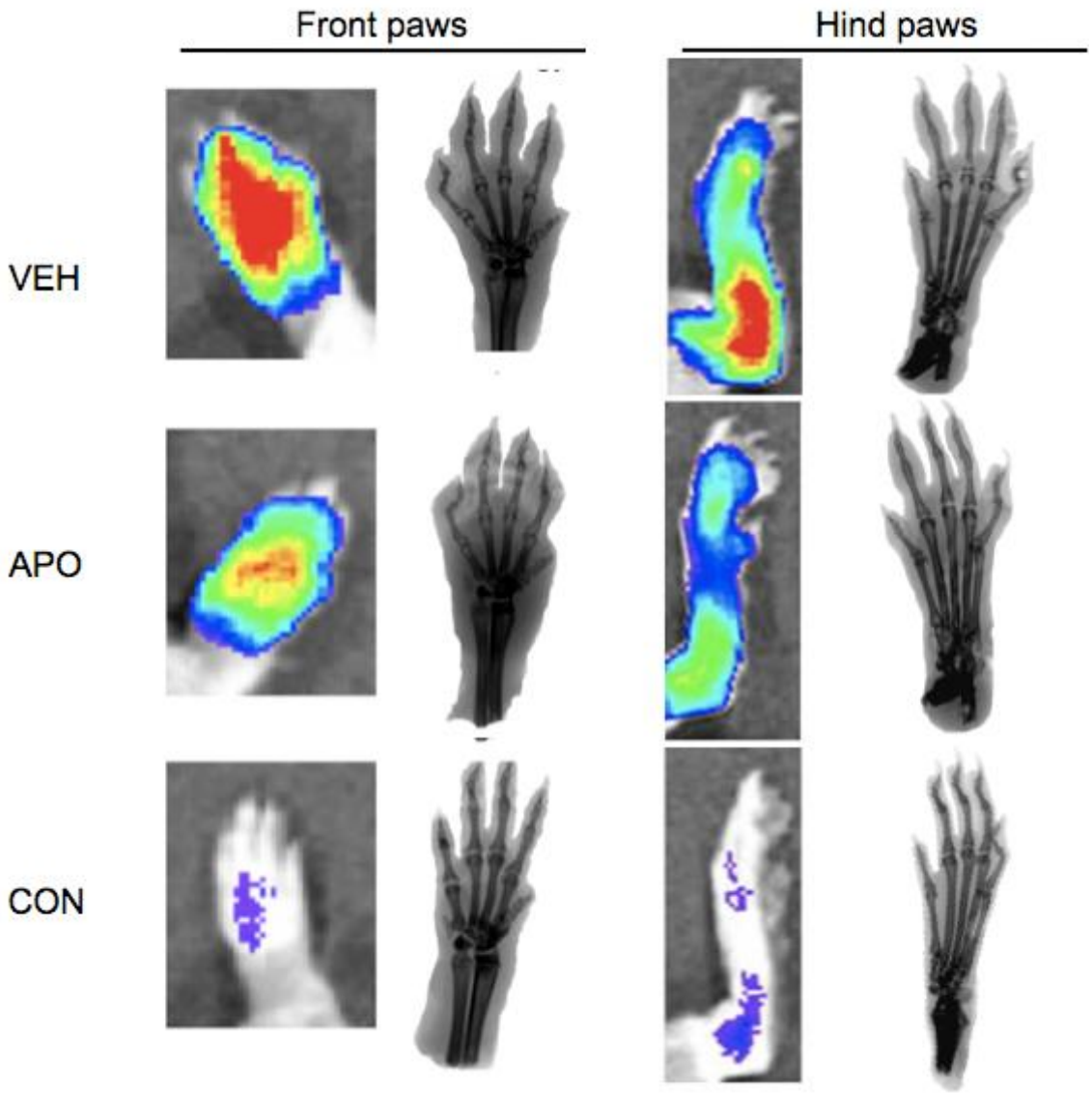

Figure 4.3.22 Fluorescence distribution and radiology

Representative front paw fluorescence images of animals in vehicle (VEH) group, APO866 (APO) group and naïve control (CON) group taken on day 32 compared with their respective radiographic images taken on day of sacrifice (day 33).

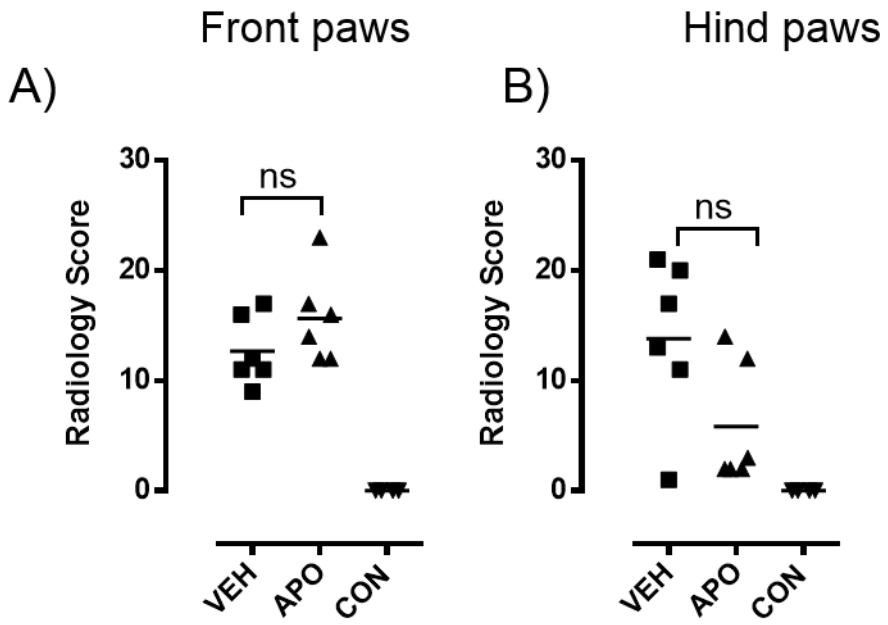

Figure 4.3.23 Effect of APO866 treatment on radiology scores

Radiology scores of animals in vehicle (VEH) group (three animals, n=6 limbs), 0.08 mg/kg/h APO866 (APO) group (three animals, n=6 limbs) and naïve control (CON) group (two animals, n=4 limbs) on the day of sacrifice (Day 33). A) front paws and B) hind paws.

Significant differences between means were determined using a two-tailed paired t test. *=P≤0.05, **=P≤0.01, ns=not significant (P>0.05).

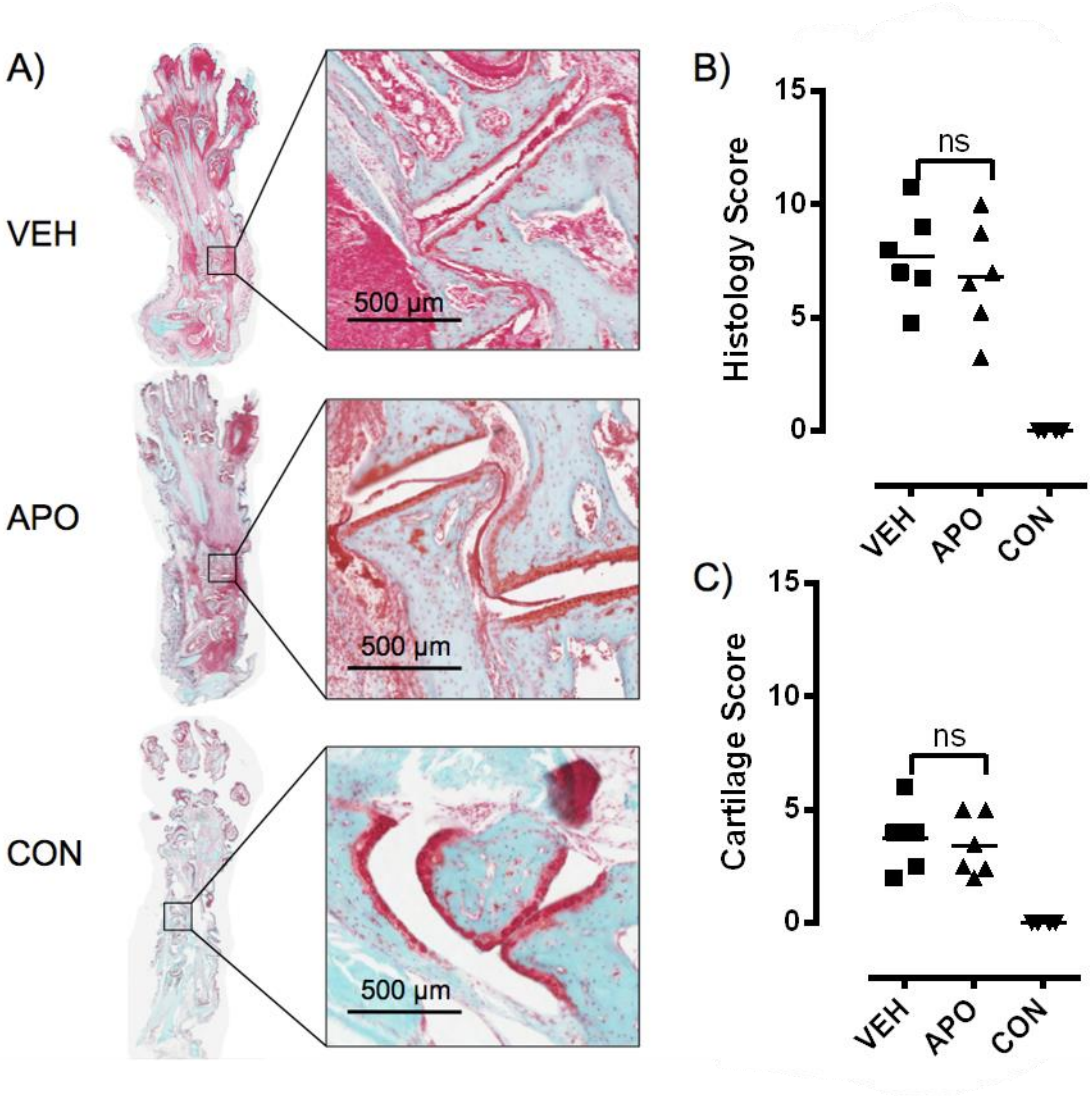

Figure 4.3.24 Histological analyses of hind paws

A) Representative histological images taken from of animals in vehicle (VEH) group (three animals, n=6 limbs), 0.08 mg/kg/h APO866 (APO) group (three animals, n=6 limbs) and naïve control (CON) group (two animals, n=4 limbs) on the day of sacrifice (Day 33). High power magnification of histological images shows the extent of pro-inflammatory infiltrate and exudate in VEH animals compared to APO. Images were scored for B) total histology score and C) cartilage erosion score. Significant differences between means were determined using a two-tailed paired t test. *=P≤0.05, **=P≤0.01, ns=not significant (P>0.05).

4.3.3.6 APO866 did not affect IgG2a antibody titres in CIA mice

Sera samples taken from animals on days 21 and 33 were tested for CII-specific IgG2a. Samples obtained from animals with established disease (CIA) and naïve control animals (CON) were compared, along with those of immunised mice with did not develop disease (no arthritis; NA). In samples taken at day 21, as expected, animals immunised with collagen had significantly greater titres of IgG2a (P=0.0136; figure 4.3.25A). By day 33, there IgG2a levels were elevated in CIA animals compared with day 21, and levels were significantly greater than in naïve controls (P=0.0392; figure 4.3.25B). There was no significant difference in IgG2a titre between VEH and APO treated animals post-treatment, confirming that APO866 does not affect the immune response to collagen in CIA mice.

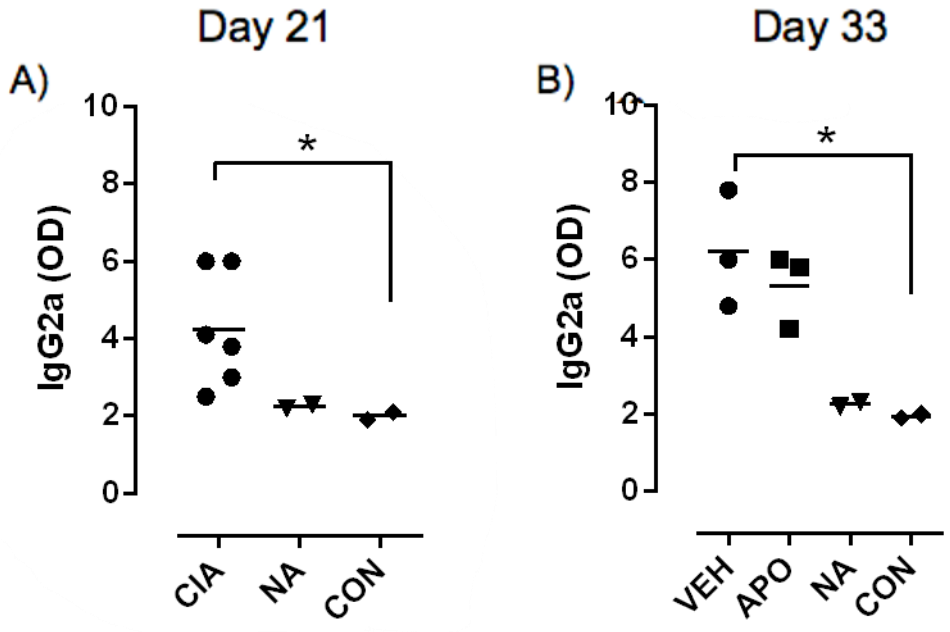

Figure 4.3.25 IgG2a antibody titre of sera at days 21 and 33

IgG2a antibody titre was determined in animals allocated to the two treatment groups (VEH and APO; n=3 animals per group), the two CIA animals that did not go on to develop arthritis (NA; n=2 animals) and the naïve control (CON; n=2) animals. A) IgG2a optical density (OD) values from sera taken at day 21. B) IgG2a OD values from sera taken at the experimental end-point on day 33. Differences between means were determined using a two-tailed paired t test. *=P≤0.05, ns=not significant (P>0.05).

4.3.3.7 APO866 did not have a significant effect on MMP gene expression

Front paws snap-frozen on the day of sacrifice (day 33) were analysed by qPCR (section 2.3.2). The effect of APO866 treatment on MMP gene expression levels was evaluated (figure 4.3.26A-D). MMP mRNA expression was not significantly different between VEH and APO866 treatment groups (P=0.843, P=0.109, P=0.253, P=0.167; MMPs -1a, 3, 9 and 13, respectively). These gene expression data are contrary to MMPSense750 fluorescent data (figure 4.3.20), which showed that APO866 significantly attenuates MMP enzymatic activity.

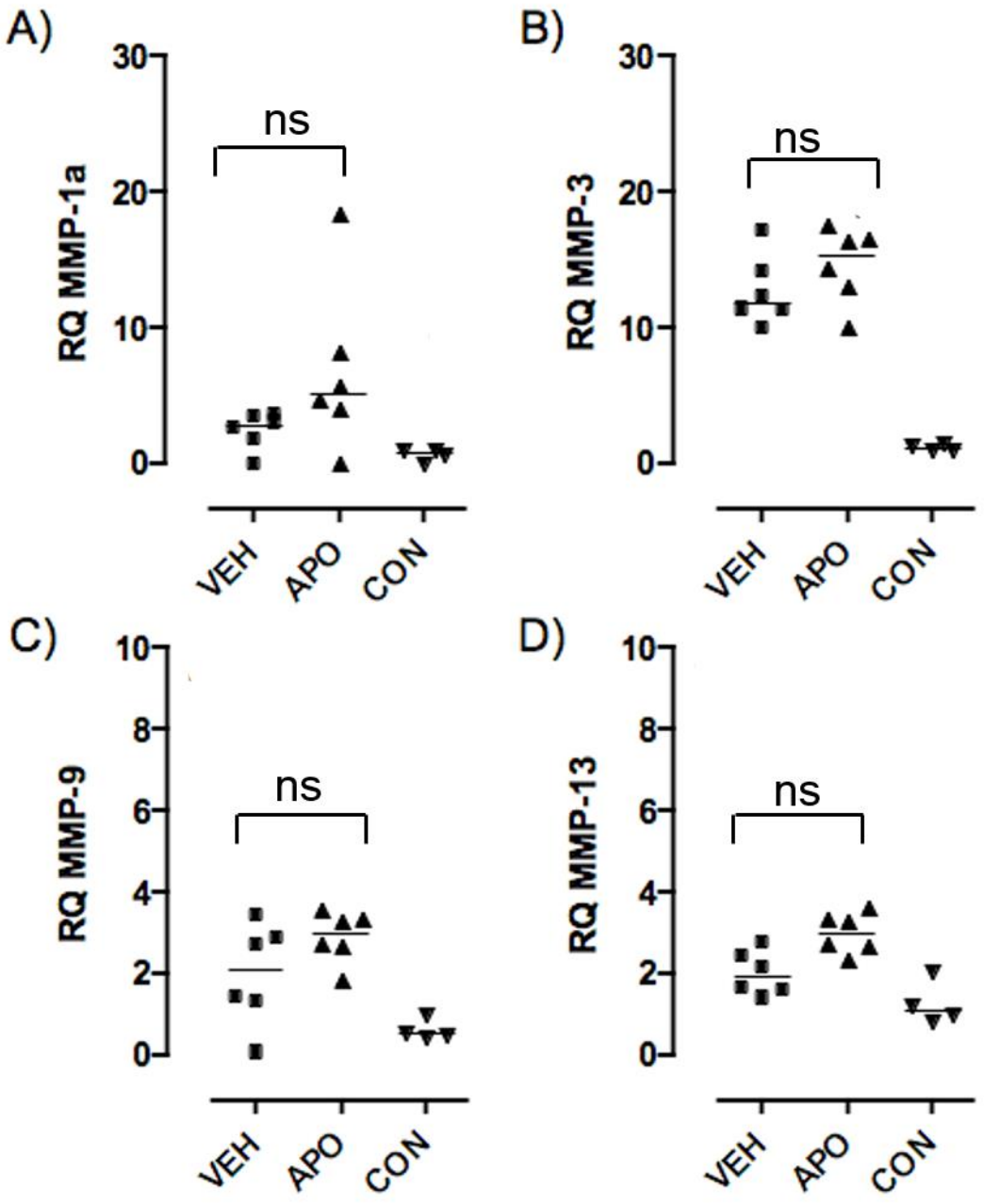

Figure 4.3.26 Real-time PCR analyses of MMP expression in front paws

Front paw cDNA of animals in vehicle (VEH) group (three animals, n=2 limbs per animal), 0.08 mg/kg/h APO866 (APO) group (three animals, n=6 limbs) and naïve control (CON) group (two animals, n=4 limbs). A) MMP-1a, B) MMP-3, C) MMP-9 and MMP-13 gene expression. Samples were plated in duplicate and relative quantities of gene expression were determined relative to the untreated control (two animals, n=4 limbs; CON). Differences between means were determined using a two-tailed paired t test. ns=not significant (P>0.05).

4.3.3.8 Immunised (no arthritis) animals were comparable to naïve controls with respect to MMP fluorescence

Two immunised mice never went on to develop CIA, and fluorescence efficiency was low in both mice up to experimental end point on day 32 (figure 4.3.27). Fluorescence values were calculated and compared to animals with established disease and naïve control animals; using ROI analysis software (figure 4.3.28). In both front and hind paws, fluorescence efficiency values (day 32) of arthritic animals were significantly greater than those of the immunised animals that did not go on to develop arthritis; (and; front paws (P=0.0009) and hind paws (P=0.0089) respectively. Fluorescence efficiency values of non-arthritic animals were comparable to the naïve controls. These data, combined with clinical score, paw diameter and IgG2a observations confirm that the animals had not developed arthritis by the experimental end-point.

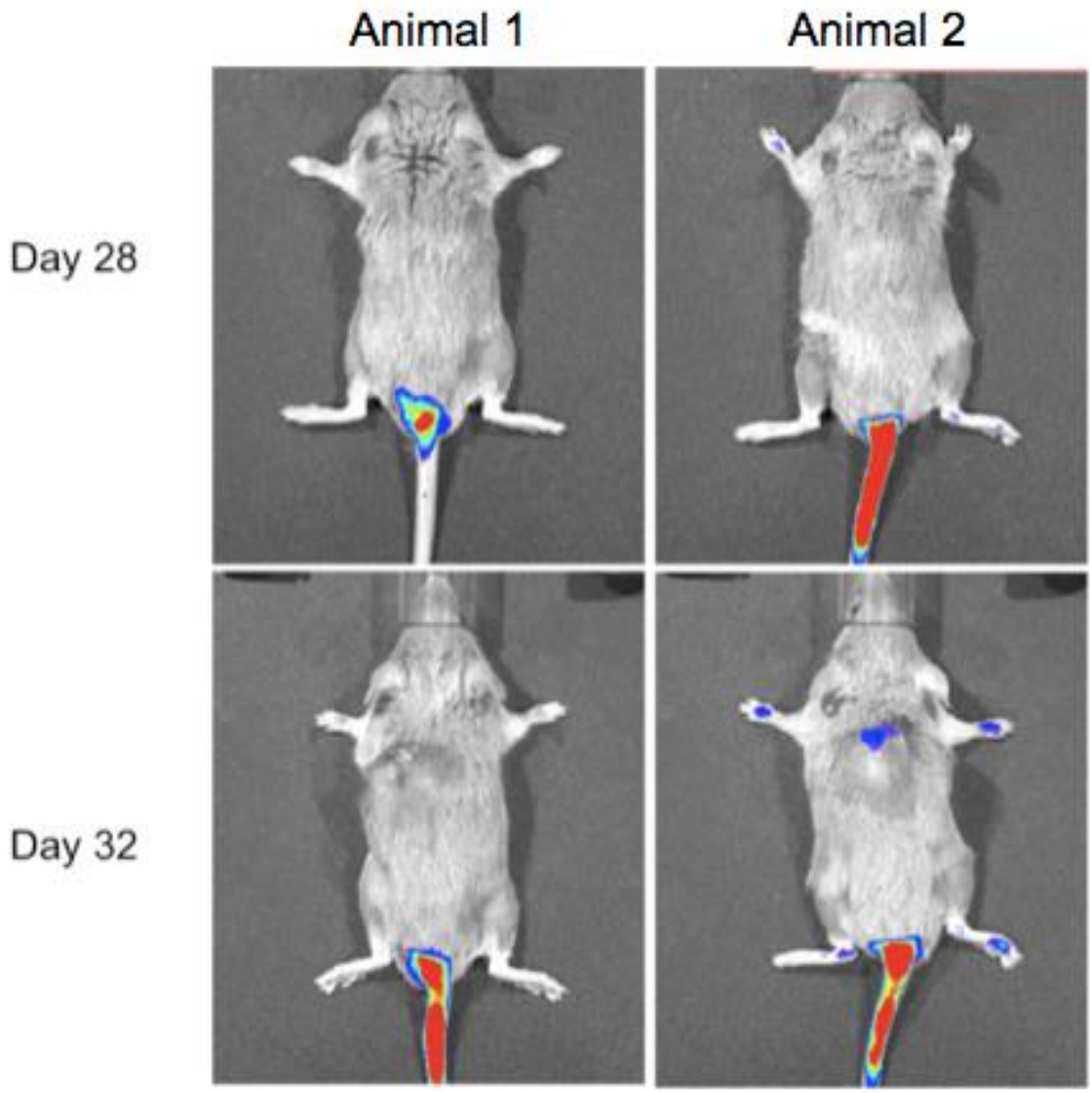

Figure 4.3.27 MMPSense750 fluorescence in animals with no arthritis

Animals (n=2) immunised with collagen that did not develop clinical signs of arthritis were each placed into vehicle and APO866 treatment groups (animal 1 and animal 2; VEH and APO, respectively) and probed and imaged with the arthritic (n=6) and control (n=2) animals. Panel above shows each animal pre-treatment (day 28), and again post-treatment (day 32).

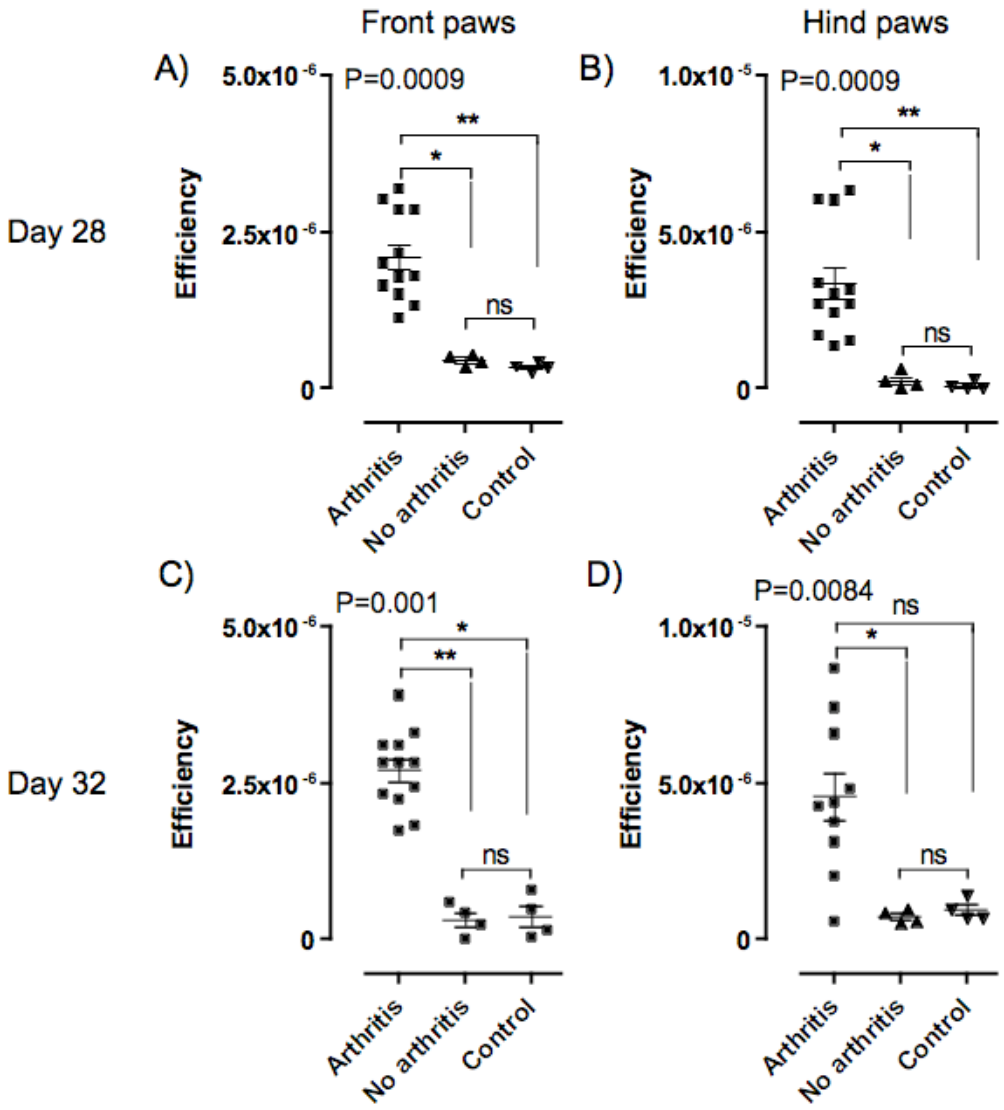

Figure 4.3.28 Comparison of MMPSense750 fluorescence efficiency of animals with and without arthritis

Raw efficiency values from day 28 and 32 corrected for background fluorescence. A) Fluorescence efficiency of front paws of animals with clinical signs of arthritis (six animals, n=12 limbs) compared to animals with no clinical signs of arthritis (two animals, n=4 limbs) and naïve control animals (two animals, n=4 limbs). B) Fluorescence efficiency of hind paws pre-treatment. Fluorescence efficiency of C) front paws and D) hind paws of animals post-treatment. Kruskal-Wallis tests with Dunn's multiple comparison post-test analyses were performed to determine the significance levels between treatment groups. **=P≤0.01, *=P≤0.05, ns=not significant (P>0.05).

4.3.4 Using archived CIA tissue to study the concentration-dependent effect of APO866 upon MMP gene expression within an inflamed joint

MMPSense750 FAST imaging data demonstrated that APO866 treatment reduced the biological activity of MMPs *in vivo* (figure 4.3.20) whilst real-time PCR data showed that APO866 enhanced MMP expression in the joint (figure 2.3.26). The small number of animals used in the study could have contributed to the disparity in the data. For this reason archived tissue, harvested from a sufficiently powered (six mice per group), unpublished study, were evaluated to study the relationship between APO066 and MMP expression in CIA joints. In this study, mice with established CIA had been treated for 12 days with either 0.08 mg/kg/h or 0.12 mg/kg/h APO866. A control group received vehicle (propylene glycol in saline). All medicaments were administered via minipumps (as above). A fourth group of naïve age-matched mice received no treatment. To use more mice to perform additional *in vivo* CIA studies was deemed unethical when archived tissues were available to serve our experimental purpose.

Real-time PCR analyses were performed (section 2.3.2), and all values were determined relative to naïve control mice (figure 4.3.29). Overall, Kruskal Wallis analyses indicated a significant difference between all four treatment groups (VEH, 0.08 mg/kg/h APO, 0.12 mg/kg/h APO, and CON) for all MMPs analysed by qPCR (P=0.001, P=0.0019, P=0.0063, P=0.0008; MMPs -1, -3, -9 and -13, respectively). Samples from animals treated with 0.12 mg/kg/h APO866 had MMP gene expression levels comparable to the naïve control, indicating a dose-dependent attenuation of MMP expression compared with untreated vehicle controls.

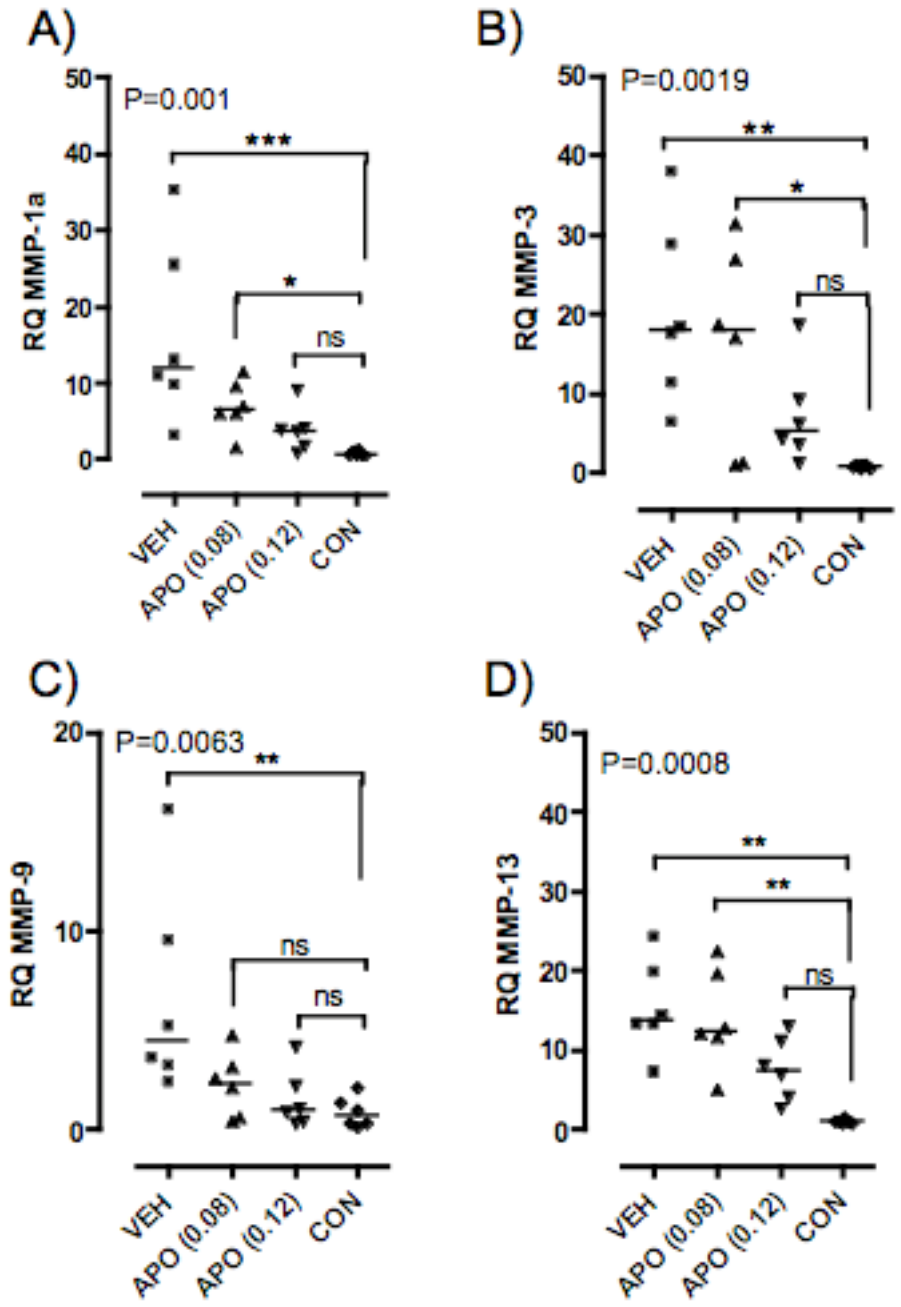

Figure 4.3.29 Effect of treatment duration and dosage on MMP expression levels

Archived paw samples were compared for relative quantities of MMP gene expression. For each treatment group, one front paw from each animal was homogenised (n=6 mice, one paw per animal) and real-time analyses were performed. Individual ΔC_T values were related to naïve controls (n=6 mice, one paw per animal). QPCR was performed on samples plated in duplicate and RQ analyses were performed for A) MMP-1a, B) MMP-3, C) MMP-9 and D) MMP-13. Kruskal-Wallis tests with Dunn's multiple comparison post-test analyses were performed to determine the significance levels between treatment groups. **=P≤0.01, *=P≤0.05, ns=not significant (P>0.05).

4.3.5 Comparison of MMPSense750 fluorescence with other disease parameters

One of the objectives of this chapter was to establish an *in vivo* imaging protocol suitable for longitudinal studies using the CIA model. Subsequently, the next objective was to determine how MMP enzymatic activity relates to other conventional disease parameters, such as clinical score. In order to do this, the data from the two independent animal experiments utilising MMPSense750 FAST (described in sections 4.2.2 and 4.2.3) were combined. The pooled dataset comprised of three naïve control animals, and five untreated CIA animals with established disease. Data from APO866-treated animals and CIA animals that did not develop signs of disease (section 4.3.3.8) were not incorporated.

4.3.5.1 MMPSense750 fluorescence was significantly correlated with clinical score and paw diameter

Firstly, fluorescence efficiency values were related to the respective arthritis index scores obtained from the animals at the time of imaging. Comparisons were made after the administration of both the first and second i.v. injections on days 28 and 32-34 respectively. The first injections of imaging probe were administered at the first sign of established disease on day 27 (median clinical score=1) and animals imaged 24 hours thereafter. At this stage, MMPSense750 fluorescence was significantly associated with front paw clinical score ($P=0.0002$; figure 5.3.30A), but not hind paw clinical score ($P=0.1259$; figure 5.3.30B) or paw diameter readings ($P=0.1635$; figure 5.3.30C). For both experiments using MMPSense750, the second set of probe injections was administered when most animals had reached the advanced stages of arthritis (median clinical score=4.0), which occurred between days 32-34. At this point, there was a highly significant association between fluorescence efficiency and clinical score in both front paws ($P\leq0.0001$; figure 5.3.30D) and hind paws ($P=0.0005$; figure 5.3.30E), as well as paw diameter measurements ($P\leq0.0001$, figure 5.3.30F).

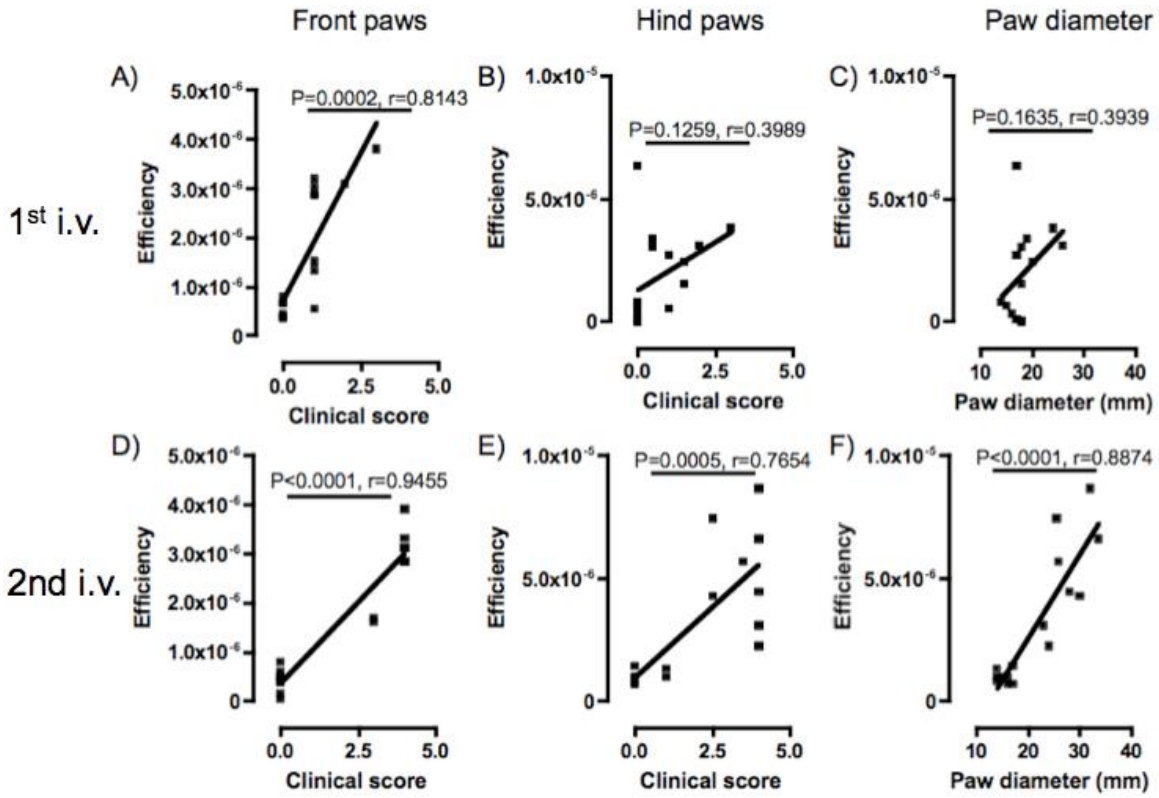

Figure 4.3.30 Correlation of MMPSense750 FAST fluorescence efficiency and conventional disease markers in early and late arthritis

Fluorescence efficiency values obtained from ROI analyses after the first (day 28; seven animals, n=14 limbs) and second (days 32-34; eight animals, n=16 limbs) i.v. injections of MMPSense750 FAST probe were related to respective clinical score and paw diameter observations from time of probe administration. Data shown are a combination of two individual experiments involving CIA and naïve animals injected with MMPSense750 probe. A) Front paw, B) Hind paw clinical scores, and C) hind paw diameters related to fluorescence efficiency values obtained after first i.v. D) Front paw and E) Hind paw clinical scores, and F) hind paw diameter related to fluorescence efficiency after administration of second i.v. Correlation analyses were performed using Pearson's Correlation Coefficient.

4.3.5.2 MMPSense750 fluorescence was significantly correlated with radiological and histological damage and MMP mRNA expression

In experiments two (section 4.3.2) and three (section 4.3.3), animals were sacrificed on days 34 and 33, respectively. For the former, only hind paws were harvested for x-ray imaging. However, for the latter experiment, both front and hind paws were imaged. The MMPSense750 fluorescence efficiency values taken prior to sacrifice were significantly associated with radiology score in both front paws (P=0.0006; figure 4.3.31A) and hind paws (P=0.0349; figure 4.3.31B). In addition, histology and cartilage erosion scores of the affected hind paws were also significantly correlated with MMPSense750 fluorescence efficiency (P=0.0007 and P=0.035; figures 4.3.31C and 4.3.31D, respectively), indicating that MMP activity is highest in paws with the greatest abundance of pro-inflammatory infiltrate and cartilage erosion.

Finally, MMP fluorescence readings of hind paws from day of sacrifice were related to respective relative quantities of MMP gene expression (figure 4.3.32), as quantified by real-time qPCR. With the exception of MMP-9 (P=0.005; figure 4.3.32B), MMP gene expression was significantly correlated with MMPSense fluorescence efficiency (P=0.0041, P≤0.0001, P=0.0033; MMPs -1, -3 and -13, respectively).

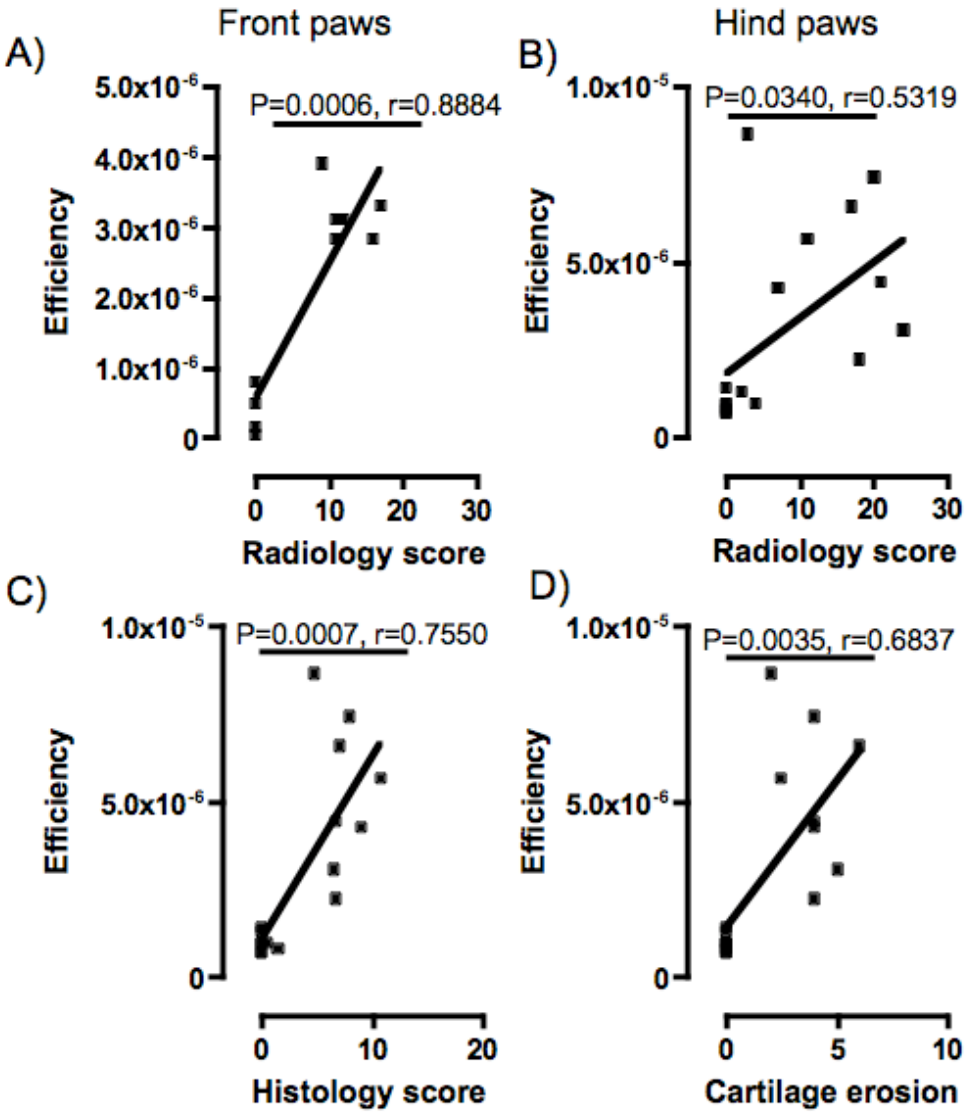

Figure 4.3.31 MMPSense750 fluorescence and radiology

Fluorescence efficiency values obtained from ROI analyses after the first (day 28; seven animals, n=14 limbs) and second (days 32-34; eight animals, n=16 limbs) i.v. injections of MMPSense750 FAST probe were related to respective MMPSense750 efficiency values obtained 6 hours after the second i.v. injection of probe (days 32-34) were related to respective radiology scores of A) front, and B) hind paws harvested at time of sacrifice on the same day. Fluorescence efficiency was also related to C) histology, and D) cartilage erosion scores of hind paws harvested on the day of sacrifice (day 32-34). Front paw observations were taken from one experiment only (n=10 limbs), whilst hind paw observations were combined from two independent experiments using MMPSense750 (n=16 limbs). Correlation analyses were performed using Pearson's Correlation Coefficient.

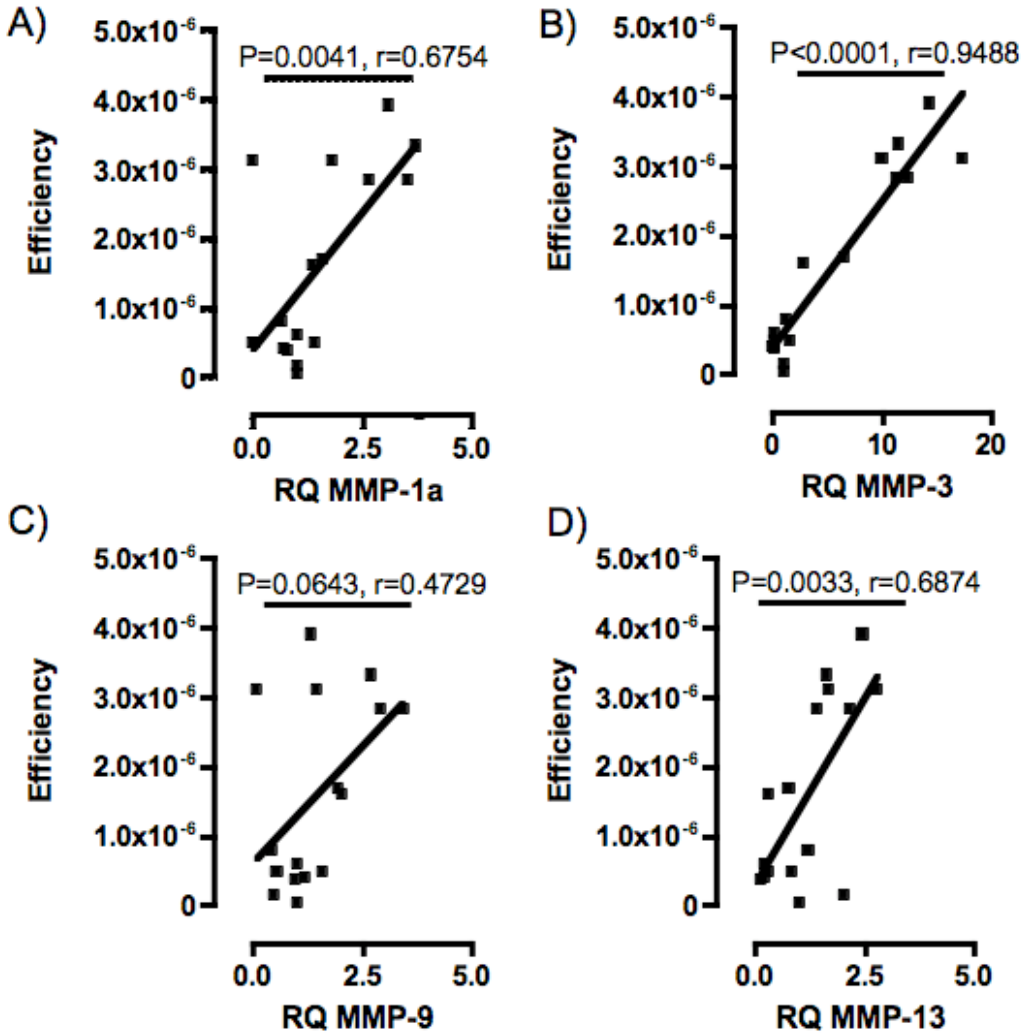

Figure 4.3.32 MMPSense750 fluorescence and relative expression of MMPs

MMPSense750 efficiency values of front paws obtained 6 hours after the second i.v. injection of probe (days 32-34) were related to relative quantity of gene expression (RQ) data obtained from real-time PCR analyses of RNA extracted from front paws harvested on day of sacrifice (days 32-34). Data shown are a combination of two individual experiments involving CIA animals injected with MMPSense750 probe. RQ values were determined by relating ΔC_T values of arthritic animals (n=10 limbs) to those of a naïve control animals (n=6 limbs). Individual RQ values for A) MMP-1a B) MMP-3 C) MMP-9 and D) MMP-13 were correlated to the respective front paw fluorescence efficiency values. Correlation analysis was carried out using Pearson's Correlation coefficient.

4.4 Discussion

4.4.1 Murine collagen-induced arthritis was induced in experimental animals

DBA-1 mice were chosen for their genetic susceptibility to CIA, which has been widely reported in the literature (Courtenay et al., 1980, Brand et al., 1996). Arthritis incidence in this strain is typically 80-100% (Brand et al., 2007). Of the eighteen animals immunised with collagen throughout the course of the three experiments, fourteen animals exhibited signs of disease; meaning incidence in these studies (approximately 78%) was slightly lower than anticipated. Low arthritis incidence is typically attributed to denatured CII, or a poor quality emulsion due to insufficient mixing of the CII with Freund's complete adjuvant (Brand et al., 2007). In the present study, the CII was made up fresh for each experiment (as detailed in section 2.2.1), and the emulsion was homogenised thoroughly in a glass syringe and tested prior to use by dropping into icy water. The age of the animals can also be ruled out as a problem, as they were all aged between 7-8 weeks when purchased. Animals were given time to acclimatise to their environment and appeared healthy prior to the start of the study. Whilst every effort was made to ensure accurate and reproducible delivery of the collagen emulsion into the animals, it is possible that the slightly lowered incidence of disease noted in this study may relate to the efficiency of collagen delivery.

Disease onset occurred typically within 25 days of the first intradermal injection of CII. In experiment three, disease onset failed to occur at this point; however, a single intra-peritoneal injection of LPS rapidly potentiated the onset of arthritis, and synchronised disease in most of the animals. The addition of LPS is associated with increased production of anti-CII IgG and IgG2a antibodies as well as various kinds of cytokines (such as 1L-1β), exacerbating the autoimmune joint inflammation (Caccese et al., 1992). As expected, the induction of arthritis in all animal experiments resulted in a characteristic monophasic progression of disease which included paw swelling and erythema in individual limbs, and an increase in hind paw diameter (Brand et al., 2007). A subjective clinical scoring system showed that disease progressively worsened in all animals with established disease, with many reaching the maximum allowable clinical score within 10 days of disease onset.

4.4.2 MMP enzymatic activity was monitored successfully in vivo with NIRF imaging probes

MMP activatable fluorescent probes were used to study local MMP enzymatic activity within murine joints in both diseased and naïve mice. Firstly, the commercially-available probe, MMPSense680, was tested on animals with established arthritis. In the first experiment, MMPSense680 was detected in the affected paws of the animals 24 hours post-injection. The localisation of the fluorescence is similar to that seen in studies by Wunder and colleagues, who tested a cathepsin-specific imaging probe in CIA animals (Wunder et al., 2004). Observations of individual limbs hinted that paws with less swelling did not fluoresce as intensively as those with a greater degree of swelling. Overall, the preliminary data indicated that MMPs are a promising biomarker for monitoring longitudinal disease progression in this animal model. However, one limitation of using MMPSense680 was that the Kodak *in vivo* imaging system used to detect its fluorescence emissions did not permit an efficient flow of anaesthetic agent (see below).

The preliminary observations of the MMPSense680 study were followed up with two experiments using another imaging probe, MMPSense750 FAST. This probe, although similar in terms of specificity, has been reported to possess a smaller molecular weight, and supposedly a faster rate of clearance (Groves et al., 2010). In addition, this probe allowed imaging in the IVIS 200 system, which contained a gas anaesthesia manifold; allowing for easier handling of the animals within the chamber. It was anticipated this probe would be more suitable for longitudinal studies, as animals could be injected with fluorescent probes twice during the course of the study. As with MMPSense680, MMPSense750 FAST fluorescence was enhanced in affected limbs of CIA animals. Arthritic animals injected with the probe showed significantly higher levels of fluorescence compared with non-arthritic animals. This corroborates previous published data, which showed a 7-fold increase in fluorescent intensity in arthritic paws compared with non-arthritic paws (Wunder et al., 2004).

When re-probed and re-imaged, fluorescence was enhanced in animals in the advanced stages of disease compared to early disease. As these imaging probes are quenched in the absence of MMP activity, the data in this chapter suggest that MMP activity is enhanced as disease progresses. Interestingly, in early disease, some fluorescence readings were elevated despite only mild paw swelling. Subsequent scoring showed that these limbs went on to develop advanced disease. This suggests that MMP activity becomes elevated in some paws prior to clinical manifestation of disease, indicating that MMP fluorescence may be useful as a predictive marker of disease onset.

Longitudinal data acquired through *in vivo* imaging with MMPSense probes were compared with end-point disease parameters such as radiology, histology and qPCR analyses of MMP gene expression. Combined from the two experiments utilising MMPSense750 showed a positive correlation between MMP fluorescence and the degree of radiological and histological damage, which had been hinted at in the MMPSense680 study. As with MMPSense680, distinct zones of intense fluorescence in pseudocolour overlays coincided with areas with a large degree of inflammatory infiltrate and cartilage erosion in corresponding histology sections. This suggests the presence of inflammatory cells and possibly chondrocytes producing excessive amounts of MMPs locally, and ties in with previous observations in RA (Ainola et al., 2005) and in the CIA model (Seeuws et al., 2010). Although MMPSense fluorescence was associated with an increase in extent of cartilage erosion, other parameters of radiological damage such as osteopenia were not observed. This is possibly due to the acute nature of the disease progression, meaning that although cartilage was affected, the short duration of the disease left insufficient time for the development of bone erosions. If disease had been allowed to progress further, it is likely that more extensive radiological damage may have occurred. It is also worth noting that joints with cartilage damage show a preference for worsening of this damage, rather than the development of bone erosions (van der Heijde, 2011). Therefore, extent of MMP production is unlikely to predict the degree of radiological damage.

Data combined from experiments two and three indicated a significant correlation between MMPSense750 FAST fluorescence and corresponding MMP gene expression data, for all MMPs with the exception of MMP-9. This is interesting, as although MMPSense750 FAST has a broad activation profile, it is particularly susceptible to MMP-9 activation (refer to figure 2.15). The specificity of the probe for MMP-9 may explain why some paw extracts yield MMP-9 gene expression, yet the respective MMPSense fluorescence values are high.

This chapter focused on a variety of MMPs known to be upregulated in the RA synovium, including MMPs -1, -3, -9 and -13 (Konttinen et al., 1999, Yoshihara et al., 2000, Tchetverikov et al., 2004). Generally, MMP expression analysed by qPCR was enhanced in CIA animals compared with naïve controls. This ties in with previous studies, that have shown upregulation of MMPs -1, -3 (Mun et al., 2009), -9 and -13 (Oestergaard et al., 2006) in the joint tissue of CIA animals. More recently, an increase in MMP-3 levels has been associated with many pathological features of CIA, including inflammation, cartilage destruction and bone erosion (Seeuws et al., 2010); indicating that expression and activity of these MMPs is a useful indicator of extent of cartilage erosion.

4.4.3 A short treatment with APO866 in established arthritis reduced arthritis index and MMP activity, but not MMP gene expression

For the final experiment, MMPSense750 FAST was used to determine the effect of APO866 treatment on disease severity in the CIA model longitudinally. The dose of 0.08 mg/kg/h was chosen for this study, as previous work within the group showed that this dose was sufficient to reduce clinical score and paw diameters compared to the untreated vehicle. After four days of treatment, APO866-treated animals had significantly lower clinical scores compared to the untreated vehicle control. A previous study by Busso *et al* (2008) found that APO866 treatment results in significantly reduced mean arthritic score within 10 days of the commencement of treatment (Busso et al., 2008). In this study, APO866 was administered intraperitoneally at doses of 2-10 mg/kg every 12 hours, for 14-15 days from the first signs of disease. The lowest dose, equivalent to 0.17 mg/kg/h, was lower than the dose used in this chapter. The concentration of APO866 used in this chapter was carefully considered, and equivalent to the maximum tolerated dose in humans (Holen et al., 2008). The method of continuous drug infusion by minipump has numerous advantages over administering drugs by injection. The main advantage is that minipump infusion involves less researcher intervention. In addition, studies comparing the two methods of administration show that continual drug infusion allows for greater bioavailability and less wasted compound (Bedard et al., 2011, Kondo and Togari, 2011). This may explain why a comparable therapeutic effect was seen in the current study, despite the relatively low dose of APO866 used.

Despite the therapeutic effects observed with respect to arthritis index, radiological and histological damage was not affected by a short APO866 treatment compared with the vehicle control. This suggests that although disease had begun to regress in response to APO866 treatment, a large degree of damage had already occurred due to the rapid nature of the disease progression. These findings are in contrast with those of Busso and colleagues, who observed significant decreases in inflammatory infiltrate and synovial hyperplasia in histological sections of APO866-treated animals (Busso et al., 2008). Sera levels of NAMPT have been associated with a higher degree of radiological damage in patients with RA (Rho et al., 2009); however, APO866 did not significantly affect radiology score compared with the vehicle control. Again, this could be attributed to the timing and dosage of APO866 administration.

In contrast with MMP fluorescence data, MMP mRNA expression was slightly enhanced in APO866-treated animals compared with the controls receiving vehicle, although this effect was not statistically significant. It is unclear why MMP gene expression remained high, whilst MMP enzymatic activity was attenuated by APO866. One possibility is that APO866 inhibited NAMPT produced by circulating T lymphocytes

and synoviocytes, thus reducing MMP fluorescence. However, the dosage used may have been insufficient to inhibit NAMPT activity in cells within deeper tissues of the inflamed joint, such as the joint cartilage.

4.4.4 APO866 treatment reduced MMP gene expression in murine front paws in a time and dose-dependent manner

Following qPCR analyses of the current studies in this chapter, archived samples from animals treated for different dose regimens were used for qPCR analyses. In contrast to findings from the short-term APO866 treatment, expression of all MMPs was significantly attenuated in a time and dose dependent manner. Busso and colleagues observed a dose-dependent effect in their studies in the CIA model, with maximal therapeutic response at the highest dose of 10 mg/kg. The beneficial effect of APO866 was apparent within ten days following the commencement of treatment (Busso et al., 2008). Although this study did not perform analyses of MMP gene expression, histological examination of tissues indicated greater retention of Safranin O staining of cartilage in APO866-treated animals; suggesting attenuation of MMP expression. These data support the findings of this chapter, that APO866 efficacy is apparent between 4-14 days of commencement of treatment.

4.4.5 APO866 has no impact upon IgG2a production

Sera taken from animals in experiment three was also tested for CII-specific IgG2a, a marker for antibody response to collagen. During disease development, anti-collagen antibodies bind to the joint cartilage and initiate the complement cascade. In the current study, IgG2a titres were analysed in sera, as IgG2a production is associated with activated Th1 (T helper type I) cells-which drive the immune response resulting in inflammation (reviewed by Brand et al., 2003). The Th2-associated IgG1 subclass is also detectable in diseased animals; however, mice that develop CIA generally have a high ratio of IgG2a:IgG1 (Brand et al., 1996). In the current study, vehicle and APO866-treated animals showed no significant differences in IgG2a levels. This is in contrast to anti-TNF receptor and anti-B cell treatments, which actively lower levels of Th1 driven IgG2a antibodies (Mukherjee et al., 2003, Yanaba et al., 2007), suggesting that therapeutic efficacy of APO866 is not due to direct reduction of auto-antibodies.

4.4.6 A multi-parameter approach can accurately assess the effects of NAMPT blockade

Taken together, these data suggest that traditional longitudinal disease parameters such as clinical score, cartilage erosion and radiology may not provide an accurate reflection of MMP gene expression and enzymatic activity *in vivo*. Conversely, MMP activity and expression data, taken alone, do not sensitively reflect the efficacy of APO866 treatment; particularly when assessing such short-term treatment regimens as

those used in this current study. Clinical score and paw diameter observations remain the best markers for disease, whilst traditional radiological and histological analyses provide the best insight into the extent of joint inflammation and cartilage erosion. However, *in vivo* imaging could emerge as a useful tool in assessing local MMP activity in joints and treatment response longitudinally. The same animal can potentially be re-probed and re-imaged multiple times, meaning valuable longitudinal data can be obtained using fewer animals. Although the probes used in this study only assess MMP activity, a variety of commercially-available probes have been developed to assess other aspects of disease, such as bone turnover. Quantitative PCR analyses did not yield a difference in MMP gene expression between vehicle and APO866 after four days of treatment. However, it was very effective at showing a time and dose-dependent effect of APO866 on MMP gene expression. The advantage of qPCR analysis is that once RNA has been extracted from paws, a number of target genes can be assessed, so a large amount of data can be generated quickly. Therefore, a multi-parameter approach provides the most comprehensive means to monitor CIA disease and APO866 efficacy.

4.4.7 APO866 may dampen local MMP activity at sites of cartilage invasion

Quantitative PCR analyses of murine front paws in this chapter showed a significant increase in expression of MMPs -1a, -3, -9 and -13 in CIA animals compared with naïve controls. MMPs -1 and -3 are both predominantly expressed in the synovial cells comprising the pannus that invades the articular cartilage. In contrast, MMPs -9 and -13 are generally expressed in the neutrophils and macrophages (MMP-9) and chondrocytes (MMP-13). These data, combined with MMP fluorescence distribution data, suggest that the synovial cells are the major source of MMP expression and activity. For future studies, localisation of MMP activity could be confirmed by immunohistochemical analyses, with the use of antibodies that specifically recognise neoepitope sequences generated by MMP-mediated cleavage of aggrecan (Fosang et al., 2003).

4.4.8 Summary

In this chapter, a combination of established and novel techniques were employed to monitor disease progression in a murine arthritis model, with the eventual aim of assessing the efficacy of NAMPT blockade by APO866. It was discovered that near infra-red fluorescent imaging probes can assess both the extent and localisation of MMP activity in the live animal; providing novel insights into the process of cartilage degradation in animal disease models. MMP enzymatic activity increased in line with paw swelling and erythema in affected limbs, highlighting it as a useful marker of inflammation as well as cartilage catabolism. MMP enzymatic activity was not directly

related to radiological and histological markers of disease in affected limbs, as well as MMP gene expression.

Treatment with APO866 attenuated disease progression in animals, causing a reduction in clinical score. There was no significant effect on cartilage degradation, histology and radiology scores, although this may be due the short duration of the treatment. Finally, qPCR analyses of archived samples confirmed that APO866 has a time and dose-dependent effect on MMP gene expression, suggesting that NAMPT plays an important role in the underlying processes involved in matrix destruction in inflammatory disease.

Chapter 5: The effect of iNAMPT blockade on articular cartilage destruction *ex vivo*

5.1 Introduction

The principle aim of this chapter is to assess the direct effect of NAMPT inhibition on cytokine-induced articular cartilage destruction *ex vivo,* using chondrocyte monolayer and bovine explant culture systems.

5.1.1 Assessment of articular cartilage breakdown *ex vivo*

The mechanical properties of cartilage are highly dependent on the integrity of its extracellular matrix (ECM), which consists primarily of type II collagen and supramolecular aggregates of aggrecan and hyaluronic acid, stabilised by link protein. The initial step in cartilage degeneration is the enzymatic degradation of aggrecan by aggrecanases (e.g. ADAMTS-4 and -5) and MMPs (e.g. MMP-1 and -3), resulting in its fragmentation (reviewed by Cawston and Young, 2010). The ensuing loss of GAG-bearing aggrecan fragments from the ECM compromises the water holding capacity of the tissue and exposes the underlying collagen framework, making it more vulnerable to biomechanical load and other degradative enzymes, particularly collagenases such as MMPs -1 and -13 (figure 5.1.1). Further enzymatic degradation, coupled with load, results in fatigue failure of the collagen framework, cell death and tissue destruction (reviewed by Aigner et al., 2006).

Researchers employ a combination of techniques to elucidate the sequence of catabolic events involved in articular cartilage destruction using both cartilage explants and chondrocyte cultures. The metabolism of chondrocytes grown as monolayers can differ from those occurring within cartilage, as chondrocytes undergo de-differentiation in monolayer growth conditions, becoming fibroblastic within a few passages. Chondrocytes retain their *in vivo* phenotype with greater fidelity in cartilage explants, as they remain embedded within their native 3D ECM (Sondergaard et al., 2006). Moreover, the degradative processes resulting in the progressive breakdown of this ECM can be fully evaluated. Explants are typically extracted from the full depth of the articular cartilage tissue that lines bovine or porcine synovial joints, and cultured *ex vivo* in supplemented medium for extended periods of time. To simulate arthritis, the cartilage explants are exposed to catabolic agents (e.g. interleukin-1) and the subsequent loss of cartilage integrity over time assessed by a variety of sensitive biochemical and histological assays. These systems thus permit appraisal of the therapeutic efficacy of anti-rheumatic agents. Several groups have used articular cartilage explant cultures to

examine the effect of the DMARDs, namely Methotrexate, Leflunomide and Sulfasalazine on IL-1β-induced PG loss (Van Der Veen et al., 1996, Neidel et al., 1998, Panico et al., 2003, Lakey and Cawston, 2009). In these studies, to mimic the chronic exposure to cytokine assault, culture media containing IL-1β either with or without DMARDs were replenished every few days.

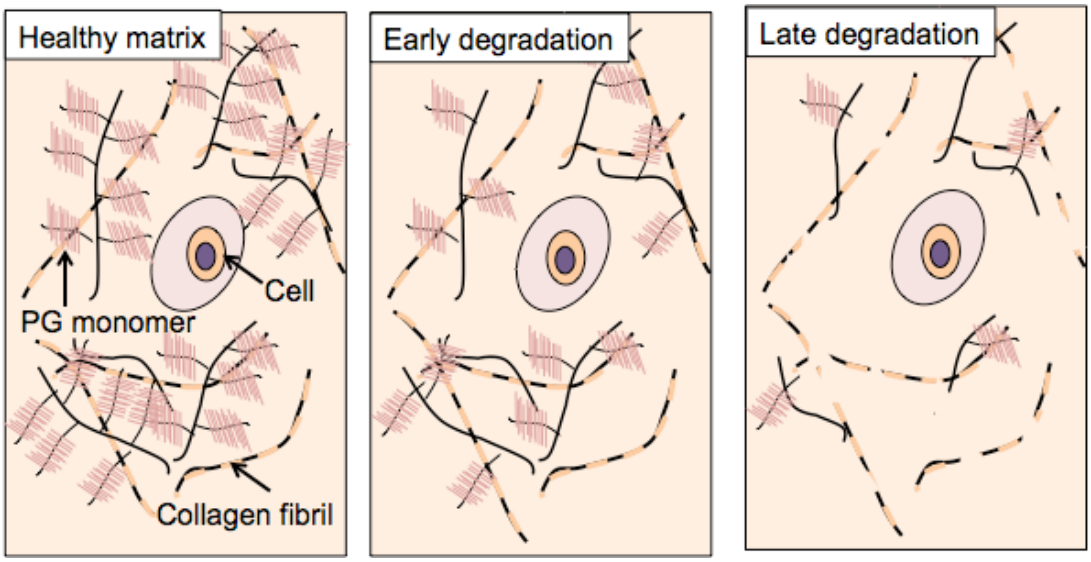

Figure 5.1.1 Destruction of matrix components in articular cartilage

Healthy cartilage owes its properties to an organised network of collagen fibrils and highly hydrophilic, supramolecular aggregates of aggrecan and hyaluronic acid, stabilised by link protein. PG loss occurs during early cartilage degradation. Continued PG depletion eventually weakens the collagen fibril network, resulting in matrix degradation.

5.1.2 Role and regulation of iNAMPT in chondrocyte-mediated catabolism

In this chapter, articular cartilage explant cultures were used to investigate the role of intracellular NAMPT (iNAMPT) in a model of chronic cytokine assault. Previous work shows that eNAMPT is upregulated in the serum and synovial fluid of patients suffering from rheumatoid arthritis (Nowell et al., 2006), and that synovial fluid eNAMPT positively correlates with the degradation biomarker of collagen II (CTX-II), and aggrecan (AGG1 and AGG2) (Duan et al., 2011). Furthermore, NAMPT protein is immunolocalised at sites of pannus invasion into the articular cartilage of patients with RA (Brentano et al., 2007). The results of chapter four have also shown that the inhibition of NAMPT *in vivo*, using the small molecule selective inhibitor APO866, reduces MMP expression and activity in the paws of animals with collagen-induced arthritis (section 4.3.3). Together,

these observations suggest an active role for NAMPT in local degradative processes in articular cartilage.

The NAMPT or NAM salvage pathway is not the only pathway involved in NAD^+ biosynthesis; there are at least three other known pathways for generating NAD^+, including the *de novo* pathway involving Tryptophan and QPRT, and the Preiss-Handler pathway involving NA and NAPRT (section 1.3.4). However, NAMPT may be unique amongst these enzymes, in that it has been shown to be upregulated by a variety of stimulators, including cytokines, Toll-like ligands and hypoxia (Brentano et al., 2007, Bae et al., 2006). With regards to human and murine chondrocytes, NAMPT mRNA and protein expression has been shown to be upregulated six-fold by the addition of 10 ng/ml IL-1β (Gosset et al., 2008). Up until now however, the expression of the other rate-limiting NAD biosynthesis enzymes (NAPRT and QPRT) in joint cells has not been investigated.

The Gosset study (Gosset et al., 2008) showed that, like the synovial fibroblasts described in section 1.1.2 of this thesis, the addition of eNAMPT not only upregulated pro-degradative MMPs in chondrocytes, it also upregulated ADAMTS -4 and -5 and the catabolic mediator, prostaglandin E_2 (Gosset et al., 2008). A variety of cofactors depend on NAD^+ availability to perform their functions, HDACs, which can act as potent transcriptional coactivators or corepressors (Roth et al., 2001). Studies have shown that inhibition of iNAMPT in human and rabbit chondrocytes reduce intracellular NAD^+ levels and the activity of a NAD+-dependent, chromatin-modifying enzyme and HDAC, silent mating type information regulation 2 homolog 1 (SIRT1) (Dvir-Ginzberg et al., 2008, Hong et al., 2011). Reduction in SIRT1 activity in this way resulted in chondrocyte dedifferentiation, with reduced gene expression of collagen 2a(α1), 2b(α1) and aggrecan *in vitro* (Hong et al., 2011, Dvir-Ginzberg et al., 2008). Young and colleagues added NAD+ independent HDAC inhibitors to explants, and found that cytokine induced MMP expression was inhibited (Young et al., 2005).

However, these studies did not investigate the effect of iNAMPT inhibition on PG loss and MMP expression; key indicators of early degradative processes. APO866, through reduction of intracellular NAD^+, may indirectly inhibit NAD+-dependent HDACs, thereby reducing MMP expression in cartilage and the implication for NAD^+ depletion in chondrocytes warrants investigation.

5.1.3 Chapter aims

In the previous chapter, treatment with APO866 in the murine CIA model attenuated disease severity and MMP mRNA expression in a dose-dependent manner. Moreover, *in vivo* imaging showed a reduction in MMP activity within the paws of APO866-treated mice compared to vehicle-treated control mice. However, the role of

iNAMPT in cartilage-mediated MMP production is yet to be investigated. Cytokines have been shown to upregulate NAMPT gene expression *in* vitro, yet the regulation of the other NAD enzymes has not been investigated thus far.

In this chapter, the aims were to investigate the cytokine regulation of other NAD^+ enzymes in chondrocytes and to assess the impact of inhibiting iNAMPT activity on cytokine-induced cartilage breakdown.

In order to achieve these aims, the specific objectives of the chapter were as follows:

- Assess the effects of IL-1β and NAMPT antagonist, APO866, on chondrocyte gene expression *in vitro*.
- Determine the impact of APO866 on IL-1β-induced cartilage breakdown *ex vivo*, using biochemical and histological technique.
- Assess the cytotoxic effects of long-term exposure to high and low doses of APO866.
- Assess the effects of NAD^+ biosynthesis substrates NMN and NA on cartilage catabolism and cellular metabolism.

5.2 Materials and methods

5.2.1 Chondrocyte culture

Human Articular chondrocytes (HACs) were extracted as outlined in section 2.1.2.1. HACs were cultured for 24 hours in serum-free chondrocyte-specific medium supplemented with 1% (v/v) Nutridoma-SP before stimulation with 10 ng/ml IL-1β, alone or in combination with 10 nM APO866. Cells were stimulated for 24 hours, media removed and 1 ml of TRI-Reagent added to cells. RNA was extracted and qPCR performed as outlined in section 2.3.2.

5.2.2 Explant cytokine stimulation studies

All explant studies were performed on biopsy cores of full-depth articular cartilage taken from the MCP/MTP joint of 7-day old calves. Extraction and preparation of tissue for *ex vivo* culture was performed as described in section 2.1.5.1. Explants were cultured in 500 µl serum-free DMEM supplemented with 2-20 ng/ml human IL-1β, 10-100 nM APO866, and 100 µM NMN or NA. Cultures were maintained for up to 21 days, medium was removed every 48 hours and stored at -20°C, prior to analysis by DMMB assay (section 2.1.5.2), gelatin zymography (section 2.1.5.3) or LDH assay (section 2.1.6.2). Cells were then supplemented with fresh medium. At the experimental end-point, explants were halved and weighed. One half of each explant was papain digested for s-GAG analysis, whilst the remaining halves were fixed for histological analyses (section 2.3.1).

5.3 Results

5.3.1 IL-1β induces NAMPT, but not NAPRT or QPRT gene expression in HACs.

In order to determine how stimulation with IL-1β, in the presence or absence of APO866, affects the gene expression of NAD^+ biosynthesis genes *in vitro,* HACs were analysed by qPCR. The addition of 10 ng/ml IL-1β significantly enhanced NAMPT gene expression compared with untreated control cells (P=0.008; figure 5.3.1). NAMPT expression was attenuated in cells co-incubated with both IL-1β and APO866 compared with IL-1β alone (P=0.043). This effect was not significant. Expression of NAPRT and QPRT were not significantly affected by treatment with IL-1β and/or APO866 (P=0.260 and P=0.134; NAPRT and QPRT, respectively).

IL-1β alone significantly induced MMP-1 and MMP-3 mRNA levels compared with an untreated control (P=0.046 and P=0.038; MMP-1 and MMP-3, respectively; figure 5.3.2). The cDNA from cells co-incubated with both IL-1β and APO866 showed attenuated MMP gene expression compared with IL-1β alone, although this effect was not significant (P=0.067 and P=0.078; MMP-1 and MMP-3, respectively).

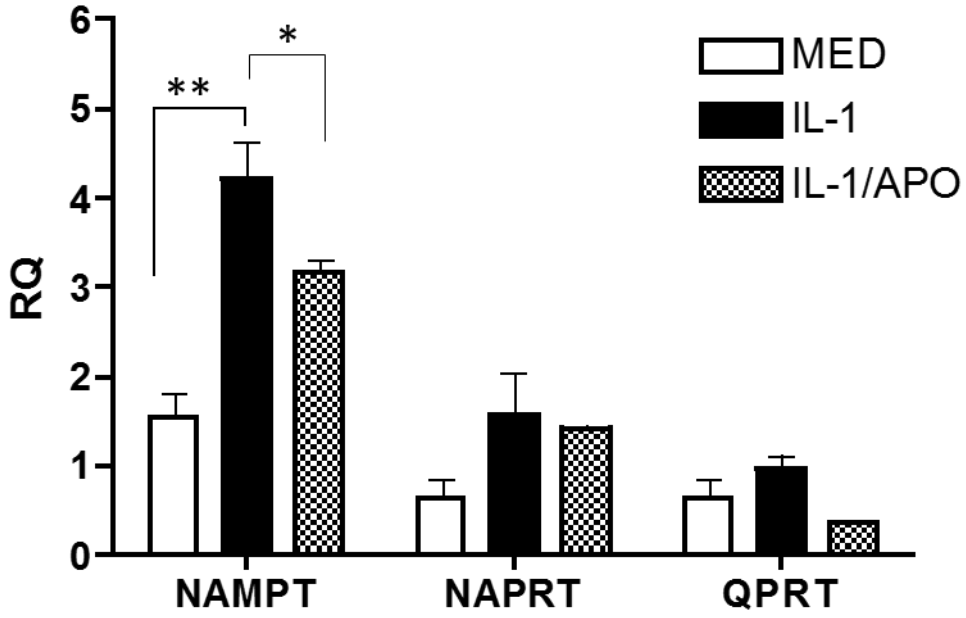

Figure 5.3.1 Effect of IL-1β and APO866 on NAD$^+$ enzyme expression in HACs

HACs (single donor, n=3 experimental replicates per condition) were stimulated for 24 hours with 10 ng/ml IL-1β alone, or in combination with 10 nM APO866. Extracted RNA samples were analysed in duplicate for NAMPT, NAPRT, and QPRT gene expression by qPCR. Samples were normalised to UBC, beta-Actin 18S rRNA and GAPDH reference genes. The relative quantity of NAMPT gene expression (RQ) in treated cells was compared to zero hour unstimulated control cells. All data points are graphically presented with mean ± standard error of the mean (S.E.M). Significance levels between means of the different treatment groups were determined using a two-tailed unpaired t test. *P≤0.05, **=P<0.01.

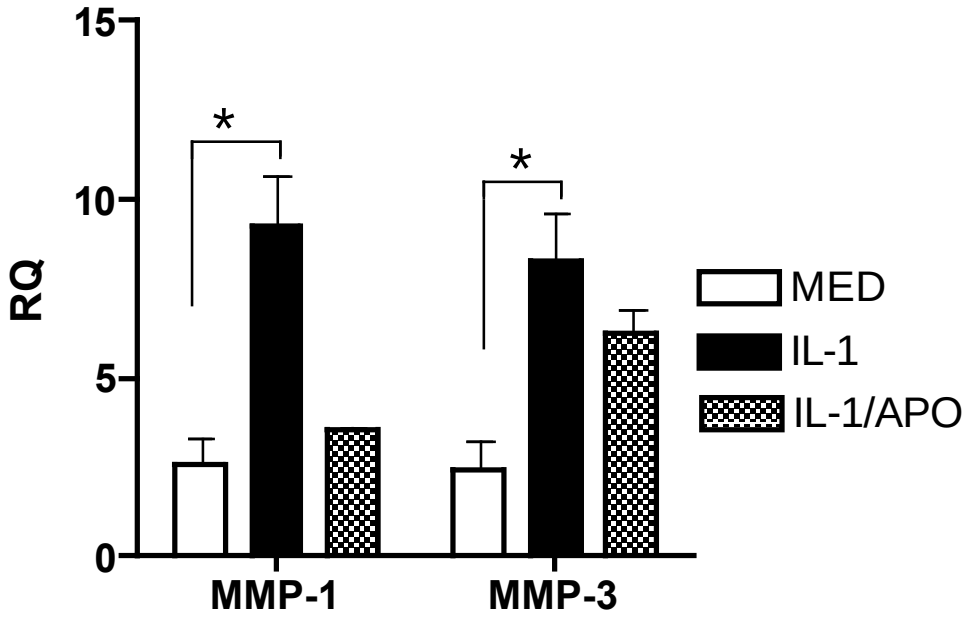

Figure 5.3.2 Effect of IL-1β and APO866 on MMP expression in HACs

HACs (single donor, n=3 experimental replicates per condition) were stimulated for 24 hours with 10 ng/ml IL-1β alone or in combination with 10 nM APO866. Extracted RNA samples were analysed in duplicate for MMP-1 and MMP-3 gene expression by qPCR. Samples were normalised to UBC, beta-Actin, 18S rRNA and GAPDH reference genes. The relative quantity of MMP gene expression (RQ) in treated cells was compared to zero hour unstimulated control cells. All data points are graphically presented with mean ± standard error of the mean (S.E.M). Significance levels between means of the different treatment groups were determined using a two-tailed unpaired t test. *=P≤0.05.

5.3.2 APO866 attenuates IL-1β-mediated PG depletion *ex vivo*

Following on from monolayer culture analyses, the effects of IL-1β on cartilage metabolism were explored in full-depth cultures of bovine articular cartilage, with specific focus on the rate of proteoglycan release. Overall, there was a significant difference in s-GAG loss between explants cultured in medium alone, and explants continually incubated with low dose (2 ng/ml) IL-1β, as determined by Two-way Analysis of variance (P≤0.0001; figure 5.3.3). However, Bonferroni post-test analyses showed that there was no significant difference at any given time point. As expected, time had an overall significant effect on s-GAG release (P≤0.0001). Explants cultured in media alone showed continuous Safranin O staining throughout the tissue, with a distinct zone of depletion nearer the cartilage superficial zone. However, explants incubated with low doses of IL-1β exhibited complete loss of PG staining from the superficial zone, and some evidence of loss in the deeper zone (figure 5.3.4). Analysis of supernatants from explants treated with low doses of IL-1β and APO866 showed only a slight attenuation of s-GAG release into the media, but showed the greatest retention of Safranin O staining out of all the cultured explants.

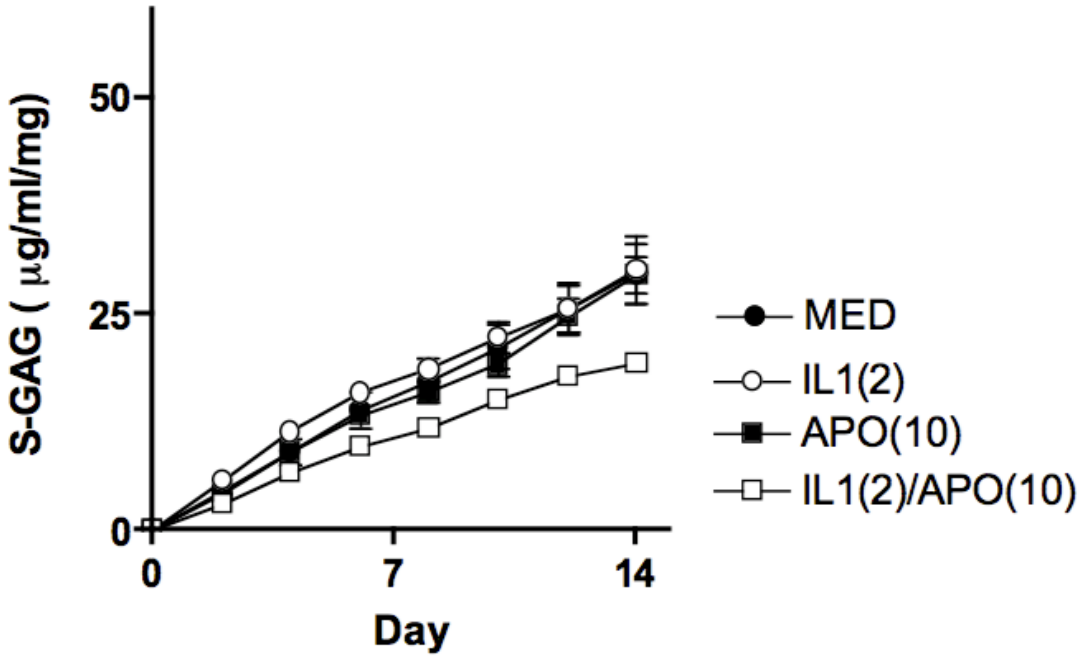

Figure 5.3.3 Effect of low-dose cytokine and APO866 on s-GAG release

Bovine cartilage explants (n=3 explants per condition) were cultured for 14 days in the presence of 2 ng/ml IL-1β (IL-1(2)) with or without 10 nM APO866 (APO(10)). Levels of s-GAG in explant culture supernatants were determined by DMMB assay and presented as cumulative s-GAG loss over the experimental culture period. Differences in s-GAG release were determined by two-way ANOVA. s-GAG, sulphated glycosaminoglycans;

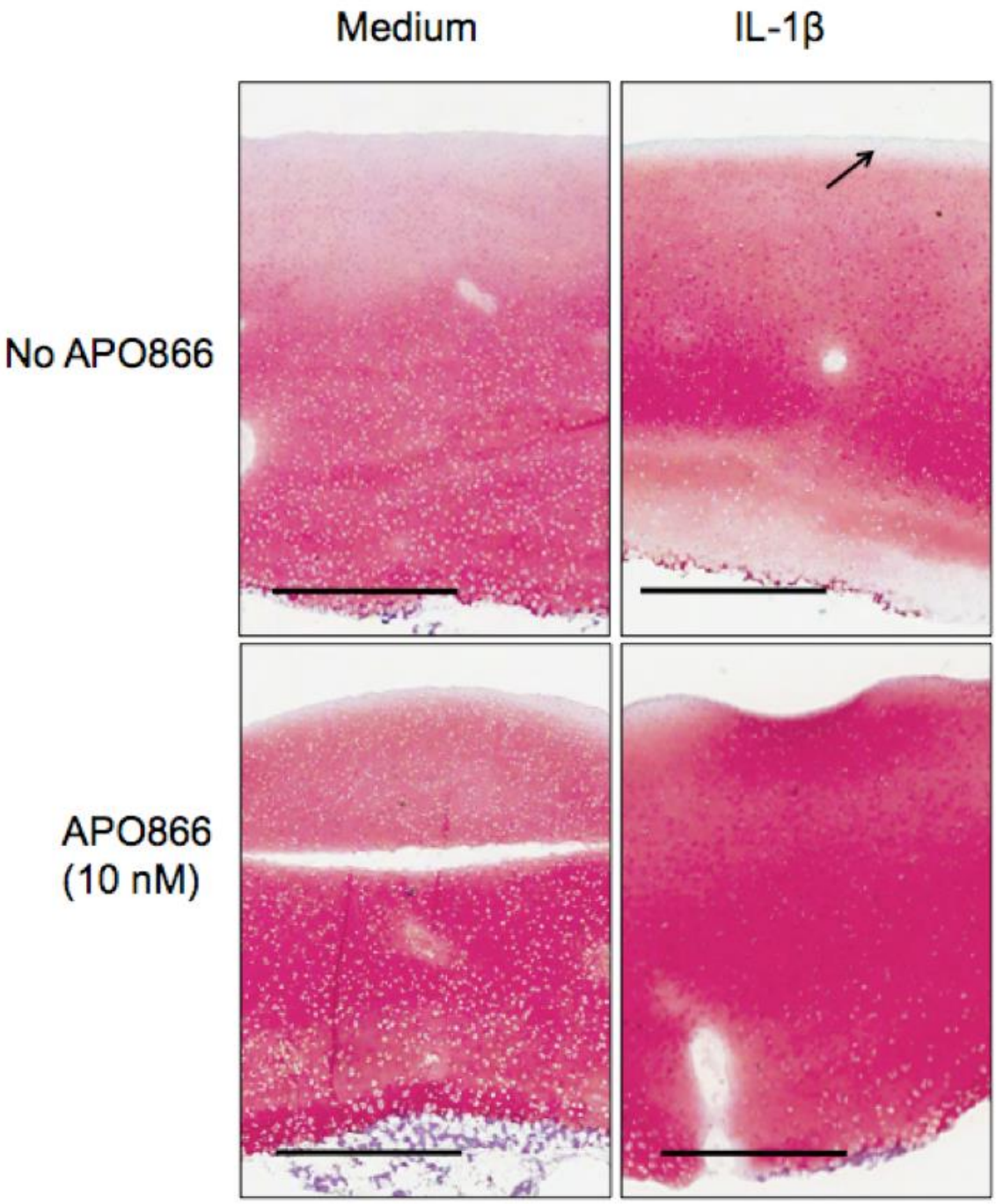

Figure 5.3.4 Proteoglycan content of explants after low dose IL-1β and/or APO866 exposure

Bovine cartilage explants (n=3 explants per condition) were cultured for 14 days in serum free medium, or supplemented with 2 ng/ml human IL-1β (IL-1), 10 nM APO866 (APO), or a combination of the two (IL-1/APO). At the end of the culture period explants (n=1 explant per condition) were fixed, sectioned and stained with Safranin O. The intensity of the red Safranin O staining was used as an indicator of PG content within the cartilage. Scale bars indicate 500 μm. The arrow indicates PG depletion from the articular surface.

Supernatants of explants cultured in the presence of high dose (20 ng/ml) IL-1β contained greater levels of s-GAG than those with 2 ng/ml IL-1β (figure 5.3.5A). Overall, two-way ANOVA analyses showed that these higher doses of IL-1β had a highly significant effect on s-GAG release, differing significantly in mean levels of s-GAG release from the fourth day of culture onwards, as determined by Bonferroni post-test analyses. This was reflected in analyses of papain digests, with IL-1β treated explants containing markedly lower levels of residual s-GAG (8.94 ± 5.08 μg/ml/mg; figure 5.3.5B) compared with those cultured in medium alone (32.49 ± 12.65 μg/ml/mg). However, residual s-GAG levels in papain cartilage extracts did not differ between treatment groups overall (P=0.0578). Cartilage explants were analysed histologically for extent of PG depletion (figure 5.3.6), by assessing loss using both subjective and objective scoring systems (refer to figures 5.3.7A and 5.3.7B). Explants incubated in medium alone showed some PG depletion from the articular surface and the edges of the tissue, with fast green counter stain visible in these regions (figure 5.3.6). In contrast, explants treated with high dose IL-1β exhibited extensive loss of Safranin O staining, corroborating DMMB data (figure 5.3.5).

As with lower doses of APO866, higher doses (100 nM) had no significant effect on s-GAG release compared with the medium control (figure 5.3.5A). However, explants incubated in high dose APO886, in combination with high dose IL-1β, showed significant differences in mean s-GAG values, compared to those incubated in IL-1β alone, becoming extremely significant (P≤0.0001) after six days of explant culture (figure 5.3.5A). Papain digests also showed greater retention of s-GAG in explants cultured with IL-1β and APO866 (34.81 ± 12.52 μg/ml/mg), compared to those cultured in IL-1β alone (figure 5.3.5B), which was also reflected in both subjective and objective histology scoring (P=0.039 and P=0.0051, respectively).

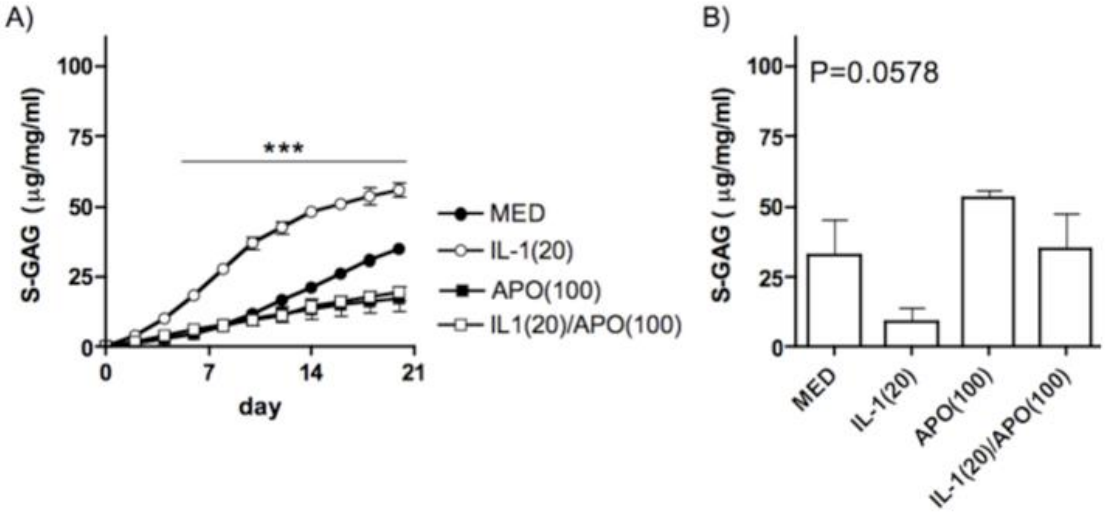

Figure 5.3.5 Effect of high-dose cytokine and APO866 on s-GAG release

Bovine cartilage explants (n=3 explants per condition) were cultured for 21 days in the presence of 20 ng/ml IL-1β with or without 100 nM APO866. A) Levels of s-GAG in explant culture supernatants were determined by DMMB assay, and presented as cumulative s-GAG loss over the experimental culture period. The difference in s-GAG release between IL-1β and IL-1/APO treated explants over time was determined by two-way ANOVA. Astrices indicate significance levels between mean s-GAG values of IL-1β treated explants compared to IL-1/APO ***P≤0.0001 B) Levels of residual explant s-GAG, were assessed in papain digests of the explants and differences determined by Kruskal Wallis One-way ANOVA with Dunn's multiple comparison post-tests. All s-GAG values were corrected for explant wet weight. Error bars depict S.E.M.

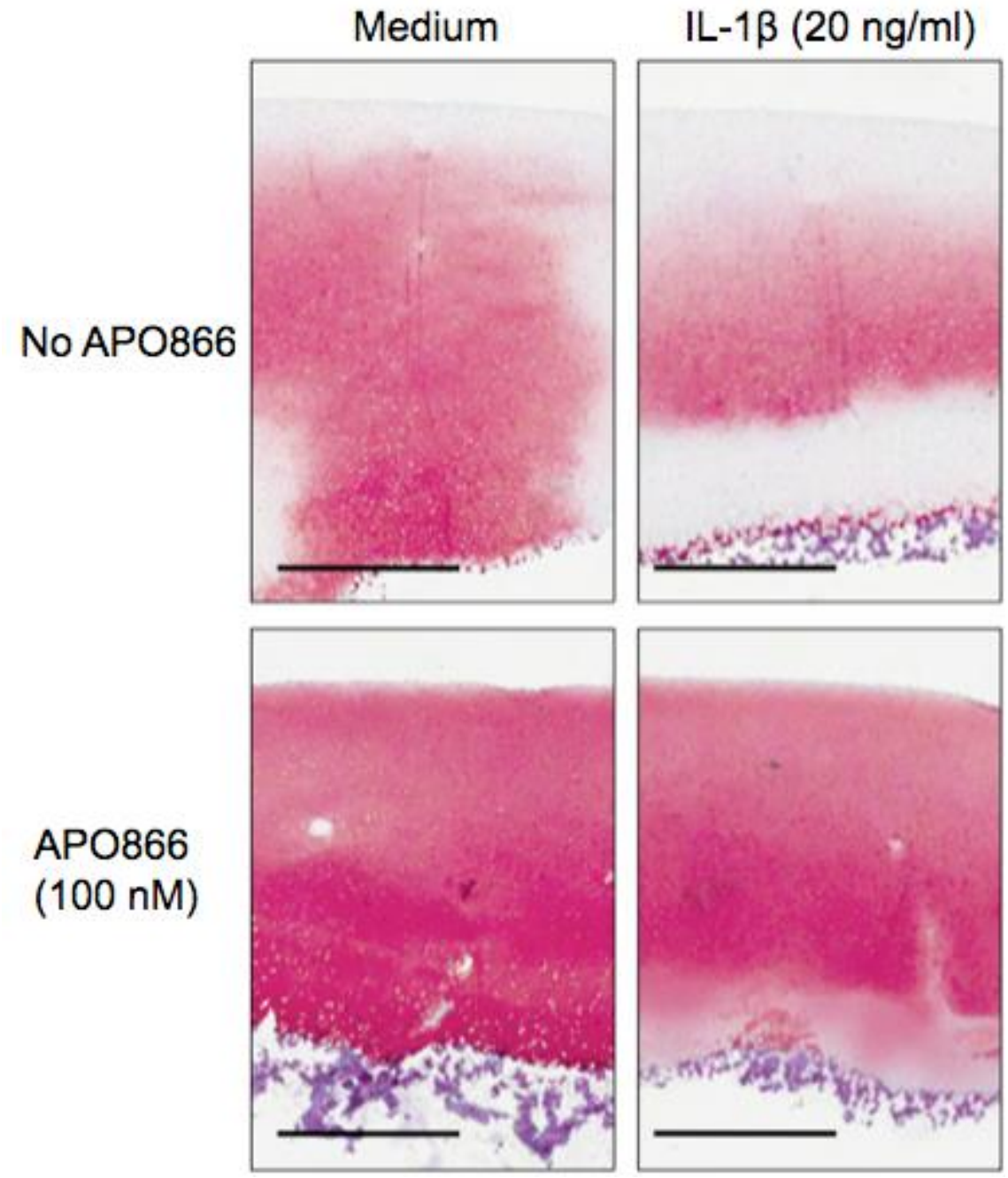

Figure 5.3.6 Proteoglycan content of explants after high dose IL-1β and/or APO866 exposure

Bovine cartilage explants (n=3 explants per condition) were cultured for 21 days in serum free media alone, or supplemented with 20 ng/ml IL-1β alone or in combination with 100 nM APO866. Explants were assessed for PG loss by Safranin O staining. Scale bars indicate 500 μm.

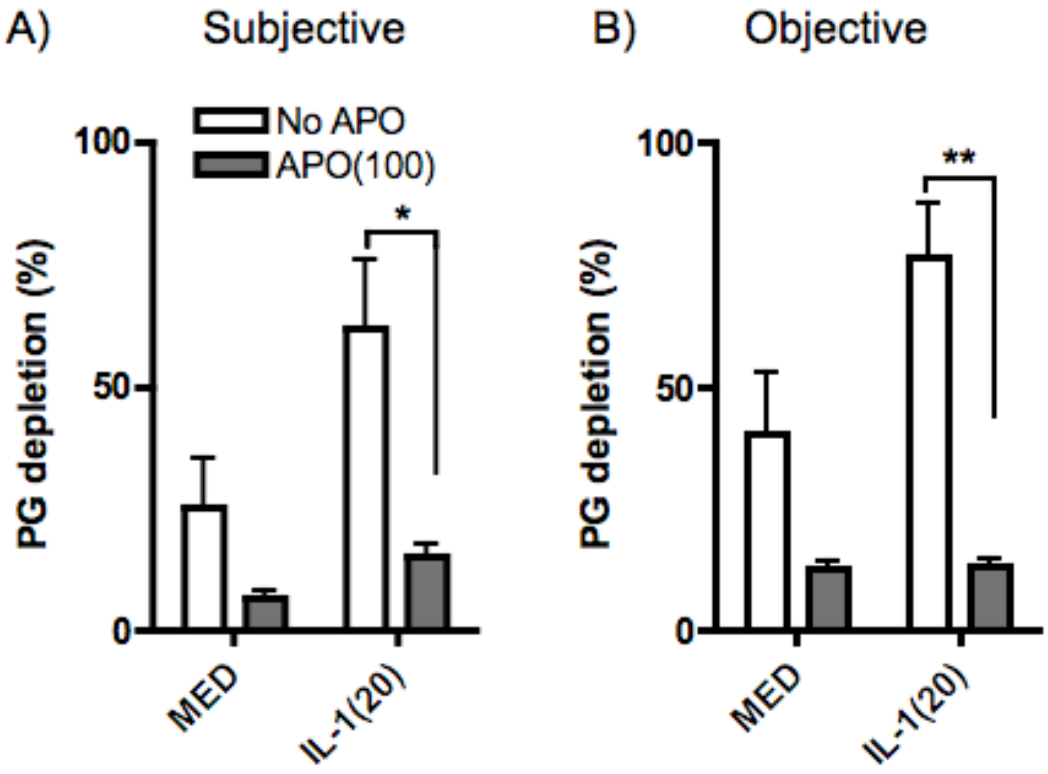

Figure 5.3.7 Histological assessment of proteoglycan loss

Bovine cartilage explants (n=3 explants/histological sections per condition) were scored for extent of PG depletion in the presence or absence of high dose (20 ng/ml) IL-1β and high dose (100 nM) APO866. Bars represent mean ± standard error of the mean (S.E.M). A) Subjective and B) objective scoring of explants was performed. Two-tailed unpaired t-tests were performed to determine the significant differences between treatment groups. *=P≤0.05, **=P≤0.01.

5.3.3 APO866 causes cell death in cartilage explants

High power examination of histological sections revealed that long-term *ex vivo* culture affects both the morphology and viability of chondrocytes within the cartilage ECM. The lacunae of cartilage cores fixed immediately upon extraction, T_0, were replete with chondrocytes with well-stained nuclei (figure 5.3.8[i]). Cartilage explants cultured in either media alone or IL-1β had a similar histological appearance to T_0 explants (figure 5.3.8).

The histological appearance of cartilage explants treated with APO866 was strikingly different to untreated controls: many lacunae contained cellular debris (figure 5.3.8[ii]) with weakly stained or shrunken nuclei, or were devoid of cells (figure 5.3.8[iii]). Explants co-incubated with APO866 in combination with IL-1β also exhibited a large degree of cell loss, with an abundance of empty lacunae (figure 5.3.9). This indicated that long-term exposure to APO866 had an adverse effect on explants.

To assess cytotoxicity, culture supernatants were analysed every 2-3 days for lactate dehydrogenase (LDH) release. Supernatants of explants cultured in medium alone or 2-20 ng/ml IL-1β, contained negligible levels of LDH throughout the culture period (figure 5.3.10). However, supplemented media from explants exposed to APO866 at even the lowest doses tested in this experimental system (10 nM), showed significant levels of LDH at day 12 of culture (figure 5.3.10A). At the lower doses, 10 nM APO866, together with 2 ng/ml IL-1β shifted the peak of LDH release from days 12 to day 10 of culture. However, at the higher doses 100 nM APO866, together with 20 ng/ml IL-1β did not shift the peak of LDH release (Figure 5.3.10B). The patterns of LDH release observed indicated a sudden and nearly complete expiration of chondrocytes as a direct result of APO866 treatment.

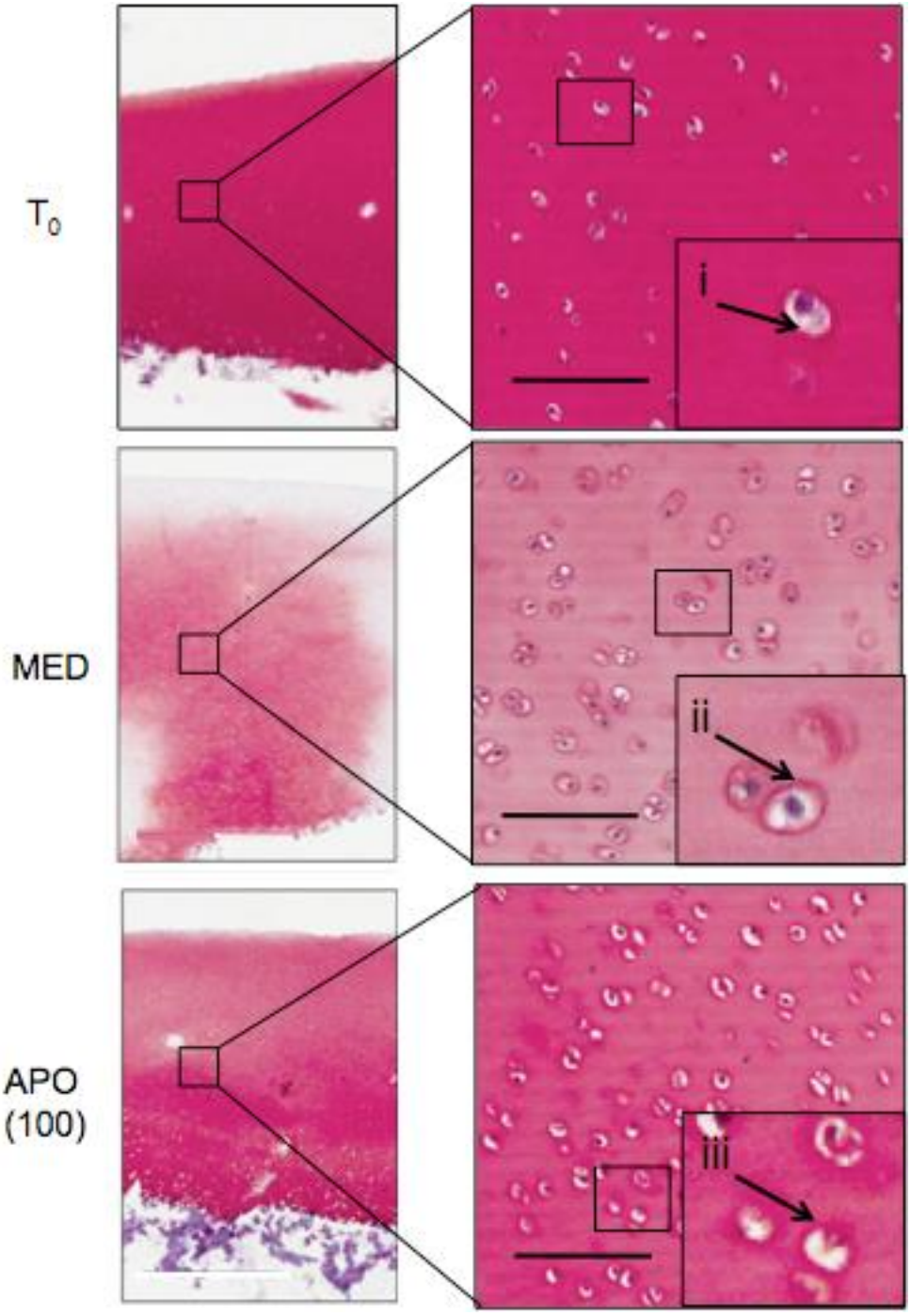

Figure 5.3.8 Morphological characteristics of chondrocytes *ex vivo*; Explants cultured with or without high dose APO866

Representative histology of explants immediately fixed upon dissection (T_0), or cultured for 21 days in medium alone (MED) or with 100 nM APO866 [APO(100)]. Sections of the mid-zone stained with Safranin O are shown. i) and ii*)* High power image of healthy cells within the lacuna, showing dark blue nuclear staining of chondrocytes within the ECM, **iii**) High power image of cells with no haematoxylin staining, indicating dying or dead cells within the lacuna. Scale bars indicate 100 μm.

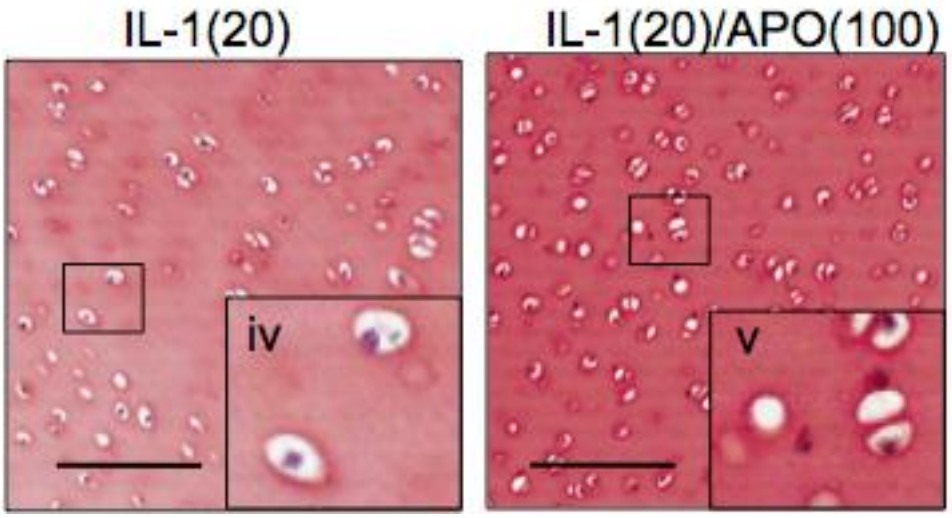

Figure 5.3.9 Morphological characteristics of chondrocytes *ex vivo;* Explants cultured with high dose APO866, with or without high dose IL-1β

Representative histology of explants cultured for 21 days in 20ng/ml IL-1β [IL-1 (20)] or IL-1β with 100 nM APO866 [IL-1(20)/APO(100)]. Sections of the mid-zone stained with Safranin O are shown. iv) High power of healthy cells within the lacuna, v*)* high power of cells with no hematoxylin staining. Scale bars indicate 100 μm.

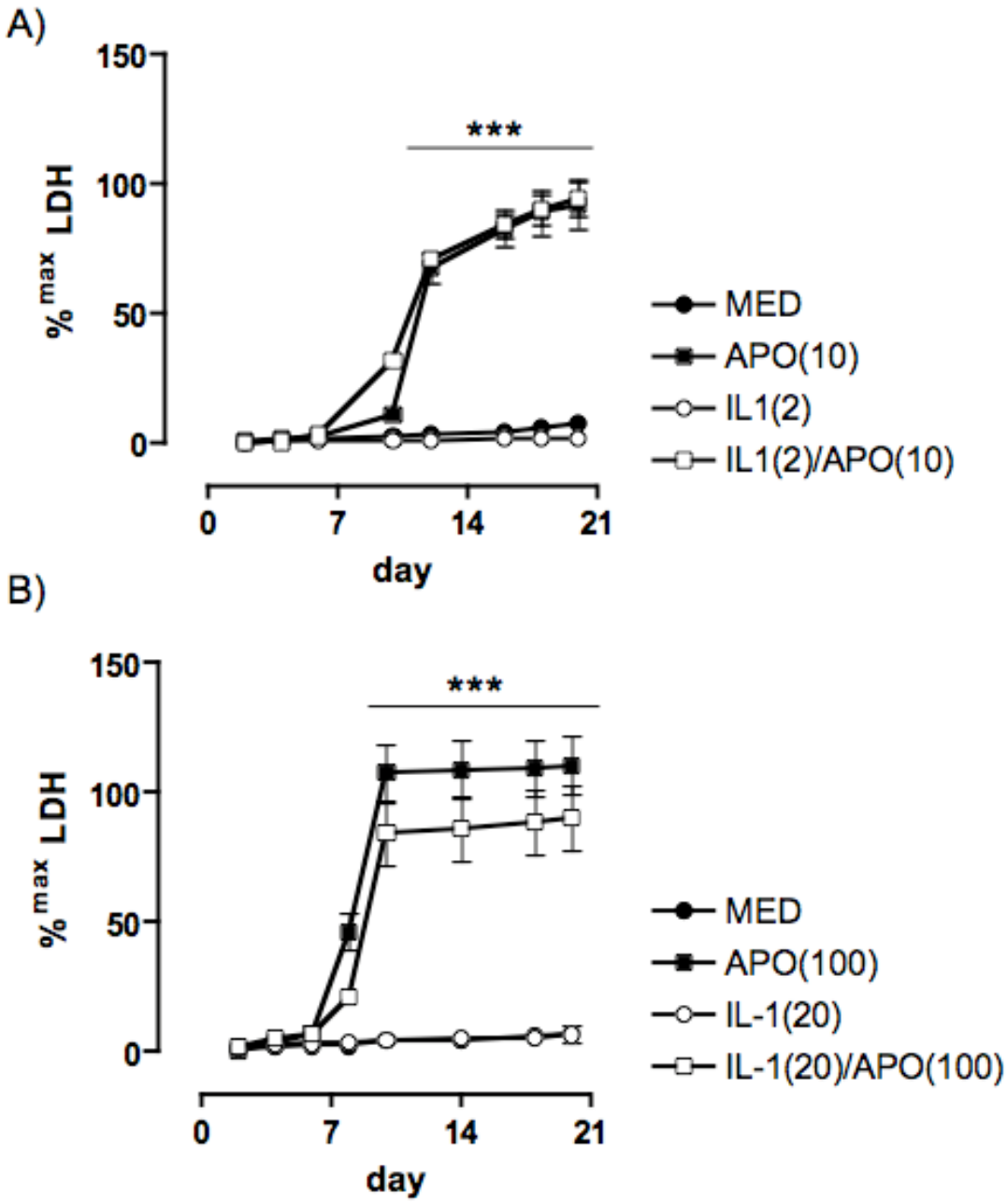

Figure 5.3.10 Effect of APO866 on LDH release from explants

Explant supernatants taken after every 48 hours of culture (n=3 samples per time point) were analysed for LDH release from cells. Fluorescence intensity values (in relative fluorescent units) were normalised to a maximum LDH release control sample, and are presented as percentage maximum LDH release in a cumulative plot. In two independent experiments, explants were stimulated with: A) 2 ng/ml IL-1β, alone or in combination with 10 nM APO866, or B) 20 ng/ml IL-1β, with or without 100 nM APO866. The differences in LDH release were determined by two-way ANOVA. Astrices indicate significance levels between mean $\%^{max}$ LDH values of treatment groups. ***=P≤0.0001

5.3.4 The NAD+ precursors, NMN and NA, rescue APO866 induced chondrocyte cell death

Due to the role of NAMPT as a NAD+ biosynthetic enzyme, it was hypothesised that the release of LDH in medium from APO866-treated chondrocytes may have been attributed to a catastrophic depletion of intracellular NAD^+ in these cells, resulting in chondrocyte cell death. The effects of both NMN and NA on cartilage rescue were tested; NMN is the product of the NAMPT enzyme, whilst NA is the precursor of NAD^+ via an alternative pathway, involving NAPRT. Both the addition of either NMN or NA (100 μM) prevented APO866-induced LDH release into the culture supernatants (figure 5.3.11A and B). The addition of either NMN or NA also prevented APO866-induced LDH release in IL-1β-stimulated explants.

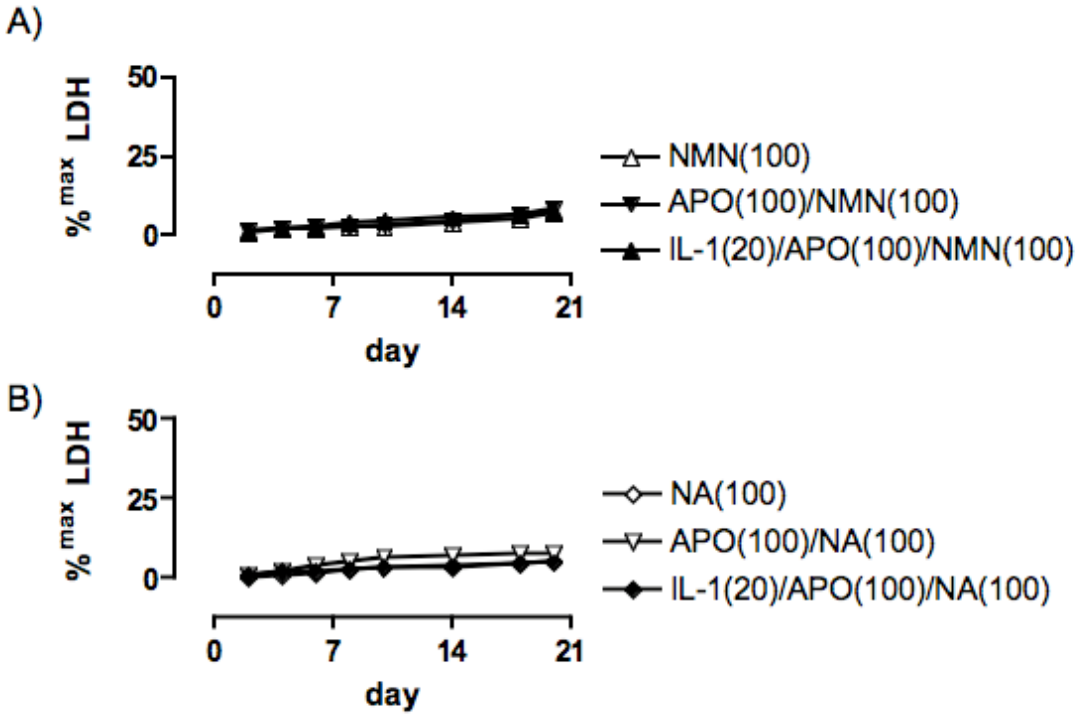

Figure 5.3.11 Effect of NMN and NA on explant cell viability

Explant supernatants taken after every 48 hours of culture (n=3 samples per time point) were analysed for LDH release from cells. Fluorescence intensity values (in relative fluorescent units) were normalised to a maximum LDH release control sample, and are presented as percentage maximum LDH release in a cumulative plot. In two independent experiments, explants were stimulated with: A) 100 μM NMN or B) 100 μM NA, alone or with 20 ng/ml IL-1β and 100 nM APO866, The difference in LDH release between the treatment groups over time was determined by two-way ANOVA.

5.3.5 NMN and NA enhance IL-1β -induced s-GAG loss and MMP activity

During the first 10 days of explant culture, NMN alone or in combination with APO866 had no significant effect on s-GAG release compared to the medium control (figure 5.3.12A). In contrast, NA alone significantly attenuated s-GAG release compared with the medium control, with cumulative s-GAG release becoming significantly altered from day 12 of explant culture (5.3.12B).

Compared to explants co-cultured with high doses of IL-1β and APO866, the addition of 100 μM NMN enhanced s-GAG release in explants, with levels exceeding those observed in the presence of IL-1β alone from the tenth day of explant culture, as determined by two way ANOVA and Bonferroni post-tests (figure 5.3.13A). The addition of 100 μM NA also significantly enhanced s-GAG release in explants co-cultured with high doses of IL-1β and APO866; an effect seen in the first six days of culture; before reaching a plateau at levels normally seen with IL-1β alone (figure 5.3.13B).

At the experimental end-point, papain digests showed there was no significant difference in s-GAG retention between explants cultured with or without high dose IL-1β ($P=0.1592$), or between explants cultured in high dose APO866 with or without IL-1β ($P=0.2827$; figure 5.3.14). However, explants treated with APO866 combined with NMN exhibited significantly higher levels of s-GAG compared with the medium control ($P=0.03$). NA also enhanced s-GAG retention in APO866-treated explants compared with the medium control. However, this effect was not significant ($P=0.182$). In contrast, incubation of explants with a combination of high doses of IL1β, APO866 and NMN caused a significant loss of s-GAG from explants ($P=0.0002$) compared to explants incubated with high dose APO866 and NMN alone. This was not apparent in explants cultured with NA ($P=0.0862$).

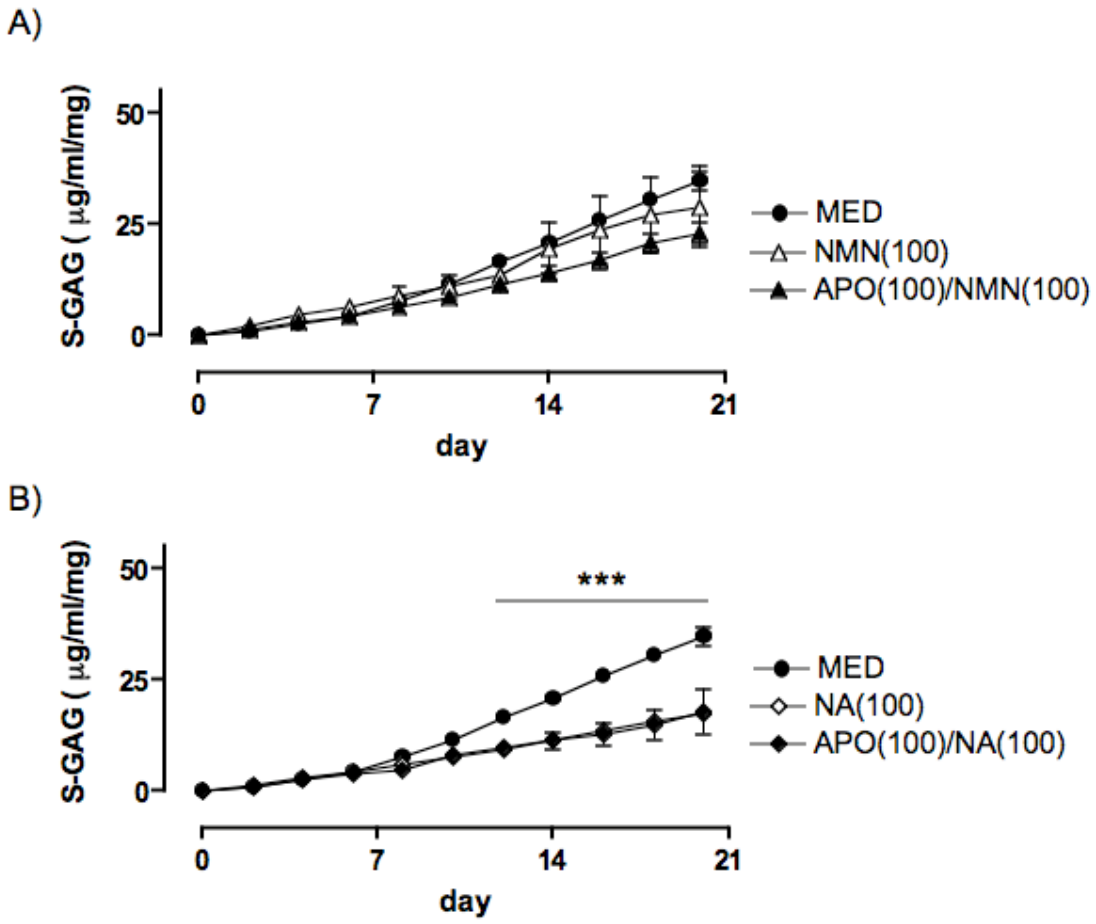

Figure 5.3.12 Effect of NMN and NA on APO866-induced s-GAG release from explants

Culture supernatants (n=3 per condition) were analysed for s-GAG content by DMMB assay. All s-GAG values obtained from culture supernatants were corrected for explant wet weight. A two-way analysis of variance was performed to determine the effects of 100 µM A) NMN [NMN(100)] and B) NA [NA(100)] on s-GAG release in the presence or absence of 100 nM APO866 [APO(100)], compared with the medium control (MED). Astrices indicate significance levels between mean cumulative s-GAG values of treatment groups. ***=P≤0.0001.

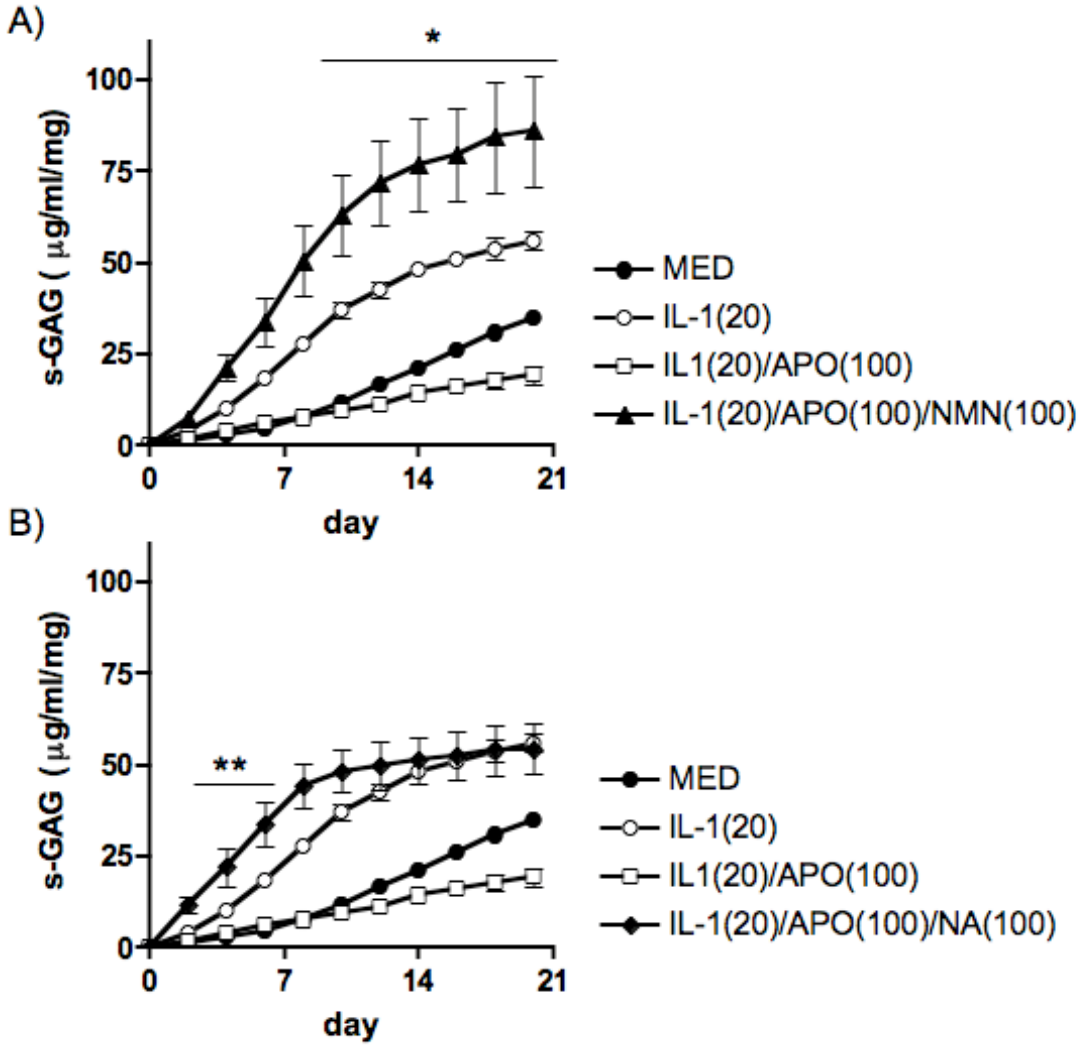

Figure 5.3.13 Effect of NMN and NA on IL-1β induced s-GAG release

Culture supernatants (n=3 per condition) were analysed for s-GAG content by DMMB assay. All s-GAG values obtained from culture supernatants were corrected for explant wet weight. A two-way analysis of variance was performed to determine the effects of 100 µM A) NMN [NMN(100)] and B) NA [NA(100)] on s-GAG release in the presence or absence of 20 ng/ml IL-1β [IL-1(20)] and 100 nM APO866 [APO(100)], compared with the medium control (MED). Astrices indicate significance levels between mean cumulative s-GAG values of treatment groups. *=P≤0.05, **=P≤0.01.

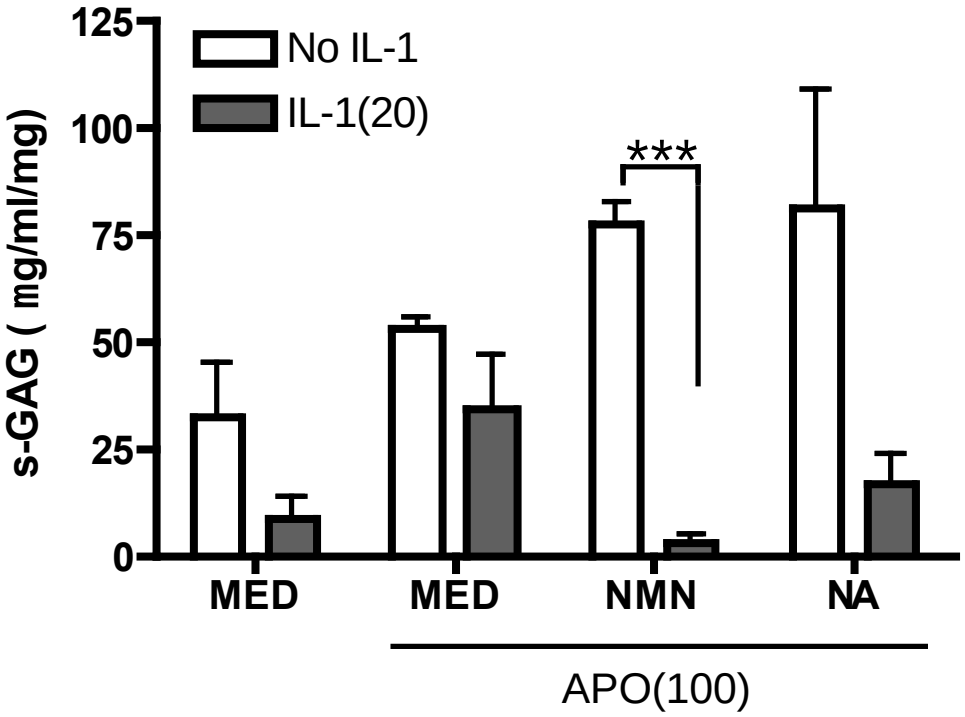

-

Figure 5.3.14 Effect of NMN and NA on GAG retention in cartilage extracts

Bovine cartilage explants (n=3 explants per condition) were papain digested and levels of s-GAG determined by DMMB assay. Two-tailed unpaired t-tests were performed to determine significance levels between means of explants treated with 100 nM APO866 [APO(100)] alone, or combined with 100 μM NMN or NA. All treatments were in the presence or absence of 20 ng/ml IL-1β Astrices indicate statistical significance levels between explant s-GAG retention in the presence or absence of 20 ng/ml IL-1β. ***=P≤0.0001.

Gelatin zymography was performed on culture supernatants to determine whether increases in IL-1β-induced s-GAG release in the presence of NMN and NA coincided with an increase in gelatinase release and activity. Gelatin zymograms showed diffuse bands of both pro- and active MMPs -2 and -9 (figure 5.3.15). Supernatants from explants stimulated with 20 ng/ml IL-1β alone showed enhancement in total MMP-2 and MMP-9 activity from around 12 days, with MMP-9 showing a greater propensity to increase at this time. Concurrent with the mass cell death observed at around day 10 in explants treated with 100 nM APO866 (figure 5.3.10), the addition of APO866 decreased release of MMP -2 at this time point, with MMP-9 bands barely detectable at any time point. Chondrocyte rescue with either NMN or NA shifted the enhancement of gelatinase activity from day 12 to day 10, and total MMP-2 activity was significantly enhanced in these explants.

These observations were reinforced by densitometry analyses (performed as described in section 2.1.5.3), which indicated that mean levels of MMP-2 and MMP-9 activity in supernatants were significantly attenuated in explants cultured with a combination of IL-1β and APO866 compared with those incubated with IL-1β alone (figure 5.3.16A and B), from days 10 (MMP-2) and 12 (MMP-9). In contrast, the addition of either 100 μM NMN or NA in IL-1β/APO866-treated explants enhanced the activity of MMP-2 and MMP-9 (figure 5.3.16C and D). Supernatants of IL-1β/APO866-treated explants co-cultured with NMN showed significantly greater mean levels of MMP-2 compared with those incubated with IL-1β alone (figure 5.3.16C). Although the NMN or NA treatments had an overall significant effect on MMP-9 release ($P \leq 0.0001$), Bonferroni post-tests did not detect a significant difference at any given time point.

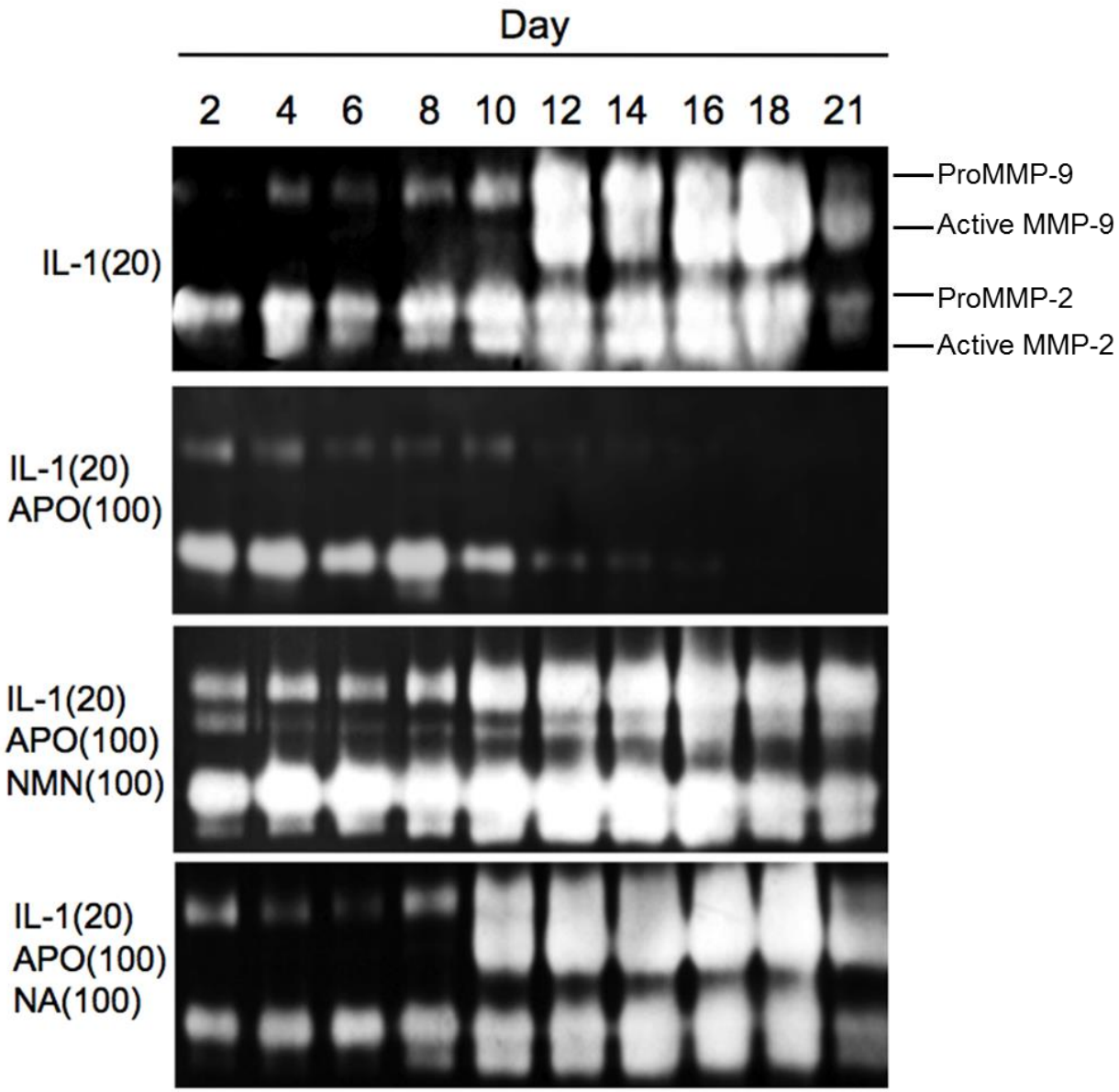

Figure 5.3.15 Gelatin zymograms of explant supernatants

Explant culture supernatants were analysed for MMP-2 and -9 activity using gelatin zymography. Explants were cultured for a total of 21 days in the presence of 20 ng/ml IL-1β, alone [IL-1(20)] or in combination with 100 nM APO866 [IL-1(20)/APO866(100)]. In addition, groups of explants were cultured with the above in combination with 100 μM of NMN [IL-1(20)/APO(100)/NMN(100)] or NA [IL-1(20)/APO(100)/NA(100)]. Supernatants from each day of medium refreshment (days 2-21) were loaded sequentially onto an SDS-PAGE gel. Three gels were run per experimental condition (n=3), each containing a series of culture supernatants from a single explant. A representative gel from each condition is shown.

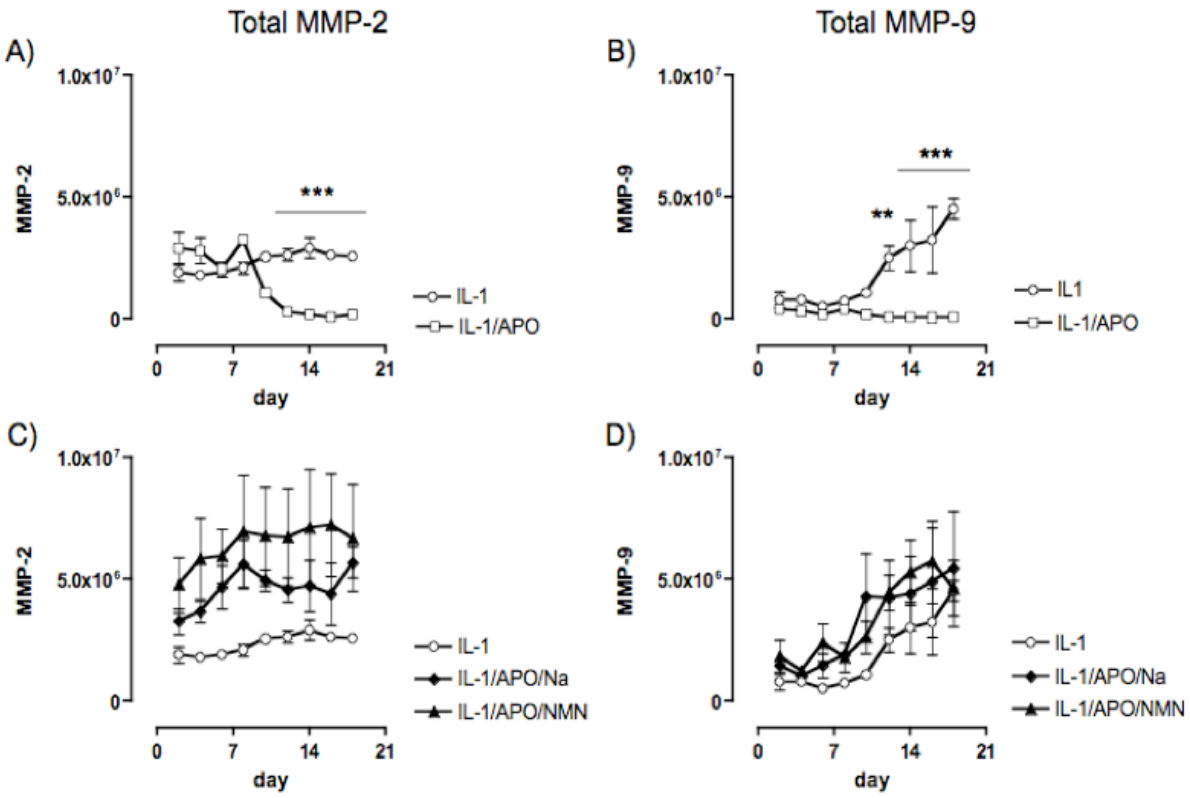

Figure 5.3.16 The effect of NMN and NA on cytokine-induced MMP activity

Densitometry analysis was performed on gelatin zymograms (n=3 gels per treatment group) to determine the mean net intensity values for bands pertaining to total MMP-2 and MMP-9. Net intensity of A) total MMP-2 and B) total MMP-9 from explant supernatants incubated with 20 ng/ml IL-1β with or without 100 nM APO866. Error bars depict S.E.M. A two-way analysis of variance was performed to determine the differences in net intensity between IL-1β (IL-1), and IL-1β/APO866 (IL-1/APO) treatment groups. Net intensity of C) total MMP-2 and D) total MMP-9 in IL-1β/APO866-treated explant supernatants supplemented with 100 μM NMN (IL-1/APO/NMN) or NA (IL-1/APO/NA). A two-way ANOVA was performed to determine differences in net intensity between the treatment groups. **=P≤0.01, ***=P≤0.0001.

5.4 Discussion

5.4.1 APO866 had no significant effect on IL-1β-induced MMP expression in human chondrocytes

Studies performed on human primary chondrocytes in this chapter confirmed that NAMPT gene expression is significantly induced by IL-1β, which ties in with previous published work in murine (Gosset et al., 2008) and rabbit (Hong et al., 2011) chondrocytes. However, expression of NAPRT and QPRT were not affected. These findings suggest that neither the alternative salvage pathway or the *de novo* pathway are affected by cytokine signalling, and that the Nam salvage pathway is the preferred pathway for NAD^+ biosynthesis in chondrocytes. It also suggests that NAMPT may be required for cytokines such as IL-1β to mediate a response.

The action of iNAMPT on cytokine-mediated induction of MMPs -1 and -3 was also investigated and the results show that co-incubation of IL-1β with APO866 did not significantly affect IL-1β-induced MMP gene expression in HACs, although expression was slightly attenuated. Previous studies in human chondrocytes have shown that addition of APO866 causes a reduction in cartilage-specific gene expression (Dvir-Ginzberg et al., 2008). Although these experiments were performed in non-activated cells, the results suggested that intracellular NAD^+ indirectly affects the regulation of matrix turnover in chondrocytes. IL-1β induces expression of MMP-1, -3 and -13 in HACs through activation of NF-κB and MAPK signalling pathways (Liacini et al., 2002, Tsutsumi et al., 2008). NAMPT and SIRT have been shown to boost activation of ERK and p38 MAP kinases. Inhibition of NAMPT with APO866 inhibited activation of these kinases. Overexpression of a dominant negative Sirt1 retrovirus had a similar effect, suggesting both are essential for IL-1β-induced ERK signalling (Hong et al., 2011). Therefore, manipulation of sirtuins through reductions in cellular NAD^+ may reduce IL-1β induced MMP transcription. IL-1β-induced MMP transcription was not completely attenuated by APO866, suggesting that IL-1β may continue to signal through NF-κB.

5.4.2 APO866 attenuation of IL-1β-induced s-GAG loss in explants is due to cytotoxicity

In contrast to medium controls, explants exposed to cytokine stimulation exhibited a time and dose-dependent increase in s-GAG release into the surrounding medium. These data demonstrate that cytokine stimulation causes an induction of catabolic protease production within the native chondrocytes, resulting in cleavage and subsequent loss of cartilage ECM components. This was confirmed in papain digests of cartilage explants, as cytokine stimulation resulted in significantly lower levels of s-GAG retention compared with explants cultured in medium alone. Gelatin zymography indicated that expression of MMP-9 is markedly induced by around day 12 of culture.

This late onset of MMP activity compared with aggrecanase activity has been observed in other explant culture studies, where type II collagen-derived fragments are typically detected in supernatants between 14-21 days of culture (Karsdal et al., 2008, Wang et al., 2009a). Taken together with the findings from the DMMB assays, these data suggest IL-1β stimulation caused enhanced loss of cartilage ECM components through the upregulation of proteolytic enzymes such as MMPs.

Explants incubated with APO866 exhibited a sharp decrease in s-GAG and MMP release from around day 10 of culture. Both inducible MMP-9 and constitutively expressed MMP-2 were greatly attenuated. It was originally thought that this was due to a therapeutic effect of APO866. However, these observations coincided with a complete loss of cell viability; suggesting the drop in MMP release was in fact a result of catastrophic cell death.

5.4.3 APO866-induced cytotoxicity is prevented by NMN and NA

The concentrations of APO866 used in *ex vivo* culture ranged from 10-100 nM; the latter dose has been previously used in murine chondrocytes stimulated for 24 hours (Jacques et al., 2012). Studies in murine and human monocytes showed that 4 hours stimulation with 100 nM APO866 does not affect cell viability, despite proven depletion of intracellular NAD^+ (Busso et al., 2008). Additionally, a study in HeLa cells showed that 100 nM APO866 causes an initial reduction in NAD^+ after 6 hours of exposure, followed by a plateau phase, before the advent of further depletion after 24-96 hours APO866 exposure (Pittelli et al., 2010). Unfortunately NAD^+ levels could not be quantified in explants, as attempts to extract the cofactor from cells proved unsuccessful. However, a gradual drop of NAD in chondrocytes, as a result of chronic exposure to APO866 may explain the cytotoxic effect of APO866 on explants.

Intracellular NAMPT catalyses the conversion of Nam to NMN, which is subsequently converted to NAD^+ by NMNAT-1 (figure 1.8). In this chapter the addition of NMN (i.e. bi-passing iNAMPT activity) rescued chondrocytes from APO866-induced cytotoxicity, suggesting that depletion of cellular NAD^+ was indeed the cause of cell death in these explants. This could also be confirmed in future studies by the addition of NAD^+ to explants or cells, or through quantification of intracellular NAD^+ in the explants. The importance of iNAMPT to cell survival is not surprising, as the Nam salvage pathway is the main means of NAD^+ production in mammals (reviewed by Bogan and Brenner, 2008). In addition to Nam, NA is an alternative precursor of NAD^+ via the Preiss-Handler pathway (figure 1.8).

Incubation of explants with NA also inhibited APO866-induced chondrocyte cytotoxicity, demonstrating that in the absence of iNAMPT chondrocytes can utilise

alternative pathways of NAD^+ biosynthesis. Together, these data confirm that the inhibition of iNAMPT by APO866 has a rate-limiting effect on cell viability and that chondrocyte viability is NAD^+ dependent. The fact that NA is able to rescue chondrocytes from iNAMPT-depletion suggests that NAD^+ may also be synthesised independently of iNAMPT in these cells. A pre-clinical study has shown that the addition of NA *in vitro* can inhibit APO866-induced cytotoxicity in cancer cell lines (Olesen et al., 2010). Besides this study, there has been little research into the effects of depletion and repletion of NAD^+ *in vitro*. NAD^+ depletion has also been shown to have a cytotoxic effect in T lymphocytes, where APO866 causes autophagic cell demise (Bruzzone et al., 2009). As with the current study, activated T lymphocytes were more sensitive to NAMPT inhibition than resting cells (Bruzzone et al., 2009). It is thought that transformed cells (e.g. cancer cells or activated cells) have a higher basal turnover of NAD^+, and so are particularly sensitive to depletion of this cofactor. Additionally, some cell lines (e.g. HepG2) are unable to utilise NA (Hasmann and Schemainda, 2003), highlighting a possible mechanism for targeted inhibition of activated cells. Both NMN and NA not only counteracted the cytotoxic effects of APO866, they also appeared to enhance cytokine-mediated induction of catabolic proteases; as apparent by enhanced and accelerated release of S-GAG and detection of MMP activity by gelatin zymography. This suggests that regulation of catabolic proteases in chondrocytes is NAD^+ dependent, though not necessarily iNAMPT dependent. It also indicates that an increase in cellular NAD+ availability may have a downstream effect on transcription of MMPs and other matrix-degrading enzymes.

5.4.5 Summary

The findings of this chapter show that iNAMPT is important for both cartilage matrix turnover and also chondrocyte survival (summarised in figure 5.4.1). Real-time PCR analyses indicate that NAMPT is the only NAD^+ biosynthesis enzyme induced by IL-1β stimulation of human chondrocytes, hinting that the Nam salvage pathway is associated with pro-inflammatory and pro-degradative processes. Inhibition of iNAMPT activity *in vitro* suggested that NAMPT is involved in IL-1β-induced MMP gene expression. However, inhibition of iNAMPT by APO866 in long-term cartilage explant culture resulted in complete chondrocyte cell death within 10 days. This cytotoxicity is attributed to a catastrophic depletion of intracellular NAD^+, as the addition of NAD^+ metabolites, NMN and NA, prevented cytotoxicity presumably through the replenishment of NAD^+. These data suggest that cell survival and cartilage catabolism are NAD^+ dependent.

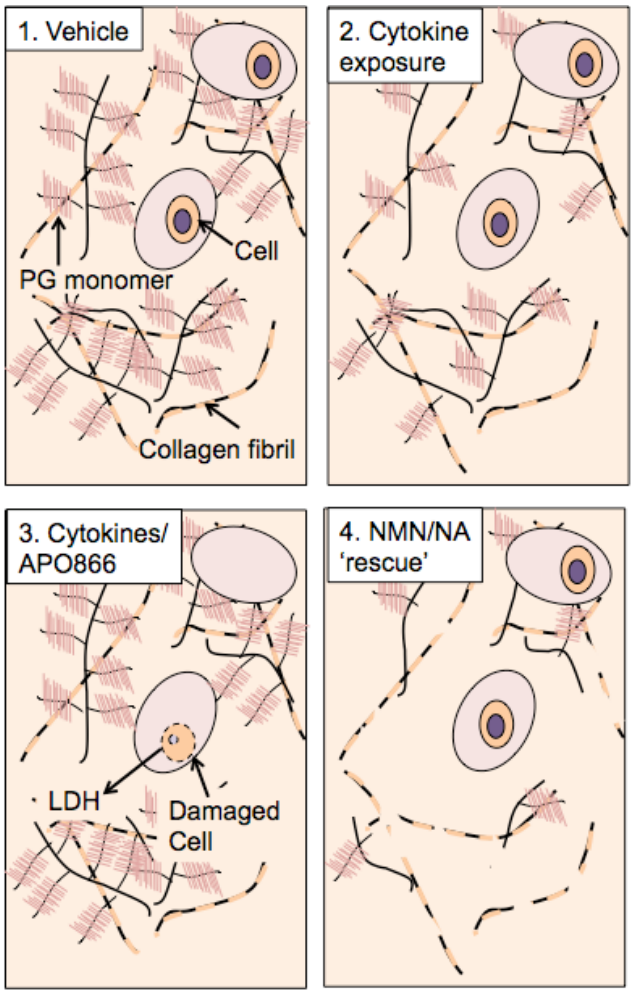

Figure 5.4.1 Summary schematic of chondrocytes and cartilage integrity *ex vivo* Panel 1: chondrocytes within the cartilage matrix, which most components remaining intact. Panel 2: Pro-inflammatory cytokine stimulation results in rapid loss of s-GAG, followed by eventual breakdown of collagen fibrils. Panel 3: Co-incubation with cytokines and NAMPT antagonist APO866 inhibits s-GAG loss, though subsequently cell damage and cytotoxicity occurs in a time and dose-dependent manner. Panel 4: The cytotoxic effects of APO866 can be counteracted with the addition of either NAMPT product NMN or alternative NAD^+ precursor NA. However, cytokine stimulation in the presence of these co-factors exacerbates s-GAG loss from the cartilage extracellular matrix.

Chapter 6: Regulation of iNAMPT in synovial fibroblasts *in vitro*

6.1 Introduction

In RA, fibroblast-like synoviocytes within the synovial intimal lining of the diarthrodial joint become phenotypically distinct from normal fibroblasts. These fibroblasts are one of the major constituents of 'pannus', the invasive granulation tissue that invades and erodes the joint articular cartilage and bone, along with synovial macrophages. Synovial fibroblasts are believed to be the primary effectors of articular cartilage destruction in RA (reviewed by Bartok and Firestein, 2010). They play a key role in the perpetuation of disease through the production of pro-inflammatory cytokines such as IL-1β (section 1.2.3) and proteases such as MMPs (section 1.2.4) that contribute to the breakdown of the articular cartilage tissue. This has been demonstrated in cadherin-11 knockout mice. These mice, which lack a synovial intimal lining, are protected from arthritis-induced cartilage damage, but not bone erosion (Lee et al., 2007).

Understanding of the pathogenesis of RA has been greatly facilitated by the use of fibroblasts isolated from the synovial tissues of diseased patients, often named fibroblast-like synoviocytes (FLS) or RASFs in the literature (Bartok and Firestein, 2010). RASFs are the major NAMPT-expressing cells in synovial tissue, and NAMPT is predominantly expressed at sites of cartilage invasion in these tissues (Brentano et al., 2007). In RASFs, NAMPT is upregulated in response to LPS, TLR ligand Poly(I-C), TNFα and IL-1β (Brentano et al., 2007). To my knowledge, the above findings are the only published findings concerning the regulation of NAMPT in human RASFs. This study demonstrates the contribution of NAMPT to the inflammatory milieu within an RA joint. This could subsequently promote articular cartilage degradation. The latter will be explored in this chapter.

There are several possible mechanisms whereby NAMPT could modulate RASF-dependent joint inflammation and degenerative processes; by virtue of its cytokine-like activity, its role in NAD^+ biosynthesis, or both. My work will contribute to the elucidation of NAMPT-dependent degenerative and inflammatory mechanisms in RASFs.

NAD^+ plays a major role as a coenzyme in numerous oxidation-reduction reactions, including the generation of ATP (Ziegler, 2000). Recently, a functional link between NAD^+ metabolism and inflammation has been proposed; in a human monocytic THP-1 cell line, intracellular NAD^+ levels promote TNFα synthesis in activated cells. It was shown that SIRT6, a member of the sirtuin family, regulates TNFα production at a

post-transcriptional step in these cells (Van Gool et al., 2009). It is possible that NAD^+ levels could control sirtuin activity, impacting upon MMP expression. The impact of sirtuins on MMP expression has not been published previously, therefore the proof of concept mechanistic studies described in this chapter will explore the role of sirtuins in modulating cytokine-mediated MMP expression by RASF.

Sirtuins, along with PARPs, are "NAD^+-consuming" proteins that require NAD^+ as a substrate for their activities. They are a group of HDACs that couple protein deacetylation to NAD^+ hydrolysis, to form O-acetyl-ADP-ribose and Nam. Deacetylation impacts upon the function of many transcription factors, affecting a wide variety of cellular functions (reviewed in North and Verdin, 2004). There are seven types of sirtuins in mammals (SIRT1-7), of which SIRT1 is the most extensively studied. Of relevance here, Revollo *et al* (2004) found that upregulation of iNAMPT increased the transcriptional regulatory function of SIRT1 in mouse fibroblasts by increasing cellular NAD^+ (Revollo et al., 2004).

The exact role of sirtuins in RA disease pathogenesis has yet to be elucidated. SIRT1 is elevated in RA synovial tissues, and like NAMPT is predominantly localised within the synovial lining (Niederer et al., 2011). In addition, SIRT1 expression is induced upon stimulation with the pro-inflammatory cytokine TNFα, and SIRT1 overexpression increases LPS- and TNFα-induced IL-6 and CXCL8 production in RASFs (Niederer et al., 2011). However, despite this apparent pro-inflammatory effect, many studies have reported a potential anti-degradative role for sirtuins. Oxidative stress-dependent reduction of SIRT1 causes an increase in MMP-9 expression in human monocytes (Nakamaru et al., 2009), and sirtuin enhancer resveratrol inhibits MMP-2 and -9 expression in stimulated human sarcoma cells (Lee and Kim, 2011). Finally, SIRT1 knockdown increases the basal expression of MMPs -1 and -3 in human dermal fibroblasts (Ohguchi et al., 2010). The regulation of sirtuins by NAD^+, and their subsequent role in MMP expression in RASFs, has yet to be investigated *in vitro*.

6.1.2 Chapter aims

The constitutive expression of NAMPT in RASFs (Brentano et al., 2007) and its upregulation in response to cytokine stimulation suggest a possible role in cartilage destruction at the articular cartilage-pannus interface. However, it is unclear whether NAMPT exerts its activity directly as a cytokine-like molecule, or indirectly through regulation of intracellular NAD^+. A greater understanding of the regulation of NAMPT in synovial fibroblasts may provide novel insights into mechanisms of RA disease pathogenesis, and help to ascertain a link between NAMPT, intracellular NAD^+ and MMP expression. Therefore, using human RASFs, the specific objectives of this chapter were:

- To determine the effect of pro-inflammatory cytokines on iNAMPT gene expression *in vitro.*
- To study the expression of alternative, rate-limiting, NAD^+ biosynthetic pathway enzymes in response to pro-inflammatory cytokine stimulation.
- To investigate the effect of the cytokines IL-1β, TNFα and OSM on expression of MMPs -1 and -3.
- To measure the expression of NAD^+ dependent deacetylase SIRT1.
- To evaluate the effect of sirtuin and PARP antagonists on cytokine-mediated MMP protein expression.

6.2 Materials and methods

Human RASFs were extracted and cultured as detailed in section 2.1.2.2. Cells were seeded onto 12-well plates ($3x10^4$ cells/ml). Cells were serum-starved for 48 hours prior to stimulation assays. Stimulations were then performed as described below. The media was removed and 1 ml of TRI-Reagent® then added to cells. RNA was extracted and qPCR performed as outlined in section 2.3.2.

6.2.1 Cytokine dose response

A dose response of the pro-inflammatory cytokines IL-1β, TNFα and OSM was carried out to determine the concentration required to induce NAMPT gene expression in RASF cell lines. Cytokine solutions (up to 20 ng/ml) were freshly prepared in serum-free medium, they were added to RASFs that had been serum-starved for 48 hours in advance of stimulation. Control wells contained RASF incubated in serum-free medium only. Experiments ended 6 hours post-stimulation when RASF were homogenised with TRI Reagent®.

6.2.2 Cytokine time course

A short-term time course assay was performed to determine the timing of gene expression of NAMPT and other genes of interest. RASFs were incubated for up to 6 hours with cytokine solutions (1 ng/ml of IL-1β, TNFα or OSM) prepared with serum-free medium. Cytokine stimulations were run in parallel on the same RASF cell line. At endpoint medium was aspirated and stored and TRI Reagent added to the cells in each well. A zero hour control was made by washing serum-starved unstimulated cells with PBS and adding TRI Reagent® immediately.

6.2.3 NAD^+ depletion assay

As iNAMPT is a rate-limiting NAD^+ enzyme (Revollo et al., 2004), the effect of iNAMPT inhibition on intracellular NAD^+ levels in RASFs was determined using both in-house and commercially-available NAD^+ detection assays (section 2.1.4). RASFs were seeded into T25 tissue culture flasks at a cell density of $2x10^5$ cells/ml in complete tissue culture medium containing 10% FBS. Cells were left to settle for 48 hours, or until cells appeared to have entered the exponential phase of growth. This was estimated from observations using an inverted microscope. Cells were then washed in PBS and treated with culture medium supplemented with 5% FBS (serum was maintained to keep cells in exponential growth) and 10 nM APO866. Flasks were cultured for 0, 24, 48 and 72 hours. At the end of the designated culture periods, culture supernatants were collected for analysis of cell viability (section 2.1.6.2) and cells were extracted for NAD^+ quantification (refer to section 2.1.4).

6.2.4 Sirtuin and PARP antagonist assay

Serum-starved RASF were stimulated for periods of 6, 24, and 48 hours in the presence of 10 ng/ml IL-1β alone, or in combination with either 100 μM EX557 or 100 μM PJ34 (Sigma-Aldrich Ltd, Dorset, UK), specific inhibitors of SIRT1 and PARP-1, respectively. Serum-starved cells were pre-incubated with the inhibitors for one hour prior to cytokine stimulation. At the end of the stimulation periods, cell culture supernatants were transferred to 2 ml microcentrifuge tubes and stored at -70°C for analysis by MMP-1 and MMP-3 protein levels by ELISA, as described in section 2.1.3.

6.3 Results

6.3.1 NAMPT is upregulated by inflammatory cytokines in RASFs

In the first experiment, a dose response was performed on three RASF lines, to determine if NAMPT gene expression could be induced by cytokine stimulation. RASFs were stimulated with escalating doses of IL-1β, TNFα or OSM (section 6.2.1) and NAMPT mRNA expression analysed by qPCR. IL-1β was the most potent inducer of NAMPT expression, with doses of 20 ng/ml resulting in a mean 30-fold increase in gene expression compared to untreated control cells cultured for the same period of time (figure 6.3.1A). However, there was great variability in the data, meaning there was no overall significant difference between IL-1β treatment groups, as determined by Kruskal-Wallis analyses (P=0.225). NAMPT expression increased in a concentration-dependent manner upon addition of TNFα, and Kruskal Wallis analyses indicated a significant difference between treatment groups (P=0.043).Maximum upregulation was apparent in cells stimulated with 5 ng/ml of TNFα (figure 6.3.1B). OSM caused a small (but non-significant) dose-dependent increase in NAMPT expression that reached its maximum level at 10 ng/ml (P=0.139, figure 6.3.1C).

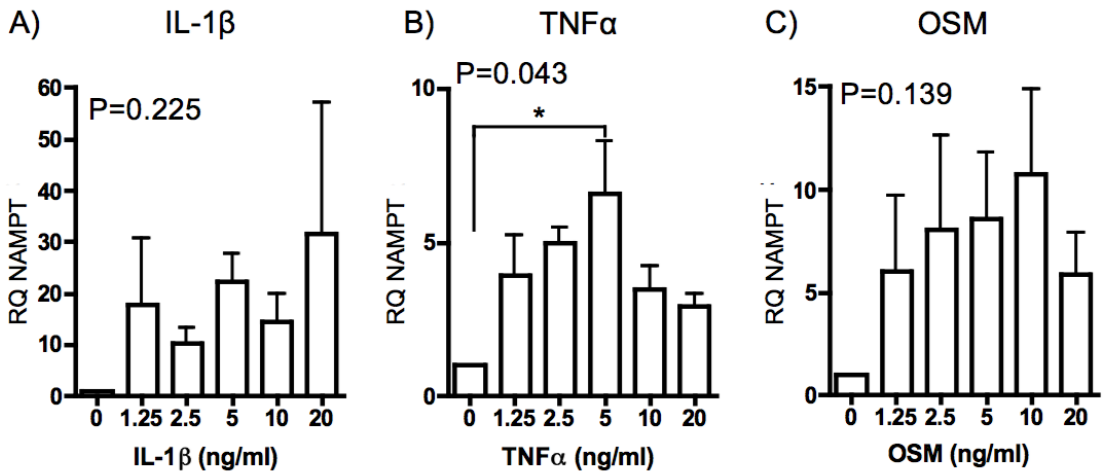

Figure 6.3.1. Dose effect of pro-inflammatory cytokines on NAMPT gene expression

Human RASFs (n=3 cell lines, with one biological replicate per condition) were washed and stimulated for 6 hours with varying doses of pro-inflammatory cytokines A) IL-1β, B) TNFα and C) OSM. RNA was extracted from cells, reverse-transcribed and analysed in duplicate for NAMPT expression using real-time quantitative PCR. The ΔC_T values for cytokine-stimulated samples were determined and normalised to the C_T values of reference genes 18S rRNA, Beta-Actin and GAPDH. The relative quantities of NAMPT gene expression (RQ) were determined by relating ΔC_T values of cytokine-stimulated samples to unstimulated control cell samples. All error bars depict the standard error of the mean (S.E.M). Kruskal-Wallis tests with Dunn's multiple comparison post-test analyses were performed to determine the significance levels between treatment groups. *=P≤0.05

NAMPT was induced by all three cytokines assayed, with induction at the lowest concentration of 1.25 ng/ml. A concentration of 1 ng/ml was used in the following experiment to determine the timing of NAMPT gene expression in RASFs from 0-6 hours post-stimulation. All cytokines had a stimulatory effect on NAMPT gene expression, within one hour of cytokine stimulation (figure 6.3.2). Stimulation of cells with IL-1β resulted in a significant upregulation of NAMPT expression at 4 and 6 hours post stimulation (P=0.024; figure 6.3.2A). Although TNFα elevated NAMPT expression, there was no overall significant difference between treatment groups (P=0.253; figure 6.3.2B). Like IL-1β, OSM stimulation resulted in a significant upregulation of NAMPT expression at 4 and 6 hour time points, with a significant difference in expression between treatment groups overall (P=0.018; figure 6.3.2C).

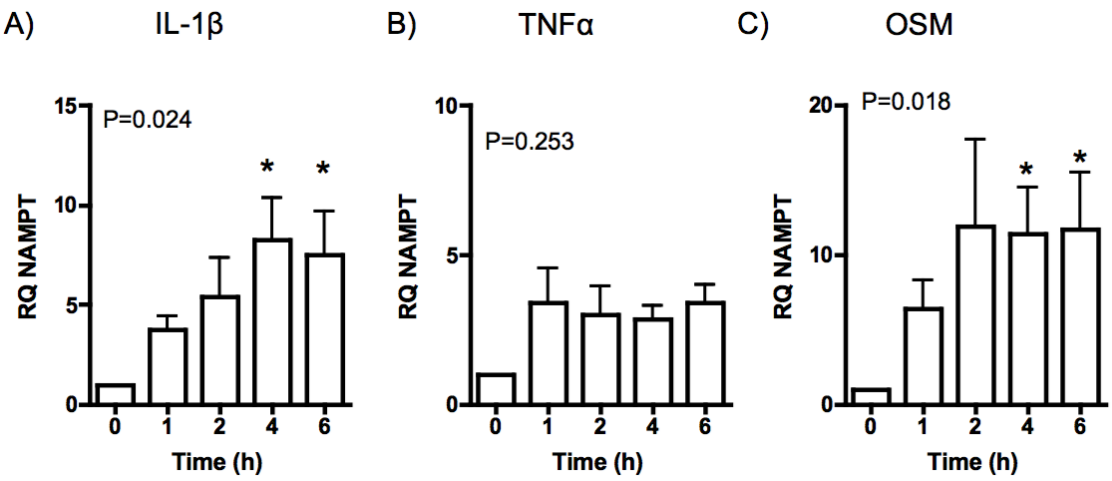

Figure 6.3.2 Cytokine-induced NAMPT gene expression over time in RASFs

Human RASFs (n=5 cell lines, one biological replicate per cell line) were stimulated for 0-6 hours with 1 ng/ml of cytokines A) IL-1β, B) TNFα and C) OSM and analysed in duplicate for NAMPT gene expression by qPCR. The ΔC_T values for cytokine-stimulated samples were normalised to the C_T values of reference genes 18S rRNA, Beta-Actin and GAPDH. The relative quantity of NAMPT gene expression (RQ) in treated cells was compared to zero hour unstimulated control cells. All error bars depict the standard error of the mean (S.E.M). Kruskal-Wallis tests with Dunn's multiple comparison post-test analyses were performed to determine the significance levels between treatment groups. *=P≤0.05.

6.3.2 Regulation of alternative NAD^+ enzymes by inflammatory cytokines

In the previous chapter, it was shown that IL-1β induces iNAMPT expression in chondrocytes, but does not affect expression of NAPRT and QPRT, enzymes involved in alternative NAD^+ pathways (section 5.3.1). In this chapter, expression of these genes in response to cytokine stimulation was explored in RASFs. Expression IDO was also analysed by qPCR. Like QPRT, IDO is a rate-limiting enzyme in the *de novo* NAD^+ biosynthesis pathway (Iqbal and Zaidi, 2006).

Over a culture period of 6 hours, all three cytokines failed to induce expression of Preiss-Handler pathway gene NAPRT (P=0.598, P=0.144 and P=0.884; IL-1β, TNFα and OSM, respectively; figure 6.3.3). As with NAPRT, expression of QPRT was not significantly affected by cytokine stimulation, as determined by Kruskal Wallis One way ANOVA (P=0.185, P=0.288 and P=0.554; IL-1β, TNFα and OSM, respectively; figure 6.3.4A-C). However, expression was slightly enhanced compared with samples from medium control (0h) cells IDO expression was also not affected by the addition of IL-1β (P=0.623; figure 6.3.4D) or TNFα (P=0.394; figure 6.3.4E). There was no significant difference between OSM treatment groups (P=0.078); however, Dunn's multiple comparison post-tests showed that IDO expression is significantly induced at 6 hours post-stimulation, compared with the zero hour control (figure 6.3.4E). This implies that IDO is induced by OSM stimulation in a time-dependent manner in human RASFs.

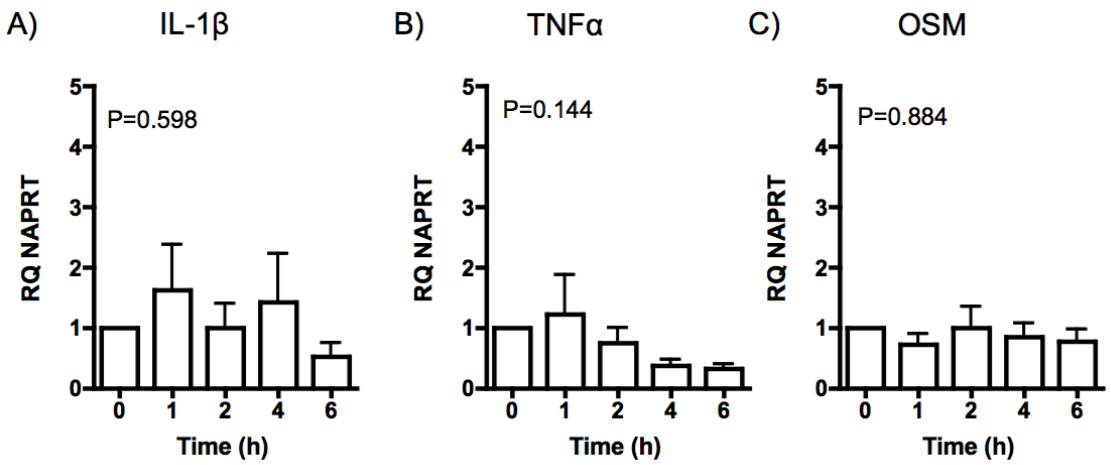

Figure 6.3.3 Effect of cytokine stimulation on regulation of Preiss-Handler NAD^+ pathway gene expression

Human RASFs (n=5 cell lines, one biological replicate per time point) were stimulated for 0-6 hours with 1 ng/ml of cytokines A) IL-1β, B) TNFα or C) OSM. Samples were plated in duplicate and analysed by real-time qPCR for NAPRT, gene expression. The ΔC_T values for cytokine-stimulated samples were normalised to the C_T values of reference genes 18S rRNA, Beta-Actin and GAPDH. The relative quantity of NAPRT gene expression (RQ) in treated cells was compared to zero hour unstimulated control cells. All error bars depict the standard error of the mean (S.E.M). Kruskal-Wallis tests with Dunn's multiple comparison post-test analyses were performed to determine the significance levels between treatment groups.

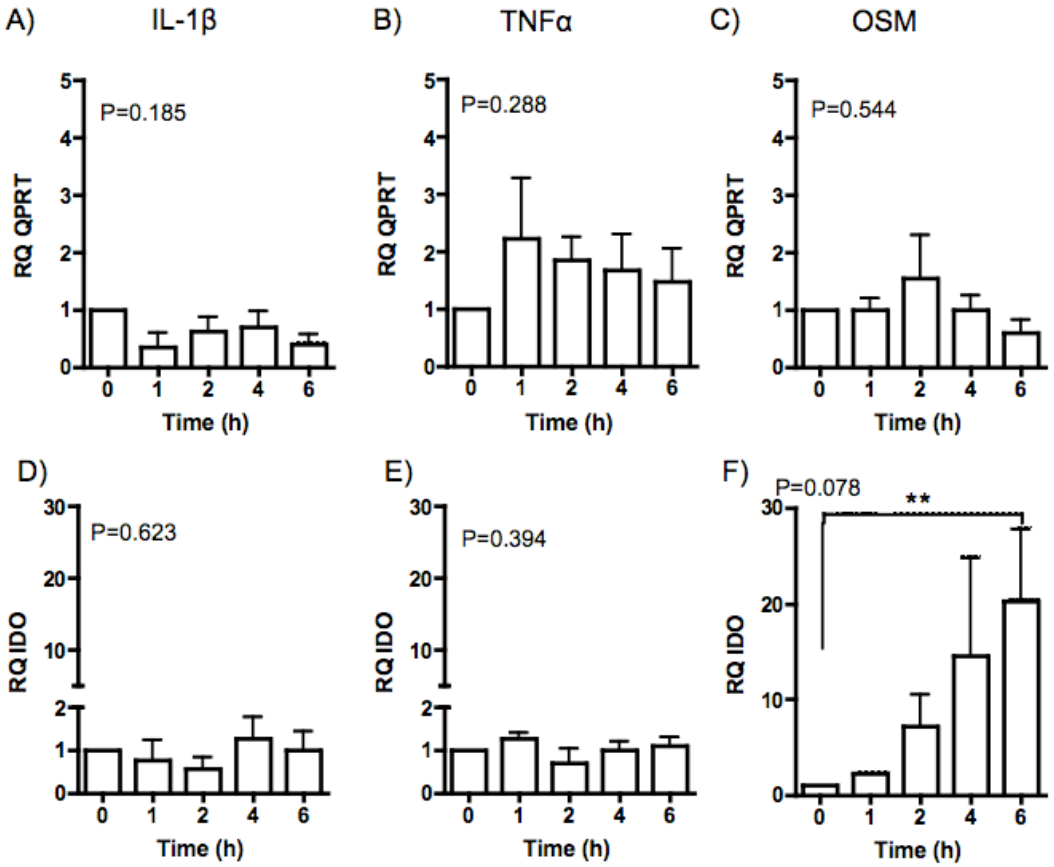

Figure 6.3.4 Effect of cytokine stimulation on regulation of *de novo* NAD$^+$ pathway gene expression

Human RASFs (n=5 cell lines, one biological replicate per time point) were stimulated for 0-6 hours with 1 ng/ml of cytokines IL-1β, TNFα or OSM. Samples were analysed in duplicate by real-time qPCR for QPRT and IDO gene expression. The ΔC_T values for cytokine-stimulated samples were normalised to the C_T values of reference genes 18S rRNA, Beta-Actin and UBC. The relative quantities of QPRT and IDO gene expression (RQ) in treated cells were compared to zero hour unstimulated control cells. All error bars depict the standard error of the mean (S.E.M). Kruskal-Wallis tests with Dunn's multiple comparison post-test analyses were performed to determine the significance levels between treatment groups. **=P≤0.01.

6.3.5 MMP-1 and MMP-3 are upregulated by IL-1 β in RASFs

Expression of MMPs -1 and -3 in response to cytokine stimulation was also analysed. In contrast to NAMPT gene expression (figure 6.3.2), MMP gene expression was generally induced at later time points (4 hours post-stimulation). IL-1β caused an overall significant induction of MMP-1 gene expression compared to the zero hour control, as determined by Kruskal-Wallis tests (P=0.049). In particular, MMP-1 expression was significantly enhanced at 6 hours post stimulation compared with the unstimulated control (figure 6.3.5A). MMP-1 expression appeared enhanced in TNFα treated RASFs; however, there was no significant difference in RQ values between time points (P=0.08; figure 6.3.5B). Despite being a strong inducer of NAMPT, OSM had a comparably minimal effect on MMP-1 expression over time (P=0.69; figure 6.3.5C), with RQ values comparable to unstimulated (zero hour) control samples. MMP-3 was significantly induced by IL-1β stimulation in RASFs in a time-dependent manner (P=0.046; figure 6.3.5D). TNFα induced MMP-3 gene expression in two of the three cell lines, but due to the variability observed between the groups, there was no overall effect on MMP-3 expression by this cytokine (P=0.175; figure 6.3.5E). As with MMP-1, OSM had no stimulatory effect on MMP-3 gene expression (P=0.095; figure 6.3.5F).

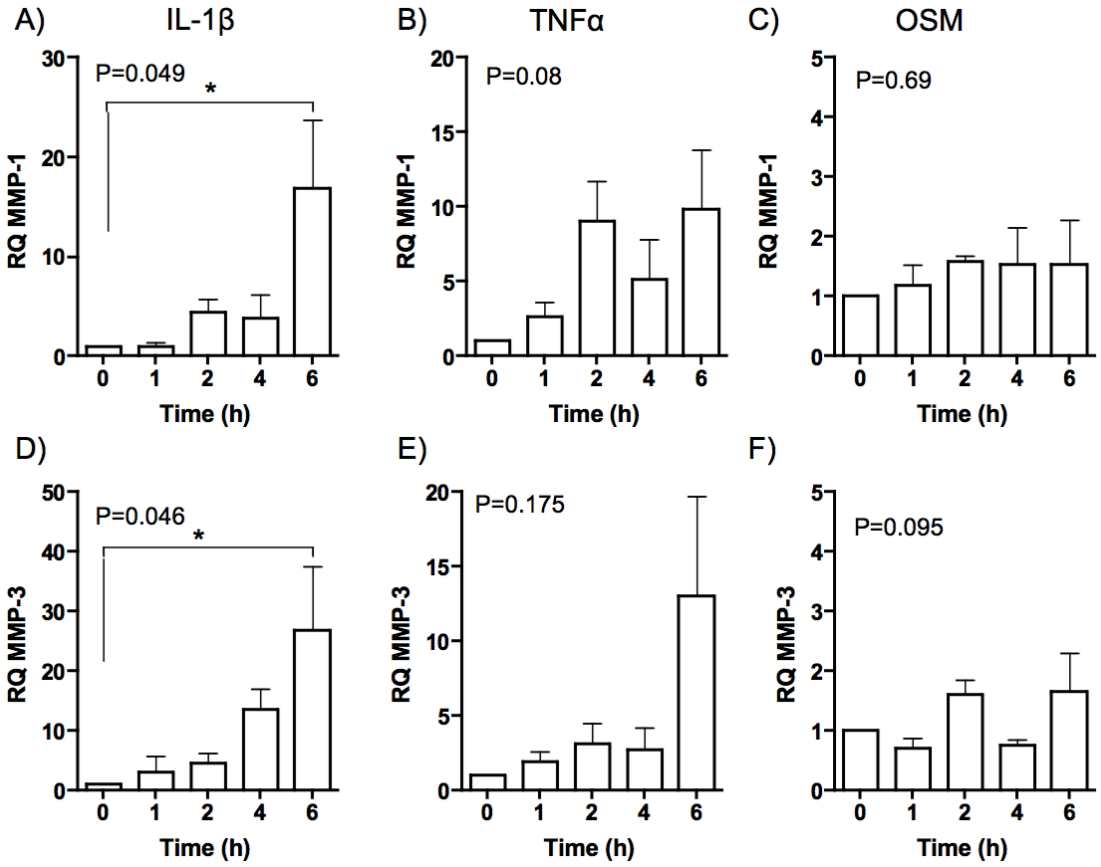

Figure 6.3.5 The effect of pro-inflammatory cytokines on MMP gene expression

Human RASFs (n=3 cell lines, one biological replicate per time point) were assayed for MMP-1 and MMP-3 gene expression in response to stimulation with 1 ng/ml of cytokines A) IL-1β, B) TNFα and C) OSM. MMP-3 gene expression was also monitored in response to D) IL-1β, E) TNFα and D) OSM. The ΔC_T values for cytokine-stimulated samples were normalised to the C_T values of reference genes 18S rRNA, Beta-Actin and GAPDH. . The relative quantities of MMP gene expression (RQ) in treated cells were analysed in duplicate using real-time quantitative PCR, compared to washed zero hour unstimulated control cells. All data points are graphically presented with mean ± standard error of the mean (S.E.M). Kruskal-Wallis tests with Dunn's multiple comparison post-test analyses were performed to determine the significance levels between treatment groups. *=P≤0.05.

6.3.6 In-house NAD^+ assay lacks sensitivity

In order to confirm a role for iNAMPT in NAD^+ metabolism in RASFs, resting (unstimulated) cells were cultured for up to 72 hours in the presence of 10 nM APO866, and intracellular NAD^+ levels determined. Cells were cultured in complete medium and extracted at the point of established growth. Initially, an in-house NAD^+ assay was developed, and cell extracts from untreated human RASFs were prepared as in section 2.1.4.1 and tested. The addition of the cycling buffer led to a rapid colorimetric change; however, the colour of the test samples differed greatly from the standards, yielding a reddish-brown colour instead of the expected purple colour of the top standards (figure 6.3.6A). The optical density (OD) values of NAD^+ standard did not conform to standard linear or polynomial curves, therefore a standard curve was generated using a Michaelis-Menton nonlinear regression and unknown test values were interpolated from the curve (figure 6.3.6B). From five of the six values initially tested, the mean value of NAD^+ detected was 12.7 ± 0.71 µg/ml. However, one cell source contained a higher level of NAD^+ (26.3 ± 1.53 µg/ml), despite an identical extraction procedure (figure 6.3.6C). The assay was repeated on samples from cells treated with 10 ng/ml IL-1β, 10 nM APO866, or a combination of both (section 6.2.3). Samples were extracted from proliferating cells at 24 and 48 hours post-stimulation. The purpose of this assay was to determine if APO866 could reduce cellular NAD^+, and to find out if NAD^+ depletion was more marked in activated cells. Although NAD^+ appeared to be detected at both time points (figure 6.3.7), the assay lacked the sensitivity and reproducibility required to accurately quantify differences over time. Therefore, a commercial NAD^+ assay was used in further studies.

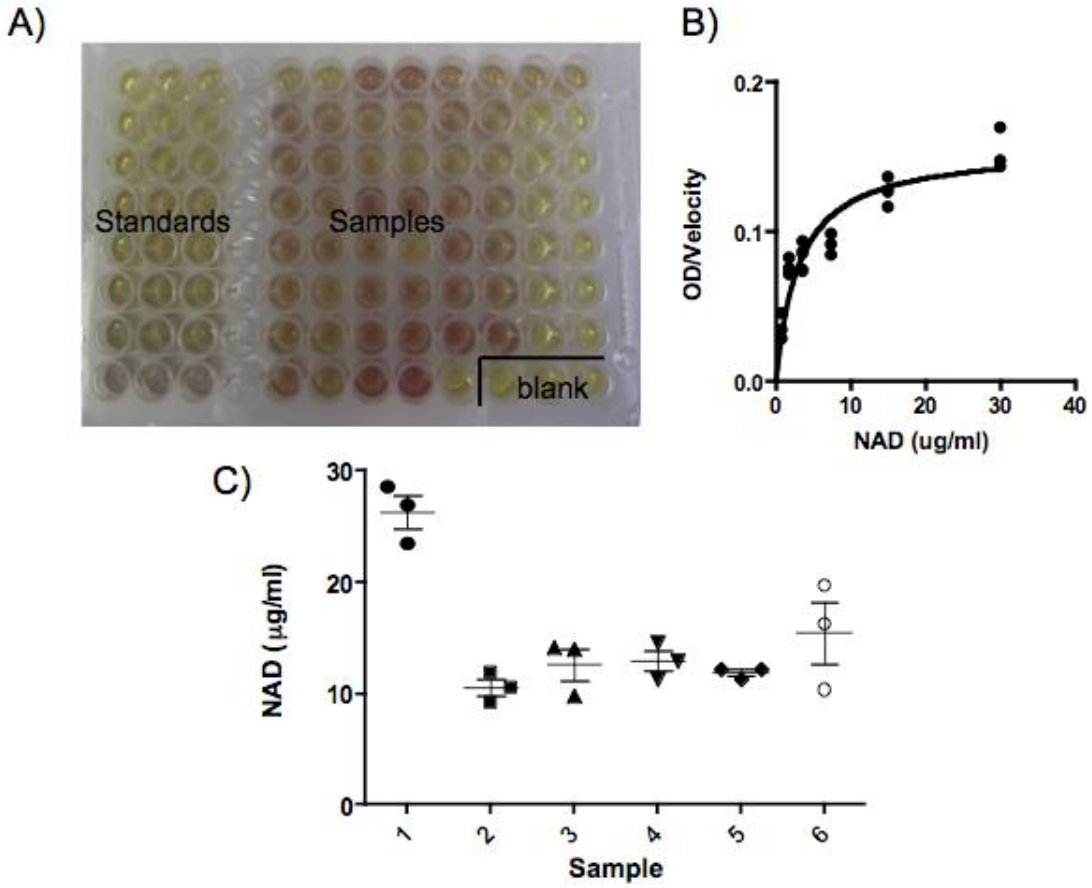

Figure 6.3.6 Testing and optimisation of in-house NAD$^+$ assay

Cell extracts from actively proliferating human RASFs (one cell line with six experimental replicates) were prepared and tested for levels of intracellular NAD$^+$ (section 2.1.4.1). Samples were plated in duplicate alongside a NAD$^+$ standard of known concentrations ranging from 0.9375-30 µg/ml, and a cycling buffer was added, resulting in a colourimetric change. A) Typical plate layout, showing the serially diluted NAD$^+$ standard and samples. B) A Michaelis-Menton standard curve, showing OD readings of samples in triplicate. C) The NAD$^+$ levels of the six individual samples, in triplicate. The mean ± standard error of the mean (S.E.M) of individual replicates are plotted.

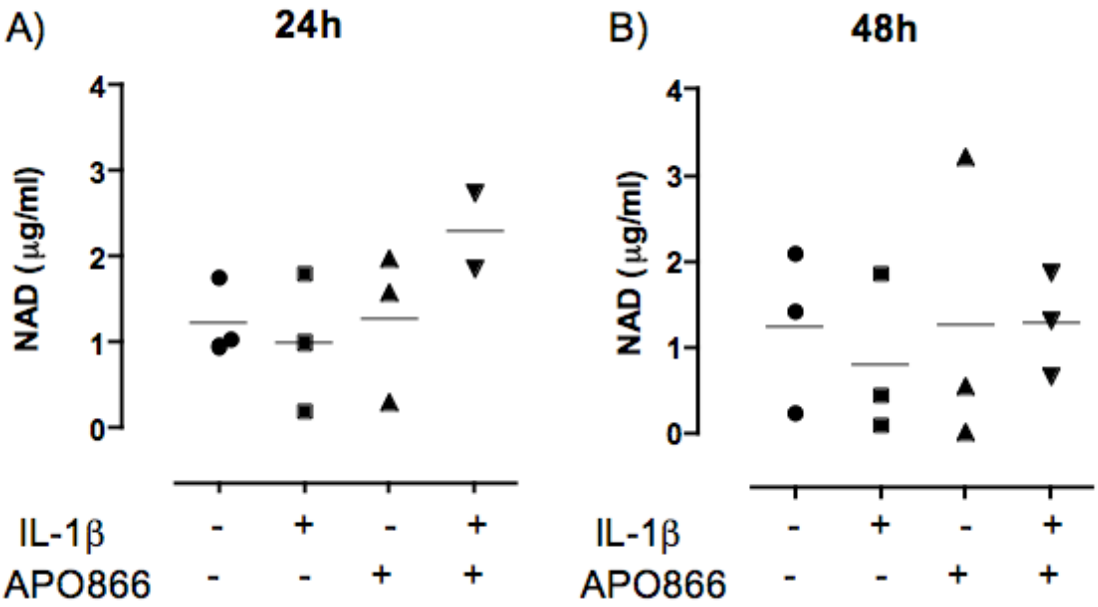

Figure 6.3.7 Detection of NAD^+ in treated samples using the in-house assay

Human RASFs (n=3 cell lines, one biological replicate per condition) were stimulated with a combination of 10 ng/ml IL-1β and 10 nM APO866 (section 2.2.3), and cells taken from A) 24 and B) 48 hours post-stimulation were prepared for analysis of intracellular NAD^+ (section 2.1.4.1). All data points are graphically presented with mean ± standard error of the mean (S.E.M).

6.3.7 APO866 reduces cellular NAD^+ over time in RASFs

Using a commercial NAD/NADH assay (section 2.1.4.2), cells extracted at zero hour with no APO866 treatment had the highest levels of total NAD (NADt; i.e. NADH and NAD^+) with a mean value of 10.9 pmol/10^6 cells (figure 6.3.8). Although the assay is capable of discerning between NAD+ and NADH (section 2.1.4.2), NAD^+ itself could not be accurately quantified; so only NADt data are presented (figure 6.3.8). The zero hour sample yielded a NADt value of 10.91 ± 1.58 pmol/10^6 cells, which was only just within the detection range of the assay. This suggests that the assay used lacks the sensitivity required in order to accurately quantify lower NADt values. However, APO866 treatment caused a significant time-dependent decrease in NADt levels in cell extracts over time, as determined by Pearson's correlation coefficient analysis (P=0.0012; Figure 6.3.8A). By 72 hours, cell extracts had no detectable NADt, with OD values comparable to the negative (blank) control. Culture supernatants were analysed for LDH release, and it was shown that LDH release was significantly increased over time, peaking at an average of 11.89 ± 2.18 of the percentage maximum of LDH release (P=0.012, figure 6.3.8B). This suggests a depletion in cellular NAD^+ levels is causing a detrimental effect on cell viability.

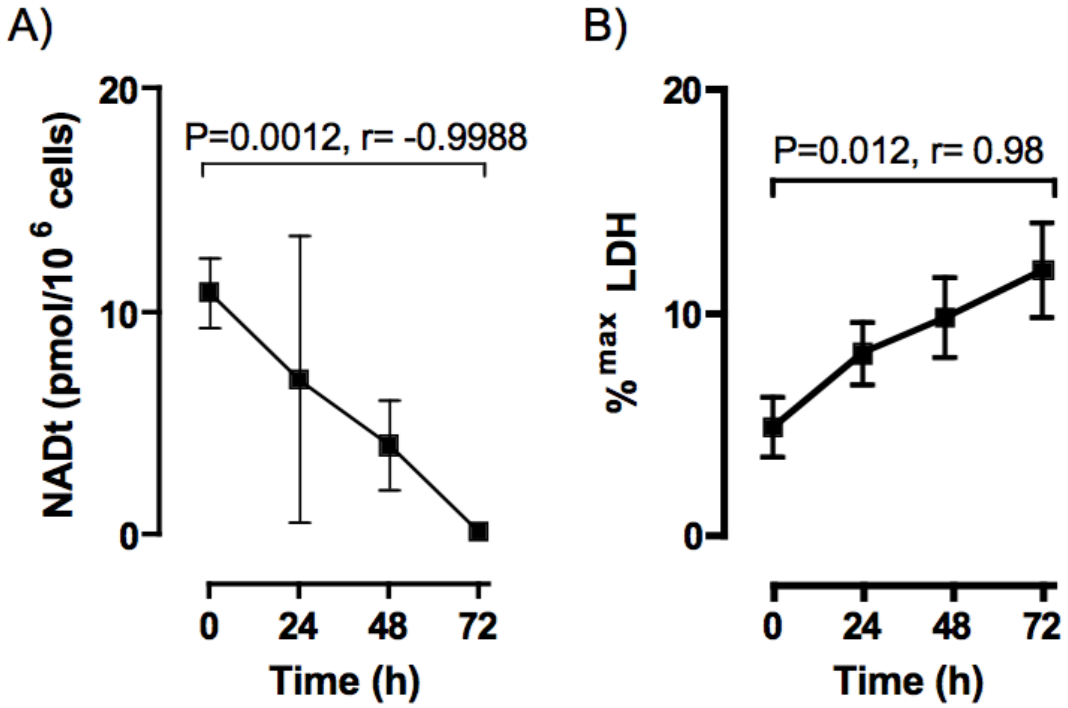

Figure 6.3.8 Effect of APO866 on intracellular NAD^+ and cell viability

Human RASFs (n=3 cell lines, one experimental replicate per time point) in log phase growth were treated with 10 nM APO866, scraped and assayed in duplicate for intracellular NADt (total NAD and NADH). A) NADt levels quantified and normalised to cell number. Pearson's correlation coefficient was used to determine the effect of APO866 treatment duration on NADt levels. All data points are graphically presented with mean ± standard error of the mean (S.E.M). B) Cell culture supernatants (n=3 cell lines) were analysed for LDH release. Fluorescence intensity values (in relative fluorescent units) were normalised to a maximum LDH release control sample, and are presented as percentage maximum LDH release in a cumulative plot.

6.3.8 SIRT1 is not induced by cytokine stimulation in RASFs

Expression of the NAD^+-dependent deacetylase SIRT1 was also studied in response to cytokine stimulation. Stimulation with IL-1β caused a slight but non-significant induction of SIRT1 gene expression in RASFs (P=0.099; figure 6.3.9A). TNFα enhanced SIRT1 expression, peaking at 2 hours post-induction. However, there was no overall significant effect on SIRT1 expression (P=0.483; figure 6.3.9B). The IL-6 family cytokine OSM failed to induce SIRT1 expression in RASFs (P=0.47, figure 6.3.9C). SIRT expression was induced in two of the three cell lines used, resulting in considerable variability. Therefore, further observations may be required to confirm whether or not IL-1β and TNFα enhance SIRT1 expression.

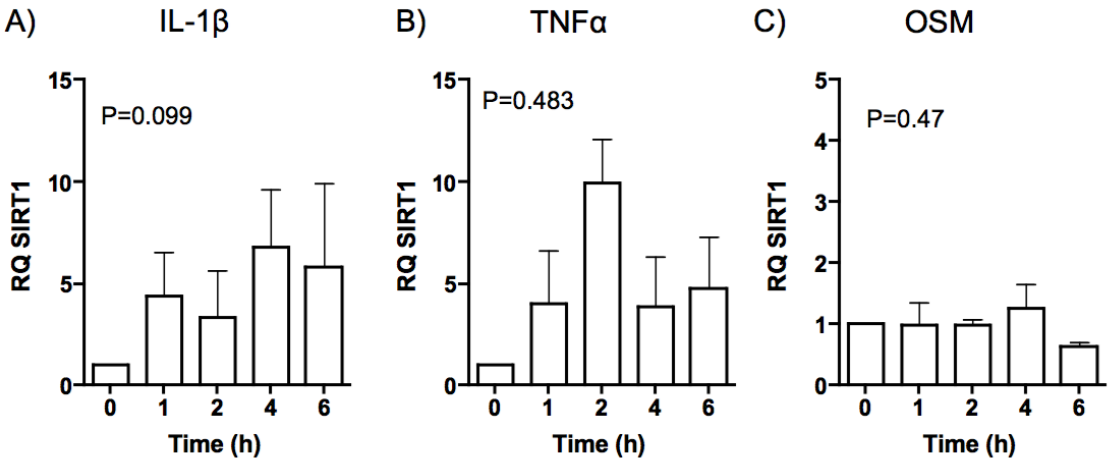

Figure 6.3.9 Cytokine-mediated expression of SIRT1 in RASFs

Human RASFs (n=3 cell lines, one biological replicate per time point) stimulated for 0-6 hours with 1 ng/ml of cytokines A) IL-1β, B) TNFα and C) OSM were analysed for SIRT1 gene expression by qPCR. The relative quantity of SIRT1 gene expression (RQ) in treated cells was compared to washed zero hour unstimulated control cells. The ΔC_T values for cytokine-stimulated samples were normalised to the C_T values of reference gene Beta-Actin. Pearson's correlation coefficient was performed to determine whether stimulation time was related to the relative quantity of SIRT1 mRNA. All data points are graphically presented with mean ± standard error of the mean (S.E.M).

6.3.9 Sirtuin inhibition enhanced IL-1 β induced MMP protein release

As RASFs stimulated with IL-1β for 6 hours showed a time-dependent increase in gene expression of NAMPT (figure 6.3.1), as well as both MMP-1 and MMP-3 (figure 6.3.5), it was investigated how the induction of NAMPT may indirectly affect downstream expression of MMPs. Through the activity of NAD^+ dependent cofactors (such as sirtuins). RASFs were stimulated with IL-1β alone or in combination with EX527 and PJ34, inhibitors of SIRT1 and PARP-1, respectively (section 6.2.4) IL-1β stimulation caused an upregulation of both MMP-1 (figure 6.3.10A) and MMP-3 (figure 6.3.10B) over time, although induction of the latter was less marked. Co-incubation with the SIRT1 inhibitor (EX527) caused a significant induction of MMP-1 protein levels compared with IL-1β alone (figure 6.3.10A). In contrast, the addition of PARP-1 inhibitor PJ34 did not affect IL-1β induced MMP-1 release. Interestingly, EX527 did not significantly enhance IL-1-β MMP-3 release (figure 6.3.10B).

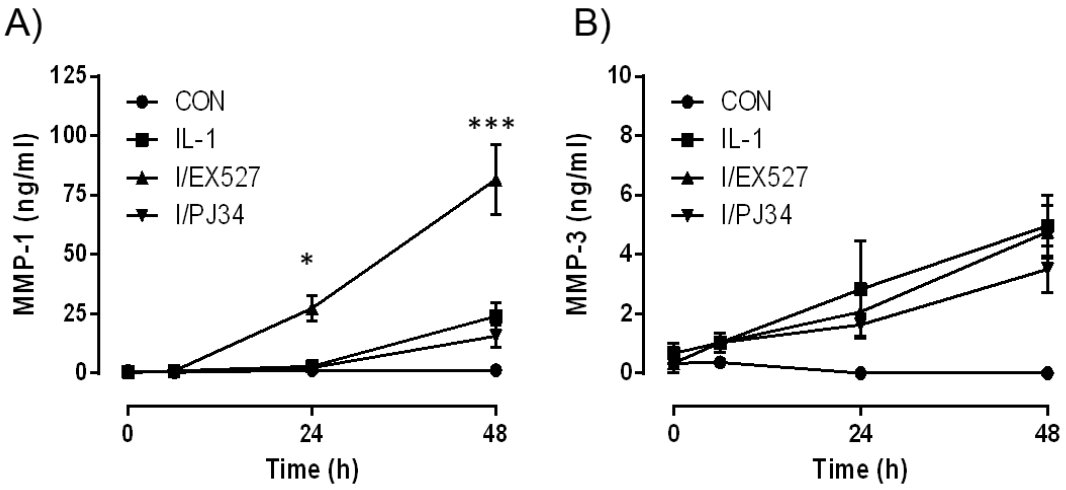

Figure 6.3.10 Effect of SIRT1 and PARP-1 antagonists on IL-1β induced MMP release

Human RASFs (n=3 cell lines) were cultured from 0-48 hours in the presence of 10 ng/ml IL-1β (IL-1), alone or100 μM EX527 (I/EX527) or PJ34 (I/PJ34). Culture supernatants were analysed for A) MMP-1 and B) MMP-3 protein levels by ELISA. Differences in MMP levels between treatment groups were determined by two-way ANOVA with Bonferroni post-tests. *=P≤0.05, ***=P≤0.001.

6.4 Discussion

Although circulating lymphocytes are thought to be a major source of NAMPT in conditions such as obesity (Friebe et al., 2011), NAMPT is also localised to the fibroblast-like synoviocytes within the intimal lining in both experimental arthritis models (Nowell et al., 2006) and in patients with RA (Brentano et al., 2007). This chapter explored the regulation of NAMPT gene expression in RASFs activated by pro-inflammatory cytokines. In addition to this, inhibitors of NAD dependent cofactors were used to determine how the rate-limiting role of NAMPT in NAD^+ biosynthesis might impact on the regulation and secretion of degradative MMPs by RASFs.

6.4.1 NAMPT is upregulated by inflammatory cytokines in RASFs

Firstly, the effect of pro-inflammatory cytokine stimulation on NAMPT gene expression was determined. NAMPT was strongly induced by the range of cytokines tested, supporting previous findings in RASFs (Nowell et al., 2006, Brentano et al., 2007). The cytokines IL-1β and TNFα are both potent inducers of NF-κB, a pivotal regulator of inflammation in RA (Firestein et al., 2009). In contrast, OSM operates mainly (although not exclusively) through the Janus kinase (JAK)/STAT signaling pathway (Kishimoto et al., 1995). The NAMPT gene promoters (both proximal and distal) are response-element rich, containing both NF-κB (Ognjanovic et al., 2001) and STAT (signal transducer and activator of transcription) (Nowell et al., 2006) binding sites, which facilitate rapid induction (summarised in section 1.3.3). The dampening effect of higher concentrations on NAMPT expression suggests control by a negative feedback mechanism. The possibility of a cytotoxic effect at these higher concentrations was ruled out, as samples were normalised prior to amplification by qPCR, to ensure they all contained equal amounts of cDNA; therefore, any differences in RQ value can be attributed to changes in levels of gene expression.

6.4.2 Alternative NAD^+ enzymes are not regulated by inflammatory cytokines

These data have demonstrated the specific and preferential induction of NAMPT above all other rate-limiting NAD^+ biosynthesis enzymes in RASFs stimulated with IL-1β, TNFα and OSM. This relates to previous findings by Iqbal and colleagues (2006), who showed that TNFα causes a time-dependent increase in NAMPT and IDO, but not QPRT, gene expression in murine macrophages (NAPRT expression was not analysed) (Iqbal and Zaidi, 2006). In contrast to these findings, the studies in this current chapter failed to detect upregulation of IDO in response to TNFα stimulation. A possible explanation is that the tryptophan biosynthesis pathway may be less predominant in RASFs compared with macrophages. IDO expression is strongly induced by Interferon gamma (IFNγ)

(Yang et al., 2010). The effect of IFNγ on the expression of NAD^+ enzymes was not investigated in this chapter; however, IFNγ is present at low levels in the synovial tissue of RA patients compared to patients with other forms of arthritis, and is undetectable in RA synovial fluid (Firestein and Zvaifler, 1987). Therefore, the tryptophan biosynthesis pathway is unlikely to contribute significantly to NAD^+ biosynthesis in RASFs stimulated with RA-associated cytokines such as IL-1β and TNFα. To my knowledge, the generation of NAD^+ via the Preiss-Handler pathway has yet to be explored in active synoviocytes. However, our group has shown that compared with NAMPT, NAPRT is expressed at very low levels in RA tissue (Moideen and Nowell; unpublished), suggesting that activated cells may not readily utilise nicotinic acid. Taken together, these data suggest that the Nam salvage pathway is the predominant pathway for generation of NAD^+ in activated RASFs.

6.4.3 IL-1β and TNFα (but not OSM) upregulate MMP-1 and -3 gene expression

IL-1β and TNFα both induced a time-dependent increase in MMP-1 and MMP-3 gene expression. The stimulatory effect of these cytokines on MMP expression in RASFs has been reported in numerous studies (Langdon et al., 1997, Brentano et al., 2007, Niederer et al., 2011). NAMPT expression appeared to preclude the induction of MMPs, with almost immediate upregulation in response to cytokine stimulation. These data originally suggested that induction of NAMPT might somehow contribute to a subsequent induction of MMP gene expression. However, this was contradicted with the results of OSM stimulation. Despite being a strong inducer of NAMPT expression, OSM failed to induce expression of MMPs -1 and -3. This suggests that iNAMPT may not be directly involved in the induction of MMPs in RASFs.

6.4.4 Activated cells have an increased requirement for NAD^+

In inflammatory arthritis, synovial fibroblasts switch from normal mesenchymal cells to an aggressive rapidly proliferating phenotype (Müller-Ladner et al., 2007). Studies in mice with glucose-6-phosphate isomerase (G6PI)-induced arthritis showed that a metabolic tracer named ^{18}F labelled fluorodeoxyglucose (^{18}F-FDG) is rapidly taken up by activated cells compared with non-activated cells, as determined by positron emission tomography-computed tomography (PET/CT) (Irmler et al., 2010). It stands to reason that an increased metabolic requirement will mean that cells have an increased requirement for NAD^+, as it is an essential cofactor involved in a broad range of biological functions (reviewed by Lin and Guarente, 2003).

The effect of cytokine stimulation on cellular NAD^+ levels appears to vary depending on cell type and cytokine involved. Iqbal and colleagues (2006) found that TNFα stimulation reduced cellular NAD^+ levels in murine macrophages, as upregulation

of NAMPT was concurrent with an upregulation of CD38, a NAD^+-degrading enzyme (Iqbal and Zaidi, 2006). This highlights the complexity of eukaryotic NAD^+ metabolism, further complicated by the cellular changes associated with activation. Unfortunately in this current study NAD^+ could not be detected in cytokine-stimulated cells. Quantifying NAD^+ by enzymatic cycling, although accessible and relatively inexpensive, does not accurately determine the relative ratios of NAD^+ and its reduced form NADH. Furthermore, enzymatic cycling techniques do not tell us the pathways involved in NAD^+ biosynthesis. This information may be obtainable using a high-performance liquid chromatography (HPLC)-based assay (Sporty et al., 2008). It is possible to isotopically label the NAD^+ precursor nicotinamide to quantify NAD^+ synthesised via NAMPT. Such a technique has been successfully applied to yeast (Sporty et al., 2008), and may help determine the differences in NAD^+ salvage pathway synthesis in both resting and activated cells. Despite the limitations of the assay used, APO866 was found to lower intracellular NAD/NADH levels in resting RASFs, reiterating findings from previous groups in a variety of cell types (Hasmann and Schemainda, 2003, Busso et al., 2008, Pittelli et al., 2010).

6.4.5 Sirtuins downregulate MMP expression in RASFs

To determine if NAD^+ biosynthesis impacts upon MMP expression, attention was focused on NAD^+-consuming factors. Various pleiotropic factors which rely on NAD^+ as a substrate have been identified, including ADP-ribose transferases, mono- and poly (ADP-ribose) polymerases, and sirtuins (Pittelli et al., 2010). Of particular interest are the sirtuins, a class of histone deacetylases that consume NAD^+ and play a role in cell longevity and ageing. The sirtuin SIRT1 is constitutively upregulated in RA synovial tissue, and is induced by TNFα in synovial fibroblasts (Niederer et al., 2011). Therefore, it was originally speculated that increased levels of cellular NAD^+ via iNAMPT might somehow positively regulate MMP gene transcription in a sirtuin-dependent manner. To test this hypothesis, EX527, a selective SIRT1 inhibitor, was added to RASFs in conjunction with IL-1β, and MMP protein levels were determined.

The addition of EX527 significantly enhanced MMP-1 protein levels in activated RASFs, suggesting an anti-degradative role for SIRT1. A similar finding has also been reported in human dermal fibroblasts, where SIRT1 inhibition increases basal and IL-1β induced expression of MMP-1 and MMP-3 proteins (Ohguchi et al., 2010). The relatively low induction of SIRT1, compared with NAMPT, in cytokine-activated cells suggests that SIRT1 upregulation may be attributed to increased NAD^+ availability. Induced SIRT1 may inhibit MMP gene expression, possibly through interactions with NF-κB; in lung cancer cell lines, SIRT1 was found to interact with and deacetylate the RelA/p65 subunit of NF-κB, inhibiting its ability to interact with promoter regions of target genes to enhance

transcription (Yeung et al., 2004). Most MMP promoters contain binding sites for a number of transcription factors, including AP-1, STAT, and NF-κB (Yan and Boyd, 2007). The promoter region of MMP-1 contains an NF-κB binding site (Vincenti et al., 1998). Although MMP-3 does not contain a functional NF-κB binding site, it does contain binding sites for other transcription factors that may interact with NF-κB (Yan and Boyd, 2007). Studies in vascular smooth muscle cells have shown that NF-κB activity is essential for upregulation of MMP-1 and -3 (Bond et al., 2001). These data suggest a possible mechanism for SIRT1-mediated inhibition of cytokine-induced MMPs, which could be explored in future work.

PARP-1 is an enzyme that modifies nuclear proteins by poly ADP-ribosylation, and is involved in cellular differentiation and DNA damage recovery (Masutani et al., 2005). The addition of specific PARP-1 inhibitor, PJ34, did not affect IL-1β induced MMP-1 and MMP-3 protein release. This is contrary to previous work, where inhibition has been shown to reduce arthritic symptoms in both mouse (Miesel et al., 1995) and rat (Kroger et al., 1996) models of arthritis. It is worth noting that work by previous groups has been carried out in various cell types/systems, and that NAD^+-dependent deacetylases may exert different regulatory effects depending on stimulus and timing. The matter is also complicated by the fact that there are seven types of sirtuins in mammals, all with differing functions and sub-cellular localisation. An in-depth study into the full effects of NAMPT and sirtuins in RA-derived cells and tissues is beyond the scope of this current study, but may help elucidate the downstream effects of NAD^+ metabolism in inflammation and possibly cartilage metabolism.

6.4.6 Summary

The findings of this chapter concerning the regulation and role of NAMPT in MMP expression are summarised in figure 6.4.1. NAMPT gene expression is upregulated in a time-dependent manner in response to cytokine stimulation in RASFs, and is the only rate-limiting NAD^+ pathway enzyme upregulated by cytokine stimulation, with the exception of IDO upregulation by OSM. This suggests an important role in metabolism in activated cells. MMP gene expression is also upregulated. Finally, the SIRT1 inhibitor EX527 enhances IL-1β mediated MMP-1 protein expression, suggesting an anti-degradative role for sirtuins such as SIRT1.

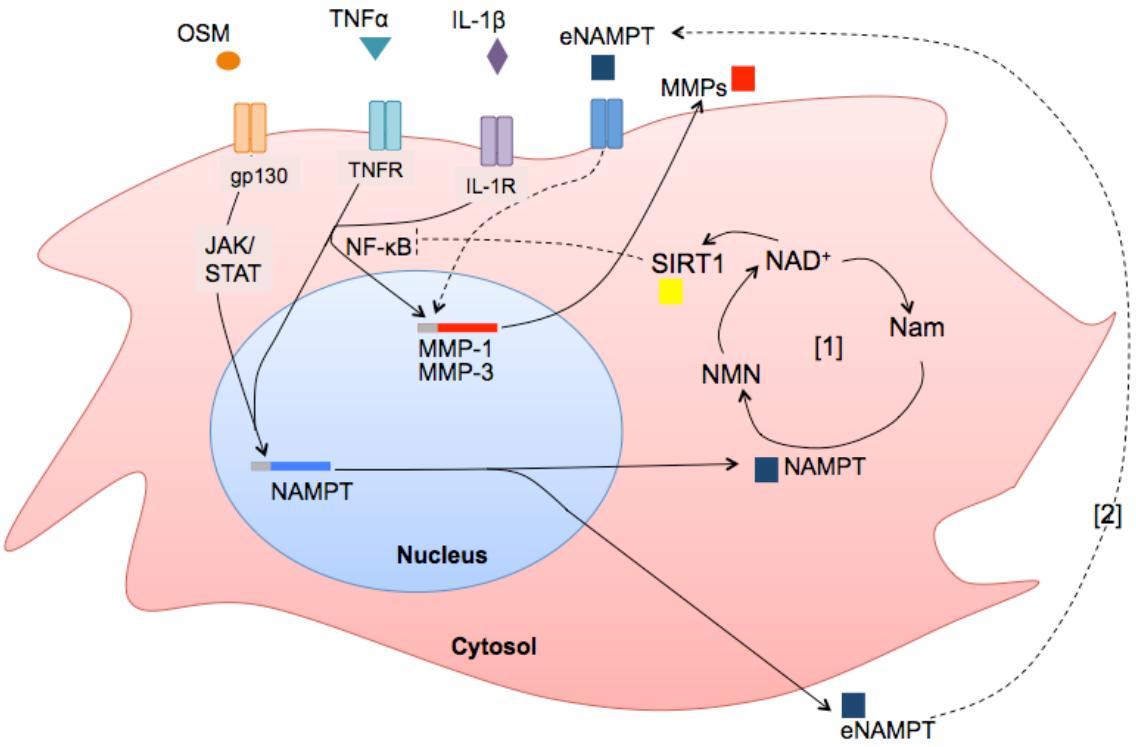

Figure 6.4.1 The regulation and role of NAMPT in MMP expression *in vitro*

This schematic represents the possible role of NAMPT in RASFs. NAMPT mRNA expression is upregulated by OSM, TNFα and IL-1β. The product of the NAMPT gene has been reported to have a dual activity. It has an enzymatic rate-limiting role in the conversion of Nam to NMN in the Nam salvage NAD^+ biosynthesis pathway **[1]**. Factors such as the protein deacetylase SIRT1 may subsequently consume NAD^+ to exert various effects with the cell **[2]** NAMPT is also thought to be secreted from cells and exert autocrine regulation via an as yet unknown receptor (investigated in chapter 4). IL-1β and TNFα (but not OSM) also induce expression of MMP-1, -3 and the NAD^+ dependent deacetylase SIRT1. SIRT1 may inhibit MMP gene transcription, possibly through interactions with the transcription factor NF-κB. Dashed lines represent possible pathways/interactions.

Chapter 7: General discussion

Previous studies have illustrated that NAMPT is a pleiotropic protein upregulated in inflammatory joint diseases such as RA (Otero et al., 2006, Nowell et al., 2006, Brentano et al., 2007). Busso and colleagues found that inhibition of NAMPT activity with the small-molecule inhibitor APO866 in a murine arthritis model decreased pro-inflammatory cytokine secretion in affected joints (Busso et al., 2008). However, little is known of the role of NAMPT in the underlying processes of cartilage destruction, which are responsible for pain and decreased mobility in RA patients. The studies described in this thesis have attempted to answer some of these questions, by studying the role and regulation of NAMPT in a variety of model systems, from monolayer culture of synovial cells to longitudinal analyses of an animal disease model. These studies further illustrate the importance of NAMPT in cellular metabolism, and how its inhibition provides a promising strategy for treatment of inflammatory arthritis. The findings presented in this thesis confirm that NAMPT has an active role in cartilage destruction, with far reaching implications in health and disease. It is induced in the principle cells involved in the production of pro-inflammatory and pro-degradative factors in arthritis disease pathogenesis, and its inhibition affects MMP expression and release both *in vitro* and *in vivo*.

7.1 eNAMPT may enhance expression of catabolic proteases in vitro

NAMPT not only functions as an intracellular enzyme, but is also actively secreted from cells as an extracellular signalling ligand, eNAMPT. The data presented in chapter 3 demonstrated for the first time that eNAMPT upregulates MMP-3 protein release in a dose-dependent manner, with no significant effects on TIMP-1, thus possibly contributing to an imbalance towards cartilage catabolism in arthritis. These findings also provided further supporting evidence of a signalling role for eNAMPT. Cell stimulations were carried out for 18 hours only, which according to results presented in chapters 6 would be insufficient for APO866 to affect cell viability or reduce intracellular NAD^+ levels. If NAMPT-mediated induction of MMP-3 was solely attributed to its enzymatic role in NAD^+ biosynthesis, then a longer period of incubation with APO866 would be required.

A role for eNAMPT as a cytokine-like molecule was further supported by its ability to induce the release of the chemokines CCL2 and CXCL8. Li and colleagues (2008) provided evidence to suggest that the cytokine-like action of eNAMPT is independent of its enzymatic activity; NAMPT mutants lacking this capability were not impaired in their ability to induce IL-6 in macrophages (Li et al., 2008a). Although many groups suggest that NAMPT functions exclusively through its role in NAD^+ biosynthesis (Yang et al.,

2006, Revollo et al., 2007a), the data presented within this chapter suggest that NAMPT may indeed have dual activity.

7.2 APO866 treatment caused a time and dose-dependent decrease in catabolic proteases in vivo

In chapter 4, a murine arthritis model was used to explore the role of NAMPT in cartilage catabolism *in vivo*. For this purpose, the CIA model was chosen, as this systemic model of disease is the most widely-studied model of RA (Brand et al., 2007). As expected, disease severity increased over time, and cartilage and joint erosions was evident in post-sacrifice analyses of radiological and histological damage. All MMPs analysed by qPCR (MMP-1, -3, -9 and -13) were enhanced in CIA animals compared with naïve controls, confirming that upregulation of MMP gene expression in this model is associated with many pathological features of CIA, including inflammation, cartilage destruction, and bone erosion.

Fluorescent imaging probes have been successfully used to monitor protease activity within the CIA model in previous studies (Wunder et al., 2004). Commercially-available MMP probes are now available which fluoresce upon cleavage by MMP enzymes within tissues, resulting in a signal that can be detected in small animal imaging systems (Kossodo et al., 2010). Therefore, *in vivo* imaging protocols for the longitudinal assessment of MMP enzymatic activity in live mice were explored, using two separate NIRF probes called MMPSense680 and MMPSense750 FAST. These imaging probes were shown to accurately determine both the extent and localisation of MMP activity in the live animal, providing novel insights into the process of cartilage degradation in animal disease models. MMP enzymatic activity (as determined from fluorescence intensity) increased in line with arthritis index scores, indicating their suitability as a marker of inflammation as well as cartilage catabolism. The fluorescent localisation of MMP activity in joints closely matched the areas of inflammatory infiltrate and cartilage erosion in corresponding histological sections. Although both MMP mRNA and protein levels were enhanced in CIA animals, there was a weak correlation between these two variables, suggesting that transcriptional regulation of MMP mRNA is not directly indicative of local MMP activity. Lack of association between these two variables may also be attributed to the low sample sizes (≤10 animals) used in CIA experiments.

A combination of the techniques mentioned above was used to assess the efficacy and bioactivity of APO866 *in vivo.* Busso and colleagues (2008) had previously shown that APO866 administered intraperitoneally (i.p.) twice daily reduced clinical scores in CIA animals in a dose-dependent manner (Busso et al., 2008). Based on these

findings, APO866 was administered to CIA animals with established arthritis as a continuous infusion, and disease was monitored over time.

Treatment with 0.08 mg/kg/h APO866 attenuated disease progression in animals, causing a significant reduction in arthritis index compared to the vehicle controls. APO866-treated animals had significantly lower levels of MMP enzymatic activity (as determined by *in vivo* imaging) compared with vehicle controls, but quantitative PCR analyses revealed that MMP gene expression was not attenuated in these tissues. Similarly, there were no significant effects on cartilage degradation, histology and radiology scores. The lack of observable effects is thought to be attributed to the short duration of the treatment. This is supported by analyses of archived samples (that had been subjected to longer and higher doses of APO866), which confirm that NAMPT has a time and dose-dependent effect on MMP gene expression. These latter results suggest that NAMPT plays an important role in the underlying processes involved in matrix destruction in inflammatory disease. In the short-term APO866 treatment study, NAMPT inhibition did not cause a significant reduction in inflammatory infiltrate and synovial hyperplasia in affected paws of CIA animals. However, related studies performed in our group involving longer treatment regimens at higher dosages have shown an effect on these parameters, and are in concordance with other studies (Busso et al., 2008).

Levels of the anti-collagen antibody IgG2a in plasma did not differ between animals treated with APO866 and those treated with the placebo, suggesting a true therapeutic response as opposed to a lack of antibody response. This is in contrast to anti-TNF receptor treatment, which elicits a therapeutic response in CIA animals by actively lowering levels of Th1 driven IgG2a antibodies (Mukherjee et al., 2003). NAMPT itself is highly induced in Th1/Th17 driven diseases such as RA (Ozgen et al., 2011), which may partly explain how APO866 intervention is so efficacious in the CIA model.

From previous studies, it is apparent that rapidly proliferating synoviocytes and invading/peripheral leukocytes are the main sources of NAMPT in inflammatory arthritis (Nowell et al., 2006, Brentano et al., 2007). MMPSense fluorescence suggests that these cells may also be major sources of MMPs within the joint, as fluorescence was enhanced in areas of the hind foot associated with enhanced levels of synovial infiltrate and exudate, apparent in histological sections. The combined data of this thesis suggest the most abundant MMPs in these tissues are likely to be MMPs -1 and -3. Articular cartilage chondrocytes are likely to be another possible source of MMPs, particularly the gelatinase MMP-9 and the collagenase MMP-13, as all of these MMPs were significantly enhanced in CIA animals. This is supported by previous studies which show evidence of eNAMPT-induced upregulation of MMPs -3 and -13 in murine articular chondrocytes

(Gosset et al., 2008). Studies in chapter 3 indicate eNAMPT controls MMP expression in fibroblasts. However, it is as yet unclear how iNAMPT may influence MMP activity.

7.3 Deprivation of iNAMPT in cartilage explants results in cell death

The studies in RASFs (Chapter 6) suggest that enzymatic iNAMPT activity does not directly affect MMP expression, despite causing a reduction of intracellular NAD^+ over time. This type of reduction in NAD^+ has also been reported in studies on HepG2 cells (Hasmann and Schemainda, 2003), HeLa cells (Pittelli et al., 2010), and human monocytes (Busso et al., 2008, Van Gool et al., 2009). In these studies, NAD^+ reduction resulted in a decrease in TNFα levels in both murine peritoneal cells (Busso et al., 2008) and human monocytes (Van Gool et al., 2009). NAD^+ reduction has also been associated with a down-regulation of cartilage-specific gene expression in human articular chondrocytes (Dvir-Ginzberg et al., 2008). The consequences of NAD^+ reduction on MMP expression have yet to be explored.

It is possible that APO866 might eventually cause a reduction in MMP expression and release through depletion of intracellular NAD^+. However, as the *in vitro* experiments were relatively short-term studies (0-72 hours), it was important to address this scenario in a longer-term study. Therefore, a bovine cartilage *ex vivo* culture system was used to study the effects of APO866 on MMP activity and cartilage catabolism over a prolonged period of time (chapter 5) APO866 was added to explants alone or in combination with IL-1β in order to determine the role of long-term iNAMPT inhibition in catabolic processes. Within 6-8 days of explant culture, APO866 reduced cytokine-mediated s-GAG and MMP release. However, upon microscopical examination, APO866 appeared to cause a reduction in the cellularity of cartilage explants, suggestive of cytotoxicity. An APO866 dose response experiment confirmed these microscopical observations, and analysis of cell viability by LDH assay showed a sudden peak of cellular toxicity in all APO866-treated explants at day 8 of culture. This cytotoxicity was attributed to a catastrophic depletion of intracellular NAD^+, as the addition of NAD^+ metabolites, NMN and NA, prevented this response, presumably through the replenishment of NAD^+.

It is likely that APO866 treatment caused cell death due to interference of the NAD^+ salvage ability of iNAMPT. This would result in a gradual depletion of NAD^+ without any Nam cycling back into the pathway. Chondrocytes within explant culture may be unable to compensate through other pathways due to a paucity of cofactors such as NA or tryptophan (figure 7.1). Cell death occurred around 6-8 days into the culture period, prior to the enhancement of MMP activation seen around day 12 in cytokine-exposed explants (figure 5.3.16). Therefore, it was not possible to determine whether iNAMPT regulates cytokine-induced MMP expression in explants. It is noteworthy that

concentrations of APO866 used in this study may be well above those that may be considered physiologically relevant in an *in vivo* setting. Furthermore, the pharmacokinetic profile of APO866 means that bioavailability *in vivo* would be significantly less than the concentrations administered in this culture system

Interestingly, both NMN and NA not only prevented APO866 induced cytotoxicity, they also enhanced s-GAG loss and MMP activity in activated explants. This suggests that increased NAD^+ availability enhances the pro-degradative effects of cytokine stimulation in chondrocytes. The exact mechanism for this enhancement remains unclear, though it suggests that increased NAD+ availability may enhance the activity of a NAD-dependent cofactor involved in downstream regulation of MMP gene expression.

The 'rescue' effect on cell viability caused by the addition of NA indicates the presence of the Preiss-Handler pathway enzymes NAPRT, NMNAT and NADSYN in chondrocytes. However, it is as yet to be determined whether these enzymes are upregulated like NAMPT in response to cytokine stimulation. Studies in RASFs in this thesis (chapter 6) and in previous published studies by Iqbal and colleagues suggest they are not (Iqbal and Zaidi, 2006).

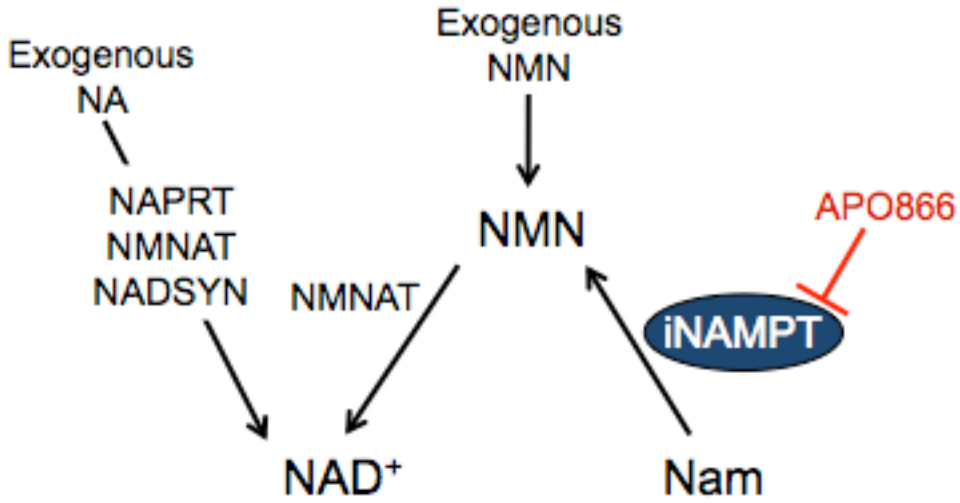

Figure 7.1 Cofactors involved in depletion and replenishment of NAD^+

Schematic showing how addition of cofactors such as NMN or NA can counteract APO866-mediated intracellular NAD^+ depletion

7.4 iNAMPT is the main rate-limiting NAD^+ enzyme induced by pro-inflammatory cytokines in the resident cells of the joint

NAMPT expression is greatly enhanced in chronically inflamed tissue, including within the structural cells of the synovial joint in RA (Nowell et al., 2006), implying active secretion by cells at sites of inflammation. In chapters 5 and 6, one of the aims was to determine the effect of pro-inflammatory cytokine stimulation on expression of intracellular (i)NAMPT in RA-derived chondrocytes and RASFs *in vitro.* In addition, the expression of alternative rate-limiting NAD^+ biosynthetic pathway enzymes was investigated. Using real-time quantitative PCR, it was shown that iNAMPT gene expression is upregulated in a time-dependent manner in response to cytokine stimulation in RASFs and human primary chondrocytes, and is the only rate-limiting NAD^+ pathway enzyme upregulated by cytokine stimulation, with no discernible effect on gene expression of NAPRT, QPRT and IDO. The highly inducible nature of iNAMPT is possibly attributed to the myriad of response elements contained within its distal and proximal promoters (Ognjanovic et al., 2001). Although induction of iNAMPT in RASFs and chondrocytes has been shown in previous studies (Nowell et al., 2006, Brentano et al., 2007, Gosset et al., 2008), this is the first time that expression of genes encoding other NAD^+ pathway enzymes has been explored in these cells, although similar findings have been observed in primary murine macrophages stimulated with TNFα (Iqbal and Zaidi, 2006). These data suggest an important role for iNAMPT in metabolism in activated or transformed cells.

7.5 iNAMPT has little effect on MMP expression in synovial joint cells

Real-time qPCR analyses showed that IL-1β upregulated both MMP-1 and MMP-3 expression in a time-dependent manner in RASFs and human primary chondrocytes. TNFα also induced MMP-1 and -3 in RASF, whilst OSM failed to induce MMPs in RASFs. Although a potent inducer of NAMPT mRNA expression, OSM failed to induce both MMP expression, suggesting that OSM stimulation affects cells in a manner distinct from IL-1β and TNFα.

It was originally hypothesised that a depletion of intracellular NAD^+ due to iNAMPT inhibition by APO866 might affect downstream MMP expression. This was thought to be due to the activity of NAD+ dependent sirtuins. As mentioned in section 6.1, sirtuins are deacetylases that perform a wide variety of functions. Yeung et al (2004) demonstrated that SIRT1 interacts with and deacetylases the p65 subunit of NF-κB (Yeung et al., 2004), which may inhibit NF-κB mediated transcription of MMPs (Vincenti et al., 1998). In RASFs (chapter 6), qPCR analysis showed that SIRT1 expression was

not effected by cytokine stimulation suggesting SIRT1 expression is regulated independently of iNAMPT. Co-incubation with IL-1β and the SIRT1 antagonist, EX527, enhanced MMP-1 protein release in RASFs, suggesting that SIRT1 silences MMP expression. It is unclear whether sirtuin-mediated regulation of MMPs is NAMPT dependent or independent. Further investigations are needed to elucidate these processes. For example, assessment of NAD^+ levels over time in cells treated with EX527 may show a gradual depletion of NAD^+, as sirtuins actively degrade this cofactor back into Nam, the substrate for NAMPT in NAD^+ salvage (figure 7.2). It is possible that blocking sirtuin activity allows a greater availability of NAD^+ for other enzymes dependent on this cofactor, which may in turn positively regulate MMP expression.

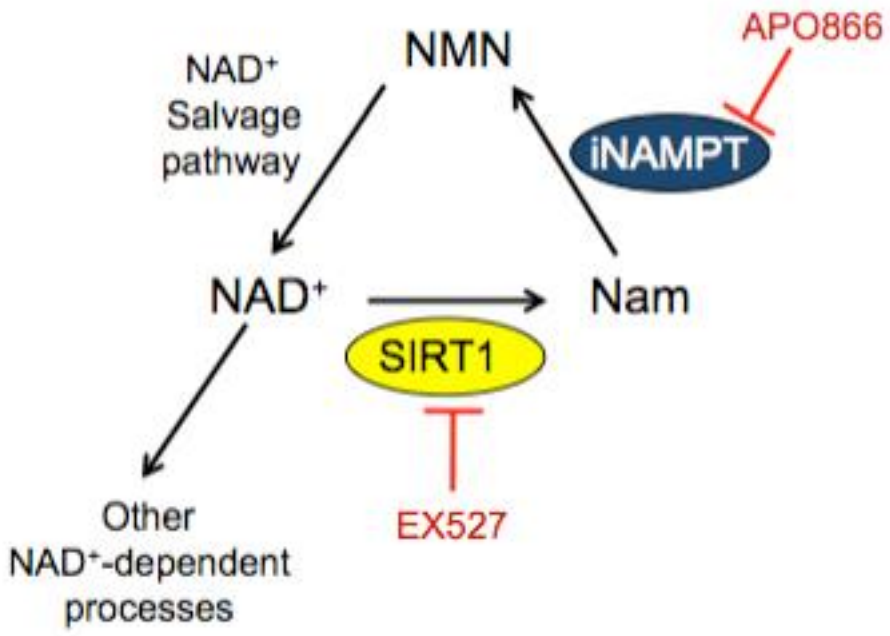

Figure 7.2 Possible effects of NAMPT and SIRT1 depletion on NAD^+ salvage

NAMPT, the rate-limiting enzyme for mammalian NAD^+ biosynthesis, is inhibited by APO866. A subsequent drop in NAD^+ availability may have a knock-on effect on activity of NAD^+-dependent factors, such as SIRT1. NAD^+ is further depleted, as SIRT1 bi-product Nam is not available to cycle back into the salvage pathway. Inhibition of SIRT1 (and other sirtuins) may initially lead to increased NAD^+ availability for other NAD^+ dependent processes, though lack of Nam salvage will also result in NAD^+ depletion, unless Nam or NMN are replenished.

7.6 Future directions

In a fibroblast cell line, addition of the eNAMPT protein was shown to enhance levels of MMP-3, CCL2 and CXCL8 protein release in a dose-dependent manner (chapter 3). Some studies suggest that the proposed signalling activities of eNAMPT may be mimicked by the addition of NMN to cells (Wang et al., 2009b, Romacho et al., 2009, Fan et al., 2011, Jacques et al., 2012), thus it would be interesting to explore whether NMN has eNAMPT mimetic effects in fibroblasts *in vitro*. The eNAMPT receptor remains unknown; however attention is currently focused on the interaction of eNAMPT with growth hormone receptor (Jacques et al., 2012). Future studies might employ a growth hormone receptor antagonist in order to confirm whether or not eNAMPT mediated MMP activity is subsequently affected.

The *in vivo* studies carried out in a murine arthritis model (chapter 4) suggest that synoviocytes and synovial lymphoid aggregates may be the major source of NAMPT and MMP production. There are commercially-available anti-NAMPT antibodies that could potentially be utilised to confirm this by immunohistochemistry (IHC). There are also IHC antibodies available that could show us the localisation and activity of pro-degradative enzymes such as MMPs and ADAMTSs. Optimising and performing these experiments is timely, but would provide key insights into the localisation and activity of NAMPT within the synovium.

In cartilage *ex vivo* cultures, APO866 significantly attenuated cytokine-induced s-GAG loss and MMP activity at the expense of cellular viability, an effect reversed by the addition of NMN or NA to explants. This experiment was only performed with APO866, NMN and NA in one dose combination (100 nM for APO866, and 100 μM for NMN and NA). A dose titration would be an interesting potential *ex vivo* study to determine if it is possible to protect articular cartilage without causing chondrocyte cytotoxicity.

Cartilage catabolism *ex vivo* was determined through release of s-GAG from explants (chapter 5). However, whilst s-GAG loss is largely reversible, collagen breakdown is not (Karsdal et al., 2008). Unfortunately, collagenase activity was not fully explored in this thesis, as assays to measure this parameter can be costly. Exploring the effect of APO866 on collagen release, possibly by hydroxyproline assay, would add real value to the existing data of this thesis.

Finally, the *in vitro* studies in RASFs (chapter 6) showed that iNAMPT is induced by the pro-inflammatory cytokines IL-1β, TNFα and OSM, and it was postulated that these cytokines might induce iNAMPT mRNA expression through activation of a myriad of key signalling pathways. It would be interesting to determine the principle pathways involved in induction of iNAMPT in response to cytokine stimulation, and this may

possibly be achieved with the use of specific inhibitors of these pathways, such as STAT and NF-κB inhibitors.

Finally, a preliminary experiment in one RASF cell line (chapter 6) suggested that SIRT1 inhibitor EX527 enhances MMP-1 (but not MMP-3) protein expression in a time-dependent manner. Confirming and elucidating the proposed anti-degradative role of sirtuins would provide key insights into the role of Nam salvage in regulation of MMP gene expression.

7.7 Concluding remarks

Taken together, the results presented within this thesis and observations published in the literature suggest that NAMPT inhibition may reduce pro-inflammatory and pro-degradative factors in affected limbs through depletion of intracellular NAD^+ in iNAMPT-sensitive cells. Activated cells appear to be more sensitive to this depletion, suggesting that high levels of NAMPT (induced as a result of cytokine-stimulation) may therefore ensure prolonged survival and enhanced proliferation at sites of inflammation.

Observations within the thesis have shown that APO866 may inhibit eNAMPT activation of MMPs in the structural cells of the joint. Targeting these cells with NAMPT-specific inhibitors such as APO866, may also actively reduce lymphocyte infiltration, by reducing chemokine synthesis locally. This is supported by observations within this thesis, which suggest that APO866 may inhibit eNAMPT induced CCL2 and CXCL8 release; subsequently preventing T-cell driven activation of the structural cells of the synovial joint. Although lymphocytes can produce MMPs such as MMP-9 (Owen et al., 2003), they mainly induce MMPs through interactions with other cell types such as synoviocytes Interestingly, activated lymphocytes are particularly sensitive to iNAMPT and NAD^+ depletion compared with resting lymphocytes (Bruzzone et al., 2009). Therefore, APO866 may well reduce MMP expression in activated lymphocytes as NAMPT inhibition was shown to impair proliferation and reduce IFNγ and TNFα production in these cells (Bruzzone et al., 2009).

Upregulated NAMPT has also been shown to delay neutrophil apoptosis in response to inflammatory stimuli (Jia et al., 2004). As neutrophils are a source of MMP-8; enhanced NAMPT and subsequent delayed neutrophil apoptosis will undoubtedly result in sustained MMP activity within the inflammatory exudate.

The work presented in this thesis has confirmed that NAMPT has an important role in cell metabolism. It is highly induced in synovial joint cells which are involved in the production of pro-inflammatory and pro-degradative factors in arthritis disease

pathogenesis. Notably, its inhibition affects MMP expression in the principle cells of a synovial joint (figure 7.3).

Many of the key findings of this thesis have been published in two peer-reviewed publications, with another expected to follow (Evans et al., 2011, Nowell et al., 2012)- see Appendices). Further experiments are required to study the downstream effects of NAMPT.

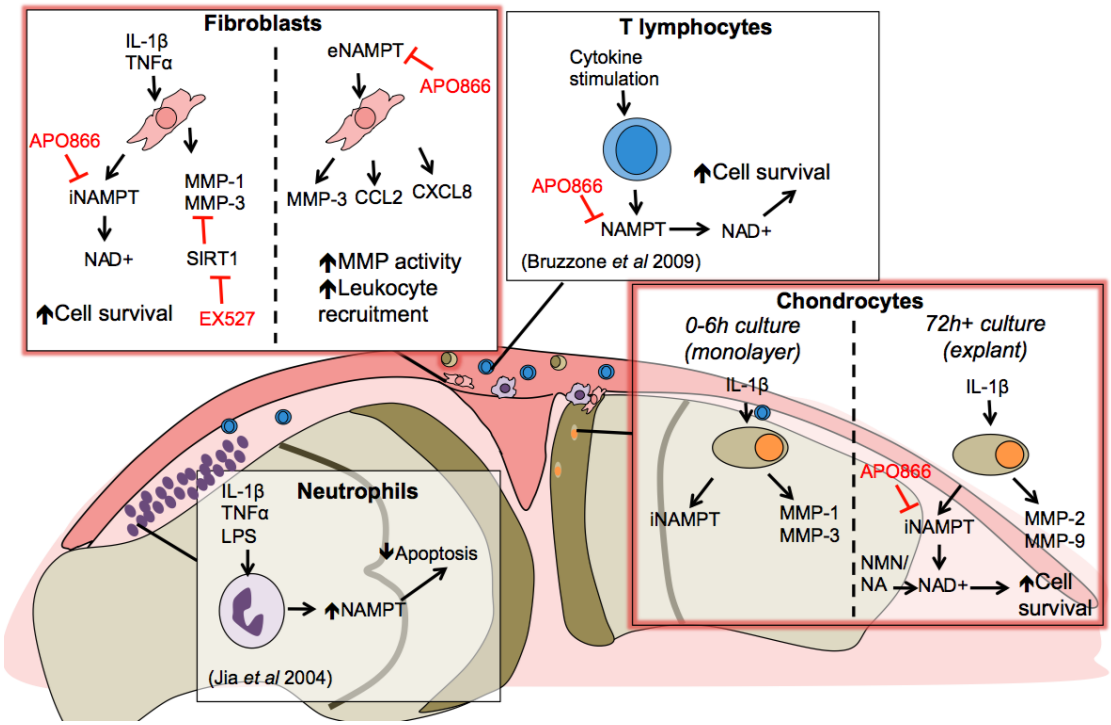

Figure 7.3 Role and regulation of NAMPT within the synovial joint

A schematic of the synovial joint, showing the main cell types involved in disease pathogenesis in rheumatoid arthritis. Findings from this thesis are summarised in the pink-bordered boxes, in addition to findings by other groups in inflammatory cells that express NAMPT.

References

ADYA, R., TAN, B. K., CHEN, J. & RANDEVA, H. S. 2009. Pre-B cell colony enhancing factor (PBEF)/visfatin induces secretion of MCP-1 in human endothelial cells: Role in visfatin-induced angiogenesis. *Atherosclerosis,* 205, 113-119.

ADYA, R., TAN, B. K., PUNN, A., CHEN, J. & RANDEVA, H. S. 2008. Visfatin induces human endothelial VEGF and MMP-2/9 production via MAPK and PI3K/Akt signalling pathways: novel insights into visfatin-induced angiogenesis. *Cardiovascular Research,* 78, 356-365.

AIGNER, T., SACHSE, A., GEBHARD, P. M. & ROACH, H. I. 2006. Osteoarthritis: Pathobiology, targets and ways for therapeutic intervention. *Advanced Drug Delivery Reviews,* 58, 128-149.

AILLAND, J., KAMPEN, W. U., SCHÜNKE, M., TRENTMANN, J. & KURZ, B. 2003. β Irradiation decreases collagen type II synthesis and increases nitric oxide production and cell death in articular chondrocytes. *Annals of the Rheumatic Diseases,* 62, 1054-1060.

AINOLA, M. M., MANDELIN, J. A., LILJESTROM, M. P., LI, T. F., HUKKANEN, M. V. & KONTTINEN, Y. T. 2005. Pannus invasion and cartilage degradation in rheumatoid arthritis: involvement of MMP-3 and interleukin-1beta. *Clin Exp Rheumatol,* 23, 644 - 650.

ALETAHA, D., NEOGI, T., SILMAN, A. J., FUNOVITS, J., FELSON, D. T., BINGHAM, C. O., BIRNBAUM, N. S., BURMESTER, G. R., BYKERK, V. P., COHEN, M. D., COMBE, B., COSTENBADER, K. H., DOUGADOS, M., EMERY, P., FERRACCIOLI, G., HAZES, J. M. W., HOBBS, K., HUIZINGA, T. W. J., KAVANAUGH, A., KAY, J., KVIEN, T. K., LAING, T., MEASE, P., M√©NARD, H. A., MORELAND, L. W., NADEN, R. L., PINCUS, T., SMOLEN, J. S., STANISLAWSKA-BIERNAT, E., SYMMONS, D., TAK, P. P., UPCHURCH, K. S., VENCOVSKÝ, J. Ô., WOLFE, F. & HAWKER, G. 2010. 2010 Rheumatoid arthritis classification criteria: an American College of Rheumatology/European League Against Rheumatism collaborative initiative. *Annals of the Rheumatic Diseases,* 69, 1580-1588.

APOXIS. 2005. *Apoxis Acquires Worldwide Rights for Novel Anti-Cancer Compound from Astellas Pharma* [Online]. Available: http://www.apoxis.com/index2.php?option=content&do_pdf=1&id=42.

ARNETT, F. C., EDWORTHY, S. M., BLOCH, D. A., MCSHANE, D. J., FRIES, J. F., COOPER, N. S., HEALEY, L. A., KAPLAN, S. R., LIANG, M. H., LUTHRA, H. S. & ET AL. 1988. The American Rheumatism Association 1987 revised criteria for the classification of rheumatoid arthritis. *Arthritis and Rheumatism,* 31, 315-324.

BAE, S.-K., KIM, S.-R., KIM, J. G., KIM, J. Y., KOO, T. H., JANG, H.-O., YUN, I., YOO, M.-A. & BAE, M.-K. 2006. Hypoxic induction of human visfatin gene is directly mediated by hypoxia-inducible factor-1. *FEBS Letters,* 580, 4105-4113.

BARTOK, B. & FIRESTEIN, G. S. 2010. Fibroblast-like synoviocytes: key effector cells in rheumatoid arthritis. *Immunological Reviews,* 233, 233-255.

BEDARD, A., MAHEUX, J., LEVESQUE, D. & SAMAHA, A. 2011. Continuous, but not Intermittent, Antipsychotic Drug Delivery Intensifies the Pursuit of Reward Cues. *Neuropsychopharmacology,* 36, 1248-1259.

BEIDERMANN, E., LOESER, R. & RATTEL, B. 2003. *Use of pyridyl amides as inhibitors of angiogenesis* [Online]. Available: http://www.freepatentsonline.com/EP1348434.html [Accessed 25th Sept 2009.

BELLOFIORE, B., MATARESE, A., BALATO, N., GAUDIELLO, F., SCARPA, R., ATTENO, M., BOCCHINO, M. & SANDUZZI, A. 2009. Prevention of Tuberculosis in Patients Taking Tumor Necrosis Factor‚ÄìÆ± Blockers. *The Journal of Rheumatology,* 83, 76-77.

BERNDT, J., KL√∂TING, N., KRALISCH, S., KOVACS, P., FASSHAUER, M., SCH√∂N, M. R., STUMVOLL, M. & BLHER, M. 2005. Plasma Visfatin Concentrations and Fat Depot-Specific mRNA Expression in Humans. *Diabetes,* 54, 2911-2916.

BIEGANOWSKI, P. & BRENNER, C. 2004. Discoveries of Nicotinamide Riboside as a Nutrient and Conserved NRK Genes Establish a Preiss-Handler Independent Route to NAD+ in Fungi and Humans. *Cell,* 117, 495-502.

BILLIPS, L. G., PETITTE, D., DORSHKIND, K., NARAYANAN, R., CHIU, C. P. & LANDRETH, K. S. 1992. Differential roles of stromal cells, interleukin-7, and kit-ligand in the regulation of B lymphopoiesis. *Blood,* 79, 1185-1192.

BOGAN, K. L. & BRENNER, C. 2008. Nicotinic Acid, Nicotinamide, and Nicotinamide Riboside: A Molecular Evaluation of NAD+ Precursor Vitamins in Human Nutrition. *Annual Review of Nutrition,* 28, 115-130.

BOND, M., CHASE, A. J., BAKER, A. H. & NEWBY, A. C. 2001. Inhibition of transcription factor NF-kB reduces matrix metalloproteinase-1, -3 and -9 production by vascular smooth muscle cells. *Cardiovascular Research,* 50, 556-565.

BRAND, D. D., KANG, A. H. & ROSLONIEC, E. F. 2003. Immunopathogenesis of Collagen Arthritis. *Springer Seminars in Immunopathology,* 25, 3-18.

BRAND, D. D., LATHAM, K. A. & ROSLONIEC, E. F. 2007. Collagen-induced arthritis. *Nature Protocols,* 2, 1269-1275.

BRAND, D. D., MARION, T. N., MYERS, L. K., ROSLONIEC, E. F., WATSON, W. C., STUART, J. M. & KANG, A. H. 1996. Autoantibodies to murine type II collagen in collagen-induced arthritis: a comparison of susceptible and nonsusceptible strains. *Journal of Immunology,* 157, 5178-5184.

BRENNAN, F. M. & MCINNES, I. B. 2008. Evidence that cytokines play a role in rheumatoid arthritis. *Journal of Clinical Investigation,* 118, 3537-3545.

BRENTANO, F., SCHORR, O., OSPELT, C., STANCZYK, J., GAY, R. E., GAY, S. & KYBURZ, D. 2007. Pre-B cell colony-enhancing factor/visfatin, a new marker of inflammation in rheumatoid arthritis with proinflammatory and matrix-degrading activities. *Arthritis and Rheumatism,* 56, 2829-2839.

BRUZZONE, S., FRUSCIONE, F., MORANDO, S., FERRANDO, T., POGGI, A., GARUTI, A., D'URSO, A., SELMO, M., BENVENUTO, F., CEA, M., ZOPPOLI, G., MORAN, E., SONCINI, D., BALLESTRERO, A., SORDAT, B., PATRONE, F., MOSTOSLAVSKY, R., UCCELLI, A. & NENCIONI, A. 2009. Catastrophic NAD+ depletion in activated T lymphocytes through Nampt inhibition reduces demyelination and disability in EAE. *PLoS ONE,* 4, e7897.

BUCKLEY, C. D., PILLING, D., LORD, J. M., AKBAR, A. N., SCHEEL-TOELLNER, D. & SALMON, M. 2001. Fibroblasts regulate the switch from acute resolving to chronic persistent inflammation. *Trends in Immunology,* 22, 199-204.

BURRAGE, P. S., MIX, K. S. & BRINCKERHOFF, C. E. 2006. Matrix metalloproteinases: Role in arthritis. *Frontiers in Bioscience,* 11, 529-543.

BUSSO, N., KARABABA, M., NOBILE, M., ROLAZ, A., VAN GOOL, GALLI, M., LEO, O., SO, A. & DE SMEDT, T. 2008. Pharmacological Inhibition of Nicotinamide Phosphoribosyltransferase/Visfatin Enzymatic Activity Identifies a New Inflammatory Pathway Linked to NAD. *PLoS ONE,* 3, e2267.

CACCESE, R. G., ZIMMERMAN, J. L. & CARLSON, R. P. 1992. Bacterial lipopolysaccharide potentiates type II collagen-induced arthritis in mice. *Mediators of Inflammation,* 1, 273-279.

CAGLIC, D., GLOBISCH, A., KINDERMANN, M., LIM, N.-H., JESKE, V., JURETSCHKE, H.-P., BARTNIK, E., WEITHMANN, K. U., NAGASE, H., TURK, B. & WENDT, K. U. 2011. Functional in vivo imaging of cysteine cathepsin activity in murine model of inflammation. *Bioorganic & Medicinal Chemistry,* 19, 1055-1061.

CAWSTON, T. E. & YOUNG, D. A. 2010. Proteinases involved in matrix turnover during cartilage and bone breakdown. *Cell and Tissue Research,* 339, 221-235.

CHEN, J., ZHANG, X. M. & XU, Q. 2004. Involvement of lymphocytes with a Th1 cytokine profile in bone cell damage associated with MMP-9 production in collagen-induced arthritis. *Inflammation Research,* 53, 670-679.

CHEN, M. P., CHUNG, F. M., CHANG, D. M., TSAI, J. C. R., HUANG, H. F., SHIN, S. J. & LEE, Y. J. 2006. Elevated plasma level of visfatin/pre-B cell colony-enhancing factor in patients with type 2 diabetes mellitus. *Journal of Clinical Endocrinology and Metabolism,* 91, 295-299.

CHOY, E. H. S., SMITH, C., DORE, C. J. & SCOTT, D. L. 2005. A meta-analysis of the efficacy and toxicity of combining disease-modifying anti-rheumatic drugs in rheumatoid arthritis based on patient withdrawal. *Rheumatology,* 44, 1414-1421.

CHUNG, C. P., LONG, A. G., SOLUS, J. F., RHO, Y. H., OESER, A., RAGGI, P. & STEIN, C. M. 2009. Adipocytokines in systemic lupus erythematosus: relationship to inflammation, insulin resistance and coronary atherosclerosis. *Lupus,* 18, 799-806.

CLOSE, D. R. 2001. Matrix metalloproteinase inhibitors in rheumatic diseases. *Annals of the Rheumatic Diseases,* 60, iii62-iii67.

COURTENAY, J. S., DALLMAN, M. J., DAYAN, A. D., MARTIN, A. & MOSEDALE, B. 1980. Immunisation against heterologous type II collagen induces arthritis in mice. *Nature,* 283, 666-8.

CREE, I. A., MEERLOO, J., KASPERS, G. L. & CLOOS, J. 2011. Cell Sensitivity Assays: The MTT Assay. *Cancer Cell Culture.* Humana Press.

CUNNANE, G., FITZGERALD, O., BEETON, C., CAWSTON, T. E. & BRESNIHAN, B. 2001. Early joint erosions and serum levels of matrix metalloproteinase 1, matrix metalloproteinase 3, and tissue inhibitor of metalloproteinases 1 in rheumatoid arthritis. *Arthritis and Rheumatism,* 44, 2263-2274.

DAHL, T. B., YNDESTAD, A., SKJELLAND, M., √ÒIE, E., DAHL, A., MICHELSEN, A., DAM√•S, J. K., TUNHEIM, S. H., UELAND, T., SMITH, C., BENDZ, B., TONSTAD, S., GULLESTAD, L., FR√∏LAND, S. S., KROHG-S√∅RENSEN, K., RUSSELL, D., AUKRUST, P. & HALVORSEN, B. 2007. Increased expression of visfatin in macrophages of human unstable carotid and coronary atherosclerosis: Possible role in inflammation and plaque destabilization. *Circulation,* 115, 972-980.

DEVKOTA, A. C. & WEINHOLD, P. S. 2010. Prostaglandin E2, collagenase, and cell death responses depend on cyclical load magnitude in an explant model of tendinopathy. *Connective Tissue Research,* 51, 306-313.

DIETRICH, L. S., FULLER, L., YERO, I. L. & MARTINEZ, L. 1966. Nicotinamide Mononucleotide Pyrophosphorylase Activity in Animal Tissues. *Journal of Biological Chemistry,* 241, 188-191.

DORSHKIND, K., NARAYANAN, R. & LANDRETH, K. S. 1992. Regulatory cells and cytokines involved in primary B lymphocyte production. *Advances in Experimental Medicine and Biology,* 323.

DREVS, J., LOÌˆSER, R., RATTEL, B. & ESSER, N. 2003. Antiangiogenic Potency of FK866/K22.175, A New Inhibitor of Intracellular NAD Biosynthesis, in Murine Renal Cell Carcinoma. *Anticancer Research,* 23, 4853-4858.

DUAN, Y., HAO, D., LI, M., WU, Z., LI, D., YANG, X. & QIU, G. 2011. Increased synovial fluid visfatin is positively linked to cartilage degradation biomarkers in osteoarthritis. *Rheumatol International*.

DUNN, E., SIMS, J. E., NICKLIN, M. J. H. & O'NEILL, L. A. J. 2001. Annotating genes with potential roles in the immune system: six new members of the IL-1 family. *Trends in Immunology,* 22, 533-536.

DVIR-GINZBERG, M., GAGARINA, V., LEE, E. J. & HALL, D. J. 2008. Regulation of cartilage-specific gene expression in human chondrocytes by SirT1 and nicotinamide phosphoribosyltransferase. *Journal of Biological Chemistry,* 283, 36300-10.

EASTGATE, J., WOOD, N., DI GIOVINE, F., SYMONS, J., GRINLINTON, F. & DUFF, G. 1988. CORRELATION OF PLASMA INTERLEUKIN 1 LEVELS WITH DISEASE ACTIVITY IN RHEUMATOID ARTHRITIS. *The Lancet,* 332, 706-709.

EDWARDS, J. C. W. 2000. Fibroblast biology: Development and differentiation of synovial fibroblasts in arthritis. *Arthritis Research and Therapy,* 2, 344-347.

ERDFELDER, E., FAUL, F. & BUCHNER, A. 1996. GPOWER: A general power analysis program. 1-11.

EVANS, L. A., WILLIAMS, A. S., HAYES, A. J., JONES, S. A. & NOWELL, M. A. 2011. Suppression of leukocyte infiltration and cartilage degradation by selective inhibition of pre–B cell colony-enhancing factor/visfatin/nicotinamide phosphoribosyltransferase: Apo866-mediated therapy in human fibroblasts and murine collagen-induced arthritis. *Arthritis and Rheumatism,* 63, 1866-1877.

EYRE, D. 2002. Articular cartilage and changes in Arthritis: Collagen of articular cartilage. *Arthritis Research and Therapy,* 4 %@ 1465-9905, 30 - 35.

EYRE, D. R., WEIS, M. A. & WU, J. J. 2006. Articular cartilage collagen: an irreplaceable framework? *European Cells and Materials,* 2, 57-63.

FAN, Y., MENG, S., WANG, Y., CAO, J. & WANG, C. 2011. Visfatin/PBEF/Nampt induces EMMPRIN and MMP-9 production in macrophages via the NAMPT-MAPK (p38, ERK1/2)-NF-kappaB signaling pathway. *International Journal of Molecular Medicine,* 27, 607-615.

FARNDALE, R. W., BUTTLE, D. J. & BARRETT, A. J. 1986. Improved quantitation and discrimination of sulphate glycosaminoglycans by use of dimethylmethylene blue. *Biochimica et Biophysica Acta - General Subjects,* 883, 173-177.

FASSBENDER, H. G. 1983. Histomorphological basis of articular cartilage destruction in rheumatoid arthritis. *Collagen and Related Research,* 3, 141-155.

FEARON, U., MULLAN, R., MARKHAM, T., CONNOLLY, M., SULLIVAN, S., POOLE, A. R., FITZGERALD, O., BRESNIHAN, B. & VEALE, D. J. 2006. Oncostatin M induces angiogenesis and cartilage degradation in rheumatoid arthritis synovial tissue and human cartilage cocultures. *Arthritis and Rheumatism,* 54, 3152-3162.

FEGHALI, C. A. & WRIGHT, T. M. 1997. Cytokines in acute and chronic inflammation. *Frontiers in Biosciences,* 1, d12-26.

FELDMANN, M., BRENNAN, F. M. & MAINI, R. N. 1996a. Rheumatoid Arthritis. *Cell,* 85, 307-310.

FELDMANN, M., BRENNAN, F. M. & MAINI, R. N. 1996b. Role of Cytokines in Rheumatoid Arthritis *Annual Review of Immunology,* 14, 397-440.

FIRESTEIN, G. S., BUDD, R. C., HARRIS, E. D., MCINNES, I. B., RUDDY, S. & SERGENT, J. S. (eds.) 2009. *Kelley's Textbook of Rheumatology Volume I*.

FIRESTEIN, G. S. & ZVAIFLER, N. J. 1987. Peripheral blood and synovial fluid monocyte activation in inflammatory arthritis. ii. low levels of synovial fluid and synovial tissue interferon suggest that γgm-interferon is not the primary macrophage activating factor. *Arthritis and Rheumatism,* 30, 864-871.

FOSANG, A. J., ROGERSON, F. M., EAST, C. J. & STANTON, H. 2008. ADAMTS-5: The story so far. *European Cells and Materials,* 15, 11-26.

FOSANG, A. J., STANTON, H., LITTLE, C. B. & ATLEY, L. M. 2003. Neoepitopes as biomarkers of cartilage catabolism. *Inflammation Research,* 52, 277-282.

FRIEBE, D., NEEF, M., KRATZSCH, J., ERBS, S., DITTRICH, K., GARTEN, A., PETZOLD-QUINQUE, S., BL√ºHER, S., REINEHR, T., STUMVOLL, M., BL√ºHER, M., KIESS, W. & K√∂RNER, A. 2011. Leucocytes are a major source of circulating nicotinamide phosphoribosyltransferase (NAMPT)/pre-B cell colony (PBEF)/visfatin linking obesity and inflammation in humans. *Diabetologia,* 54, 1200-1211.

FUJIKI, K., SHIN, D. H., NAKAO, M. & YANO, T. 2000. Molecular cloning and expression analysis of the putative carp (Cyprinus carpio) pre-B cell enhancing factor. *Fish and Shellfish Immunology,* 10, 383-385.

FUJIMOTO, M., SERADA, S., MIHARA, M., UCHIYAMA, Y., YOSHIDA, H., KOIKE, N., OHSUGI, Y., NISHIKAWA, T., RIPLEY, B., KIMURA, A., KISHIMOTO, T. & NAKA, T. 2008. Interleukin-6 blockade suppresses autoimmune arthritis in mice by the inhibition of inflammatory Th17 responses. *Arthritis and Rheumatism,* 58, 3710-3719.

FUKUHARA, A., MATSUDA, M., NISHIZAWA, M., SEGAWA, K., TANAKA, M., KISHIMOTO, K., MATSUKI, Y., MURAKAMI, M., ICHISAKA, T., MURAKAMI, H.,

WATANABE, E., TAKAGI, T., AKIYOSHI, M., OHTSUBO, T., KIHARA, S., YAMASHITA, S., MAKISHIMA, M., FUNAHASHI, T., YAMANAKA, S., HIRAMATSU, R., MATSUZAWA, Y. & SHIMOMURA, I. 2005. Visfatin: A protein secreted by visceral fat that Mimics the effects of insulin. *Science,* 307, 426-430.

FUKUHARA, A., MATSUDA, M., NISHIZAWA, M., SEGAWA, K., TANAKA, M., KISHIMOTO, K., MATSUKI, Y., MURAKAMI, M., ICHISAKA, T., MURAKAMI, H., WATANABE, E., TAKAGI, T., AKIYOSHI, M., OHTSUBO, T., KIHARA, S., YAMASHITA, S., MAKISHIMA, M., FUNAHASHI, T., YAMANAKA, S., HIRAMATSU, R., MATSUZAWA, Y. & SHIMOMURA, I. 2007. Retraction. *Science,* 318, 565-565.

GARROD, A. B. 1892. The great practical importance of separating rheumatoid arthritis from gout. *The Lancet,* 2, 1033-1037.

GARTEN, A., PETZOLD, S., KˆRNER, A., IMAI, S.-I. & KIESS, W. 2009. Nampt: linking NAD biology, metabolism and cancer. *Trends in Endocrinology and Metabolism,* 20, 130-138.

GELSE, K., P√∂SCHL, E. & AIGNER, T. 2003. Collagens‚Äîstructure, function, and biosynthesis. *Advanced Drug Delivery Reviews,* 55, 1531-1546.

GOLDRING, S. R. 2003. Pathogenesis of bone and cartilage destruction in rheumatoid arthritis. *Rheumatology (Oxford),* 42, ii11 - ii16.

GOSSET, M., BERENBAUM, F., SALVAT, C., SAUTET, A., PIGENET, A., TAHIRI, K. & JACQUES, C. 2008. Crucial role of visfatin/pre-B cell colony-enhancing factor in matrix degradation and prostaglandin E2 synthesis in chondrocytes: Possible influence on osteoarthritis. *Arthritis and Rheumatism,* 58, 1399-1409.

GREEN, M. J., GOUGH, A. K. S., DEVLIN, J., SMITH, J., ASTIN, P., TAYLOR, D. & EMERY, P. 2003. Serum MMP‚Äì3 and MMP‚Äì1 and progression of joint damage in early rheumatoid arthritis. *Rheumatology,* 42, 83-88.

GRIFFITHS, R. J., PETTIPHER, E. R., KOCH, K., FARRELL, C. A., BRESLOW, R., CONKLYN, M. J., SMITH, M. A., HACKMAN, B. C., WIMBERLY, D. J. & MILICI, A. J. 1995. Leukotriene B4 plays a critical role in the progression of collagen-induced arthritis. *Proceedings of the National Academy of Sciences of the United States of America,* 92, 517-521.

GROVES, K., KOSSODO, S., HANDY, E., JENSEN, J., BLUSZTAJN, A., CUNEO, G., PETERSON, J. D. & RAJOPADHYE, M. 2010. In Vivo Imaging of Treatment Effects Using a Novel Infrared Labeled Agent MMPSense750 FAST. *In:* PERKINELMER (ed.).

HARA, N., YAMADA, K., SHIBATA, T., OSAGO, H. & TSUCHIYA, M. 2011. Nicotinamide Phosphoribosyltransferase/Visfatin Does Not Catalyze Nicotinamide Mononucleotide Formation in Blood Plasma. *PLoS ONE,* 6, e22781.

HASMANN, M. & SCHEMAINDA, I. 2003. FK866, a Highly Specific Noncompetitive Inhibitor of Nicotinamide Phosphoribosyltransferase, Represents a Novel Mechanism for Induction of Tumor Cell Apoptosis. *Cancer Research,* 63, 7436-7442.

HEMBRY, R. M., BAGGA, M. R., REYNOLDS, J. J. & HAMBLEN, D. L. 1995. Immunolocalisation studies on six matrix metalloproteinases and their inhibitors, TIMP-1 and TIMP-2, in synovia from patients with osteo- and rheumatoid arthritis. *Annals of the Rheumatic Diseases,* 54, 25-32.

HINZ, M., KATSILAMBROS, N., MAIER, V., SCHATZ, H. & PFEIFFER, E. F. 1973. Significance of streptozotocin induced nicotinamide-adenine-dinucleotide (NAD) degradation in mouse pancreatic islets. *FEBS Letters,* 30, 225-228.

HOFFLER, C. E., HANKENSON, K. D., MILLER, J. D., BILKHU, S. K. & GOLDSTEIN, S. A. 2006. Novel explant model to study mechanotransduction and cell–cell communication. *Journal of Orthopaedic Research,* 24, 1687-1698.

HOLEN, K., SALTZ, L. B., HOLLYWOOD, E., BURK, K. & HANAUSKE, A. R. 2008. The pharmacokinetics, toxicities, and biologic effects of FK866, a nicotinamide adenine dinucleotide biosynthesis inhibitor. *Investigational New Drugs,* 26, 45-51.

HOLEN, K. D., BURK, K., SCHWARTZ, G. K., SPRIGGS, D., HOLLYWOOD, E., TY, V., ALCASID, A., JILL, H., BARBER, W., KELSEN, D. & SALTZ, L. B. Dose-finding and pharmacokinetic study of FK866, an inhibitor of NAD biosynthesis. American Society of Clinical Oncology Annual Meeting, 2002. 87a.

HONCZARENKO, M., LE, Y., SWIERKOWSKI, M., GHIRAN, I., GLODEK, A. M. & SILBERSTEIN, L. E. 2006. Human Bone Marrow Stromal Cells Express a Distinct Set of Biologically Functional Chemokine Receptors. *STEM CELLS,* 24, 1030-1041.

HONG, E., YUN, H. S., KIM, J., UM, H., LEE, K., KANG, C., LEE, S., CHUN, J. & HWANG, S. 2011. Nicotinamide Phosphoribosyltransferase Is Essential for Interleukin-1β-mediated Dedifferentiation of Articular Chondrocytes via SIRT1 and Extracellular Signal-regulated Kinase (ERK) Complex Signaling. *Journal of Biological Chemistry,* 286, 28619-28631.

HOUSSIAU, F. A., DEVOGELAER, J.-P., DAMME, J. V., DEUXCHAISNES, C. N. D. & SNICK, J. V. 1988. Interleukin-6 in synovial fluid and serum of patients with rheumatoid arthritis and other inflammatory arthritides. *Arthritis and Rheumatism,* 31, 784-788.

HUEBER, A. J., ASQUITH, D. L., MILLER, A. M., REILLY, J., KERR, S., LEIPE, J., MELENDEZ, A. J. & MCINNES, I. B. 2010. Cutting Edge: Mast Cells Express IL-17A in Rheumatoid Arthritis Synovium. *The Journal of Immunology,* 184, 3336-3340.

HUGHES, C. E., CATERSON, B., FOSANG, A. J., ROUGHLEY, P. J. & MORT, J. S. 1995. Monoclonal antibodies that specifically recognize neoepitope sequences generated by 'aggrecanase' and matrix metalloproteinase cleavage of aggrecan: Application to catabolism in situ and in vitro. *Biochemical Journal,* 305, 799-804.

IMAI, S. 2009. Nicotinamide phosphoribosyltransferase (Nampt): a link between NAD biology, metabolism, and diseases. *Curr Pharm Des,* 15, 20-8.

IMAI, S. & KIESS, W. 2009. Therapeutic potential of SIRT1 and NAMPT-mediated NAD biosynthesis in type 2 diabetes. *Frontiers in Biosciences,* 14.

IQBAL, J. & ZAIDI, M. 2006. TNF regulates cellular NAD+ metabolism in primary macrophages. *Biochemical and Biophysical Research Communications,* 342, 1312-1318.

IRMLER, I., OPFERMANN, T., GEBHARDT, P., GAJDA, M., BRAUER, R., SALUZ, H. & KAMRADT, T. 2010. In vivo molecular imaging of experimental joint inflammation by combined 18F-FDG positron emission tomography and computed tomography. *Arthritis Research and Therapy,* 12, R203.

ISHIKAWA, T., NISHIGAKI, F., MIYATA, S., HIRAYAMA, Y., MINOURA, K., IMANISHI, J., NEYA, M., MIZUTANI, T., IMAMURA, Y., NARITOMI, Y., MURAI, H., OHKUBO, Y., KAGAYAMA, A. & MUTOH, S. 2005. Prevention of progressive joint destruction in collagen-induced arthritis in rats by a novel matrix metalloproteinase inhibitor, FR255031. *British Journal of Pharmacology,* 144**,** 133-143.

JACQUES, C., HOLZENBERGER, M., MLADENOVIC, Z., SALVAT, C., PECCHI, E., BERENBAUM, F. & GOSSET, M. 2012. Pro-inflammatory actions of visfatin/Nampt involve regulation of insulin signaling pathway and Nampt enzymatic activity. *Journal of Biological Chemistry*.

JÄRVINEN, T. A. H., MOILANEN, T., RVINEN, T. L. N. & MOILANEN, E. 1995. Nitric oxide mediates interleukin-1 induced inhibition of glycosaminoglycan synthesis in rat articular cartilage. *Mediators of Inflammation,* 4, 107-111.

JIA, S. H., LI, Y., PARODO, J., KAPUS, A., FAN, L., HOLSTEIN, O. D. & MARSHALL, J. C. 2004. Pre-B cell colony-enhancing factor inhibits neutrophil apoptosis in experimental inflammation and clinical sepsis. *Journal of Clinical Investigation,* 113, 1318-1327.

JONES, E. F., SCHOOLER, J., MILLER, D. C., DRAKE, C. R., WAHNISHE, H., SIDDIQUI, S., LI, X. & MAJUMDAR, S. 2012. Characterization of human

osteoarthritic cartilage using optical and magnetic resonance imaging. *Molecular Imaging and Biology,* 14, 32-39.
JOOSTEN, L. A., HELSEN, M. M., VAN DE LOO, F. A. & VAN DEN BERG, W. B. 1996. Anticytokine treatment of established type II collagen-induced arthritis in DBA/1 mice: A comparative study using anti-TNFα, anti-IL-1α/β and IL-1Ra. *Arthritis and Rheumatism,* 58, S110-S122.
JOOSTEN, L. A. B., HELSEN, M. M. A., SAXNE, T., VAN DE LOO, F. A. J. & VAN DEN BERG, W. B. 1999. IL-1 Blockade Prevents Cartilage and Bone Destruction in Murine Type II Collagen-Induced Arthritis, Whereas TNF-Œ± Blockade Only Ameliorates Joint Inflammation. *Journal of Immunology,* 163, 5049-5055.
KARSDAL, M. A., MADSEN, S. H., CHRISTIANSEN, C., HENRIKSEN, K., FOSANG, A. J. & SONDERGAARD, B. C. 2008. Cartilage degradation is fully reversible in the presence of aggrecanase but not matrix metalloproteinase activity. *Arthritis Research and Therapy,* 10.
KHAN, J. A., TAO, X. & TONG, L. 2006. Molecular basis for the inhibition of human NMPRTase, a novel target for anticancer agents. *Nature Structural and Molecular Biology,* 13, 582-588.
KIM, M. K., LEE, J. H., KIM, H., PARK, S. J., KIM, S. H., KANG, G. B., LEE, Y. S., KIM, J. B., KIM, K. K., SUH, S. W. & EOM, S. H. 2006. Crystal Structure of Visfatin/Pre-B Cell Colony-enhancing Factor 1/Nicotinamide Phosphoribosyltransferase, Free and in Complex with the Anti-cancer Agent FK-866. *Journal of Molecular Biology,* 362, 66-77.
KIM, S. R., BAE, S. K., CHOI, K. S., PARK, S. Y., JUN, H. O., LEE, J. Y., JANG, H. O., YUN, I., YOON, K. H., KIM, Y. J., YOO, M. A., KIM, K. W. & BAE, M. K. 2007. Visfatin promotes angiogenesis by activation of extracellular signal-regulated kinase 1/2. *Biochemical and Biophysical Research Communications,* 357, 150-156.
KINNE, R. W., STUHLMULLER, B. & BURMESTER, G. R. 2007. Cells of the synovium in rheumatoid arthritis. Macrophages. *Arthritis Research and Therapy,* 9, 224.
KISHIMOTO, T., AKIRA, S., NARAZAKI, M. & TAGA, T. 1995. Interleukin-6 family of cytokines and gp130. *Blood,* 86, 1243-1254.
KNUDSON, C. B. & KNUDSON, W. 2001. Cartilage proteoglycans. *Seminars in Cell & Developmental Biology,* 12, 69-78.
KO, Y., BANERJI, S. S., LIU, Y., LI, W., LIANG, J., SOULE, H. D., PAULEY, R. J., WILLSON, J. K. V., ZBOROWSKA, E. & BRATTAIN, M. G. 1998. Expression of transforming growth factor-β receptor type II and tumorigenicity in human breast adenocarcinoma MCF-7 cells. *Journal of Cellular Physiology,* 176, 424-434.
KONDA, V. R., DESAI, A., DARLAND, G., BLAND, J. S. & TRIPP, M. L. 2010. META060 inhibits osteoclastogenesis and matrix metalloproteinases in vitro and reduces bone and cartilage degradation in a mouse model of rheumatoid arthritis. *Arthritis and Rheumatism,* 62**,** 1683-1692.
KONDO, H. & TOGARI, A. 2011. Continuous Treatment with a Low-Dose B-Agonist Reduces Bone Mass by Increasing Bone Resorption Without Suppressing Bone Formation. *Calcified Tissue International,* 88, 23-32.
KONTTINEN, Y. T., AINOLA, M., VALLCALA, H., MA, J., IDA, H., MANDELIN, J., KINNE, R. W., SANTAVIRTA, S., SORSA, T., LO?PEZ-OTI?N, C., TAKAGI, M. & JUMPPANEN, M. 1999. Analysis of 16 different matrix metalloproteinases (MMP-1 to MMP-20) in the synovial membrane: Different profiles in trauma and rheumatoid arthritis. *Annals of the Rheumatic Diseases,* 58, 691-697.
KONTTINEN, Y. T., LI, T., HUKKANEN, M., MA, J., XU, J. & VIRTANEN, I. 2000. Fibroblast biology: Signals targeting the synovial fibroblast in arthritis. *Arthritis Research and Therapy,* 2, 348-355.
KOSSODO, S., ZHANG, J., JESCHKE, J., BLUSZTAJN, A., RAJOPADHYE, M., CATALANO, A. & PETERSON, J. D. 2010. Optical Imaging of MMPSense as a Biomarker of Matrix Metalloprotease Activity In vivo. *In:* MEDICAL, V. (ed.).

KROGER, H., MIESEL, R., DIETRICH, A., OHDE, M., RAJNAVOLGYI, E. & OCKENFELS, H. 1996. Synergistic effects of thalidomide and poly (ADP-ribose) polymerase inhibition on type II collagen-induced arthritis in mice. *Inflammation,* 20, 203-215.

LAKEY, R. L. & CAWSTON, T. E. 2009. Sulfasalazine blocks the release of proteoglycan and collagen from cytokine stimulated cartilage and down-regulates metalloproteinases. *Rheumatology,* 48, 1208-1212.

LANDRÉ-BEAUVAIS, A. J. 2001. The first description of rheumatoid arthritis. Unabridged text of the doctoral dissertation presented in 1800. *Joint Bone Spine,* 68, 130-143.

LANGDON, C., LEITH, J., RICHARDS, C. D. & SMITH, F. 1997. Oncostatin M stimulates monocyte chemoattractant protein-1- and interleukin-1-induced matrix metalloproteinase-1 production by human synovial fibroblasts in vitro. *Arthritis and Rheumatism,* 40, 2139-2146.

LAZARUS, R., VERCELLI, D., PALMER, L. J., KLIMECKI, W. J., SILVERMAN, E. K., RICHTER, B., RIVA, A., RAMONI, M., MARTINEZ, F. D., WEISS, S. T. & KWIATKOWSKI, D. J. 2002. Single nucleotide polymorphisms in innate immunity genes: abundant variation and potential role in complex human disease. *Immunological Reviews,* 190, 9-25.

LEBER, T. M. & BALKWILL, F. R. 1997. Zymography: A Single-Step Staining Method for Quantitation of Proteolytic Activity on Substrate Gels. *Analytical Biochemistry,* 249, 24-28.

LEE, D. M., KIENER, H. P., AGARWAL, S. K., NOSS, E. H., WATTS, G. F., CHISAKA, O., TAKEICHI, M. & BRENNER, M. B. 2007. Cadherin-11 in synovial lining formation and pathology in arthritis. *Science,* 315, 1006-1010.

LEE, S.-J. & KIM, M.-M. 2011. Resveratrol with antioxidant activity inhibits matrix metalloproteinase via modulation of SIRT1 in human fibrosarcoma cells. *Life Sciences,* 88, 465-472.

LI, H., LIU, P., CEPEDA, J., FANG, D., EASLEY, R. B., SIMON, B. A., ZHANG, L. Q. & YE, S. Q. 2008a. Augmentation of pulmonary epithelial cell IL-8 expression and permeability by pre-B-cell colony enhancing factor. *Journal of Inflammation,* 5.

LI, Y., ZHANG, Y., DORWEILER, B., CUI, D., WANG, T., WOO, C. W., BRUNKAN, C. S., WOLBERGER, C., IMAI, S. I. & TABAS, I. 2008b. Extracellular nampt promotes macrophage survival via a nonenzymatic interleukin-6/STAT3 signaling mechanism. *Journal of Biological Chemistry,* 283, 34833-34843.

LIACINI, A., SYLVESTER, J., LI, W. & ZAFARULLAH, M. 2002. Inhibition of interleukin-1-stimulated MAP kinases, activating protein-1 (AP-1) and nuclear factor kappa B (NF-κB) transcription factors down-regulates matrix metalloproteinase gene expression in articular chondrocytes. *Matrix Biology,* 21, 251-262.

LIN, L. F., LAN, S. J., RICHARDSON, A. H. & HENDERSON, L. M. 1972. Pyridine nucleotide synthesis. Purification of nicotinamide mononucleotide pyrophosphorylase from rat erythrocytes. *Journal of Biological Chemistry,* 247, 8016-22.

LIN, S.-J. & GUARENTE, L. 2003. Nicotinamide adenine dinucleotide, a metabolic regulator of transcription, longevity and disease. *Current Opinion in Cell Biology,* 15, 241-246.

LIU, N., SHANG, J., TIAN, F., NISHI, H. & ABE, K. 2011. In vivo optical imaging for evaluating the efficacy of edaravone after transient cerebral ischemia in mice. *Brain Research,* 1397, 66-75.

LUK, T., MALAM, Z. & MARSHALL, J. C. 2008. Pre-B cell colony-enhancing factor (PBEF)/visfatin: a novel mediator of innate immunity. *Journal of Leukocyte Biology,* 83, 804-816.

LUTZKY, V., HANNAWI, S. & THOMAS, R. 2007. Cells of the synovium in rheumatoid arthritis. Dendritic cells *Arthritis Research and Therapy,* 9, 219.

MANDEMA, J. W., SALINGER, D. H., BAUMGARTNER, S. W. & GIBBS, M. A. 2011. A Dose-Response Meta-Analysis for Quantifying Relative Efficacy of Biologics in Rheumatoid Arthritis. *Clin Pharmacol Ther,* 90, 828-835.

MARTIN, P. R., SHEA, R. J. & MULKS, M. H. 2001. Identification of a plasmid-encoded gene from Haemophilus ducreyi which confers NAD independence. *Journal of Bacteriology,* 183, 1168-1174.

MARUVADA, P., DMITRIEVA, N. I., EAST-PALMER, J. & YEN, P. M. 2004. Cell Cycle-dependent Expression of Thyroid Hormone Receptor-Œ≤ Is a Mechanism for Variable Hormone Sensitivity. *Molecular Biology of the Cell,* 15, 1895-1903.

MASUTANI, M., NAKAGAMA, H. & SUGIMURA, T. 2005. Poly(ADP-ribosyl)ation in relation to cancer and autoimmune disease. *Cellular and Molecular Life Sciences,* 62, 769-783.

MATSUI, H., TSUTSUMI, A., SUGIHARA, M., SUZUKI, T., IWANAMI, K., KOHNO, M., GOTO, D., MATSUMOTO, I., ITO, S. & SUMIDA, T. 2008. Visfatin (pre-B cell colony-enhancing factor) gene expression in patients with rheumatoid arthritis. *Annals of the Rheumatic Diseases,* 67, 571-572.

MAURI, C. & EHRENSTEIN, M. 2007. Cells of the synovium in rheumatoid arthritis. B cells *Arthritis Research and Therapy,* 9, 205.

MCFARLANE, S., AITKEN, J., SUTHERLAND, J. S., NICHOLL, M., PRESTON, V. G. & PRESTON, C. M. 2011. Early Induction of Autophagy in Human Fibroblasts after Infection with Human Cytomegalovirus or Herpes Simplex Virus 1. *Journal of Virology,* 85, 4212-4221.

MCGLOTHLIN, J. R., GAO, L., LAVOIE, T., SIMON, B. A., EASLEY, R. B., MA, S. F., RUMALA, B. B., GARCIA, J. G. & YE, S. Q. 2005. Molecular cloning and characterization of canine pre-B-cell colony-enhancing factor. *Biochem Genet,* 43, 127-141.

MCINNES, I. B. & SCHETT, G. 2007. Cytokines in the pathogenesis of rheumatoid arthritis. *Nat Rev Immunol,* 7, 429-442.

MESKO, B., POLISKA, S., SZEGEDI, A., SZEKANECZ, Z., PALATKA, K., PAPP, M. & NAGY, L. 2010. Peripheral blood gene expression patterns discriminate among chronic inflammatory diseases and healthy controls and identify novel targets. *BMC Medical Genomics,* 3, 15.

MIESEL, R., KURPISZ, M. & KROGER, H. 1995. Modulation of inflammatory arthritis by inhibition of poly(ADP ribose) polymerase. *Inflammation,* 19, 379-387.

MOSCHEN, A. R., GEIGER, S., GERNER, R. & TILG, H. 2009. Pre-B cell colony enhancing factor/NAMPT/visfatin and its role in inflammation-related bone disease. *Mutation Research/Fundamental and Molecular Mechanisms of Mutagenesis,* In Press, Corrected Proof.

MOSCHEN, A. R., KASER, A., ENRICH, B., MOSHEIMER, B., THEURL, M., NIEDEREGGER, H. & TILG, H. 2007. Visfatin, an Adipocytokine with Proinflammatory and Immunomodulating Properties. *Journal of Immunology,* 178, 1748-1758.

MOTA, L., SANTOS NETO, L. & CARVALHO, J. L. 2009. Autoantibodies and other serological markers in rheumatoid arthritis: predictors of disease activity? *Clinical Rheumatology,* 28, 1127-1134.

MUKHERJEE, P., WU, B., MAYTON, L., KIM, S. H., ROBBINS, P. D. & WOOLEY, P. H. 2003. TNF receptor gene therapy results in suppression of IgG2a anticollagen antibody in collagen induced arthritis. *Annals of the Rheumatic Diseases,* 62, 707-714.

MÜLLER-LADNER, U., OSPELT, C., GAY, S., DISTLER, O. & PAP, T. 2007. Cells of the synovium in rheumatoid arthritis. Synovial fibroblasts *Arthritis Research and Therapy,* 9, 223.

MUN, S. H., KIM, H. S., KIM, J. W., KO, N. Y., KIM DO, K., LEE, B. Y., KIM, B., WON, H. S., SHIN, H. S., HAN, J. W., LEE, H. Y., KIM, Y. M. & CHOI, W. S. 2009. Oral administration of curcumin suppresses production of matrix metalloproteinase

(MMP)-1 and MMP-3 to ameliorate collagen-induced arthritis: inhibition of the PKCdelta/JNK/c-Jun pathway. *J Pharmacol Sci,* 111, 13-21.
MURUGANANDHAM, M., ALFIERI, A. A., MATEI, C., CHEN, Y., SUKENICK, G., SCHEMAINDA, I., HASMANN, M., SALTZ, L. B. & KOUTCHER, J. A. 2005. Metabolic signatures associated with a NAD synthesis inhibitor-induced tumor apoptosis identified by1H-decoupled-31P magnetic resonance spectroscopy. *Clinical Cancer Research,* 11, 3503-3513.
MUSGROVE, E., RUGG, C., TAYLOR, I. & HEDLEY, D. 1984. Transferrin receptor expression during exponential and plateau phase growth of human tumour cells in culture. *Journal of Cellular Physiology,* 118, 6-12.
NAGASE, H. & WOESSNER, J. F. 1999. Matrix Metalloproteinases. *Journal of Biological Chemistry,* 274, 21491-21494.
NAHIMANA, A., ATTINGER, A., AUBRY, D., GREANEY, P., IRESON, C., THOUGAARD, A. V., TJ√∏RNELUND, J., DAWSON, K. M., DUPUIS, M. & DUCHOSAL, M. A. 2009. The NAD biosynthesis inhibitor APO866 has potent antitumor activity against hematologic malignancies. *Blood,* 113, 3276-3286.
NAKAMARU, Y., VUPPUSETTY, C., WADA, H., MILNE, J. C., ITO, M., ROSSIOS, C., ELLIOT, M., HOGG, J., KHARITONOV, S., GOTO, H., BEMIS, J. E., ELLIOTT, P., BARNES, P. J. & ITO, K. 2009. A protein deacetylase SIRT1 is a negative regulator of metalloproteinase-9. *The FASEB Journal,* 23, 2810-2819.
NATIONAL RHEUMATOID ARTHRITIS SOCIETY 2010. The Economic Burden of Rheumatoid Arthritis.
NEIDEL, J., SOVA, L., SCHROERS, B., SINTERMANN, F., MANZKE, O. & BOHLEN, H. 1998. Effects of methotrexate on normal articular cartilage in vitro and in vivo. *Annals of the Rheumatic Diseases,* 57, 414-421.
NEMETH, E., TASHIMA, L. S., YU, Z. & BRYANT-GREENWOOD, G. D. 2000. Fetal membrane distention: I. Differentially expressed genes regulated by acute distention in amniotic epithelial (WISH) cells. *American Journal of Obstetrics and Gynacology,* 182, 50-59.
NEUMANN, E., RIEPL, B., KNEDLA, A., LEFEVRE, S., TARNER, I., GRIFKA, J., STEINMEYER, J., SCHOLMERICH, J., GAY, S. & MÜLLER-LADNER, U. 2010. Cell culture and passaging alters gene expression pattern and proliferation rate in rheumatoid arthritis synovial fibroblasts *Arthritis Research and Therapy,* 12, R83.
NICE, N. I. F. H. A. C. E. 2009. The management of rheumatoid arthritis in adults.
NIEDERER, F., OSPELT, C., BRENTANO, F., HOTTIGER, M. O., GAY, R. E., GAY, S., DETMAR, M. & KYBURZ, D. 2011. SIRT1 overexpression in the rheumatoid arthritis synovium contributes to proinflammatory cytokine production and apoptosis resistance. *Annals of the Rheumatic Diseases,* 70, 1866-1873.
NORTH, B. & VERDIN, E. 2004. Sirtuins: Sir2-related NAD-dependent protein deacetylases. *Genome Biology,* 5, 224.
NOSS, E. H., CHANG, S. K., WATTS, G. F. M. & BRENNER, M. B. 2011. Modulation of matrix metalloproteinase production by rheumatoid arthritis synovial fibroblasts after cadherin 11 engagement. *Arthritis and Rheumatism,* 63, 3768-3778.
NOWELL, M. A., EVANS, L. A. & WILLIAMS, A. S. 2012. PBEF/NAMPT/visfatin: a promising drug target for treating rheumatoid arthritis? *Future Medicinal Chemistry,* 4, 751-769.
NOWELL, M. A., RICHARDS, P. J., FIELDING, C. A., OGNJANOVIC, S., TOPLEY, N., WILLIAMS, A. S., BRYANT-GREENWOOD, G. & JONES, S. A. 2006. Regulation of pre-B cell colony-enhancing factor by STAT-3-dependent interleukin-6 trans-signaling: Implications in the pathogenesis of rheumatoid arthritis. *Arthritis and Rheumatism,* 54, 2084-2095.
NOWELL, M. A., RICHARDS, P. J., HORIUCHI, S., YAMAMOTO, N., ROSE-JOHN, S., TOPLEY, N., WILLIAMS, A. S. & JONES, S. A. 2003. Soluble IL-6 Receptor Governs IL-6 Activity in Experimental Arthritis: Blockade of Arthritis Severity by Soluble Glycoprotein 130. *Journal of Immunology,* 171, 3202-3209.

OESTERGAARD, S., CHOUINARD, L., DOYLE, N., KARSDAL, M. A., SMITH, S. Y., QVIST, P. & TANK√≥, L. B. 2006. The utility of measuring C-terminal telopeptides of collagen type II (CTX-II) in serum and synovial fluid samples for estimation of articular cartilage status in experimental models of destructive joint diseases. *Osteoarthritis and Cartilage,* 14, 670-679.

OGNJANOVIC, S., BAO, S., YAMAMOTO, S. Y., GARIBAY-TUPAS, J., SAMAL, B. & BRYANT-GREENWOOD, G. D. 2001. Genomic organization of the gene coding for human pre-B-cell colony enhancing factor and expression in human fetal membranes. *Journal of Molecular Endocrinology,* 26, 107-117.

OGNJANOVIC, S. & BRYANT-GREENWOOD, G. D. 2002. Pre-B-cell colony-enhancing factor, a novel cytokine of human fetal membranes. *American Journal of Obstetrics and Gynecology,* 187, 1051-1058.

OHGUCHI, K., ITOH, T., AKAO, Y., INOUE, H., NOZAWA, Y. & ITO, M. 2010. SIRT1 modulates expression of matrix metalloproteinases in human dermal fibroblasts. *British Journal of Dermatology,* 163, 689-694.

OLESEN, U. H., THOUGAARD, A. V., JENSEN, P. B. & SEHESTED, M. 2010. A preclinical study on the rescue of normal tissue by nicotinic acid in high-dose treatment with APO866, a specific nicotinamide phosphoribosyltransferase inhibitor. *Molecular Cancer Therapeutics,* 9, 1609-1617.

OTERO, M. & GOLDRING, M. B. 2007. Cells of the synovium in rheumatoid arthritis. Chondrocytes. *Arthritis Research and Therapy,* 9.

OTERO, M., LAGO, R., GOMEZ, R., LAGO, F., DIEGUEZ, C., GOMEZ-REINO, J. J. & GUALILLO, O. 2006. Changes in plasma levels of fat-derived hormones adiponectin, leptin, resistin and visfatin in patients with rheumatoid arthritis. *Annals of the Rheumatic Diseases,* 65, 1198-1201.

OWEN, J. L., IRAGAVARAPU-CHARYULU, V., GUNJA-SMITH, Z., HERBERT, L. M., GROSSO, J. F. & LOPEZ, D. M. 2003. Up-Regulation of Matrix Metalloproteinase-9 in T Lymphocytes of Mammary Tumor Bearers: Role of Vascular Endothelial Growth Factor. *The Journal of Immunology,* 171, 4340-4351.

OZGEN, M., KOCA, S., AKSOY, K., DAGLI, N., USTUNDAG, B. & ISIK, A. 2011. Visfatin levels and intima-media thicknesses in rheumatic diseases. *Clinical Rheumatology,* 30, 757-763.

PACIFICI, M., KOYAMA, E., SHIBUKAWA, Y., WU, C., TAMAMURA, Y., ENOMOTO-IWAMOTO, M. & IWAMOTO, M. 2006. Cellular and Molecular Mechanisms of Synovial Joint and Articular Cartilage Formation. *Annals of the New York Academy of Sciences,* 1068, 74-86.

PANICO, A., CARDILE, V., GENTILE, B., GARUFI, F., FAMA, P., BONFIGLIO, G. & RONSISVALLE, G. 2003. Effects of leflunomide on human cartilage. *Il Farmaco,* 58, 983-987.

PAP, T., MÜLLER-LADNER, U., GAY, R. E. & GAY, S. 2000. Fibroblast biology. Role of synovial fibroblasts in the pathogenesis of rheumatoid arthritis. *Arthritis Research and Therapy,* 2, 361-367.

PETERS, H. C., OTTO, T. J., ENDERS, J. T., JIN, W., MOED, B. R. & ZHANG, Z. 2011. The protective role of the pericellular matrix in chondrocyte apoptosis. *Tissue Engineering Part A,* 17, 2017-2024.

PITTELLI, M., FORMENTINI, L., FARACO, G., LAPUCCI, A., RAPIZZI, E., CIALDAI, F., ROMANO, G., MONETI, G., MORONI, F. & CHIARUGI, A. 2010. Inhibition of Nicotinamide Phosphoribosyltransferase: cellular bioenergetics reveals a mitochondrial insensitive NAD pool. *Journal of Biological Chemistry,* 285, 34106-34114.

POOLE, A. R., KOJIMA, T., YASUDA, T., MWALE, F., KOBAYASHI, M. & LAVERTY, S. 2001. Composition and structure of articular cartilage: a template for tissue repair. *Clinical Orthopaedics and Related Research,* 391 Suppl, S26-33.

POWANDA, M. C., MUNIZ, O. & DIETRICH, L. S. 1969. Mechanism of rat liver nicotinamide mononucleotide pyrophosphorylase. *Biochemistry,* 8, 1869-1873.

PRÉSUMEY, J., COURTIES, G., LOUIS-PLENCE, P., ESCRIOU, V., SCHERMAN, D., PERS, Y., YSSEL, H., PÈNE, J., KYBURZ, D., GAY, S., JORGENSEN, C. & APPARAILLY, F. 2013. Nicotinamide phosphoribosyltransferase/visfatin expression by inflammatory monocytes mediates arthritis pathogenesis. *Annals of the Rheumatic Diseases*.

PRIMERDESIGN 2011. Precision nanoScript Reverse Transcription kit.

RAZA, K., FALCIANI, F., CURNOW, S. J., ROSS, E., LEE, C., AKBAR, A., LORD, J., GORDON, C., BUCKLEY, C. D. & SALMON, M. 2005. Early rheumatoid arthritis is characterized by a distinct and transient synovial fluid cytokine profile of T cell and stromal cell origin. *Arthritis Research and Therapy,* 7, R784-R795.

REAGAN-SHAW, S., NIHAL, M. & AHMAD, N. 2008. Dose translation from animal to human studies revisited. *The FASEB Journal,* 22, 659-661.

RENGEL, Y., OSPELT, C. & GAY, S. 2007. Proteinases in the joint: Clinical relevance of proteinases in joint destruction. *Arthritis Research and Therapy,* 9.

REVENKO, I. N., SOMMER, F. O., MINH, D. T., GARRONE, R. & FRANC, J.-M. 1994. Atomic force microscopy study of the collagen fibre structure. *Biology of the Cell,* 80, 67-69.

REVOLLO, J. R., GRIMM, A. A. & IMAI, S. 2007a. The regulation of nicotinamide adenine dinucleotide biosynthesis by Nampt/PBEF/visfatin in mammals. *Current Opinion in Gastroenterology,* 23, 1640179.

REVOLLO, J. R., GRIMM, A. A. & IMAI, S. I. 2004. The NAD biosynthesis pathway mediated by nicotinamide phosphoribosyltransferase regulates Sir2 activity in mammalian cells. *Journal of Biological Chemistry,* 279, 50754-50763.

REVOLLO, J. R., KORNER, A., MILLS, K. F., SATOH, A., WANG, T., GARTEN, A., DASGUPTA, B., SASAKI, Y., WOLBERGER, C., TOWNSEND, R. R., MILBRANDT, J., KIESS, W. & IMAI, S. I. 2007b. Nampt/PBEF/Visfatin Regulates Insulin Secretion in beta Cells as a Systemic NAD Biosynthetic Enzyme. *Cell Metabolism,* 6, 363-375.

RHEE, D. K., MARCELINO, J., BAKER, M., GONG, Y., SMITS, P., LEFEBVRE, V. R., JAY, G. D., STEWART, M., WANG, H., WARMAN, M. L. & CARPTEN, J. D. 2005. The secreted glycoprotein lubricin protects cartilage surfaces and inhibits synovial cell overgrowth. *The Journal of Clinical Investigation,* 115, 622-631.

RHO, R. H., SOLUS, J., SOKKA, T., OESER, A., CHUNG, C. P., GEBRETSADIK, T., SHINTANI, A., PINCUS, T. & STEIN, C. M. 2009. Adipocytokines are associated with radiographic joint damage in rheumatoid arthritis. *Arthritis and Rheumatism,* 60, 1906-1914.

ROMACHO, T., AZCUTIA, V., VÁZQUEZ-BELLA, M., MATESANZ, N., CERCAS, E., NEVADO, J., CARRARO, R., RODRÍGUEZ-MAÑAS, L., SÁNCHEZ-FERRER, C. F. & PEIRÓ, C. 2009. Extracellular PBEF/NAMPT/visfatin activates pro-inflammatory signalling in human vascular smooth muscle cells through nicotinamide phosphoribosyltransferase activity. *Diabetologia,* 52, 2455-2463.

ROMAGNANI, P., ANNUNZIATO, F., LASAGNI, L., LAZZERI, E., BELTRAME, C., FRANCALANCI, M., UGUCCIONI, M., GALLI, G., COSMI, L., MAURENZIG, L., BAGGIOLINI, M., MAGGI, E., ROMAGNANI, S. & SERIO, M. 2001. Cell cycle-dependent expression of CXC chemokine receptor 3 by endothelial cells mediates angiostatic activity. *Journal of Clinical Investigation,* 107, 53-63.

RONGVAUX, A., SHE, R. J., MULKS, M. H., GIGOT, D., URBAIN, J., LEO, O. & ANDRIS, F. 2002. Pre-B-cell colony-enhancing factor, whose expression is up-regulated in activated lymphocytes, is a nicotinamide phosphoribosyltransferase, a cytosolic enzyme involved in NAD biosynthesis. *European Journal of Immunology,* 32, 3225-3234.

ROTH, S. Y., DENU, J. M. & ALLIS, C. D. 2001. Histone Acetyltransferases *Annual Review of Biochemistry,* 70, 81-120.

ROWAN, A. D. 2001. Cartilage catabolism in arthritis: factors that influence homeostasis. *Expert Reviews in Molecular Medicine,* 3, 1-20.

ROZEN, S. & SKALETSKY, H. 2000. Primer3 on the WWW for general users and for biologist programmers. *Methods in Molecular Biology,* 132, 365-386.
RUBBERT-ROTH, A. 2012. Assessing the safety of biologic agents in patients with rheumatoid arthritis. *Rheumatology,* 51, v38-v47.
SAMAL, B., SUN, Y., STEARNS, G., XIE, C., SUGGS, S. & MCNIECE, I. 1994. Cloning and characterization of the cDNA encoding a novel human pre-B- cell colony-enhancing factor. *Molecular and Cellular Biology,* 14, 1431-1437.
SCHAGGER, H. 2006. Tricine-SDS-PAGE. *Nat. Protocols,* 1, 16-22.
SEEUWS, S., JACQUES, P., VAN PRAET, J., DRENNAN, M., COUDENYS, J., DECRUY, T., DESCHEPPER, E., LEPESCHEUX, L., PUJUGUET, P., OSTE, L., VANDEGHINSTE, N., BRYS, R., VERBRUGGEN, G. & ELEWAUT, D. 2010. A multiparameter approach to monitor disease activity in collagen-induced arthritis. *Arthritis Reseach and Therapy,* 12, R160.
SHEN, Y., CHEN, J., ZHANG, X., WU, X. & XU, Q. 2007. Human TNF-alpha gene vaccination prevents collagen-induced arthritis in mice. *International Immunopharmacology,* 7, 1140-1149.
SHERIDAN, C. 2008. Small molecule challenges dominance of TNF-[alpha] inhibitors. *Nat Biotech,* 26, 143-144.
SHERRY, S. T., WARD, M. H., KHOLODOV, M., BAKER, J., PHAN, L., SMIGIELSKI, E. M. & SIROTKIN, K. 2001. dbSNP: the NCBI database of genetic variation. *Nucleic Acids Research,* 29, 308-311.

SIEBUHR, A. S., WANG, J., KARSDAL, M. A., BAY-JENSEN, A., JIN, Y. & ZHENG, Q. 2012. Matrix Metalloproteinase-dependent turnover of cartilage, synovial membrane, and connective tissue is elevated in rats with collagen induced arthritis. *Journal of Translational Medicine,* 10, 195.
SONDERGAARD, B. C., HENRIKSEN, K., WULF, H., OESTERGAARD, S., SCHURIGT, U., BRAUER, R., DANIELSEN, I., CHRISTIANSEN, C., QVIST, P. & KARSDAL, M. A. 2006. Relative contribution of matrix metalloprotease and cysteine protease activities to cytokine-stimulated articular cartilage degradation. *Osteoarthritis and Cartilage,* 14, 738-48.
SPORTY, J. L., KABIR, M. M., TURTELTAUB, K. W., OGNIBENE, T., LIN, S.-J. & BENCH, G. 2008. Single sample extraction protocol for the quantification of NAD and NADH redox states in Saccharomyces cerevisiae. *Journal of Separation Science,* 31, 3202-3211.
STOCKWELL, R. A. 1971. The interrelationship of cell density and cartilage thickness in mammalian articular cartilage. *The Journal of Anatomy,* 109, 411-421.
SZABO, C. 1996. DNA strand breakage and activation of poly-ADP ribosyltransferase: a cytotoxic pathway triggered by peroxynitrite. *Free Radic Biol Med,* 21, 855-69.
TAK, P. P. & BRESNIHAN, B. 2000. The pathogenesis and prevention of joint damage in rheumatoid arthritis: Advances from synovial biopsy and tissue analysis. *Arthritis and Rheumatism,* 43, 2619-2633.
TANAKA, M., NOZAKI, M., FUKUHARA, A., SEGAWA, K., AOKI, N., MATSUDA, M., KOMURO, R. & SHIMOMURA, I. 2007. Visfatin is released from 3T3-L1 adipocytes via a non-classical pathway. *Biochemical and Biophysical Research Communications,* 359, 194-201.
TCHETVERIKOV, I., RONDAY, H. K., VAN EL, B., KIERS, G. H., VERZIJL, N., TEKOPPELE, J. M., HUIZINGA, T. W., DEGROOT, J. & HANEMAAIJER, R. 2004. MMP profile in paired serum and synovial fluid samples of patients with rheumatoid arthritis. *Annals of the Rheumatic Diseases,* 63, 881-3.
THIERRY-MIEG, D. & THIERRY-MIEG, J. 2006. AceView: a comprehensive cDNA-supported gene and transcripts annotation *Genome Biology,* 7 %@ 1465-6906, S12.
TOPOTARGET. 2009a. *A Phase I/II Study to Assess the Safety and Tolerability of APO866 for the Treatment of Refractory B-CLL* [Online]. Available:

http://www.clinicaltrials.gov/ct2/show/NCT00435084?term=APO866&rank=2 [Accessed November 12 2011].
TOPOTARGET. 2009b. *A Study to Assess APO866 for the Treatment of Advanced Melanoma* [Online]. Available: http://www.clinicaltrials.gov/ct2/show/NCT00432107?term=APO866&rank=3 [Accessed November 12 2011].
TOPOTARGET. 2011. *A Study of APO866 for the Treatment of Cutaneous T cell Lymphoma* [Online]. Available: http://www.clinicaltrials.gov/ct2/show/NCT00431912?term=APO866&rank=1 [Accessed November 12 2011].
TRENTHAM, D. E., TOWNES, A. S. & KANG, A. H. 1977. Autoimmunity to type II collagen an experimental model of arthritis. *The Journal of Experimental Medicine,* 146, 857-868.
TSUTSUMI, R., ITO, H., HIRAMITSU, T., NISHITANI, K., AKIYOSHI, M., KITAORI, T., YASUDA, T. & NAKAMURA, T. 2008. Celecoxib inhibits production of MMP and NO via down-regulation of NF-κB and JNK in a PGE2 independent manner in human articular chondrocytes. *Rheumatology International,* 28, 727-736.
VAN DEN BERG, W. 1998. Joint inflammation and cartilage destruction may occur uncoupled. *Springer Seminars in Immunopathology,* 20, 149-164.
VAN DEN BERG, W. 2009. Lessons from animal models of arthritis over the past decade *Arthritis Research and Therapy,* 11, 250.
VAN DER HEIJDE, D. S. E. 2011. Erosions versus joint space narrowing in rheumatoid arthritis: what do we know? *Annals of the Rheumatic Diseases,* 70, i116-i118.
VAN DER VEEN, M. J., SCHEVEN, B. A. A., VAN ROY, J. L. A. M., DAMEN, C. A., LAFEBER, F. P. J. G. & BIJLSMA, J. W. J. 1996. In vitro effects of methotrexate on human articular cartilage and bone-derived osteoblasts. *Rheumatology,* 35, 342-349.
VAN DER VEER, E., NONG, Z., O'NEIL, C., URQUHART, B., FREEMAN, D. & PICKERING, J. G. 2005. Pre-B-cell colony-enhancing factor regulates NAD+-dependent protein deacetylase activity and promotes vascular smooth muscle cell maturation. *Circulation Research,* 97, 25-34.
VAN GOOL, F., GALL√≠, M., GUEYDAN, C., KRUYS, V., PREVOT, P. P., BEDALOV, A., MOSTOSLAVSKY, R., ALT, F. W., DE SMEDT, T. & LEO, O. 2009. Intracellular NAD levels regulate tumor necrosis factor protein synthesis in a sirtuin-dependent manner. *Nature Medicine,* 15, 206-210.
VAN MEURS, J., VAN LENT, P., STOOP, R., HOLTHUYSEN, A., SINGER, I., BAYNE, E., MUDGETT, J., POOLE, R., BILLINGHURST, C., VAN DER KRAAN, P., BUMA, P. & VAN DEN BERG, W. 1999a. Cleavage of aggrecan at the Asn341–Phe342 site coincides with the initiation of collagen damage in murine antigen-induced arthritis: A pivotal role for stromelysin 1 in matrix metalloproteinase activity. *Arthritis & Rheumatism,* 42, 2074-2084.
VAN MEURS, J. B. J., VAN LENT, P. L. E. M., HOLTHUYSEN, A. E. M., SINGER, I. I., BAYNE, E. K. & VAN DEN BERG, W. B. 1999b. Kinetics of aggrecanase- and metalloproteinase-induced neoepitopes in various stages of cartilage destruction in murine arthritis. *Arthritis and Rheumatism,* 42, 1128-1139.
VANDESOMPELE, J., DE PRETER, K., PATTYN, F., POPPE, B., VAN ROY, N., DE PAEPE, A. & SPELEMAN, F. 2002. Accurate normalization of real-time quantitative RT-PCR data by geometric averaging of multiple internal control genes. *Genome Biology,* 3, research0034.1-research0034.11.
VANKEMMELBEKE, M. N., HOLEN, I., WILSON, A. G., ILIC, M. Z., HANDLEY, C. J., KELNER, G. S., CLARK, M., LIU, C., MAKI, R. A., BURNETT, D. & BUTTLE, D. J. 2001. Expression and activity of ADAMTS-5 in synovium. *European Journal of Biochemistry,* 268, 1259-1268.
VERMA, P. & DALAL, K. 2011. ADAMTS-4 and ADAMTS-5: Key enzymes in osteoarthritis. *Journal of Cellular Biochemistry,* 112, 3507-3514.

VINCENTI, M. P., COON, C. I. & BRINCKERHOFF, C. E. 1998. Nuclear factor κB/p50 activates an element in the distal matrix metalloproteinase 1 promoter in interleukin-1β-stimulated synovial fibroblasts. *Arthritis and Rheumatism,* 41, 1987-1994.

VISSE, R. & NAGASE, H. 2003. Matrix metalloproteinases and tissue inhibitors of metalloproteinases: Structure, function, and biochemistry. *Circulation Research,* 92, 827-839.

VON HEIJNE, G. 1986. A new method for predicting signal sequence cleavage sites. *Nucleic Acids Research,* 14, 4683-4690.

WALDBURGER, J. M. & FIRESTEIN, G. S. 2009. Garden of therapeutic delights: New targets in rheumatic diseases. *Arthritis Research and Therapy,* 11.

WALKER, D. 2011. Rheumatoid Arthritis. *In:* UK, A. R. (ed.).

WANG, B., CHEN, P., JENSEN, A. C., KARSDAL, M. A., MADSEN, S. H., SONDERGAARD, B. C., ZHENG, Q. & QVIST, P. 2009a. Suppression of MMP activity in bovine cartilage explants cultures has little if any effect on the release of aggrecanase-derived aggrecan fragments. *BMC Research Notes,* 2.

WANG, P., XU, T., GUAN, Y., SU, D., FAN, G. & MIAO, C. 2009b. Perivascular adipose tissue-derived visfatin is a vascular smooth muscle cell growth factor: role of nicotinamide mononucleotide. *Cardiovascular Research,* 81, 370-380.

WANG, T., ZHANG, X., BHEDA, P., REVOLLO, J. R., IMAI, S.-I. & WOLBERGER, C. 2006. Structure of Nampt/PBEF/visfatin, a mammalian NAD+ biosynthetic enzyme. *Nature Structural and Molecular Biology,* 13, 661-662.

WESTACOTT, C. I., WHICHER, J. T., BARNES, I. C., THOMPSON, D., SWAN, A. J. & DIEPPE, P. A. 1990. Synovial fluid concentration of five different cytokines in rheumatic diseases. *Annals of the Rheumatic Diseases,* 49, 676-681.

WIJBRANDTS, C. A., DIJKGRAAF, M. G. W., KRAAN, M. C., VINKENOOG, M., SMEETS, T. J., DINANT, H., VOS, K., LEMS, W. F., WOLBINK, G. J., SIJPKENS, D., DIJKMANS, B. A. C. & TAK, P. P. 2008. The clinical response to infliximab in rheumatoid arthritis is in part dependent on pretreatment tumour necrosis factor Œ± expression in the synovium. *Annals of the Rheumatic Diseases,* 67, 1139-1144.

WILCZYNSKA, K. M., GOPALAN, S. M., BUGNO, M., KASZA, A., KONIK, B. S., BRYAN, L., WRIGHT, S., GRISWOLD-PRENNER, I. & KORDULA, T. 2006. A Novel Mechanism of Tissue Inhibitor of Metalloproteinases-1 Activation by Interleukin-1 in Primary Human Astrocytes. *Journal of Biological Chemistry,* 281, 34955-34964.

WOOLEY, P. H., DILLON, A. M. & LUTHRA, H. S. 1983. Genetic control of type II collagen-induced arthritis in mice: Factors influencing disease susceptibility and evidence for multiple MHC-associated gene control. *Transplantation Proceedings,* 15, 180-185.

WOSIKOWSKI, K., MATTERN, K., SCHEMAINDA, I., HASMANN, M., RATTEL, B. & LOÃÀSER, R. 2002. WK175, a novel antitumor agent, decreases the intracellular nicotinamide adenine dinucleotide concentration and induces the apoptotic cascade in human leukemia cells. *Cancer Research,* 62, 1057-1062.

WUNDER, A., TUNG, C. H., M√ºLLER-LADNER, U., WEISSLEDER, R. & MAHMOOD, U. 2004. In vivo imaging of protease activity in arthritis: A novel approach for monitoring treatment response. *Arthritis and Rheumatism,* 50, 2459-2465.

XIE, H., TANG, S. Y., LUO, X. H., HUANG, J., CUI, R. R., YUAN, L. Q., ZHOU, H. D., WU, X. P. & LIAO, E. Y. 2007. Insulin-Like Effects of Visfatin on Human Osteoblasts. *Calcified Tissue International,* 80, 201-210.

YAN, C. & BOYD, D. D. 2007. Regulation of matrix metalloproteinase gene expression. *Journal of Cellular Physiology,* 211, 19-26.

YANABA, K., HAMAGUCHI, Y., VENTURI, G. M., STEEBER, D. A., ST.CLAIR, E. W. & TEDDER, T. F. 2007. B cell depletion delays collagen-induced arthritis in mice: Arthritis induction requires synergy between humoral and cell-mediated immunity. *Journal of Immunology,* 179, 1369-1380.

YANG, H., LAVU, S. & SINCLAIR, D. A. 2006. Nampt/PBEF/Visfatin: A regulator of mammalian health and longevity? *Experimental Gerontology,* 41, 718-726.

YANG, H., YEN, M., LIN, C., LIN, C., CHEN, Y., WENG, T., HUANG, T., WU, C. & LAI, M. 2010. A combination of the metabolic enzyme inhibitor APO866 and the immune adjuvant L-1-methyl tryptophan induces additive antitumor activity. *Experimental Biology and Medicine,* 235, 869-876.

YE, S. Q., SIMON, B. A., MALONEY, J. P., ZAMBELLI-WEINER, A., GAO, L., GRANT, A., EASLEY, R. B., MCVERRY, B. J., TUDER, R. M., STANDIFORD, T., BROWER, R. G., BARNES, K. C. & GARCIA, J. G. N. 2005. Pre-B-Cell Colony-enhancing Factor as a Potential Novel Biomarker in Acute Lung Injury. *American Journal of Respiratory and Critical Care Medicine,* 171, 361-370.

YEUNG, F., HOBERG, J. E., RAMSEY, C. S., KELLER, M. D., JONES, D. R., FRYE, R. A. & MAYO, M. W. 2004. Modulation of NF-κB-dependent transcription and cell survival by the SIRT1 deacetylase. *EMBO Journal,* 23, 2369-2380.

YING, W., SEVIGNY, M. B., CHEN, Y. & SWANSON, R. A. 2001. Poly(ADP-ribose) glycohydrolase mediates oxidative and excitotoxic neuronal death. *Proceedings of the National Academy of Sciences of the United States,* 98, 12227-32.

YOSHIHARA, Y., NAKAMURA, H., OBATA, K., YAMADA, H., HAYAKAWA, T., FUJIKAWA, K. & OKADA, Y. 2000. Matrix metalloproteinases and tissue inhibitors of metalloproteinases in synovial fluids from patients with rheumatoid arthritis or osteoarthritis. *Annals of the Rheumatic Diseases,* 59, 455-61.

YOUNG, D., LAKEY, R., PENNINGTON, C. J., JONES, D. R., KEVORKIAN, L., EDWARDS, D., CAWSTON, T. E. & CLARK, I. 2005. Histone deacetylase inhibitors modulate metalloproteinase gene expression in chondrocytes and block cartilage resorption. *Arthritis Research & Therapy,* 7, R503-R512.

ZEREZ, C. R., LEE, S. J. & TANAKA, K. R. 1987. Spectrophotometric determination of oxidized and reduced pyridine nucleotides in erythrocytes using a single extraction procedure. *Analytical Biochemistry,* 164, 367-73.

ZHANG, L. Q., HERUTH, D. P. & YE, S. Q. 2011. Nicotinamide phosphoribosyltransferase in human diseases. *Journal of Bioanalysis and Biomedicine,* 3, 13-25.

ZIEGLER, M. 2000. New functions of a long-known molecule. Emerging roles of NAD in cellular signaling. *European Journal of Biochemistry,* 267, 1550-1564.